COMPUTATION AND VERIFICATION OF WORKPIECE SHAPE IN ELECTROCHEMICAL MACHINING

A Thesis presented for the Degree of

Doctor of Philosophy

by

M.B. NANAYAKKARA, B.Sc.

Department of Production Management
and Manufacturing Technology,
UNIVERSITY OF STRATHCLYDE.

AUGUST 1977

To dear Mother

SUMMARY

This investigation was motivated by the need for accurate prediction of electrochemical machined surfaces relative to corresponding tool geometries for given sets of machining parameters.

A mathematical model was formulated which simulates the electrochemical erosion achieved by primary current distribution under steady tool feed rate, but with correction for variable efficiency.

The equations comprising the mathematical model were programmed for solution by a digital computer, using discrete steps and a quasi-steady approach. The model was not completely analytical; it utilised an empirical values for specific metal removal rates. The efficiency of machining with $NaNO_3$ electrolyte was estimated from experimental results of other investigators.

To assess the validity of the model, drilling test runs were performed with tubular electrodes having two geometries at the leading edge of the tool. Work specimens were made out of EN58J stainless steel, both NaCl and $NaNO_3$ electrolytes were used. The correlation between experimentally obtained drilled surfaces and the computer predicted surfaces were satisfactory, justifying the assumptions made during the development of the model and the numerical methods of the solution used.

This investigation has provided a method which could be successfully employed to predict the electrochemically

machined profiles relative to tool geometries. This undoubtedly helps the production engineer in achieving the desired tolerances of the finished component eliminating the high cost of trial and error techniques.

ACKNOWLEDGEMENTS

The author wishes to express his sincere thanks to his supervisor Dr. C.N. Larsson for his invaluable guidance and help without which this project work would not have been completed.

The author also wishes to express his thanks to Professor D.S. Ross, Head of the Department of Production Management and Manufacturing Technology for provision of research facilities and the opportunity of performing this study. Thanks are also due to Professor Butler of the Department of Mathematics for reading Chapter II of this thesis; also to the staff of the Production Engineering work shop for their many diverse contributions.

NOMENCLATURE

A	Atomic weight
A	Area (Chapter III)
A.C.	alternating current
b	width (Chapter III)
D.C.	direct current
E	Electrode Potential
ECM	Electrochemical Machining
F	Faraday number
f	Tool feed rate
h	inter electrode gap
he	orthogonal equilibrium gap
I	electrical current
J	electrical current density
J_o	exchange current density
l	length
m	mass
P	Pressure
Q	electrolyte flow rate
R	gas constant
R	electrical resistance
r	radius
S	conductance
T	temperature
t	time
V	electrical voltage
V_l	potential drop in electrolyte in the electrode gap (volts)

V_{sp}	specific volumetric metal removal rate (volume)
w	Land width
Z	valency
δ_d	thickness of the double layer
η_a	activation over potential
η	current efficiency
χ	electrical conductivity
ϕ	potential flux
θ	angle
ρ, ρ	density
α	transfer coefficient (Chapter II)

Suffixes

a	anode
c	cathode
conc	concentration
r	resistance

CONTENTS

CHAPTER I

INTRODUCTION AND LITERATURE REVIEW

1.1 INTRODUCTION

Difficulties experienced in machining hard alloys using conventional machining processes, demand for stress free machined surfaces and a wide variety of complex shapes have led to the development of electrochemical machines.

The electrochemical machining process is capable of producing complex forms at relatively high metal removal rates in a single pass. This process has been profitably employed in the aircraft industry - for example, in shaping of turbine blades, drilling cooling holes in gas turbines etc.

However only a limited amount of information is available on selecting process parameters. Up to the present time design of tooling due to the complexity of the process, is by a trial and error technique. For this reason the advantages of the process are not fully realised. Whatever machining process is used accuracy and repeatability are important to the industrial viability. Of the factors affecting both accuracy and repeatability of the E.C.M. process the gap between the work piece and tool is of prime importance. Accurate prediction of this gap would make the perfection of the tools easier so that greater advantage could be taken of the virtues of the process.

1.2 ELECTROCHEMICAL MACHINING PROCESS

The electrochemical machining process is controlled high rate electrolysis. In general a D.C. voltage

(rectified A.C.) is applied across two electrodes immersed in an electrolytic cell. The shaping tool is made the cathode and the piece being machined made the anode which are separated by a small gap typically between 0.05 mm and 0.50 mm (0.002 inches and 0.02 inches). Electrolyte is pumped between the gap of the electrodes as one of the electrodes is moved towards the other normally at a constant rate. The current which passes through the cell is carried by electrons in the electrodes and ions in the electrolyte.Transfer of current between the work piece and the electrolyte causes atom by atom removal of metal from the anode which is the work piece. Any part of the work piece nearer to the conducting surface (non insulated) of the cathode, or the tool, will have a higher current density than remote areas. As a result these areas which are nearer will be machined at a faster rate, and as feed of the electrode is maintained at a constant rate, the anode will take up more or less, the inverse shape of the cathode. The basic theory of the process is described in more detail by De Barr and Oliver (1).

1.3 ELECTROCHEMISTRY IN ECM

1.3.1 Electrode Process

The main role of an electrolyte in the electrochemical cell is essentially the same as with other electrochemical processes such as electroplating, fuel cells etc. where the electrolyte acts as an electrolytic

conductor between the anode and the cathode which are the work piece and the tool respectively in the case of the electrochemical machining process. It also forms the energy barriers commonly known as double layers at the electrode-electrolyte interface which control and characterise the electrochemical process occurring across these interfaces.

The mechanism of electrolyte conduction is not only different from the electronic conduction but it is also very much more complex and less understood especially in the case of electrolytes of high concentrations. In metals electrical conduction is achieved by the movement of free electrons which are found in abundance in the metal where as in electrolytes it occurs by mass transfer, i.e. by the movement of cations and anions to their respective electrodes. Conduction across the electrode electrolyte interface occurs by charge transfer in one or more electrochemical reactions.

1.3.2 Potential Distribution Across the Electrode Gap

The voltage required to pass an electric current through an electrolytic cell may be considered as the sum of several components distributed between the electrodes. The potential drop in the electrolyte across the electrode gap itself obeys Ohms law, and can be expressed as

$$(V_\ell) = \frac{J\,h}{\chi} \qquad \ldots\ldots \quad (1.1)$$

where '(V_ℓ)' the voltage drop in the electrolyte, in the electrode gap and J the local current density, 'χ' the

specific conductivity of the electrolyte. Here 'h' the gap between the electrodes is measured along current flux lines, and if the electrodes are parallel to each other 'h' will be of constant value equal to the gap distance between the electrodes. There also exists a potential difference between each electrode surface and the adjacent electrolyte layer i.e. the electrode potential, which is determined by the electrode material, and the reactive species and the current density.

1.3.3 Over Potentials

At any electrode-electrolyte interface, there is an electric double layer as shown in Fig. (1.1). It occurs at both the anode and the cathode of the cell, but the arrangement of charges or the polarities of the electrodes are in opposite directions.

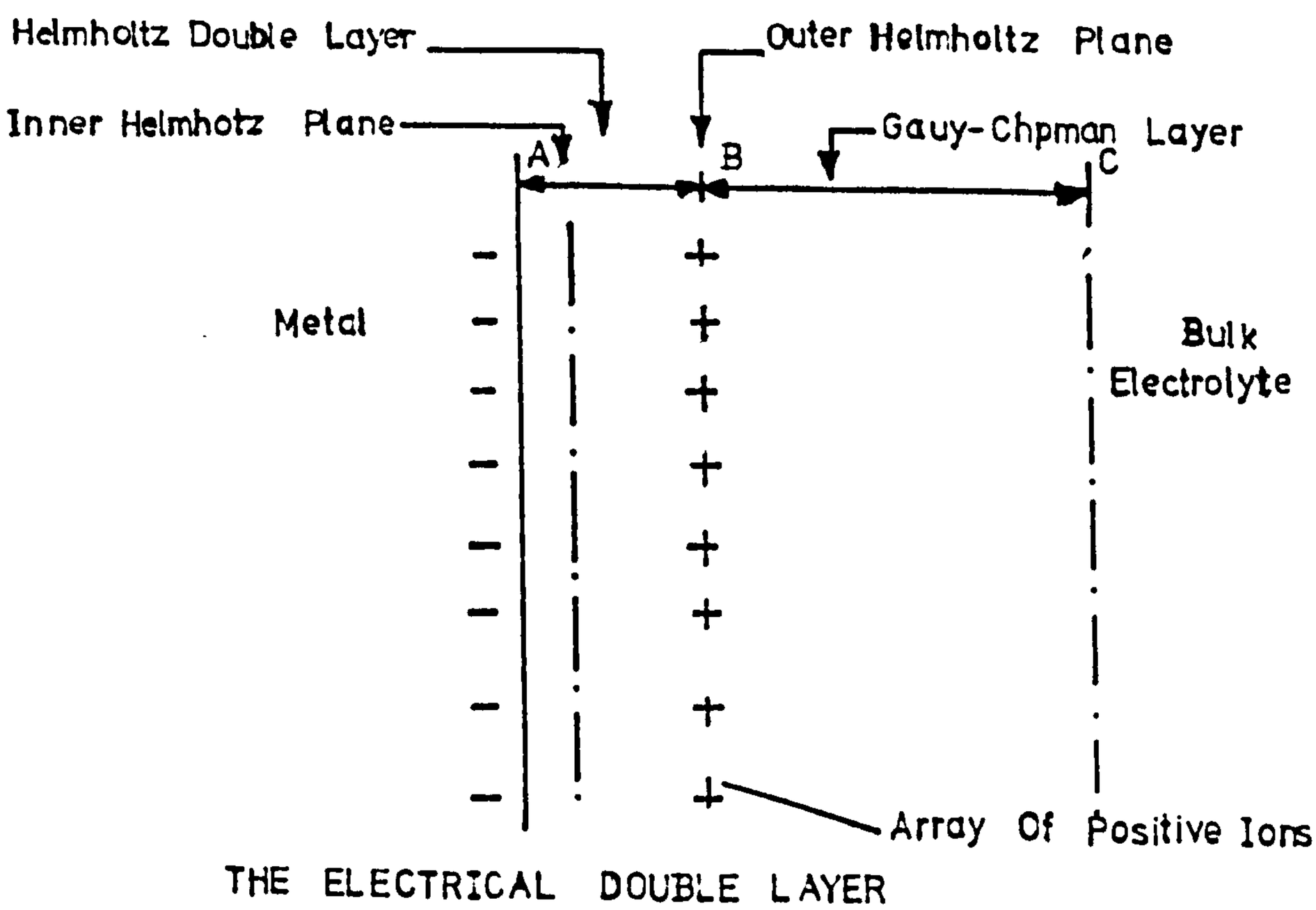

THE ELECTRICAL DOUBLE LAYER

FIG. (1.1)

A potential difference arises from the transfer into the solution of metal ions and the simultaneous discharge of ions from the solution. Equilibrium is reached when the electrons left in the metal contribute in the formation of a layer of + ve ions in the solution. The +ve charges in the solution and the negative charges in the metal forms the 'electrical double layer'. The structure of the double layer is complicated, with reference to Fig.(1.1), over the inner Helmholtz plane A, which lies very close to the metal surface, unsolvated charges which do not have water molecules attached to them may be absorbed. Beyond 'A' lies the outer Helmholtz plane, 'B' along which lies an array of +ve charges, further into the solution is the Gouy-Chapman layer, C, which is more diffuse and mobile. The bulk electrolyte with its usual properties lies outside Gouy-Chapman layer.

The rate of charge transfer reaction which occurs at the two electrodes depends upon the potential difference across the double layer, the nature of the electrode and on the nature of the double layer itself, i.e. the capacitance of the double layer which is a function of its thickness δ_d and the dielectric constant of the solvent molecules. The thickness of the double layer is also dependent on the radii of the ions present in the electrolyte (2).

If a potential difference is applied across the cell to cause anodic dissolution, then the anode will ionize at a greater rate than that of discharge of its

ions. The electrode potential is accordingly altered from its equilibrium by an amount η_a, the activation overpotential. A quantitative relationship between activation potential and current density, i.e. the rate of the electrochemical reactions occurring at the double layer is given by the Tafel equation.

At the anode

$$(\eta_a)_a = -\frac{RT}{\beta ZF} \ln J_o + \frac{RT}{\beta ZF} \ln J_a \quad \ldots\ldots (1.2)$$

and at the cathode

$$(\eta_a)_c = +\frac{RT}{(1-\beta)ZF} \ln J_o - \frac{RT}{(1-\beta)ZF} \ln J_c \quad \ldots (1.3)$$

where Z is the charge involved in the respective electrode reaction, 'β' is the symmetry factor or the transfer coefficient which is usually equal to about $\frac{1}{2}$, J_o the exchange current density, R the gas constant and T the temperature. It is worth stating at this point the extreme nature of the electrode process in ECM work, the large current densities involved and steep concentration gradients in the immediate vicinity of the electrode solution interface may result in a more complex form of activation overpotential than that expressed by the Tafel's equation.

Tafel overpotentials have been studied mainly in connection with hydrogen evolution at the cathode although some information has been collected on anodic phenomena (3). The current densities at which these overpotential values have been found were very much lower than those commonly

encountered in ECM. Typical values of exchange current density J_o and Tafel slope ($2.303 \frac{RT}{ZF}$) for electrolysis of an iron electrode in $\frac{1}{2}$ molar chloride solution are 3.16×10^{-5} Amp/cm^2 and 59 mV/decade.

Apart from the overpotentials or polarisation explained before there are another two types of over-potentials commonly associated with electrode process. As the dissolution proceeds in ECM, the movement of ions is controlled by three processes.

1. Migration, i.e. the movement of ions under the influence of the electric field.
2. Convection, i.e. the movement of ions achieved by bodily movement of the electrolyte; in ECM this is achieved by forced agitation of the electrolyte.
3. Diffusion; i.e. the movement of ions due to ion concentration gradient in solution.

In anodic dissolution, when the metal dissolution rate is faster than the rate at which metal ions can diffuse away from an electrode, a condition is reached where an ionic concentration gradient exists over a thin layer of the electrolyte adjacent to the electrode. This layer is known as the diffusion layer. A change in the electrode potential from the reversible value occurs due to this ionic concentration gradient. The numerical value of the difference between this value of potential and that of the reversible potential is known as the concentration over-potential. The other overpotential is 'Resistance overpotential', this is generally regarded as the potential

drop across a layer of electrolyte or film layer such as an oxide film on the electrode surface. The magnitude of this potential depends on the amount of current flowing in the cell and on the nature and the conductivity of the electrolyte.

Thus the external potential V required to pass a current I through an electrochemical cell can be expressed as

$$V = (E_c - E_a) + \eta_a + \eta_{conc} + \eta_r + IR \quad \ldots \quad (1.4)$$

where E_c and E_a are reversible potentials at the cathode and the anode respectively, η_a, η_{conc}, η_r and IR are contributions from activation, concentration, resistance overpotentials and potential drop in the bulk electrolyte respectively.

1.3.4 Polarisation Curves

Main features of the anodic dissolution can be clearly explained with reference to a polarisation curve. This is the curve of anode potential against current density obtained during anodic dissolution. A polarisation curve which shows the main features is shown in Fig. (1.2). For anodic potential in the range AB the anode is said to be in active state, dissolution of the anode is by removal of ions from its crystal planes, i.e. the dissolution depends on the geometry of the crystal lattice and the surface becomes etched. Tafel's equation is applicable under these conditions.

As the anode potential is increased beyond B Fig.(1.2)

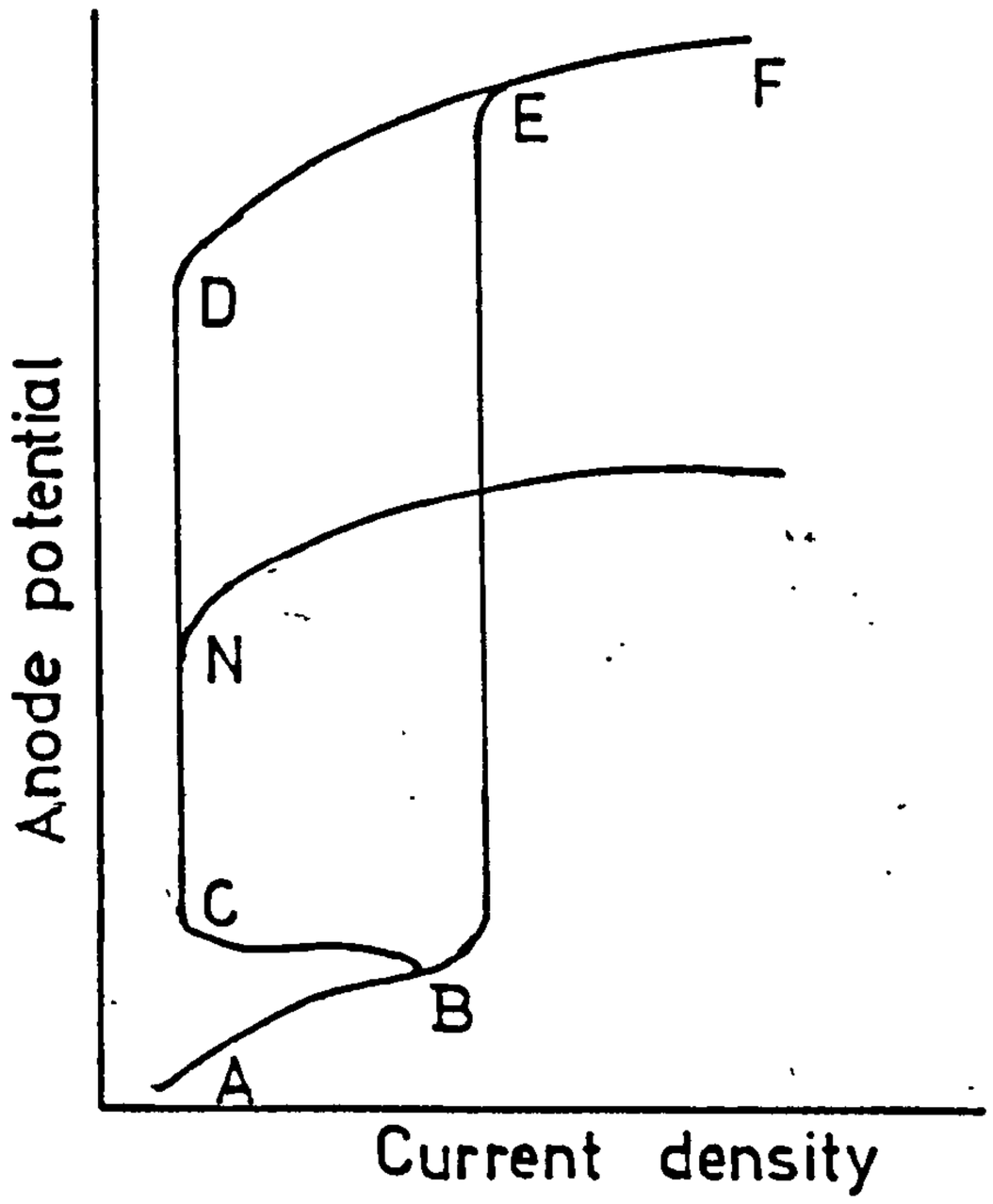

FIG. (1.2)

(1.2), an oxide film may form on the anode surface. This may hinder the reaction rate for example as shown to the level CD. The anode is then said to be passive. The oxide film may be so conductive that the passage of a greater amount of current becomes possible as shown by BE. In this case dissolution occurs in a random manner over the anode surface, is controlled by the oxide film and not by the geometry of crystal lattice. Since the dissolution occurs in a random fashion, the anode surface becomes polished.

For films with good electrical conductivity and for appropriate conditions of potential oxidation in preference to or in addition to polishing or passivity, oxidation of solution anions may take place. An example of

this is the oxidation of hydroxyl ion to form oxygen

$$4\ OH^- \longrightarrow 2H_2O + O_2 + 4e$$

This condition is shown by DF in the Fig. (1.2).

A condition which is difficult to distinguish from gas evolution is transpassivity, here the cations of the oxide film are oxidised to a soluble higher valency form. Chromium is one of the metals which exhibits this property yielding chromates.

If the passive film formed on the anode surface is exposed to a strong electrolyte of appropriate concentration, such as sodium chloride, the anions of the electrolyte will penetrate into the film causing disruption of the film. This disrupted area of the film will permit greater local current flow than the other areas of the film. Such current flow can lead to the formation of pitting on the anode surface. Pitting is most likely to occur at weak points on the electrode surface, such as at grain boundaries. This effect is shown in the polarisation curve by D and N.

1.3.5 Reactions Occurring at the Electrodes

The general ionic reactions which occur in an electrochemical cell when using acidic, neutral electrolytes are as follows; alkaline electrolytes are not used in ECM.

(i) When using acidic electrolyte (e.g. HCl), at the anode the dissolution of the metal can be expressed by

$$M = M^{Z+} + Ze$$

where M^{Z+}, the metal ion of valency Z, e is the electron charge, and at the cathode evolution of hydrogen can be expressed by

$$2H^{+} + 2e = H_2$$

Reduction of the metal ion at the cathode is a possibility (plating of the cathode) but this is very much undesirable in ECM work as this tends to alter the initial shape of the tool electrode.

(ii) When using neutral electrolytes (e.g. NaCl) there is no plating at the cathode. The metal ion liberated at the anode and the hydroxyl ion from water molecules which are found in abundance forms a metal hydroxide which is precipitated. The anode reactions are

$$M = M^{Z+} + Ze$$

for the metal dissolution and

$$M + Z\ (OH)^{-} = M(OH)_2 + Ze$$

for the formation of metal hydroxide. At the cathode is hydrogen evolution.

$$2H_2O + 2\ e = H_2 + 2OH$$

There is some evidence (4) that a large proportion of the current is not used for hydrogen evolution when nitrate electrolytes are employed. Instead the nitrate is reduced.

1.4 Machining Rates

Faraday's laws of electrolysis can be satisfactorily applied to find the machining rates if there are no side reactions. When all the current is used for machining, the mass of the metal removed from the anode assuming it to be of an element is given by

$$m = \frac{A\ I\ t}{Z\ F} \qquad \ldots\ldots (1.5)$$

where A is the atomic weight of the element, Z the valency of the ion produced, I the current, t the time and F the Faraday constant.

From equation (1.5) it can be deduced that 'f_a' the rate at which the anode surface recedes is given by

$$f_a = \frac{A\ J}{Z\ F\ \rho} \qquad \ldots\ldots (1.6)$$

where J is the current density over the anode surface and ρ the density of the anode material.

1.4.1 Steady State Machining

Under steady machining conditions that is when the gap between the tool and the work piece remains constant, the component of the feed velocity in the direction of normal erosion should be of the same magnitude as the erosion rate. If the electrodes are perpendicular to the feed direction the feed rate of f is given by

$$f = \frac{A\ J}{Z\ F\ \rho} \qquad \ldots\ldots (1.7)$$

The factor $\frac{A}{ZF\rho}$ is a constant for a given electrode combination and is usually known as the specific metal removal rate.

1.4.2 Machining of Alloys

Most industrial materials machined by E.C.M. process are alloys, ions formed by each element in the alloy during electrolytic dissolution may not necessarily have the same valency and equation (1.6) has to be modified accordingly to take into consideration different valencies of ions formed.

Larsson (5) obtained a general theoretical machining rate for an alloy by summing up the charges required to remove each element from a given volume of the alloy. The specific metal removal rate V_{sp} of the alloy (volume of the anode removed per unit charge) was given by the equation:

$$V_{sp} = \frac{100}{\rho F} \times \frac{1}{\frac{x_1 Z_1}{A_1} + \frac{x_2 Z_2}{A_2} + \frac{x_3 Z_3}{A_3} + ...} \quad cm^3\ A^{-1}\ S^{-1} \qquad ..... (1.8)$$

where 1, 2, 3, etc. are the elements of the alloy of atomic weights A_1, A_2, A_3, etc., which enter solution with valencies Z_1, Z_2, Z_3 etc.

1.4.3 Discrepancy in Predicted Machining Rates

Application of Faraday's laws in determining metal removal rates has its limitations. Many cases have been reported e.g. Mao (4) where the dissolution is less than 100% efficient as predicted by Faraday's laws. Evolution of oxygen is usually assumed to be a secondary reaction which used some of the current but other causes have been put forward for some examples at current densities lower than used for E.C.M. Faraday's laws can only predict accurately the rate at which a metal is removed from the anode if the following conditions are satisfied.

1. Valencies of ions produced must be known.
2. There must be only one electrode reaction
3. The metal must be removed by dissolution only, and not by disintegration.

Incorrect, assumed valencies may give higher or lower machining rates depending on whether the assumed valency is below or above the correct valency of the ion. Davidson (6) has reviewed the low valence state in anodic dissolution, for example there is evidence that both aluminium and copper dissolves in univalent state, but in aqueous solution the valencies are found to be three and two respectively. It has been deduced (5) that the metal initially dissolves in the univalent form and some of these ions return to the anode, then being oxidised to a higher state, drawing more current. Those ions which do not return to the anode are chemically oxidised by reacting with water. A further common example of the

incorrect choice of valency value is that of chromium. When using passivating electrolytes such as $NaNO_3$ or $NaClO_3$ part of the current is used in secondary chemical reactions such as the evolution of oxygen, thereby reducing the efficiency of the process. König (7) states that by employing passivating electrolytes the over cut i.e. the gap between the electrodes can be reduced. The reason for this is the property of the passivating layers on the anode surface, especially at the low current density areas where not all of the current is used in metal dissolution. There is evidence for disintegration of anode during anodic dissolution. Straumanis (8) has observed disintegration of gold during anodic dissolution. He states further that the amount of metal disintegrated increased with decrease in current density and increase in purity. Metals such as silver, beryllium and magnesium have been observed to disintegrate partially at low current densities. Current efficiencies of over 100% obtained for E.C.M. with electrolytes such as NaCl may be due to contributions from partial anodic disintegration and so a low value for valency may be erroneously assumed.

1.5 MACHINING ACCURACY AND REPEATABILITY

Accuracy in E.C.M. depends on accurate prediction of the work shape relative to the geometry of the tool, that is prediction of the gap between tool and the work piece for all points on the work surface. P.E.R.A. (9)

Konig (7,10), Tipton (11), Collet (12), Krylov (13), have formulated expressions for the prediction of the side gap Fig. (1.4). Due to the complexity of the processes accurate prediction of the side gap is very laborious and involves complicated mathematics. In normal practise side gap is defined as a function of the frontal equilibrium gap which is relatively easy to predict and itself is a function of process parameters.

1.6 Frontal Equilibrium Gap

Frontal equilibrium gap is usually defined as the smallest gap between the two electrodes which occurs after infinite time of machining. The sections of the tool and the work piece being parallel to each other and the constant feed direction of the moving electrode (usually the cathode) and the current flux being normal to the surfaces. In practical electrochemical machining equilibrium gap is reached after a short period of machining, which will be noted when the machining current reaches a steady value, other process parameters being kept constant.

1.6.1 Expression for Frontal Equilibrium Gap

Consider a section of two plane parallel electrodes in an electrolytic tank connected to D.C. (rectified A.C.) supply. Neglecting overpotential effects and assuming the process is 100% efficient the rate of metal removal from the anode surface is given by

$$(V_{sp}) \times J$$

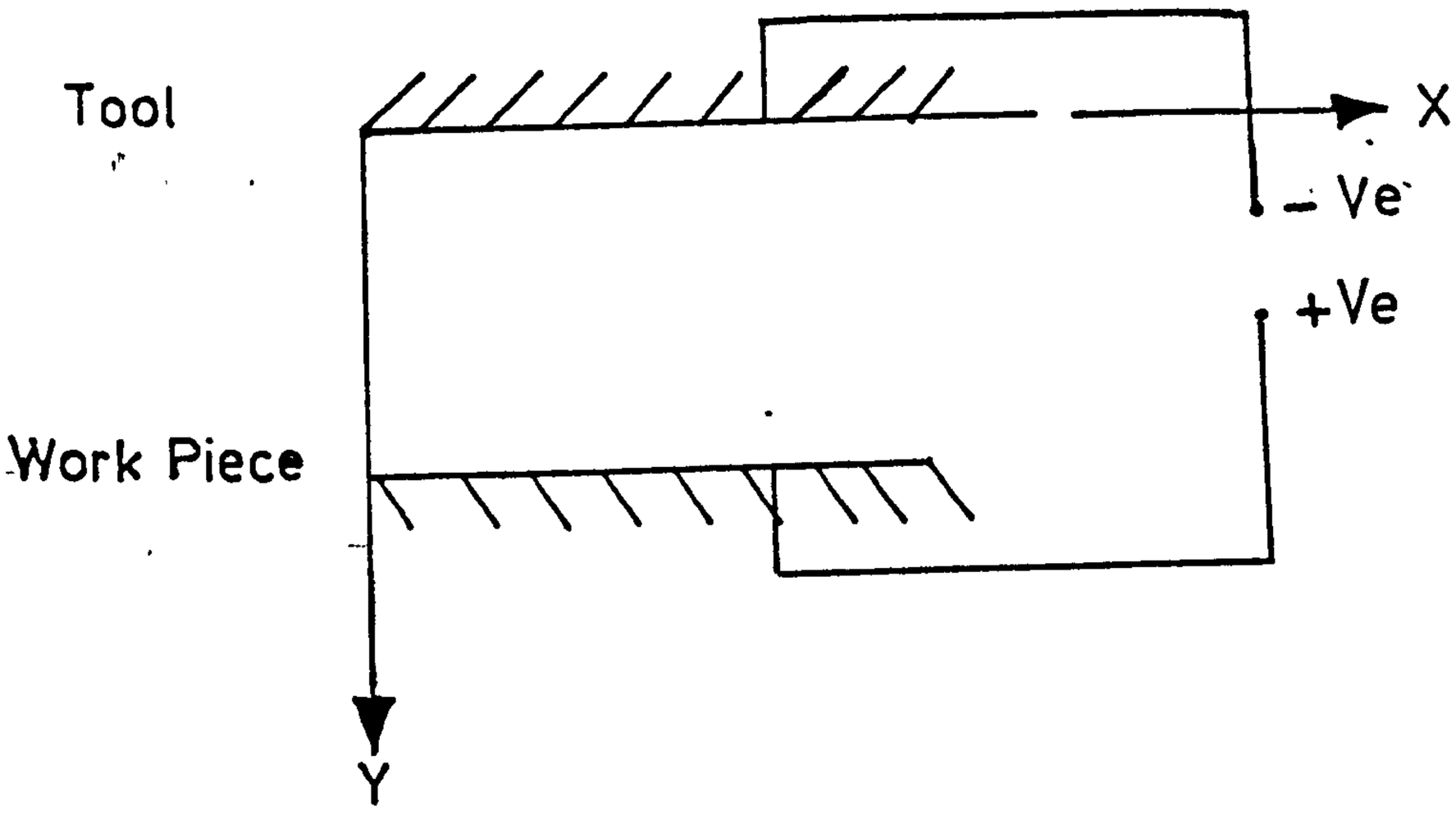

FIG. (1.3)

where (V_{sp}) is the specific metal removal rate from the anode surface; in other words it is the volume of metal removed per Coloumb. J is the current density in the region considered. The value of J is dependent on 'X' conductivity of the electrolyte and the gap 'h' between the two electrode surfaces and is given by

$$J = \frac{V_\ell \cdot \kappa}{h} \qquad \ldots\ldots (1.9)$$

where V is ohmic drop across the resistance of the solution .

From (1) and (2) the rate of change of gap 'h' between the electrodes when both electrodes are stationary is given by

$$\frac{dh}{dt} = \frac{(V_{sp}) \times V_\ell \times \kappa}{h} \qquad \ldots\ldots (1.10)$$

If one of the electrodes is fed towards the other at a constant feed rate 'f' then rate of change of the gap h

from (1.10) is

$$\frac{dh}{dt} = \frac{(V_{sp}) \times V \times \chi}{h} - f$$

Under steady machining, that is when the gap between the electrodes remains constant (time independent) $\frac{dh}{dt} = 0$. The magnitude of constant gap is given by

$$h_e = \frac{(V_{sp}) \times V \times \chi}{f} \quad \ldots\ldots (1.11)$$

h_e is commonly known as the equilibrium gap. Accurate prediction of equilibrium is very important and it is discussed in section (1.11).

1.7 PREDICTION OF OVERCUT

The prediction of overcut is important when the process is used commercially. The earliest published literature in English regarding the prediction of overcut was a research report by P.E.R.A. (9). The elements of their analysis can be considered with reference to Fig. (1.4).

Overcut at any point 'P' on the work surface which was formed by a drilling tool having a straight leading edge, and a non insulated land width W was defined as

$$h = h_c + \int_0^u \frac{dh}{du} \cdot du \quad \ldots\ldots (1.12)$$

'h_c' is the overcut opposite the leading edge and $\frac{dh}{du}$ the change of gap with respect to position along the uninsulated tool region. $\frac{dh}{du}$ was evaluated in two steps

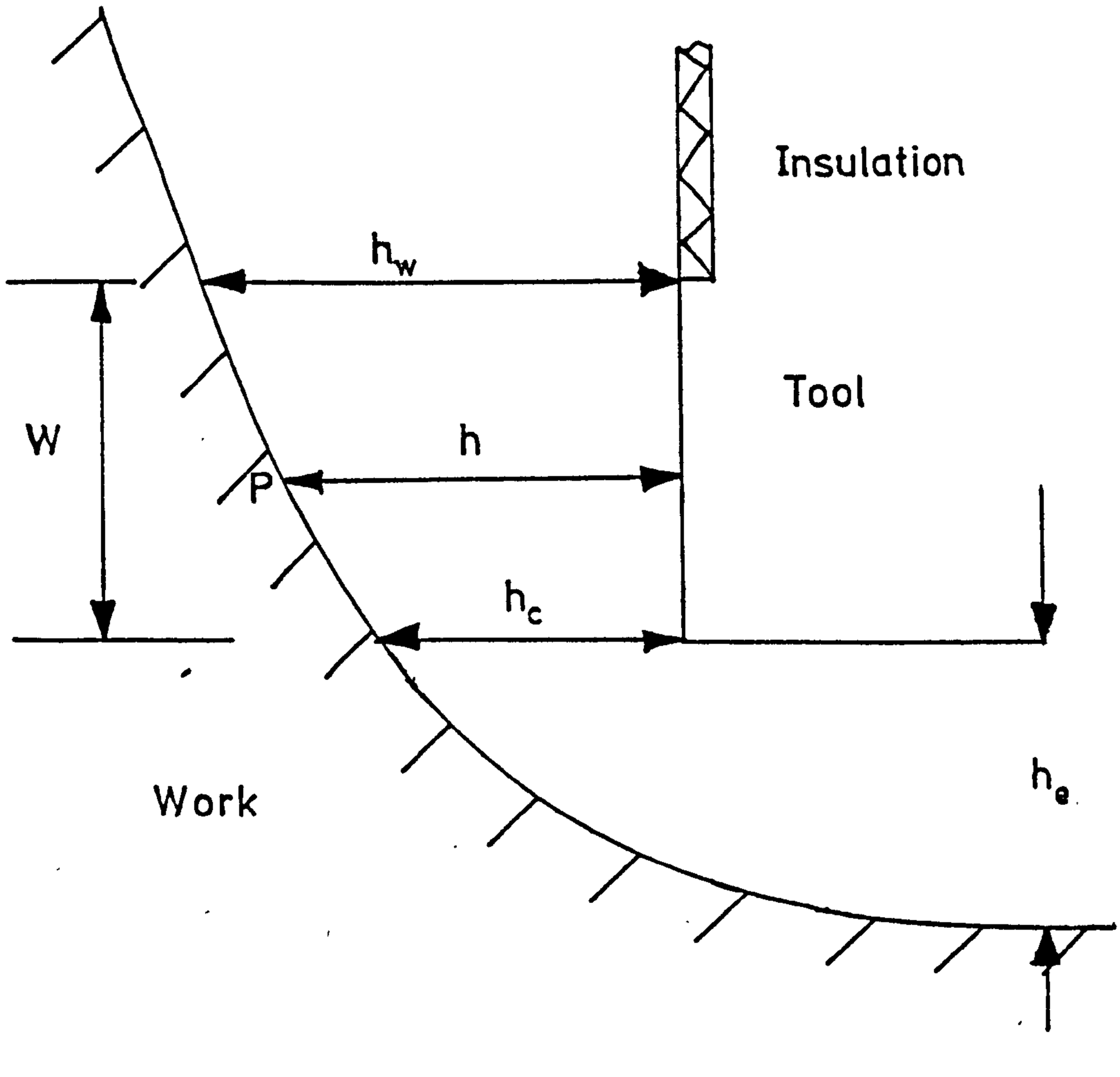

FIG. (1.4)

by expressing $\frac{dh}{du}$ as the division of $\frac{dh}{dt}$ and $\frac{du}{dt}$. Since the tool moves at a steady rate $\frac{du}{dt} = f$ the tool feed rate. $\frac{dh}{dt}$ is the rate of change of gap. P.E.R.A. (9) defined $\frac{dh}{dt}$ as

$$\frac{dh}{dt} = \frac{\text{Machining parameter}}{\text{gap}}$$

here the machining parameter is $V_{sp} \times V_L \times \chi_o$ and the gap is the radial gap, from equation (1.10) it implies that P.E.R.A.(9) has assumed normal or orthogonal distribution of current and has considered only erosion in the radial direction, for a large radius where the field is approximately orthogonal.

The gap h_c was found numerically in terms of the frontal equilibrium gap using a relaxation method. The relaxation analysis was based on solving Laplace's equation for potential distribution between boundaries ABC and SPTU Fig. (1.4) bounded by steady state erosion condition $\frac{\partial V}{\partial N}$ Cos θ = Constant.

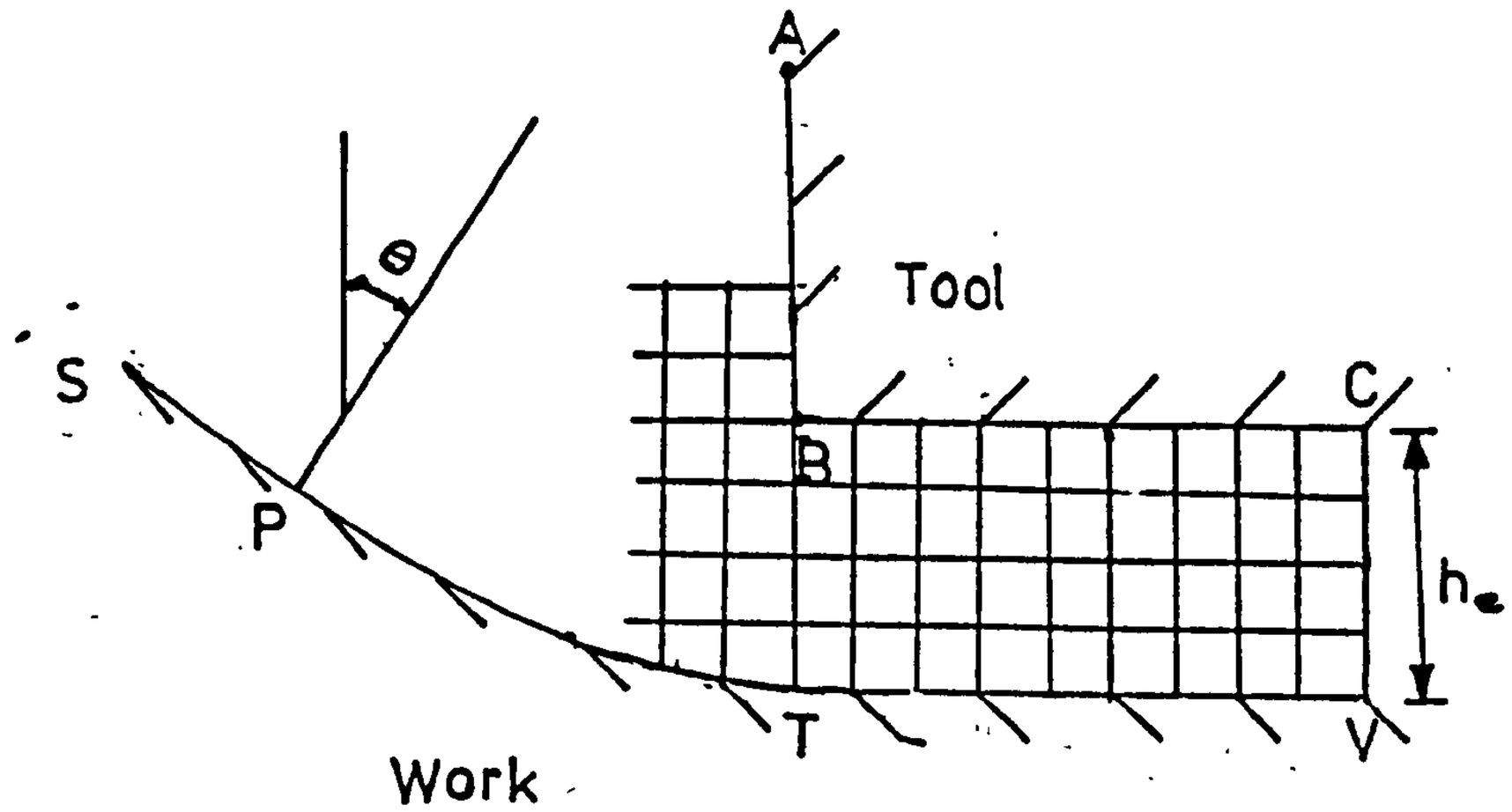

FIG. (1.5)

Solution of Laplace's equation requires a closed region of known boundary conditions. In this report (9), boundaries chosen were not clearly explained.

The overcut opposite A was found by integrating equation (5) within limit O and 'W' where W is the land width, h_w the overcut opposite A is given by

$$h_w = \left[2he.w + (1.7\ he)^2\right]^{\frac{1}{2}} \quad \ldots\ (1.13)$$

This analysis has neglected the machining due to current flux which protrude on to the work surface beyond the uninsulated region of the boundary. The factor 1.7 was given by their numerical analysis for the ratio of h_c/h_e.

Konig (10) considered the stray current machining, defined the side gap at three different regions along the tool boundary. The gap 'h_o' which is generated by radius 'r' at the corner of the tool, the gap (h_s - h_o) generated by the cylindrical non insulated part of the tool and the gap (h_w - h_s) which was caused by stray current machining.

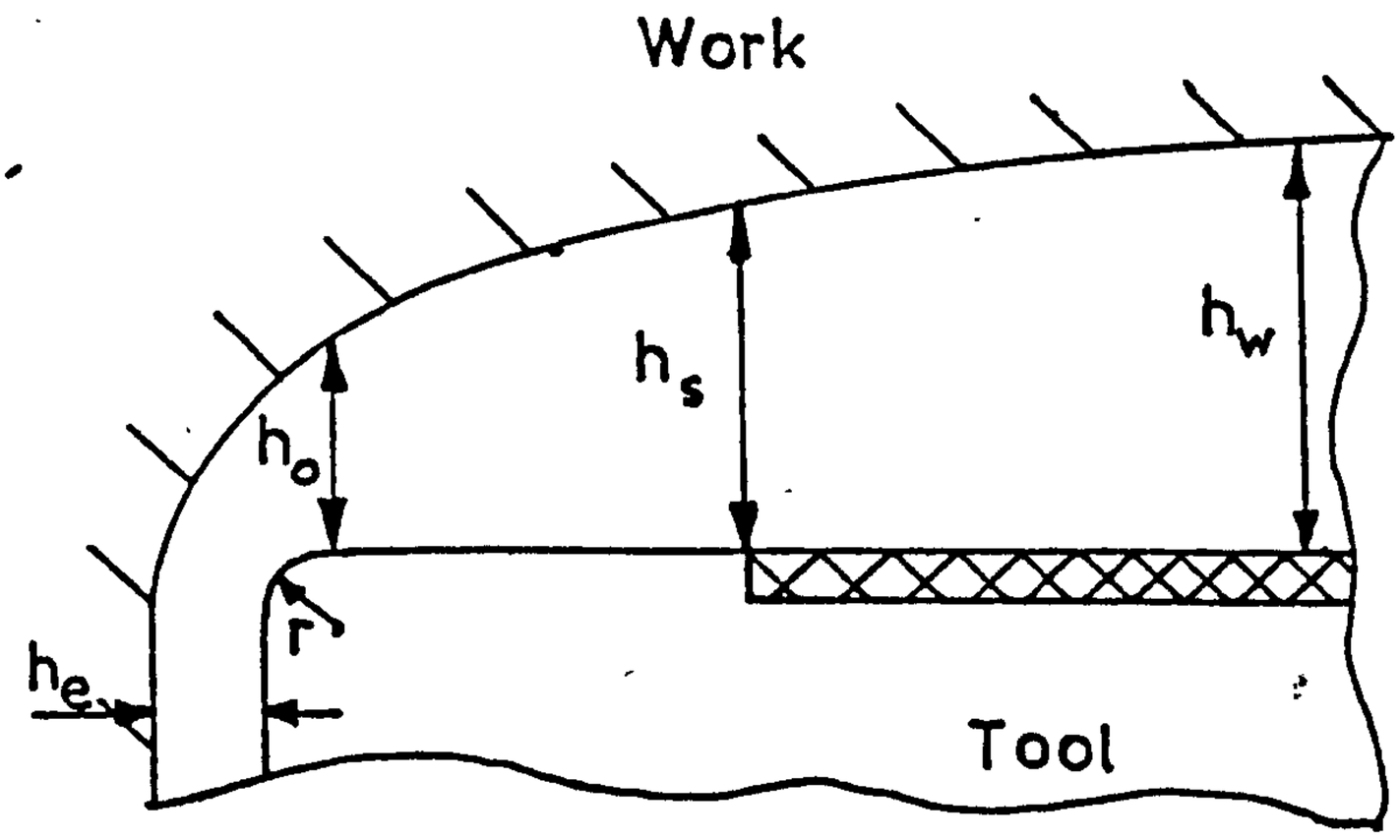

FIG. (1.6)

An empirical formula was derived to calculate the gap h_o. For a drilling tool having no land width and the corner radius within the limits 1 mm $\leq$ r $\leq$ 5 mm, h_o is given by

$$h_o = (0.1 + h_e)(0.314r + 1.17) \quad \ldots\ldots (1.14)$$

and

$$h_o = 2h_e + 0.1 \quad 6.238(r-1) \quad \ldots\ldots (1.15)$$

for tools having land width $\geq$ 1 mm and the corner radius within the limits 1 mm $\leq$ r $\leq$ 5 mm. Knowing gap h_o, gap

$h_s - h_o$ was calculated from the parabolic equation obtained from the condition

$$\frac{dh}{dt} = \frac{\text{machining parameter}}{h}$$

which was the same assumption made by P.E.R.A. (9). The additional increase in the overcut due to stray currents machining which was $(h_w - h_s)$, was found empirically. The quoted value was 0.65 of the frontal equilibrium gap. The equation for total overcut will not be influenced by the incorrect assumption for the gap $h_w - h_o$, due to the fact the $(h_w - h_s)$ was determined empirically. However the work carried out by Tipton (11) in prediction of the machined anode profile and prediction of overcut is more general. Tipton (11) developed a conducting paper analogue technique to predict the work shape relative to the tool geometry. Since tool dimension and feed rate were taken as fraction of the equilibrium gap and as some fraction of the equilibrium gap per unit time, for a given geometry of a tool, only one prediction will be necessary. The other work shapes for different process parameters, and similar geometries could be found by scaling up or down depending on the magnitude of the frontal equilibrium gap. Tipton (11) further developed the method to solve the problem numerically using a digital computer. However this computer method is only suitable for prediction of work shapes produced by simple tool geometries with no insulation boundaries and where the feed direction is nearly normal to the work surface. Thus it ignores the stray

current machining. He also extended the simple theory of prediction of the frontal equilibrium gap to predict the equilibrium gap formed when the tool surface is inclined to the feed direction.

Assuming all the current is distributed in the radial direction, he derived a formula to predict the gap formed by an uninsulated cylindrical tool. Leong (14) employed a similar approach in the derivation of formula for the overcut. Modified formulae were obtained by P.E.R.A. (9) and Konig (10) using form factors to fit the experimental results.

Collet et al (12) have used a complex variable approach for predicting overcut. The maximum overcut and the overcut opposite the leading edge for a plane faced tool with insulation on the outside and for a plane faced tool with no insulation was given. An initial guess of the form of the solution was assumed, in order to predict the work shape when the boundary conditions were satisfied but the uniqueness of the solution, which is of the utmost importance, was not discussed. There may be several forms of the guessed solution which satisfy the boundary conditions yielding a solution for the Laplace equation for a free boundary problem. From their analysis Collet et al (12) predicted that the final over-cut obtained from the plane faced cylindrical drilling tool with insulation on the outside cylindrical surface to be of the same magnitude as the frontal equilibrium gap. The gap opposite the leading edge was found to be 0.731 of

the equilibrium gap. For tools with no insulation the gap increased with the length of the tool and the predicted value of the gap at the leading edge was found to be 1.159 of the frontal equilibrium gap.

1.8 PREDICTION OF TOOL SHAPES

Procedures for the prediction of tool shape to produce the required work surfaces are not very well established at present time due to difficulties in locating insulated tool boundaries. A way of finding a tool shape is to use several guessed tool shapes and to solve the Laplace equation which satisfies the boundary conditions. This method will be very time consuming and is difficult to make into a computer program to produce the desired tool shape automatically. Krylov (13) attempted to solve the problem of finding tool shapes to produce a given work shape but he assumed the potential of the tool boundary to be a constant. That is the tool has no insulated boundaries. The mathematical approach employed yields a continuous analytic function for tool shapes which are of no practical importance. As stated in this report this approach does not lead to a well posed mathematical problem and results are quoted for three theoretical work shapes -given by equations

(a) $y = x^4$

(b) $y = e^{-x^2}$

and (c) $y = \sin x$

Tipton (11) has outlined an approach to solve the

problem of finding tool shape to produce the required work shape. The two dimensional work boundary was defined numerically in the X, Y plane with Y as the feed direction. Fig. (1.7). He assumed that in equili-

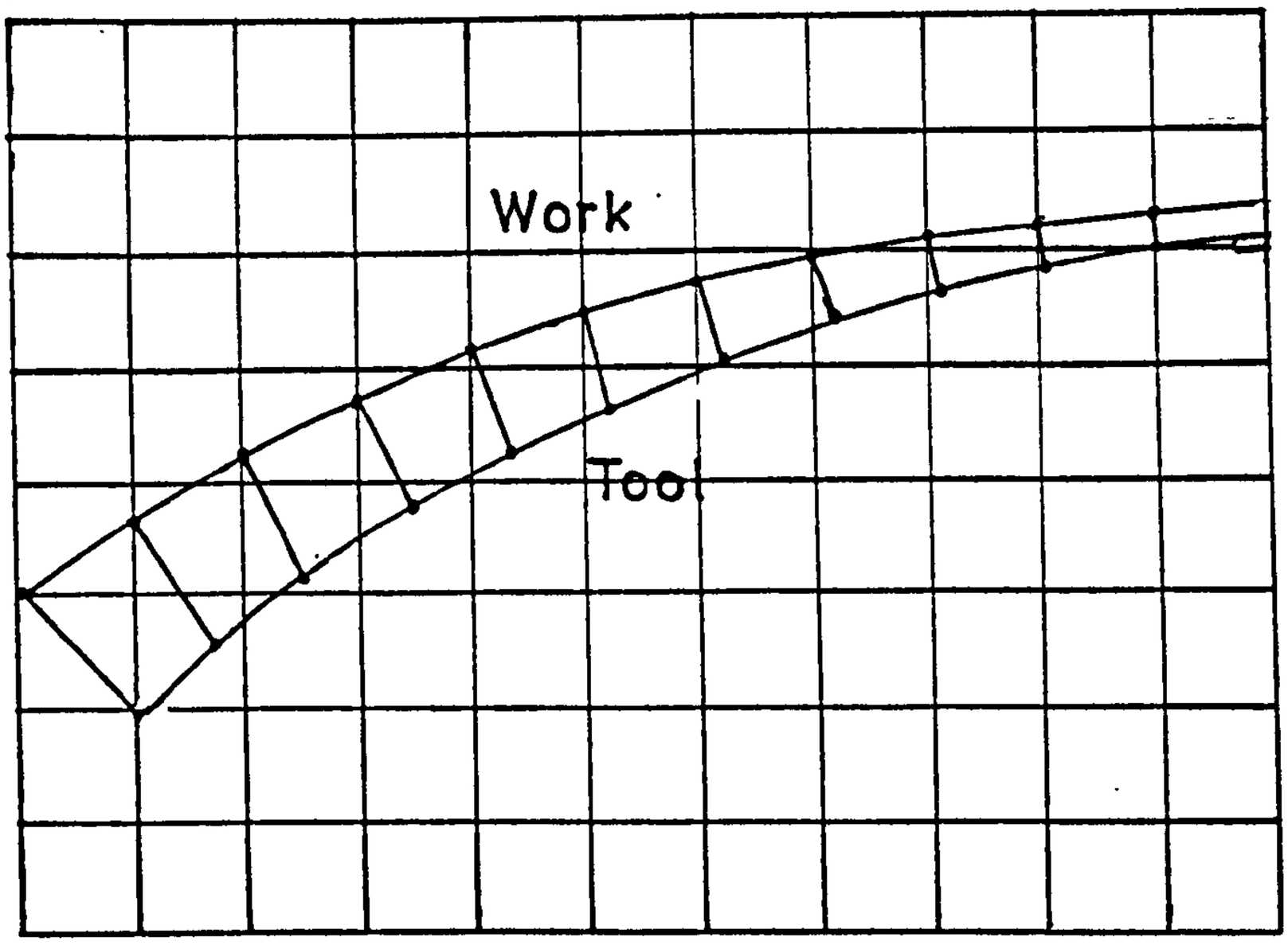

FIG. (1.7)

brium machining condition, the normal current density is a constant which is correct if efficiency does not vary with current density, hence he deduced that constant current increment should flow through each of the adjacent coordinates on the work boundary. This assumption is not true, as explained in Chapter II, section (2.6.3) that normal current density varies from point to point on the work surface as 'sin γ' where 'γ' is the angle between the -ve feed vector and tangent to the work surface at the point considered. But Tipton's (11) deduction is a valid one. Method of Curvilinear Rectangles (see Wright (15)) has been used to find the required tool boundary. Since

this method only predicts tool shapes with constant potential tool boundaries, as stated in this report this procedure is not suitable to predict most tool shapes for even relatively simpler work surfaces.

1.9 EFFECT OF PROCESS PARAMETERS

Repeatability of the E.C.M. process in forming components depends on how the process parameters are controlled. The side gap directly or indirectly depends on the process parameters. From equation (1.11) it should be clear that the frontal equilibrium gap could be controlled directly by dependent process parameters such as cell voltage, electrolyte conductivity and feed rate of the tool or work piece. The dependence of other process parameters such as electrolyte flow rate, temperature, forward pressure, back pressure on the frontal equilibrium gap has been studied by many authors for example Thorpe and Zerkle (16), Hopenfeld and Cole (17), Konig (7), Leong (14).

The prediction of equilibrium gap in electro-chemical machining in relation to non-uniform electrolytic conductivity was first investigated by Tipton (11,18). Complexity of the problem was reduced by considering the conductivity of the electrolyte as temperature dependent. Hopenfeld and Cole (17) developed an equation which describes the functional relationship between process parameters based on a mathematical model incorporating a bubble layer. A further equation which predicts the local current distribution along the anode length was formulated.

In the experimental model the electrode gap was kept constant and the variation of current density along the anode length was sought. This was said to be analogous to the actual physical case at equilibrium but in fact at equilibrium the current density along anode length is constant providing dissolution efficiency remains constant.

Thorpe and Zerkle (16) used a similar approach to that of Hopenfeld and Cole (17). A one dimensional, two phase, fluid flow theory was formulated for the electrolyte behaviour in the frontal electrode gap occurring in the diesinking process using axially symmetric shallow cavities, both void fraction and temperature effects were included in determination of the frontal equilibrium gap of the cavity produced. Numerical results were given for both flat and spherical bottomed cavities under steady machining conditions. Both radial forward flow and radial reverse flow has been considered.

1.9.1 Electrolyte Pressure Requirements

The electrolyte, apart from acting as the electrolytic conductor between the anode and the cathode in the ECM cell, is also used to flush away the eroded metal, to take away the liberated gases and the heat generated during the process. This requires sufficient flow of electrolyte through the electrode gap. Since the electrode gap is small high pressures are required to pump the electrolyte through the gap.

The pressure of the electrolyte at the entrance to

the ECM cell is commonly known as the forward pressure, usually this is controlled by a valve in line with the cell and by a by-pass valve through which excess electrolyte is taken back to the electrolyte tank. The required pressure depends on the pressure distribution in the electrode gap which depends on the geometry of the electrodes. Chikamori (19) has shown that for circular electrodes the pressure distribution obeys the pressure distribution derived mathematically from Bernoulli's equation.

Cavitation in low pressure areas appears to be responsible for some defects e.g. flow marks on the work piece surface. The possibility of cavitation can be reduced by applying back pressure. Back pressure is the pressure of the electrolyte as it leaves the ECM Cell, but as this also reduces the volumetric flow a compromise has to be reached. Back pressure is applied by restricting the electrolyte outlet from the machining zone or in a totally enclosed cell by having a throttling valve in the outlet pipeline. Another advantage of having back pressure is it shifts the boiling temperature of the electrolyte to higher value. Leong (14) found that increase in back pressure gave smaller overcut, when other operating parameters flow rate, voltage, inlet temperature and feed rate kept constant, but one would expect the contrary. Increase in back pressure also reduces the magnitude of the bubble layer which effectively increases conductivity. Referring to equation (1.11) increase in

conductivity gives a larger value for the equilibrium gap hence a larger value for the overcut.

Chickamori et al (19) studied the flow of electrolyte in electrochemical die-sinking process. For circular electrodes Bernoulli's equation was used to express the pressure distribution in the electrode gap. The obtained equation for pressure loss P_r (Kg/cm^2) due to viscous forces is

$$P_r = \frac{6\mu Q}{\pi h^3} \log_{10} \frac{r_1}{r} \times 3.83$$

where μ the coefficient of viscosity ($Kg.s/m^2$)

Q flow rate (ℓ/min)

r the distance from centre (mm)

$2r_1$ the outside diameter of the electrode (mm)

Study of the experimental curves and theoretical curves obtained revealed that above certain flow rates negative pressure zones occur between the electrodes, which means that voids could be formed readily by cavitation. The critical gap range when the pressure loss increases rapidly, was found to be 0.1 and 0.3 mm. To prevent occurrence of cavitation which deteriorates the accuracy of electrochemically machined surface Chickamori (19) suggests the use of small flow rate and large gap distance or very small gap distance below 0.1 mm. The occurrence of cavitation was observed to be near the aperture where the flow velocity becomes large. For rectangular electrodes this may be prevented up to some extent by the

use of slit aperture for the electrolyte flow. A characteristic of this aperture is that the minimum flow section, (circumferential length of the aperture x electrode gap distance), can be increased more than that of the circular ones.

1.9.2 Limitation of Feed Rate due to Electrolyte Boiling

With reference to equation (4) it could be deduced that by making the feed rate large, small equilibrium gaps could be attained, which implies that the work surface produced would closely resemble the inverse tool shape. In actual practice the feed rate is limited by a number of factors which are indirectly dependent on the process parameters of equation (1.11). High feed rates which imply small gaps means low flow rates, and high current densities. This increases the rate at which the electrolyte is heated. If the flow rate is not sufficient the heat generated by the current will cause the electrolyte to reach its boiling point and process failure will occur. Feed rate limitations due to electrolyte boiling and hydrogen evolution are described by P.E.R.A. (9).

Assuming that the total electrical energy supplied to the tool work electrodes system appears as heat and neglecting heat losses to the surroundings via tool holder etc., P.E.R.A. derived a general expression for feed rate in terms of the temperature rise to the boiling point of the

electrolyte. This equation predicts the maximum allowable feed rate at which the electrolyte boils. The authors of this paper found that the predicted feed rates could not be attained in practice. The maximum attainable feed rates being approximately half that predicted by the formula.

1.9.3 Limitation of Feed Rate due to Gas Evolution

Hydrogen gas liberated at the cathode during the machining process, forms a layer of bubbles surrounding the cathode thereby reducing the conductivity of the electrolyte and thus the metal removal rate. Therefore the amount of hydrogen in the electrolyte limits the feed rate. The reduction in conductivity will also give gap sizes smaller than those predicted by formulae assuming constant conductivity neglecting the effect of hydrogen.

P.E.R.A. (9) assumed that the maximum feed possible depends on the volumetric concentration of the evolved gases in the electrolyte. They considered ECM in a narrow channel gap of constant width between the two electrodes and further assumed that the evolution and dissolution of the gas do not change the volume of the incompressible electrolyte between inlet and outlet ports of the cell. They also neglected any solubility effects and assumed that the pressure gradient is unaffected by the presence of hydrogen. The values of feed rate predicted by this method for a 40% volumetric concentration of hydrogen in the electrolyte were found to be very close to the maximum values obtained experimentally.

1.9.4 Other Factors Affecting Attainable Feed Rate

The amount of gas mixed in the electrolyte was found by PERA to be the predominating factor in determination of the maximum feed rate. As liberated gas forms voids in the gap, the voltage gradient in the gap exceeds the electric strength an arc will occur, Loutrel et al (20) suggests that after the arc is initiated the heat produced will vapourize the surrounding electrolyte causing the void to grow larger, if the voltage gradient is high as in extreme machining case the arc will grow. This local heating causes the electrolyte to boil, which causes process failure. Bhattacharyya et al (21) considered the problem of optimization of metal removal rate subjected to the constraints of electrolyte boiling, hydrodynamic instability, consequential choking and passivation of work surface. Numerical relationship between electrolyte flow velocity at the entrance to the cell and the maximum tool feed for machining iron in NaCl solution is given.

Thorpe and Zerkle (16) also give choking as a limiting factor although in practice Clark (22) could not find a choking situation experimentally.

CHAPTER II

VARIABLE NONORTHOGONAL DIFFERENCE SCHEME TO PREDICT THE FREE BOUNDARY OF A LAPLACIAN REGION

2.1 INTRODUCTION

In practical electrochemical machining the most important condition is machining with constant feed rate at a given constant applied d.c. potential difference. This results in establishing an equilibrium gap between the tool electrode (cathode) and the work electrode (anode); it is immaterial whether the tool is fed towards a fixed work surface at a constant feed rate or vice versa.

The rate of dissolution of the anode depends on the current density at the anode surface; hence on the potential distribution in the gap between the two electrodes. Tipton (11)has solved the problem of potential distribution to find the work shape in electrochemical machining using a conducting paper analogue method and a numerical method based on finite differences employing a square mesh to enclose the region. The developed computer program which was used to predict the work profile did not consider the insulated part of the tool boundary, and as stated is only suitable for simple tool geometries whose profile sections are linear including steps in the direction of the tool feed. A method of successive approximation was used to solve the field problem, where the potential value at each grid point inside the region was repeatedly adjusted until the values at all points satisfied the difference equation which corresponds to the Laplace equation within a given tolerance. Initial values of potentials at grid points

inside the electrode gap which were required to begin the computation for the first iteration were found by linear interpolation along vertical grid lines between the tool boundary and the work boundary. Computer predicted work shapes for three different tool geometries having linear tool sections were presented, namely for a tool with a vertical step, a 'V' shaped tool having a line of symmetry and for a tool section of the shape of a saw-tooth having lines of symmetry at each end. There seems to be no other published work on numerical methods or classical methods for the prediction of work profile in E.C.M. except for theoretical work done by Collett et al (12) which was reviewed in Chapter I.

In actual E.C.M. the tool shapes have more complex geometries than those which can be treated by the numerical method presented by Tipton.(11,18) Therefore there is a need for a method which can be used to predict most E.C.M. shapes. The numerical method which is described in this Chapter is more general and can be easily applied to predict most E.C.M. shapes. It is based on the analogue method detailed by Tipton(11) except for the erosion condition which defines the work boundary, being treated in a different manner (see section (2.7.3)).

2.2 REASONS FOR NUMERICAL APPROACH

Laplace equation is perhaps the most widely studied of all elliptic partial differential equations, and there exist a multitude of techniques, both analytical and

numerical, for its resolution subject to appropriate boundary conditions. Practically any standard text on classical analysis contains many possible functions $\phi(x,y)$ which satisfy

$$\nabla^2\phi = \frac{\partial^2\phi}{\partial x^2} + \frac{\partial^2\phi}{\partial y^2} = 0 \qquad \ldots (2.1)$$

The choice of that linear combination which is sufficient to describe the solution of a particular boundary value problem can only successfully be achieved if the region in which the equation must be solved has a peculiarly simple geometry; namely rectangular or circular. For more complex geometries, and in particular for 'FREE BOUNDARY VALUE PROBLEMS', this task becomes hopelessly involved. In any case, even if such an analytical approach were feasible for a free boundary value problem it is expected that a numerical method would have to be used at some stage to determine the free boundary. There is therefore a case for using a numerical technique right from the beginning.

2.3 REASONS FOR USING METHOD OF FINITE DIFFERENCES

There are a number of numerical techniques that can be used to obtain a solution from partial differential equations which describe a field, but the one which is well established, and which can be applied equally to linear, or nonlinear problems, to steady state or transient ones independent of boundary conditions or boundary shapes is the method of 'Finite Difference'.

It consists of values of the function describing the field at discrete points spread over the region, the other required information is derived from these points values in the same manner as if the point values were obtained by physical experiment. The method of obtaining the solution by finite difference technique consists of replacing the partial differential equation of the field by a simple algebraic equation expressed in terms of the corresponding point values of the field, and essentially the problem reduces to solution of a system of simultaneous equations.

2.4 MESH SELECTION

It was earlier mentioned that the method of obtaining a solution by finite differences requires the replacement of the partial differential equation of the field by a system of simple algebraic equation in terms of the values of the field function at discrete points distributed over the region. Before these equations are constructed it is important to decide what distribution of the discrete points in the field should be considered. Although any distribution could be used the problem becomes very much simplified if a regular distribution is used. The common practice is to take nodal points of a regular grid as discrete points, in which case all nodal points are orientated in the same manner with respect to their immediate neighbours. This ensures that the resulting finite difference equations have the same form for each point.

The most important of all meshes is the square mesh,

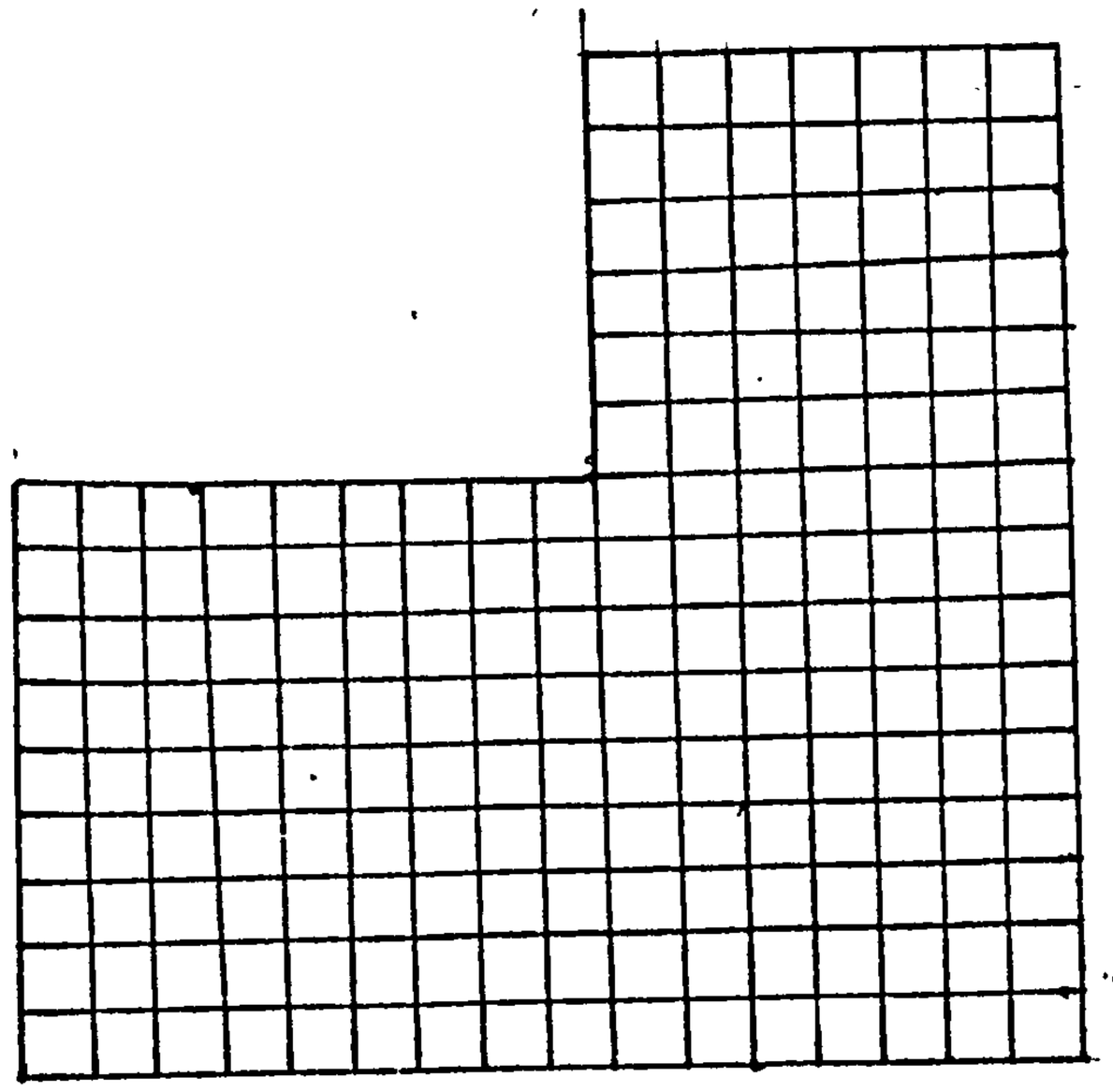

(a)

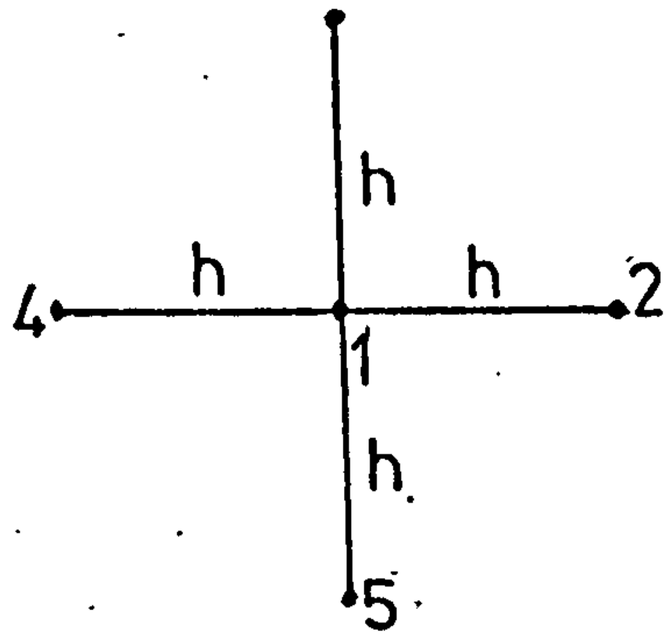

(b)

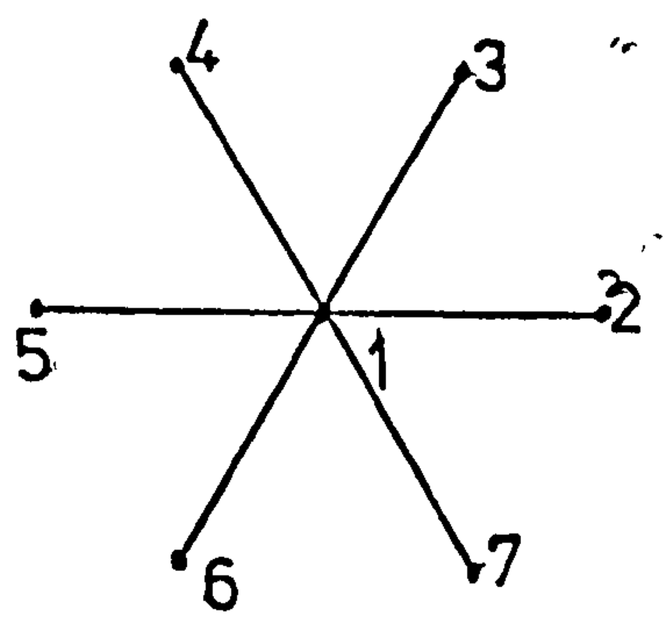

(a) Square Mesh

(b) Equilateral Triangular Mesh

FIG 2.1

and the other regular mesh in common use is the equilateral-triangular mesh Fig. 2.1 . Other types of mesh such as one of curvilinear squares may be employed depending on the boundary shape of the region.

2.5 STANDARD DIFFERENCE SCHEME, FORMATION OF DIFFERENCE EQUATION

2.5.1 The solution of Laplace's equation using finite differences

The finite difference form of Laplace equation for the potential Ø is obtained by replacing the differential equation

$$\frac{\partial^2 \phi}{\partial x^2} + \frac{\partial^2 \phi}{\partial y^2} = 0 \qquad \ldots(2.1)$$

by

$$\frac{\Delta^2 \phi}{(\Delta x)^2} + \frac{\Delta^2 \phi}{(\Delta y)^2} = 0 \qquad \ldots(2.2)$$

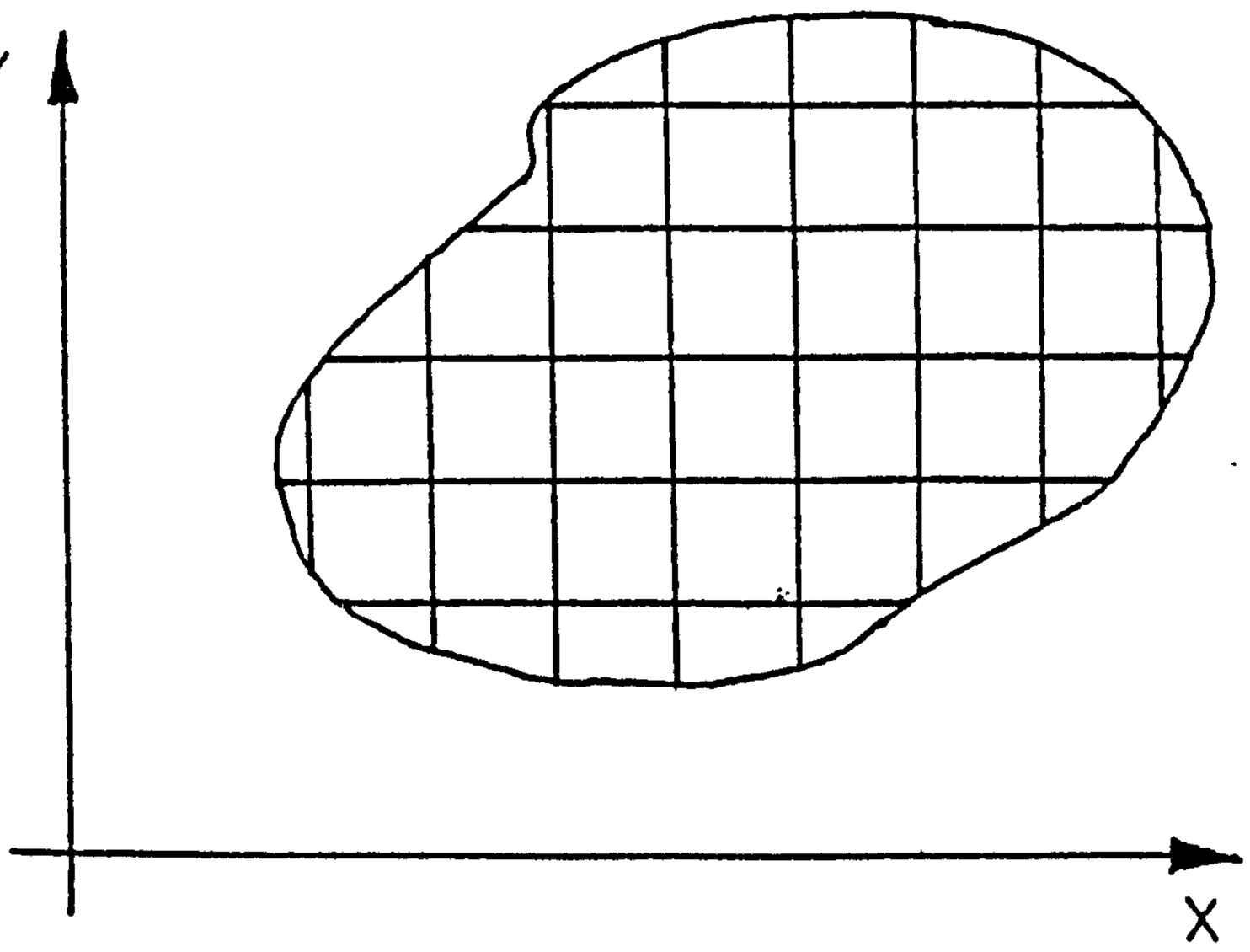

FIG. (2.2) LAPLACIAN REGION BOUNDED BY A CLOSED BOUNDARY

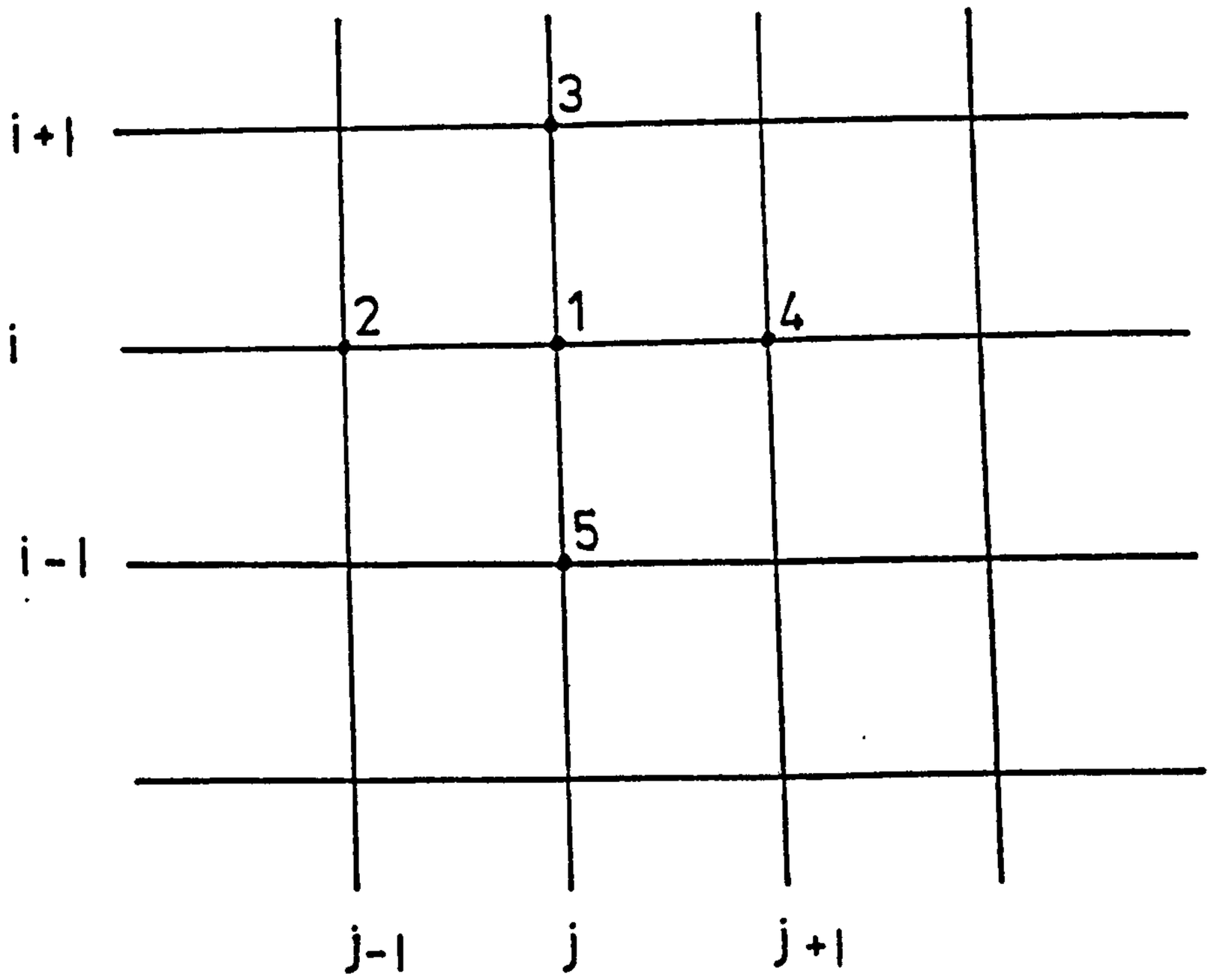

FIG. (2.3)

Consider a general point of the square mesh of spacing h(i,j). The four adjacent points 2, 3, 4 and 5 forms what is known as a regular star. Referring to Fig. (2.3) the forward and backward differences are

$$\left(\frac{\Delta\phi}{\Delta x}\right)_{4,1} = \frac{\phi_{j+1,i} - \phi_{i,j}}{h} \quad , \quad \left(\frac{\Delta\phi}{\Delta x}\right)_{2,1} = \frac{\phi_{i,j} - \phi_{i,j-1}}{h}$$

respectively.

The second central difference quotient is given by

$$\frac{\Delta^2\phi}{(\Delta x)^2} = \frac{\left(\frac{\Delta\phi}{\Delta x}\right)_{4,1} - \left(\frac{\Delta\phi}{\Delta x}\right)_{2,1}}{h}$$

$$= \frac{\phi_{i,j+1} - 2\phi_{i,j} + \phi_{i,j-1}}{h^2} \qquad \ldots \quad (2.3)$$

and by similar reasoning

$$\frac{\Delta^2\phi}{(\Delta y)^2} = \frac{\phi_{i+1,j} - 2\phi_{i,j} + \phi_{i-1,j}}{h^2} \qquad \ldots (2.4)$$

adding (2.3) and (2.4)

$$\frac{\Delta^2\phi}{(\Delta x)^2} + \frac{\Delta^2\phi}{(\Delta y)^2} = \frac{\phi_{i,j+1} + \phi_{i+1,j} + \phi_{i,j-1}, \phi_{i-1,j} - 4\phi_{i,j}}{h^2}$$

Hence

$$\phi_{i,j} = \frac{\phi_{i,j+1} + \phi_{i+1,j} + \phi_{i,j-1} + \phi_{i-1,j}}{4} \qquad \ldots (2.5)$$

Thus a simple equation is obtained which relates the potential at each nodal point to the potentials of the four neighbouring points of a square mesh. The boundary of the Laplacian region does not necessarily fall on nodal points of the square mesh; the boundary may intersect the grid lines of the mesh to form irregular stars as shown in FIG. 2.4 . Here a different equation has to be used in relating the potential at a grid point to that of the neighbouring points. It should be noted that an irregular star should not contain more than two short arms; three short arms would imply a too coarse mesh(11). The derivation of the equation relating the potentials for an irregular star is given in most texts in numerical analysis. With reference to FIG. 2.4 ; if the length between 1 and 3 is βh and that between 1 and 4, αh where $\beta \leq 1$ and $\alpha \leq 1$.

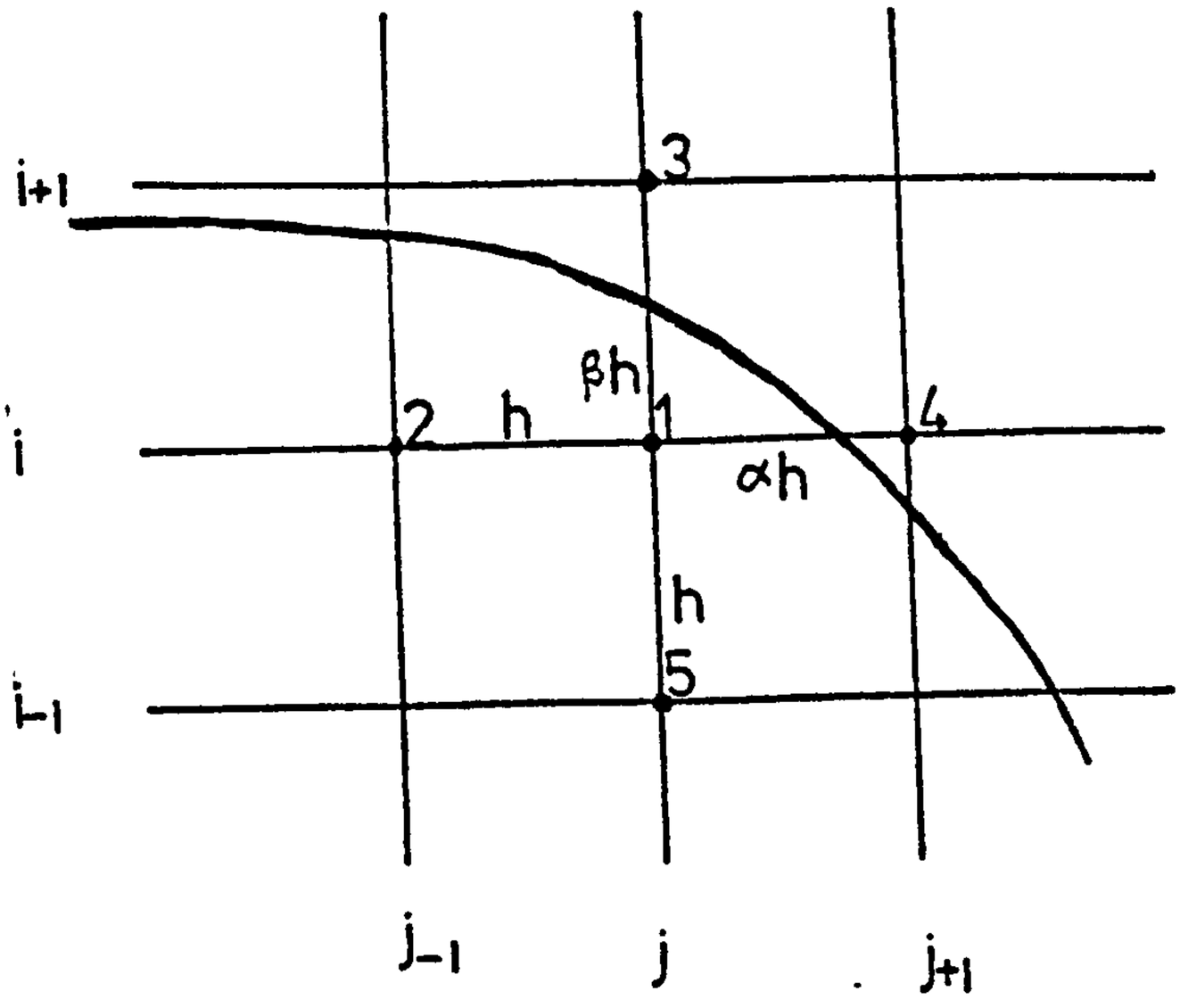

FIG. (2.4) LAPLACIAN BOUNDARY FORMING AN IRREGULAR STAR

The difference equation which defines the potential ϕ_1 at 1 in terms of the potential of the neighbouring points is

$$\frac{\phi_4}{\beta(1+\beta)} + \frac{\phi_3}{\alpha(1+\alpha)} + \frac{\phi_2}{(1+\beta)} + \frac{\phi_1}{(1+\alpha)} = \left(\frac{1}{\alpha} + \frac{1}{\beta}\right) \phi_1 \quad \ldots (2.6)$$

when $\alpha = \beta = 1$ this equation reduces to equation (2.5).

2.5.2 Techniques of Solving the Difference Equations

For smaller regions having few grid points, field distribution can be found by hand computation of the set of simultaneous equations which was obtained by writing the difference equation for each grid point as explained in

section (2.5.1). The ways of acceleration of computation by methods of relaxation and over relaxation can be found in most texts in numerical methods. (For example refs.23-24) But practical field problems contain meshes of very large numbers of grid points and 10,000 grid points are not unusual(23). In those cases hand computation becomes impossible and a computer has to be employed.

The ideas involved in machined computation are identical to those encountered in hand computation, since the computation is based on the same finite difference equations. There are several papers dealing with reducing the number of iterations involved for the convergency of the solution. The line iteration method used can be classified into two main groups. As detailed by Arms and Gates(24) the potential values at all nodes were adjusted line by line of the mesh the lines being either vertical or horizontal. In the other technique potential values of the field were adjusted by vertical lines or horizontal lines as explained in a paper by Peaceman and Rachford(25) . The above methods are capable of producing a solution of given accuracy with fewer iterations.

Before deciding on the application of standard difference scheme, and the technique of solution, it is necessary to know the boundary shapes and boundary conditions encountered in E.C.M.

2.6 STEADY STATE ELECTROCHEMICAL MACHINING

In practical electrochemical machining initially the tool is set at a precalculated gap from the workpiece depending upon the process parameters voltage, feed rate and conductivity of the electrolyte. Depending upon the geometries of the electrodes, sections of the workpiece near to the uninsulated boundary of the tool will have higher current densities than those sections which are relatively far from the uninsulated tool boundary. As a result those sections nearer to the tool electrode will erode at a faster rate than sections which are far from the cathode surface. As the tool is fed towards the workpiece the work surface attains an equilibrium shape and this shape 'generates' into the workpiece at the given tool feed rate. Most of the machining takes place in sections of the workpiece which are opposite the uninsulated parts of the tool section, erosion of the workpiece opposite the insulated tool boundaries drops along the insulated length. Erosion in this region occurs only from the current flux which protrudes from uninsulated tool boundaries. As a result drilled holes with parallel walls can be produced from E.C.M. With reference to FIG. 2.5 , in the region opposite the leading edge of the tool most of E.C.M. takes place and the current density reaches a constant steady value at equilibrium conditions. This section of the workpiece recedes at the same rate as that of the tool feed velocity.

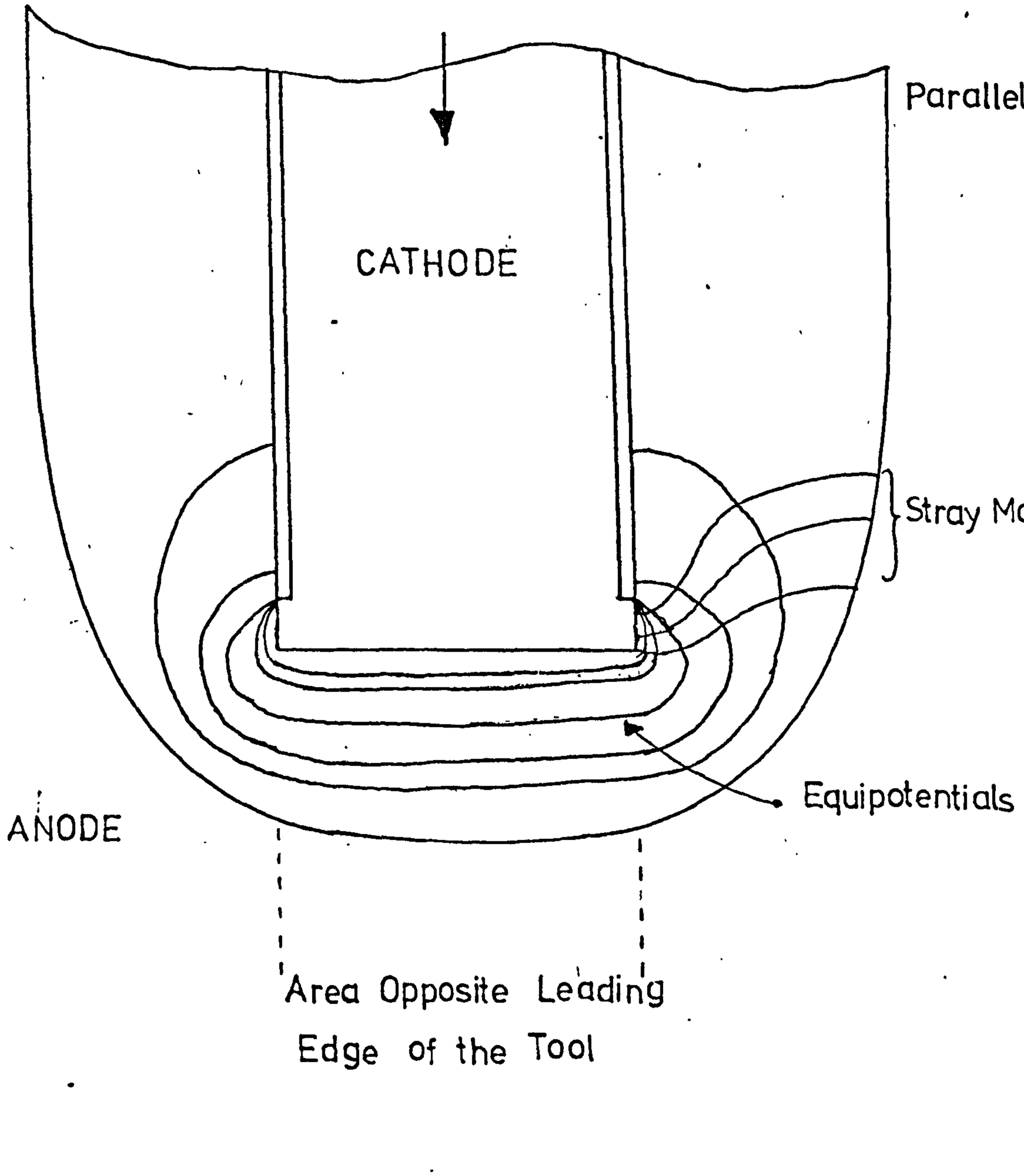
Parallel Wall
CATHODE
Stray Machinir
ANODE
Equipotentials
Area Opposite Leading
Edge of the Tool

FIG.2.5

2.6.1 Types of Electrochemical Boundaries

Boundary Conditions

By whatever method is used in solving the potential distribution equation it is necessary to know the boundary conditions.

a) Conducting boundaries:-

In the absence of an overpotential, dependent on the local current density, the potential of the electrode which is usually uniform can be specified.

b) Insulated boundaries:-

The flux normal to the insulated boundary is zero; here the method of electrical images can be used to construct a series of fictitious nodal points outside the insulating boundary having identical potential values as their counterparts.

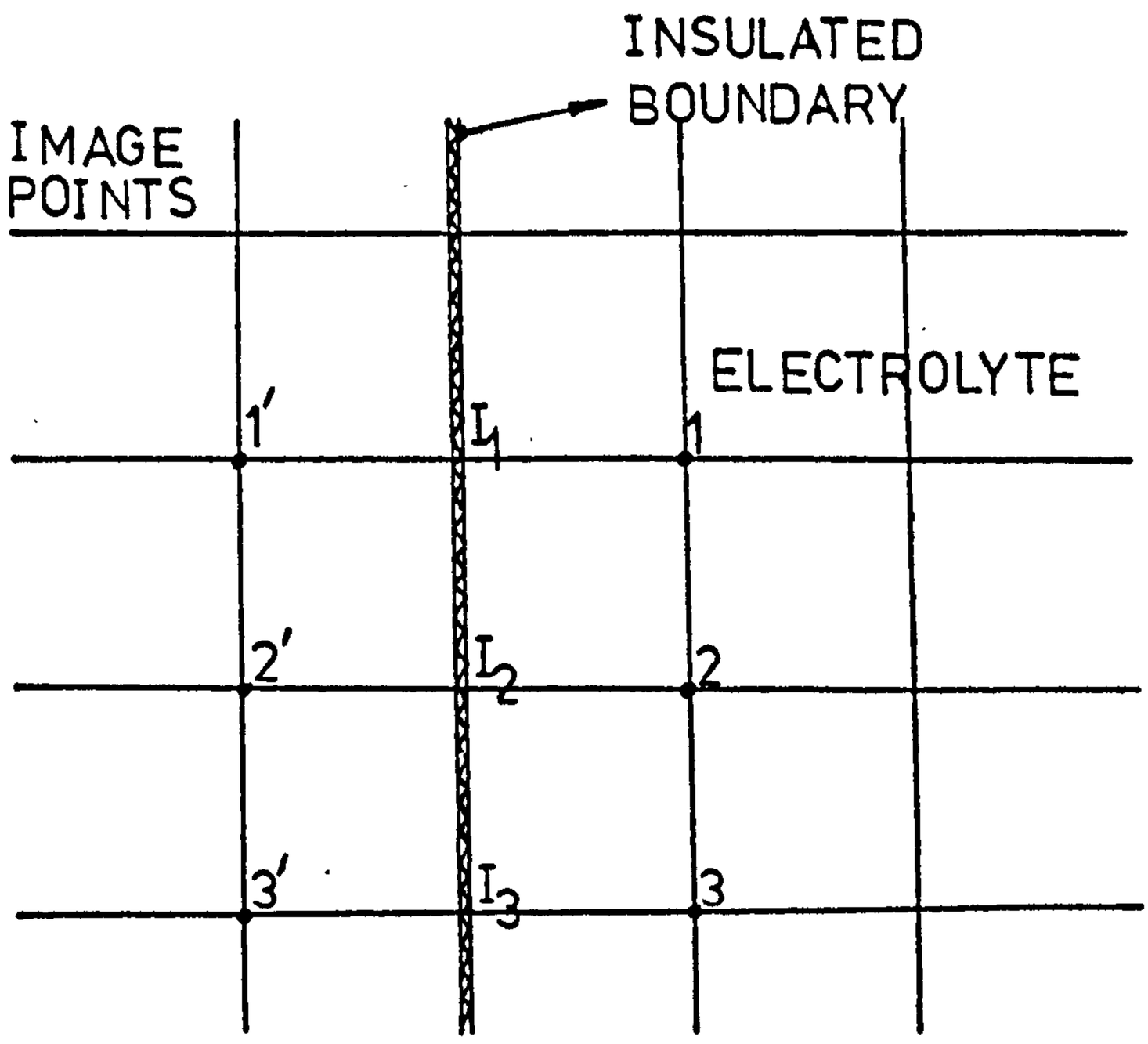

FIGURE (2.6)

With reference to FIG. (2.6)

$\phi_1 = \phi_1'$; $\phi_2 = \phi_2'$; $\phi_3 = \phi_3'$ etc.

The mesh points on the boundary are then treated as a point within the Laplace region in applying the equation $\nabla^2\phi = 0$.

c) <u>Electrochemical boundaries which are defined by the current dependent overpotential:-</u>

In this region neither the potential nor the current is specified at the boundary; only their approximate functional relationship is known.

For a linear overpotential where the potential of the electrode ϕ_e is related to the potential on the electrolyte side ϕ_B by

$$\phi_B = \phi_e - b.J$$

where b is the slope of the local current density J and

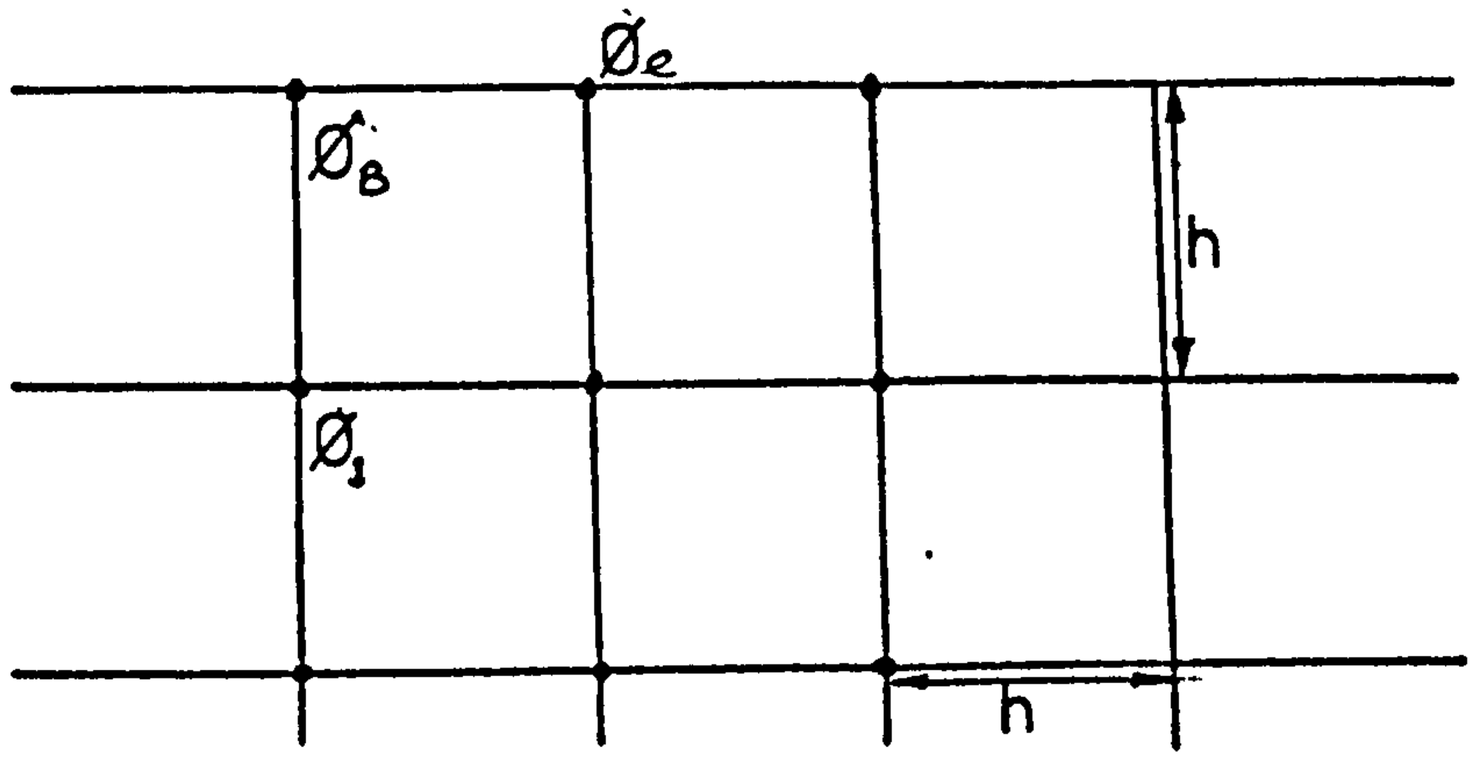

FIGURE (2.7)

potential Ø curve (26). Then

$$\phi_B = \phi_e - \frac{bk}{h}(\phi_B - \phi_1)$$

$$\phi_B = \phi_e + \frac{(bk)/h \times \phi_1}{1 + (bk)/h} \qquad \ldots (2.7)$$

k is the conductivity of the electrolyte solution.

Another type of electrochemical boundary is where the relationship between potential and current density is expressed by Tafel polarization.

Where $\phi_B = \phi_e - \beta \ln \frac{J}{J_o}$ ... (2.8)

$= RT/\alpha nF$, J_o the exchange current density, α the transfer coefficient.

Evaluation of the potential at the solution side of the boundary involves a trial-and-error procedure [5].

2.6.2 Machining Equation

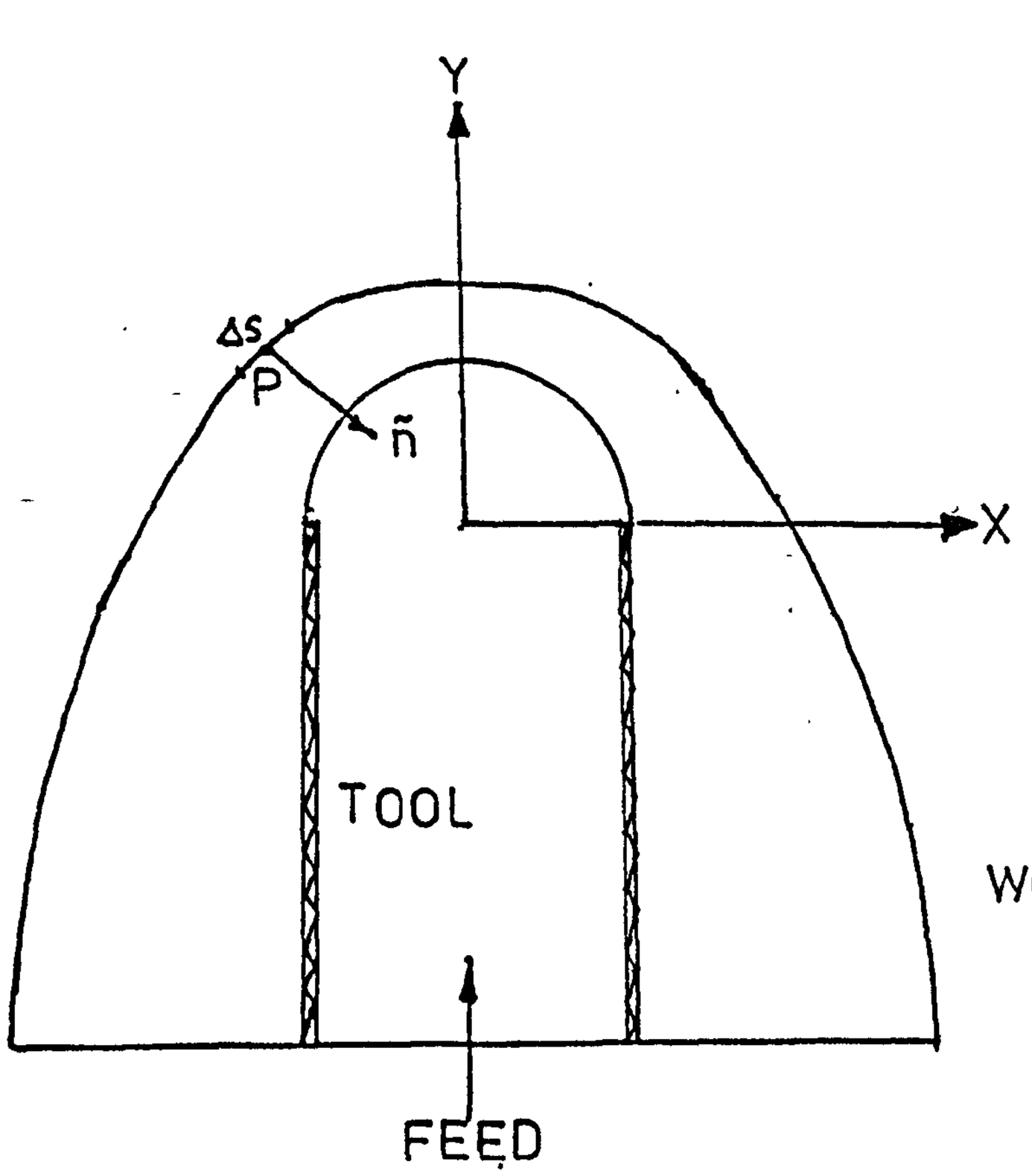

FIG. (2.8) SECTION THROUGH THE SYMMETRICAL AXIS

Consider any point P on the work surface produced by an axi symmetric semi cylindrical electrochemical tool. The relationship between the normal potential gradient and the current density at P is

$$\chi \times \frac{\partial \phi}{\partial N} = J$$

where χ is the conductivity of the electrolyte, and 'J' the current density at P. The normal erosion rate of the work surface is directly proportional to the normal potential gradient and the normal erosion rate is

$$(V_{SP}) \times J$$

$$= (V_{SP}) \times \chi \times \frac{\partial \phi}{\partial N} \qquad \ldots (2.9)$$

where V_{SP}, the volumetric metal removal rate per Coloumb.

2.6.3 Erosion Condition

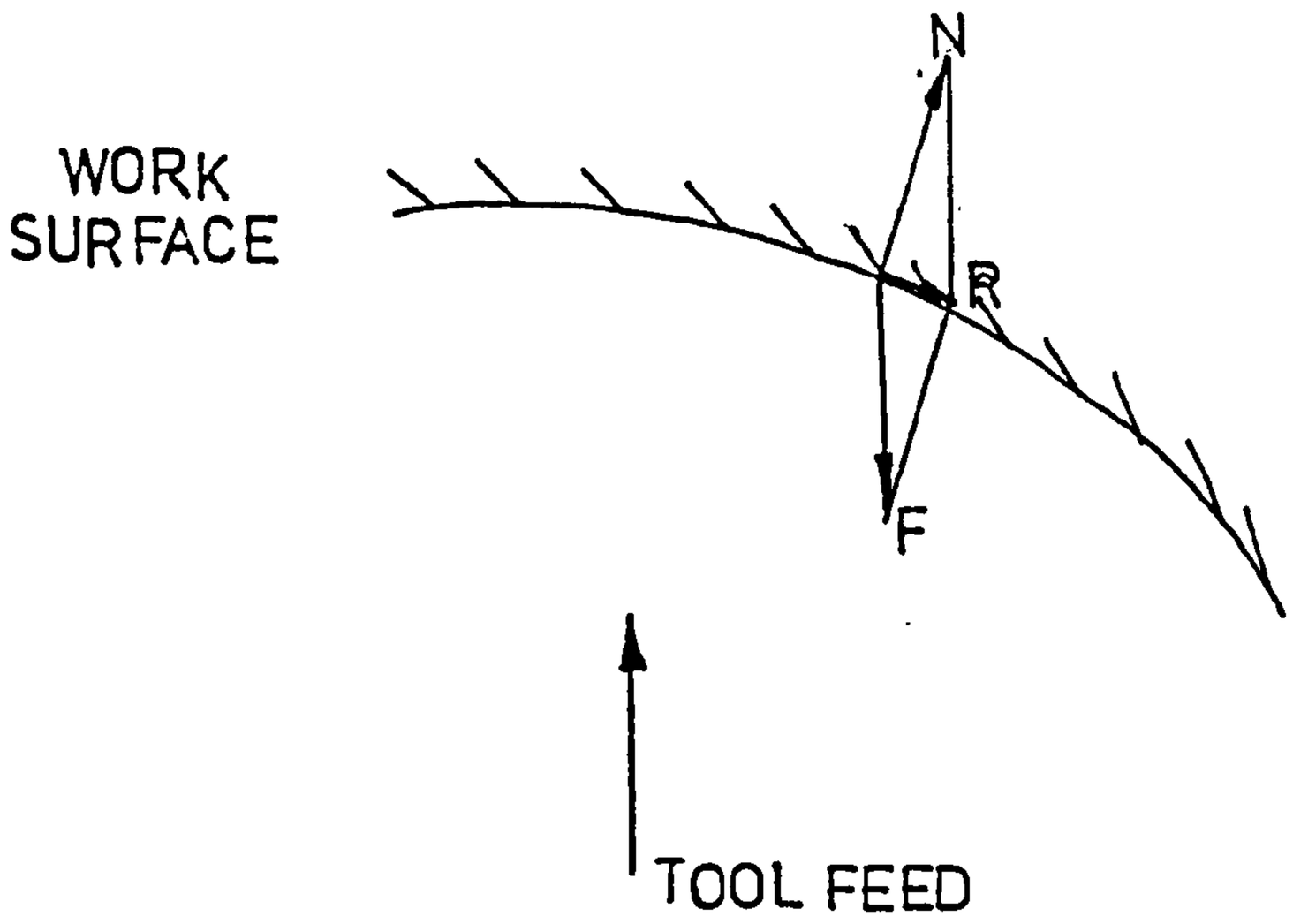

FIGURE (2.9)

In FIG. 2.9 PN denotes the magnitude of the normal erosion vector at point P on the work surface, PF denotes the negative tool feed velocity vector, and PR the resultant of these two vectors.

If the system has attained steady state machining condition, this shape of work surface remains unaltered, i.e. the resultant of the normal erosion vector and, negative feed vector should lie along the tangent to the work surface at point P. If 'θ' the angle between the resultant and the negative feed direction, then

$$\frac{PN}{PF} = \sin\theta \qquad \ldots (2.10)$$

The magnitude of PN is given by equation (2.9), and PF is the tool feed velocity.

2.7 DIFFICULTIES IN APPLYING STANDARD DIFFERENCE SCHEME TO PREDICT ECM REGIONS

A typical section of the gap between tool electrode and work electrode when using a tool having a cylindrical leading edge is shown in FIG. 2.10 . The gap AB is the equilibrium gap and is taken as unity which usually lies between 0.12 mm and 0.5 mm.

The other dimensions given are approximate nominal values commonly encountered in electrochemical drilling measured with respect to the frontal equilibrium gap AB. This is the region for which Laplace equation for potential distribution has to be applied in order to find the primary current distribution in the electrode

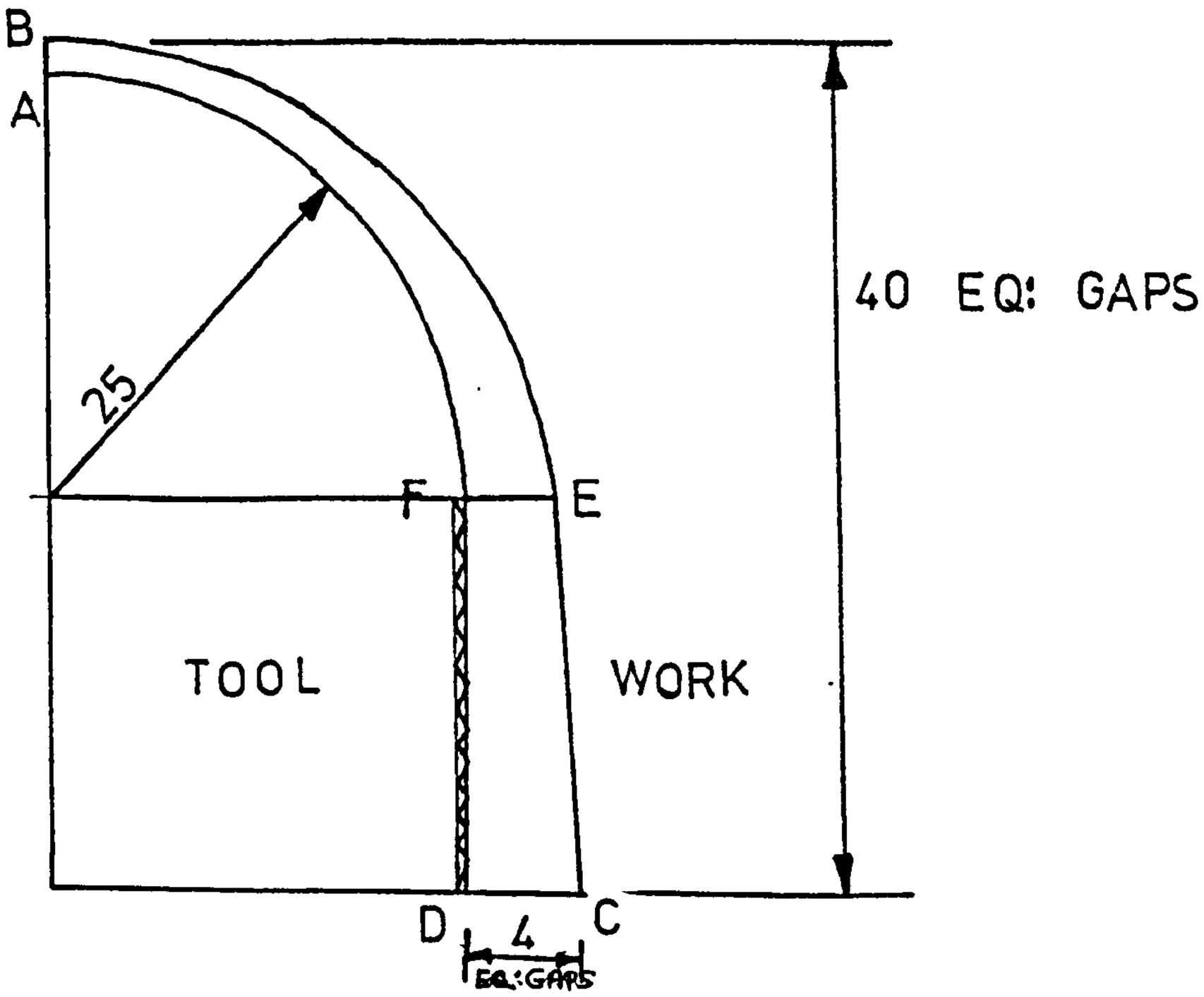

FIG. (2.10) ABCD THE GAP BETWEEN ELECTRODES

gap. Most other electrode gaps for which Laplace equation has to be solved have more complex geometries than the one shown in FIG. 2.10 . This makes application of standard difference scheme [illegible] difficult. Since the gap between the electrodes is the factor determining tolerance of a component manufactured by ECM its accurate prediction is vital. The acceptable error usually falls below 0.1 of the equilibrium gap. Therefore if a standard difference method is used in conjunction with a square mesh or a rectangular mesh, because of curved boundaries of the region and the closer solution required, a very fine mesh has to be used. In other words this means solution of a large number of equations. This procedure

requires more computer time and will be very expensive.

The other alternative, using an orthogonal curvilinear mesh (radial lines and circles) becomes more involved even if the work boundary is fixed. FIG. 2.11 shows an orthogonal curvilinear mesh superimposed on the curved part of the electrode gap. To include the

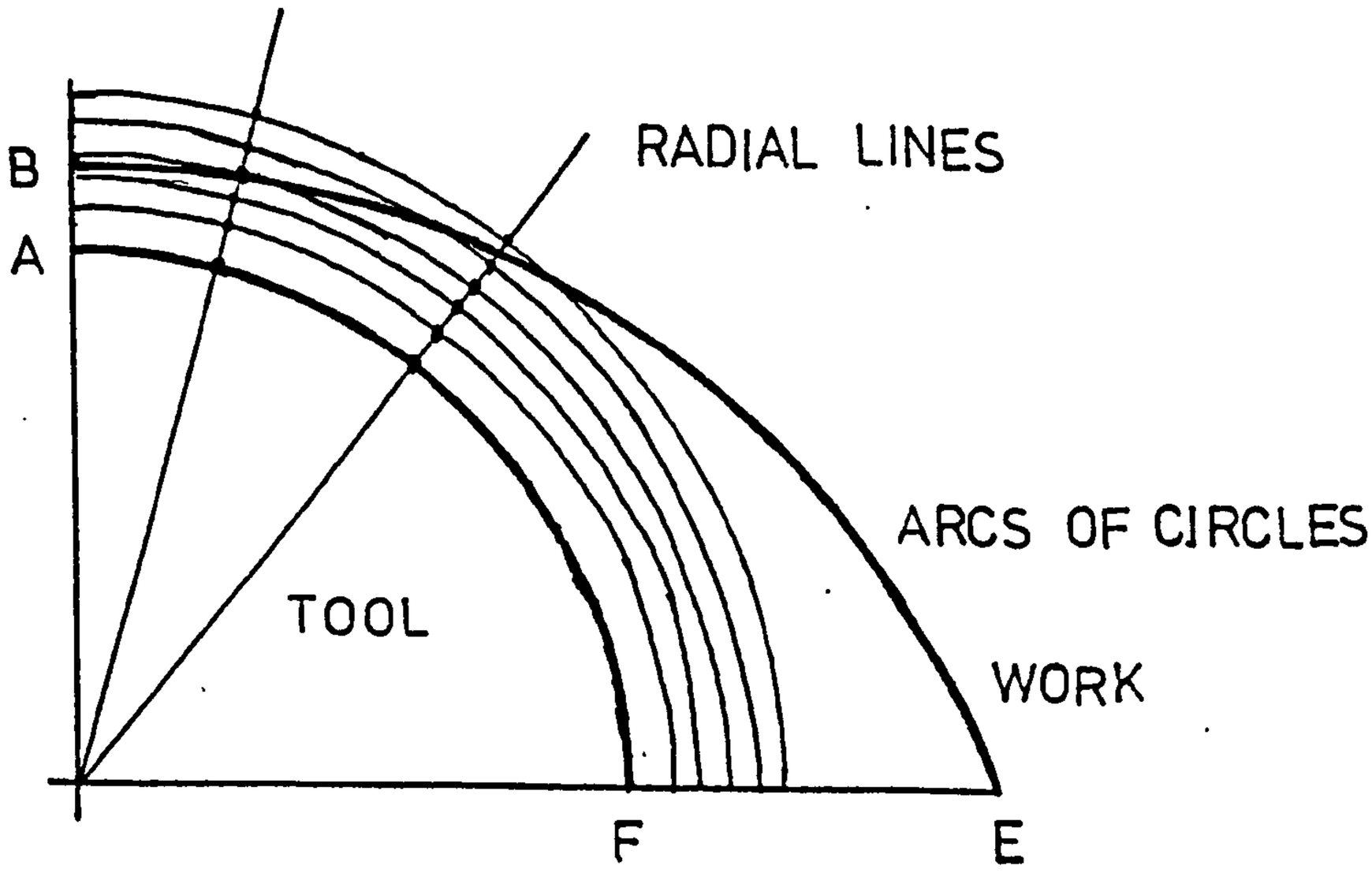

FIGURE (2.11)

work boundary in the mesh a larger number of circular lines have to be considered, most of these curved lines of the mesh will lie outside electrode gap. Potential values of the nodes of the outermost boundary have to be guessed in forming the finite difference equations.

The straight part of the problem has to be treated using square or rectangular mesh. But for a free boundary problem this procedure fails due to difficulty in locating the free boundary in each iteration, since nodal points do not necessarily lie on the boundary.

The answer to this problem is a variable non orthogonal finite difference mesh with nodal points which can be located on the free boundary at each iteration.

2.8 POLYNOMIAL APPROXIMATION METHOD TO SOLVE THE FIELD DISTRIBUTION

It has been shown in section (2.3) that the potential at any nodal point is a function of potentials of neighbouring points and their positions from the point under consideration. Thus the potential at any point in the region can be expressed using a polynomial of the form $\emptyset = f(x,y)$, where $\emptyset$ could be expressed as a quadratic or cubic or a higher order function in x and y. For example $\emptyset$ may be expressed as

$$\emptyset = Ax^3 + By^3 + Cx^2y + Dy^2x + Exy \; Q \; Fx + Gy + H \qquad \ldots(2.11)$$

or

$$\emptyset = Ax^2 + By^2 + Cx + Dy + E \qquad \ldots(2.12)$$

To evaluate $\emptyset$, knowing the co-ordinates, functions A, B, C, D etc. have to be evaluated.

Therefore if equation (2.11) is used to express $\emptyset$, nine equations have to be found to evaluate the above mentioned functions, or five equations if the polynomial given by (2.12) is used.

The boundaries of most Laplace regions are of constant potential (conducting surface) or surfaces where the potential gradient is a constant or zero (insulated boundaries). To find the required condition when using equation (2.12) in expressing potential at a point,

partially differentiating (2.12) with respect to x and y.

$$\frac{\partial \phi}{\partial x} = 2Ax + C$$

$$\frac{\partial^2 \phi}{\partial x^2} = 2A$$

$$\frac{\partial \phi}{\partial y} = 2By + D$$

$$\frac{\partial^2 \phi}{\partial y^2} = 2B$$

$$\therefore \quad \nabla^2 \phi = 0 = 2A + 2B \qquad \ldots(2.13)$$

This is true for any inner point in the Laplace region. For boundaries along or parallel to co-ordinate axis, and having constant potential gradients

$$\frac{\partial \phi}{\partial x} = K_1 = 2Ax + C$$

and $\qquad \ldots(2.14)$

$$\frac{\partial \phi}{\partial y} = K_2 = 2By + D$$

where K_1 and K_2 are constants.

If the points were chosen in such a way that the point under consideration is the origin in a system of local co-ordinates, x = 0, y = 0, the condition given by equation (2.14) becomes

$$\frac{\partial \phi}{\partial x} = K_1 = C \qquad \text{and}$$

$$\ldots(2.15)$$

$$\frac{\partial \phi}{\partial y} = K_2 = D$$

This way of choosing the co-ordinate system is very useful if a higher order polynomial is used to define the potential function, since the terms $\frac{\partial^2 \phi}{\partial x^2}$, $\frac{\partial^2 \phi}{\partial y^2}$, $\frac{\partial \phi}{\partial x}$ and $\frac{\partial \phi}{\partial y}$ will contain terms which are multiples of x and y, which become zero when x = 0, and y = 0.

2.8.1 FORMULATION OF THE DIFFERENCE SCHEME

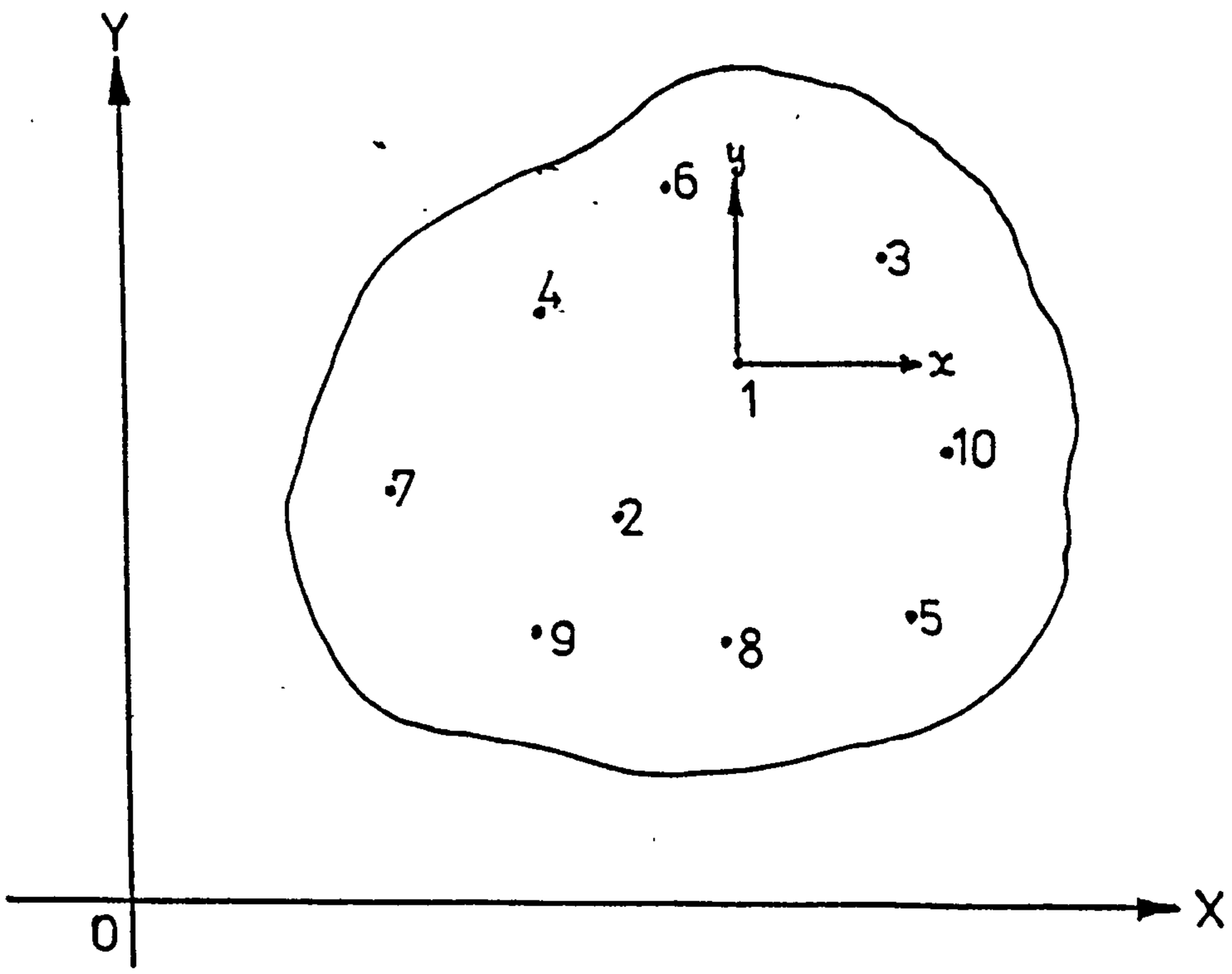

FIGURE (2.12)

Consider a set of discrete points 1, 2, 3, ... etc. in a Laplace region. Let the potential values of these points be ϕ_1, ϕ_2, ϕ_3 ... etc. respectively, having co-ordinates (X_1, Y_1), (X_2, Y_2), (X_3, Y_3) ... etc. respectively. Assume that the potential at a point in the region can be expressed using equation (2.12).

Therefore for any general point in the region

$$\emptyset = AX^2 + BY^2 + CX + DY + E$$

To evaluate A, B, C, D and E as mentioned earlier five equations have to be found. Consider points 1, 2, 3, 4 and 5. These points were so chosen because point 3 is symmetrically positioned among the remaining four points. Whenever it is possible points should be selected in this manner for the simple reason the mesh point under consideration receives information from the whole of the surrounding area. Otherwise the points may be chosen in any suitably desired manner. The corresponding potential equations for these points are

$$\emptyset_1 = AX_1^2 + BY_1^2 + CX_1 + DY_1 + E$$

$$\emptyset_2 = AX_2^2 + BY_2^2 + CX_2 + DY_2 + E$$

$$\emptyset_3 = AX_3^2 + BY_3^2 + CX_3 + DY_3 + E \qquad \ldots (2.16)$$

$$\emptyset_4 = AX_4^2 + BY_4^2 + CX_4 + DY_4 + E$$

$$\emptyset_5 = AX_5^2 + BY_5^2 + CX_5 + DY_5 + E$$

Now if the origin of co-ordinate is shifted to point 1, or in other words if the co-ordinate of the surrounding four points were taken with respect to a system of local co-ordinates having the origin at point 1, where points 1, 2, 3, etc. have co-ordinates (x_1, y_1), (x_2, y_2), (x_3, y_3) etc. respectively, with respect to the new system, where $(x_1 = 0,\ y_1 = 0)$, $(x_2 = X_2 - X_1,\ y_2 = Y_2 - Y_1)$, $(x_3 = X_3 - X_1,\ y_3 = Y_3 - Y_1)$ ... etc. respectively. The set of equations (2.16) can be written as

$$\begin{aligned}
\phi_1 &= ax_1^2 + by_1^2 + cx_1 + dy_1 + e \\
\phi_2 &= ax_2^2 + by_2^2 + cx_2 + dy_2 + e \\
\phi_3 &= ax_3^2 + by_3^2 + cx_3 + dy_3 + e \qquad \ldots (2.17) \\
\phi_4 &= ax_4^2 + by_4^2 + cx_4 + dy_4 + e \\
\phi_5 &= ax_5^2 + by_5^2 + cx_5 + dy_5 + e
\end{aligned}$$

where a, b, c, d and e are the corresponding functions in the system of local co-ordinates. The set of equations given by (2.17) can be written in the matrix form

$$\begin{bmatrix} \phi_1 \\ \phi_2 \\ \phi_3 \\ \phi_4 \\ \phi_5 \end{bmatrix} = \begin{bmatrix} x_1^2 & y_1^2 & x_1 & y_1 & 1 \\ x_2^2 & y_2^2 & x_2 & y_2 & 1 \\ x_3^2 & y_3^2 & x_3 & y_3 & 1 \\ x_4^2 & y_4^2 & x_4 & y_4 & 1 \\ x_5^2 & y_5^2 & x_5 & y_5 & 1 \end{bmatrix} \begin{bmatrix} a \\ b \\ c \\ d \\ e \end{bmatrix}$$

or if the position matrix is denoted by $[P]$ and $[M] = [P]^{-1}$, then

$$\begin{bmatrix} a \\ b \\ c \\ d \\ e \end{bmatrix} = \begin{bmatrix} m_{11} & m_{12} & m_{13} & m_{14} & m_{15} \\ m_{21} & & & & \\ & & & & \\ & & & & \\ m_{51} & & & & m_{55} \end{bmatrix} \begin{bmatrix} \phi_1 \\ \phi_2 \\ \phi_3 \\ \phi_4 \\ \phi_5 \end{bmatrix} \qquad \ldots (2.18)$$

2.8.2 Extraction of the required combination of functions a,b,c etc. to satisfy the Laplace region

The conditions to be satisfied for different boundary conditions are given in section (2.8). The

corresponding combination of function could be easily obtained from the equation (2.18) conditions

(1) For a point within the Laplace region: a + b = 0,

i.e.

$$(m_{11} + m_{21})\phi_1 + (m_{12} + m_{22})\phi_2 + (m_{13} + m_{23})\phi_3 + (m_{14} + m_{24})\phi_4 + (m_{15} + m_{25})\phi_5 = 0 \quad \ldots (2.19)$$

(2) For a boundary point where $\frac{\partial \phi}{\partial x} = 0$ i.e. C = 0

$$m_{31}\phi_1 + m_{32}\phi_2 + m_{33}\phi_3 + m_{34}\phi_4 + m_{34}\phi_5 = 0 \quad \ldots (2.20)$$

(3) For a boundary point where $\frac{\partial \phi}{\partial y} = 0$, i.e. D = 0

$$m_{4,1}\phi_1 + m_{4,2}\phi_2 + m_{4,3}\phi_3 + m_{4,4}\phi_4 + m_{4,5}\phi_5 = 0 \quad \ldots (2.21)$$

(4) For a boundary point where ϕ = K (constant) i.e. a conducting boundary, E = 0

$$m_{51}\phi_1 + m_{52}\phi_2 + m_{53}\phi_3 + m_{54}\phi_4 + m_{55}\phi_5 = 0 \quad \ldots (2.22)$$

For any other boundary condition the required information can be easily extracted from equation (2.18).

2.8.3 Method of Solution

Method of solution involves setting up a set of equations similar to the set of equations given in (2.17), the number of equations in the set being dictated by the number of terms in the polynomial defining ϕ. Using the matrix inversion technique the inverted matrix M (refer equation (2.18)) can be formed; knowing the location of the point, i.e. a boundary point or an inner point, the required combination of functions may then be extracted.

an equation similar to that of (2.19), (2.20), (2.21) or (2.22) is formed. This procedure can be repeated for all grid points. Simultaneous solution of all the equations formed in the above manner gives the field distribution of the region. Thus this scheme provides a variable, nonorthogonal finite difference mesh where nodal points can be located on the free boundary at each iteration.

2.8.4 Grid Point Selection

It was mentioned earlier, that the grid points required for the formation of the set of equations can be selected in any desired manner. For the work described in this thesis grid points were chosen as follows. The point number 1 always refers to the grid point under consideration.

(1) A point within the region.

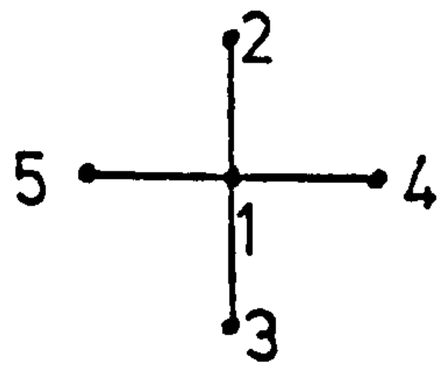

The points were so selected to form a star as shown.

(2) point on a conducting boundary

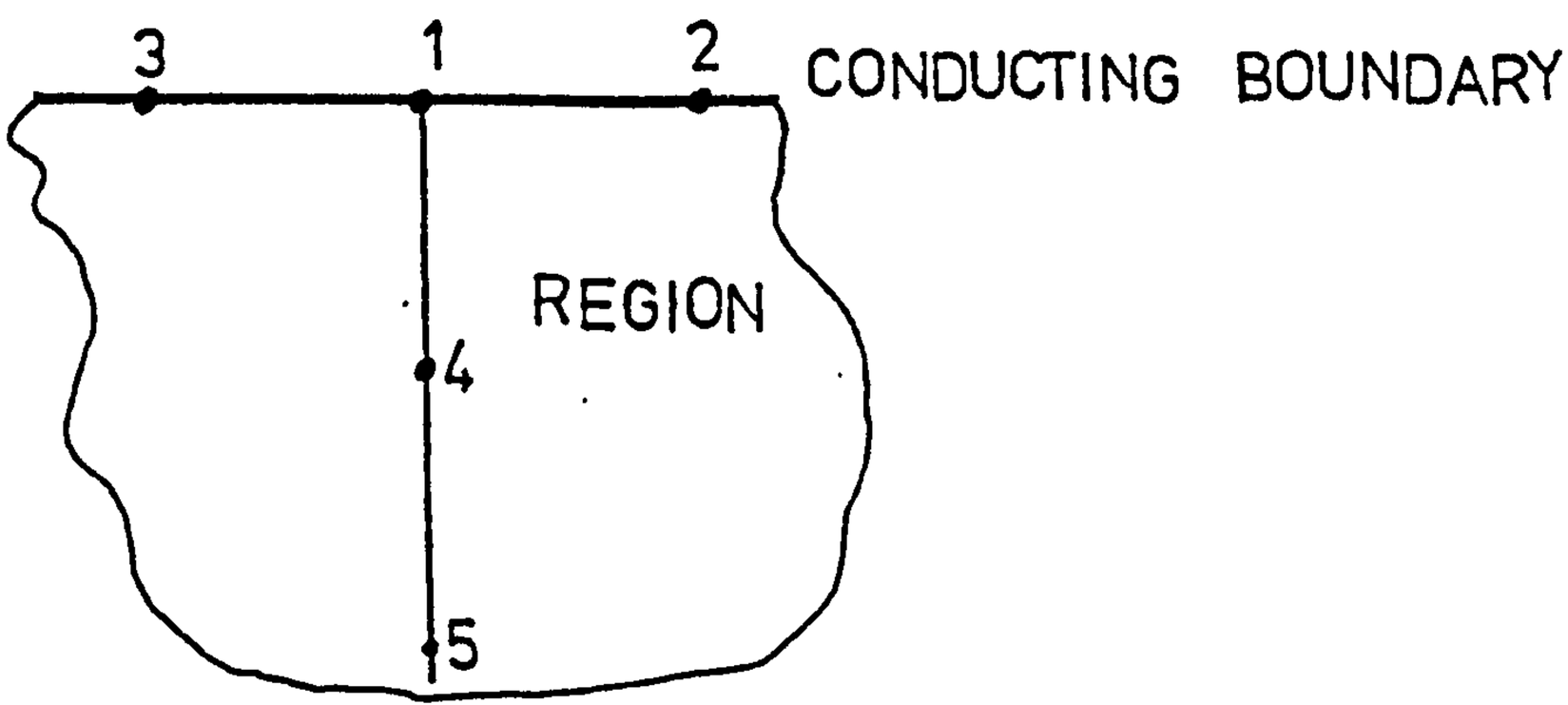

the points were chosen as shown.

(3) Point on a boundary where $\frac{\partial \phi}{\partial x} = 0$, or $\frac{\partial \phi}{\partial y} = 0$

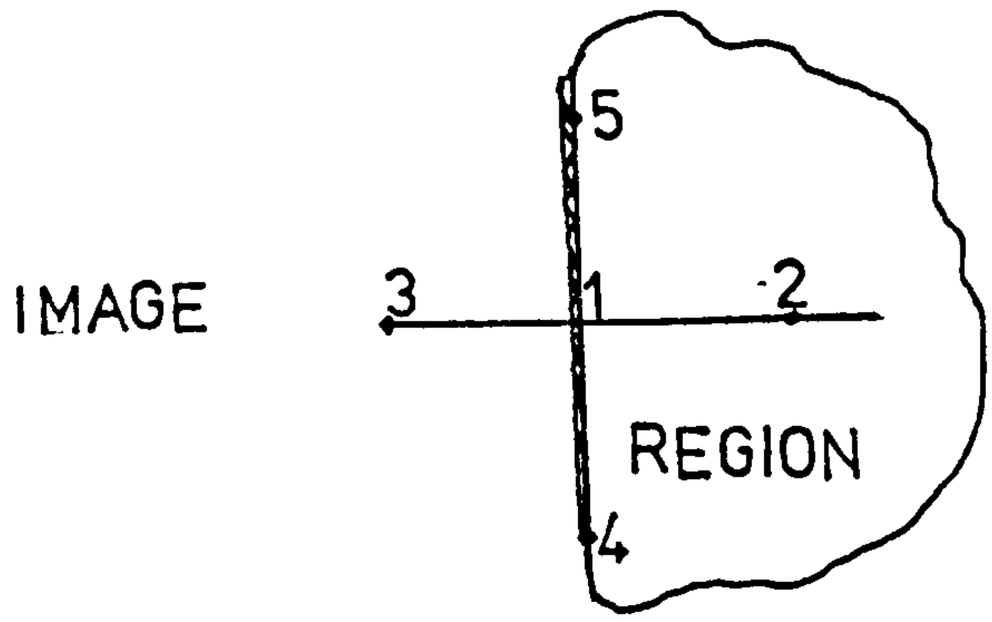

A image point 3 was constructed and the point was treated as an inner point.

2.8.5 The Mesh

The required mesh depends on the geometry of the Laplacian region and the choice is quite arbitrary. For example if the region is of rectangular form, mesh could be formed with lines parallel to the sides of the rectangle, or if the region is a segment of a circle, radial lines, and circular arcs could be employed to form the mesh. The mesh employed for the region bounded by the tool shown in FIG. 4.5a and the work boundary is detailed in section 2.10.2 .

2.9 COMPARISON OF SOLUTION FOUND BY VARIABLE NON-ORTHOGONAL DIFFERENCE SCHEME WITH THAT OF AN EXACT SOLUTION

It was thought at this point to use five term polynomial given by equation (2.12) to define the potential at a grid point, in the prediction of the primary current distribution in steady state electrochemical machining.

There are certain advantages in using a five term rather than a higher order polynomial because the computation involves the inversion of the matrices. The size of the matrix to be inverted is determined by the number of terms in the polynomial and the number of matrices to be inverted is equal to the number of grid points. Since this number is quite large (about 200 grid points), computation could be an expensive procedure. Also the rounding off errors involved in inversion of large matrices could be of significant order and the use of higher order polynomial might not necessarily yield a closer solution to the actual field. On the other hand in using a polynomial such as given by equation (2.12), the truncation error involved in not considering the product of x and y terms may be significant. To check both systems, and to compare the significance of using a higher order polynomial, a known problem in potential distribution was solved using both the equations

$$\emptyset = Ax^3 + By^3 + Cx^2y + Dy^2x + Exy + Fx + Gy + L \qquad (2.11)$$

and

$$\emptyset = A_1x^2 + B_1y^2 + C_1x + D_1y + E \qquad (2.12)$$

This was so chosen because to evaluate the function A, B, C etc. in (2.11) and A1, B1, C1 etc. in (2.12), required the consideration of five nodal points and nine nodal points respectively, hence the point under consideration could be so chosen, that other points surround it in a symmetrical manner. The problem considered was to evaluate the potential distribution in

the region bounded by two conducting cylinders of infinite length.

POTENTIAL DISTRIBUTION IN THE REGION BOUNDED BY TWO CHARGED CONCENTRIC CYLINDERS OF INFINITE LENGTH

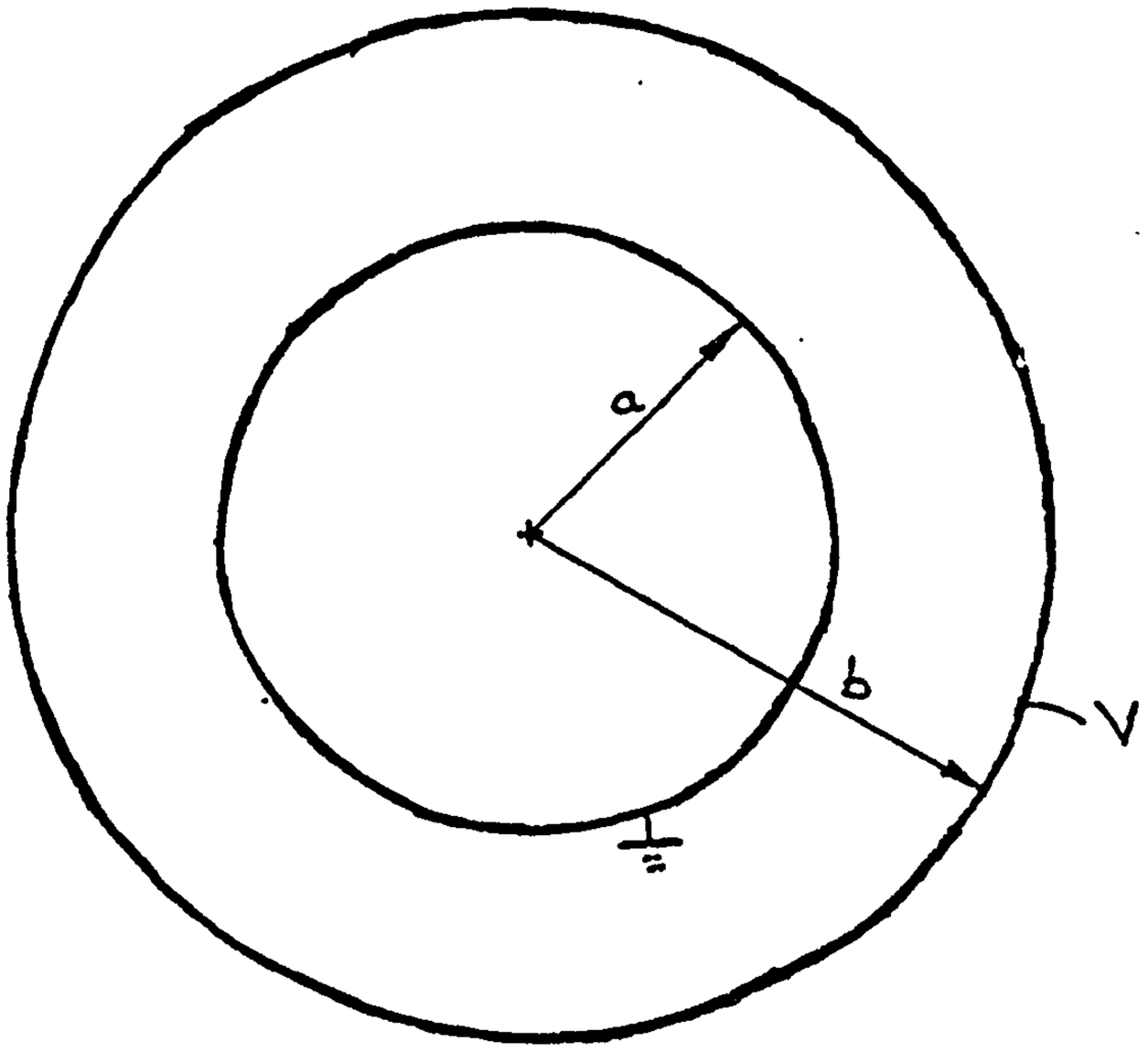

FIGURE (2.13)

The region under consideration is the space between the two cylinders. In circular-cylindrical co-ordinates (r, ψ , Z), the Laplace equation is of the form.

$$\nabla^2\phi = \frac{\partial^2\phi}{\partial r^2} + \frac{1}{r}\times\frac{\partial\phi}{\partial r} + \frac{1}{r^2}\times\frac{\partial^2\phi}{\partial\psi^2} + \frac{\partial^2\phi}{\partial Z^2} = 0 \qquad (2.23)$$

Since the cylinder is considered to be long and the two surfaces are concentric conductors Ø is independent of Z. Hence equation (2.23) reduces to

$$\nabla^2\phi = \frac{d^2\phi}{dr^2} + \frac{1}{r}\times\frac{d\phi}{dr} = 0 \qquad (2.24)$$

The general solution of this equation is

$$\emptyset = L + M \ln r \qquad (2.25)$$

where L and M are arbitary constants.

The boundary conditions are

$r = a$, $\emptyset = 0$, (earthed)

$r = b$, $\emptyset = V$, (the applied voltage)

on substitution in equation (2.25)

$$L + M \ln (a) = 0 \qquad (2.26)$$

and $L + M \ln (b) = V$

which gives

$$L = -V \ln (a)/\ln(b/a)$$

$$M = V/\ln (b/a)$$

Hence from equation (2.25) $\emptyset$ at any radial distance r is given by

$$\emptyset = V \cdot \frac{\ln(r/a)}{\ln(b/a)} \qquad (2.27)$$

Taking as an example the value of $\emptyset$ for

$a = 25$

$b = 26$

$V = 12$ at r = 25.4, 25.7, and 25.9 from the equation are

$$\emptyset_{(25.4)} = 4.8566\,24$$

$$\emptyset_{(25.7)} = 8.4492\,59$$

$$\emptyset_{(25.9)} = 10.8219\,96$$

Correct to 4 decimal places.

The corresponding values for $\emptyset$ obtained from

numerical solutions using the 'Difference Scheme" given in section (2.8) are given in tables (2.14)and (2.15) Setting up the problem for numerical analysis, and details of the nine point scheme is given in Appendix (A.3).

It is clearly seen from the tables (2.14)and (2.15) that there is hardly any difference in the predicted values from both schemes and they very closely resemble the values obtained from the exact solution. The potential distribution defined by equation (2.12) gave values almost identical to those obtained from the exact solution. Theoretically the higher order polynomial should give a more accurate solution than the lower order polynomial but in this case did not. The very small difference in potential values between the calculated and analytical values could have originated from the rounding off errors in the matrix inversion procedure and from truncation error of the assumed function. The very small difference in the answers obtained between the exact solutions and this difference scheme justifies the use of potential distribution defined by equation (2.12) in conjunction with the difference scheme explained in section (2.8), for the prediction of potential distribution of regions bounded by curved surfaces. This difference scheme has been used throughout the work explained in this thesis, in prediction of the primary current distribution between the tool electrode and the work electrode in steady state 'Electro-Chemical Machining'

r = 25 mm	r = 25·4 mm	r = 25·7 mm	r = 25·9 mm	r = 26 mm
PHI(1)= 0.000046	PHI(2)= 4.855947	PHI(3)= 8.448601	PHI(4)=10.820652	PHI(5)=12.000000
PHI(6)= 0.000001	PHI(7)= 4.855873	PHI(8)= 8.448588	PHI(9)=10.820590	PHI(10)=12.000000
PHI(11)= 0.000065	PHI(12)= 4.855909	PHI(13)= 8.448615	PHI(14)=10.820615	PHI(15)=12.000000
PHI(16)= 0.0	PHI(17)= 4.855967	PHI(18)= 8.448578	PHI(19)=10.820605	PHI(20)=12.000000
PHI(21)= 0.0	PHI(22)= 4.855889	PHI(23)= 8.448625	PHI(24)=10.820688	PHI(25)=12.000000
PHI(26)= 0.0	PHI(27)= 4.856007	PHI(28)= 8.448682	PHI(29)=10.820751	PHI(30)=12.000000
PHI(31)= 0.0	PHI(32)= 4.856078	PHI(33)= 8.448655	PHI(34)=10.820772	PHI(35)=12.000000
PHI(36)= 0.0	PHI(37)= 4.856016	PHI(38)= 8.448667	PHI(39)=10.820760	PHI(40)=12.000000
PHI(41)= 0.0	PHI(42)= 4.856039	PHI(43)= 8.448627	PHI(44)=10.820821	PHI(45)=12.000000
PHI(46)= 0.0	PHI(47)= 4.855739	PHI(48)= 8.448124	PHI(49)=10.820722	PHI(50)=12.000000
PHI(51)= 0.0	PHI(52)= 4.855760	PHI(53)= 8.448159	PHI(54)=10.820721	PHI(55)=12.000000
PHI(56)= 0.0	PHI(57)= 4.856063	PHI(58)= 8.448709	PHI(59)=10.820860	PHI(60)=12.000000
PHI(61)= 0.0	PHI(62)= 4.856061	PHI(63)= 8.448673	PHI(64)=10.820728	PHI(65)=12.000000
PHI(66)= 0.0	PHI(67)= 4.856001	PHI(68)= 8.448629	PHI(69)=10.820771	PHI(70)=12.000000
PHI(71)= 0.0	PHI(72)= 4.856012	PHI(73)= 8.448694	PHI(74)=10.820749	PHI(75)=12.000000
PHI(76)= 0.0	PHI(77)= 4.855896	PHI(78)= 8.448627	PHI(79)=10.820704	PHI(80)=12.000000
PHI(81)= 0.0	PHI(82)= 4.855871	PHI(83)= 8.448526	PHI(84)=10.820604	PHI(85)=12.000000
PHI(86)=-0.000028	PHI(87)= 4.855881	PHI(88)= 8.448619	PHI(89)=10.820628	PHI(90)=12.000000
PHI(91)= 0.0	PHI(92)= 4.855878	PHI(93)= 8.448590	PHI(94)=10.820594	PHI(95)=12.000000
PHI(96)= 0.000000	PHI(97)= 4.855963	PHI(98)= 8.448658	PHI(99)=10.820738	PHI(100)=12.000097

FIG.2.14 $\phi = Ax^3 + By^3 + Cx^2y + Dxy^2 + Ex^2 + Fy^2 + Gx + Hy + J$

r = 25 mm	r = 25·4 mm	r = 25·7 mm	r = 25·9 mm	r = 26·mm
PHI(1)= 0.0	PHI(2)= 4.856580	PHI(3)= 8.449145	PHI(4)=10.820889	PHI(5)=12.000000
PHI(6)= 0.0	PHI(7)= 4.856518	PHI(8)= 8.449123	PHI(9)=10.820829	PHI(10)=12.000000
PHI(11)= 0.0	PHI(12)= 4.856516	PHI(13)= 8.449120	PHI(14)=10.820824	PHI(15)=11.999987
PHI(16)= 0.0	PHI(17)= 4.856588	PHI(18)= 8.449075	PHI(19)=10.820812	PHI(20)=11.999998
PHI(21)= 0.0	PHI(22)= 4.856488	PHI(23)= 8.449104	PHI(24)=10.820880	PHI(25)=11.999999
PHI(26)= 0.0	PHI(27)= 4.856596	PHI(28)= 8.449162	PHI(29)=10.820905	PHI(30)=11.999999
PHI(31)= 0.0	PHI(32)= 4.856627	PHI(33)= 8.449097	PHI(34)=10.820933	PHI(35)=11.999987
PHI(36)= 0.0	PHI(37)= 4.856490	PHI(38)= 8.449095	PHI(39)=10.820886	PHI(40)=11.999998
PHI(41)= 0.0	PHI(42)= 4.856544	PHI(43)= 8.449062	PHI(44)=10.820935	PHI(45)=11.999998
PHI(46)= 0.0	PHI(47)= 4.856508	PHI(48)= 8.449043	PHI(49)=10.820872	PHI(50)=11.999987
PHI(51)= 0.0	PHI(52)= 4.856488	PHI(53)= 8.449018	PHI(54)=10.820843	PHI(55)=12.000000
PHI(56)= 0.0	PHI(57)= 4.856535	PHI(58)= 8.449050	PHI(59)=10.820930	PHI(60)=11.999998
PHI(61)= 0.0	PHI(62)= 4.856562	PHI(63)= 8.449060	PHI(64)=10.820871	PHI(65)=11.999987
PHI(66)= 0.0	PHI(67)= 4.856524	PHI(68)= 8.449040	PHI(69)=10.820911	PHI(70)=11.999987
PHI(71)= 0.0	PHI(72)= 4.856591	PHI(73)= 8.449159	PHI(74)=10.820907	PHI(75)=11.999999
PHI(76)= 0.0	PHI(77)= 4.856474	PHI(78)= 8.449092	PHI(79)=10.820867	PHI(80)=11.999987
PHI(81)= 0.0	PHI(82)= 4.856485	PHI(83)= 8.449019	PHI(84)=10.820796	PHI(85)=11.999998
PHI(86)= 0.0	PHI(87)= 4.856516	PHI(88)= 8.449121	PHI(89)=10.820829	PHI(90)=11.999998
PHI(91)= 0.0	PHI(92)= 4.856518	PHI(93)= 8.449121	PHI(94)=10.820829	PHI(95)=12.000000
PHI(96)=-0.000000	PHI(97)= 4.856580	PHI(98)= 8.449145	PHI(99)=10.820888	PHI(100)=12.000000

FIG.2.15 $\phi = Ax^2 + By^2 + Cx + Dy + E$

2.10 PREDICTION OF WORKBOUNDARY BY SOLVING THE FIELD DISTRIBUTION IN THE LAPLACIAN REGION BY POLYNOMIAL APPROXIMATION METHOD

The tool electrodes used in the ECM experiments are shown in FIG. (4.5.). These were made out of brass bars drilled through the axis to form a passage for the electrolyte flow. In 'a' the leading edge of the tool was machined to form a semi-circular section beyond which the outside surface of the tool was insulated. In 'b' the leading edge of the tool was straight and at the edge was a small corner radius to facilitate electrolyte flow, followed by an uninsulated boundary which is commonly known as the land width. Symmetry of the tool electrode requires only one quarter section through the axis of symmetry to be considered.

Presentation of the three dimensional electro-chemical die-sinking problem in two dimensions assumes orthogonal current flux distribution instead of radial current flux distribution, but since the radius of tool electrode 'QG' FIG. (2.15) is large compared to the equilibrium gap EB, the error involved is not significant.

With reference to FIG. (2.15), BGC is the quarter section of the tool boundary, 'O' the origin of global co-ordinate axis coincides with the centre of arc BG. GC is the insulated section of the tool boundary which is parallel to 'Y' axis.

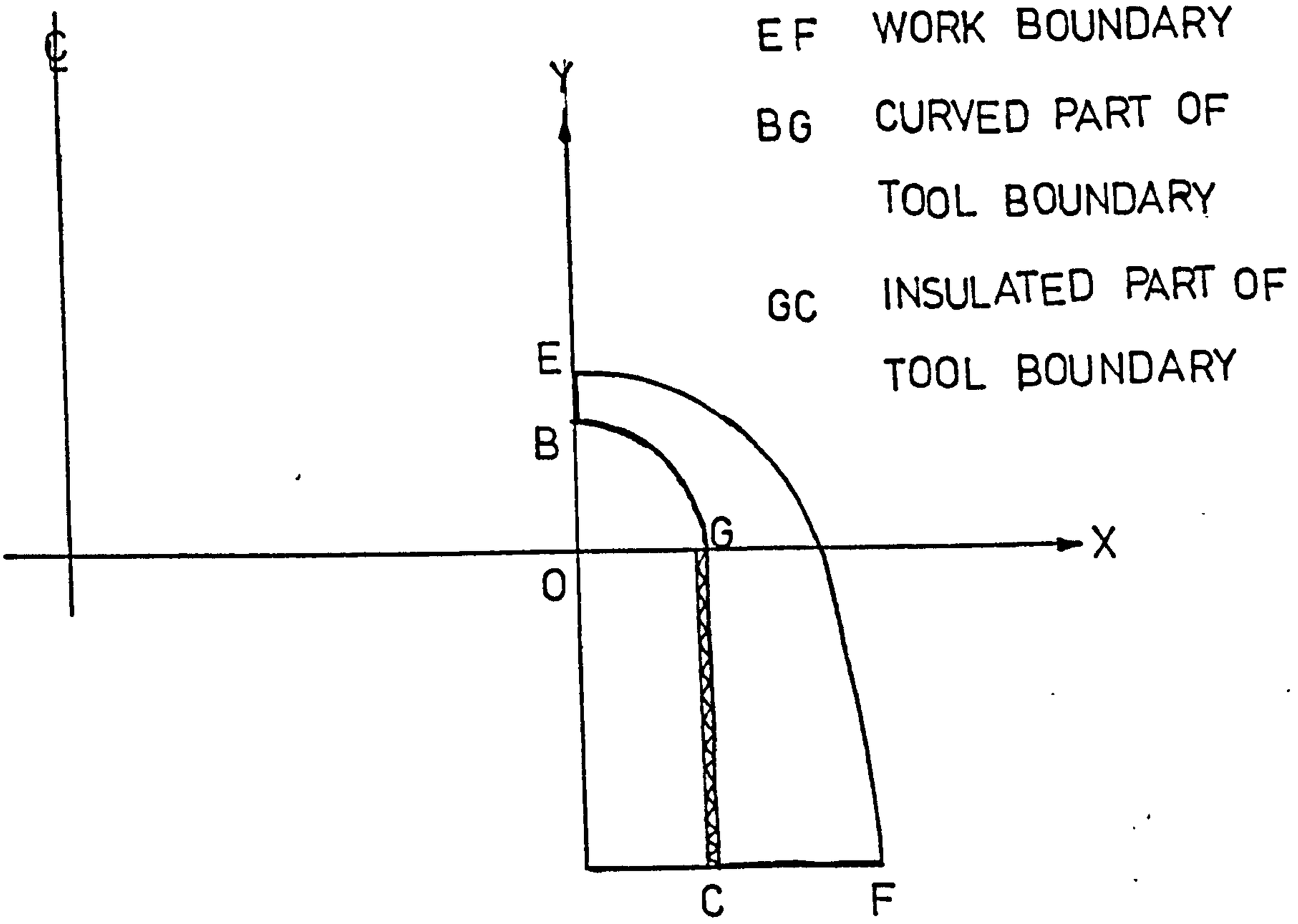

FIGURE 2.16

2.10.1 Assumptions and Boundary Conditions

For the solution $\nabla^2\phi = 0$ a closed section with known boundary conditions has to be found.

(a) Boundary BE:- The point E on the work surface is directly opposite the point 'B' on the tool surface. BE is parallel to the feed direction, and by symmetry BE is a line of constant current.

That is $\frac{\partial\phi}{\partial x} = 0$ on BE.

(b) Boundary CF:- If the boundary CF (here it is taken parallel to the X axis) is taken relatively far down the insulated boundary as shown in FIG. (2.15), with reasonable accuracy it could be stated that variation of potential in the vicinity across the line CF is negligible; thus CF is a boundary where $\frac{\partial\phi}{\partial y} = 0$.

(c) Boundary GC:- Since there is no current flux across GC, normal flux across GC is zero. Thus GC is a boundary where $\frac{\partial \phi}{\partial n} = 0$.

(d) Boundaries BG and EF:- Since the uninsulated section of the tool boundary BG and the work boundary EF are metal conductors; it is assumed that potential along BG and EF is constant and to have a zero magnitude and the positive applied potential respectively.

2.10.2 Setting up the mesh

Since tool geometry is known it is convenient to take the centre of the radiused section of the semi-cylindrical surface of the tool as the origin of the global co-ordinate axis. An initial guess was made on the work boundary shape, in this case it was assumed to be made up of a circular section continued with a parabolic section having the same gradient at the point of coincidence, as shown in FIG. (2.17). The initial normal gap at all places between the tool electrode and work surface was taken to be a fraction of the frontal equilibrium gap (theoretical orthogonal equilibrium gap). The transverse lines of the mesh were chosen by considering the circular and straight sections of the tool separately. For the circular region the tool was divided by radial lines drawn through the origin 'O'. The straight section of the gap was divided by lines parallel to the 'X' axis. Since most of the constant potential lines reach the insulated tool boundary near to

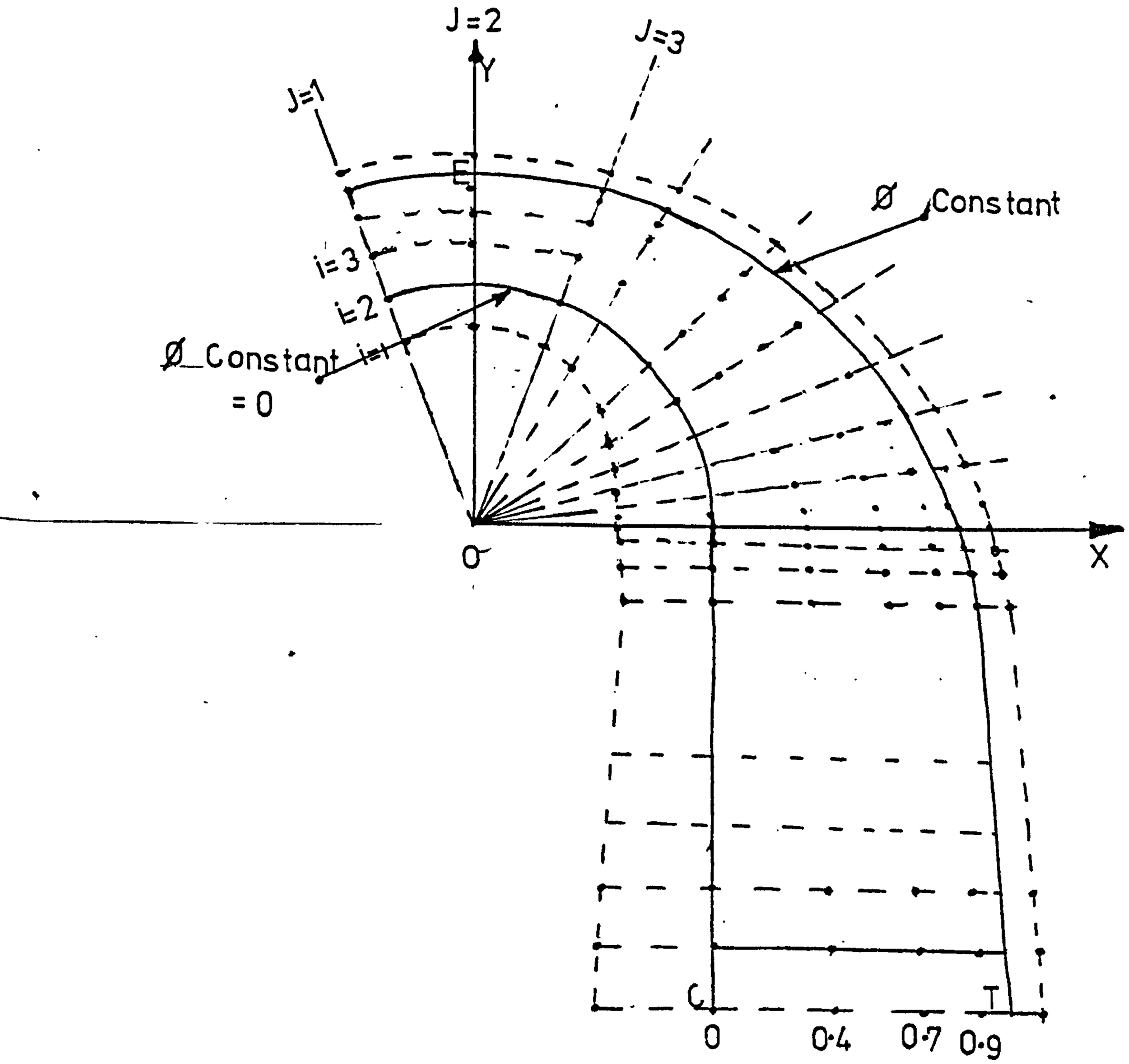

FIGURE 2.17

the leading edge FIG. 2.17. Closer packed transverse lines were taken in this area for both circular and straight regions. The number of these lines was chosen arbitrarily.

The potential gradient at the work surface along a

transverse line is found by dividing the difference of potential between the work boundary and the potential nearest to the work boundary on the particular line by the length of their separation along the line. Hence the potential gradient obtained is more accurate if the distance between these is as small as possible. To achieve this and at the same time to keep the number of simultaneous equations to a manageable level the longitudinal lines of the mesh were not equally spaced but positioned in the gap at 0.4, 0.7, and 0.9 of the gap moving from the tool boundary towards work boundary giving the least distance near the work boundary.

2.10.3 Method of Solution

For each grid point of the region depending upon its condition, equation (2.19), (2.20), (2.21) or (2.22) was formed. The set of equations so formed was simultaneously solved to obtain the potential distribution. To apply the erosion condition equation (2.9) was used to correct the work boundary i.e. to shift the points on the work boundary, the normal erosion rate had to be evaluated. Even though the transverse lines along which the potential gradient was found were normal to the tool boundary they were not normal to the work boundary, hence the normal erosion rate on the work surface had to be evaluated.

2.10.4 Normal Potential Gradient

Consider the work surface at potential $\emptyset_1$ and assume the 0.9 longitudinal line be an equipotential at $\emptyset_2$ in the

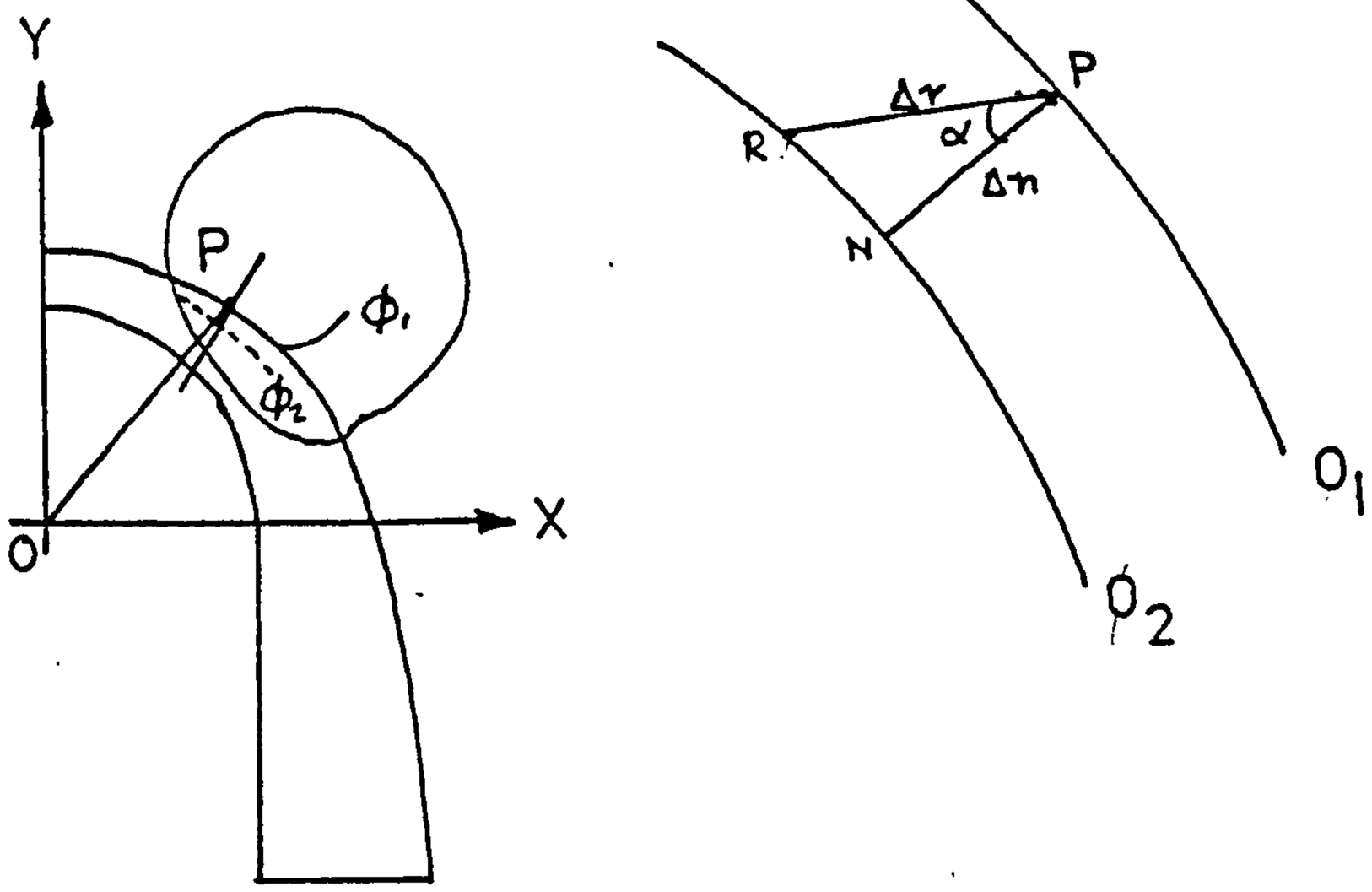

FIG. 2.18

region where it is cut by the radial line OP Fig. 2.17. If the radial line cuts the 0.9 longitudinal at R let the distance RP be Δr_o. Let a line PN normal to the work surface meet the 0.9 longitudinal at N such that PN equals Δn. If the angle between RP and PN is 'α' then assuming RN to be straight and parallel to the work surface

$$\Delta n = \Delta r \cdot \cos\alpha$$

Hence

$$\frac{\partial \phi}{\partial r} = \lim_{\Delta r \to 0} \frac{\phi_1 - \phi_2}{\Delta r}$$

$$= \lim_{\Delta n \to 0} \frac{\phi_1 - \phi_2}{\Delta n} \cdot \cos\alpha$$

$$= \frac{\partial \phi}{\partial N} \cdot \cos\alpha$$

where $\frac{\partial \phi}{\partial r}$ is the directional derivative along RP.

Therefore

$$\frac{\partial \phi}{\partial N} = \frac{\partial \phi}{\partial r} \cdot \sec \alpha \qquad (2.28)$$

Equation (2.28) defines the magnitude of the normal potential gradient in terms of a known radial potential gradient. Under equilibrium machining condition, the erosion rate on the work surface point E on FIG. 2.16 where the tool feed direction is the same as the normal to the work surface, has the same magnitude as that of the feed velocity of the tool. Since the potential gradient is directly proportional to the erosion rate

$$(V_{sp}) \cdot K \cdot \frac{\partial \phi}{\partial N} = f \qquad (2.29)$$

From equation (2.10) θ_r the angle between the negative tool feed direction and the tangent to the surface is given by

$$\sin(\theta_r) = \frac{(Vsp) \cdot K \cdot (\partial \phi / \partial N)r}{f}$$

$$\therefore \quad \sin(\theta_r) = \frac{(\partial \phi / \partial N)_2}{(\partial \phi / \partial N)_1} \qquad (2.30)$$

where suffix 'r' denotes any general point on the work surface and suffix 1 the nodal point on the work surface i.e. point E FIG. (2.17)where the feed direction is the same as the normal to the surface. For each grid point on the work boundary two values of 'θ' were found, 'θ_g' which is calculated from the geometry of the guessed work shape, and 'θ_r' from the erosion condition using

equation (2.30). If the assumed work surface is the true equilibrium work profile θ_g has the same value as θ_r for all grid points on the surface. Since the assumed work shape is not the true equilibrium shape θ_g values were corrected using the formula

$$\theta_{correc} = FAC \times \theta_r + (1 - FAC) \times \theta_g \qquad (2.31)$$

In the computer program which is given in Appendix (2.2), a value of 0.1 was used for FAC. Care must be taken not to over correct the value θ_g. This could result in oscillating the solution rather than settling on to the equilibrium work shape. Using FAC = 0.1 a solution within 0.05 equilibrium gaps was obtained within about 6 iteration.

Each time the'gap' between the electrodes was calculated along the 'J' lines. The new shape of the corrected work surfaces was treated as the guessed shape for the second iteration. This procedure was continued until the change in electrode gap between two successive iterations was less than same factor of the equilibrium gap (0.05 he).

CHAPTER III

TEMPERATURE DISTRIBUTION IN THE INTER-ELECTRODE GAP

3.1 REVIEW

Temperature of the electrolyte plays a vital part in electrochemical machining, change in temperature effects the conductivity, flow and dimensions of the electrode gap. Since ionic solutions have a large negative thermal coefficient of resistance which is greatest at low concentration, an increase in temperature always gives an increase in conductivity of the electrolyte. The amount by which the conductivity changes for a unit change in temperature depends on the nature and concentration of the electrolyte. For example calculated values of temperature coefficients for specific conductance using equation (3.1), and data from Ref. (30) between 40°C and 60°C for 10% wt./vol. solutions of sodium chloride and sodium nitrate are 1·61 $10^{-2}{}^{o}C^{-1}$ and 1·05 $10^{-2}\ {}^{o}C^{-1}$ respectively, and for 20% wt./vol. solutions sodium chloride and sodium nitrate are 1·67 $10^{-2}\ {}^{o}C^{-1}$ and 1·18 $10^{-2}\ {}^{o}C^{-1}$ respectively.

There are several references which deal with conductivity changes due to concentration variations and temperature changes in the electrolyte (30, 31). Specifically in the content of electrochemical machining, the approximate relationship between conductivity and temperature is given by the equation.

$$\chi = \chi_o\ (1 + \alpha . \Delta T) \qquad (3.1)$$

where

ΔT = change in temperature

α = temperature coefficient of specific conductance.

χ_o = the conductivity at inlet temperature.

Wolosewicz (30) considered both changes in concentration of the electrolyte and temperature on its conductivity. The increase in temperature of the electrolyte also improves the flow characteristics due to reduction in viscosity at elevated temperatures. The effect of temperature on the electrode gap dimensions and the equilibrium gap dimension is treated in Ref. (1). There should be an increase in gap dimension along downstream of the electrode length due to increase in electrolyte conductance although this may be compensated by the presence of hydrogen bubbles which were liberated at the cathode. Clark, (22) developed an equation to predict the temperature rise within the bubble layer, on the basis of the assumption of a cubic packing of hydrogen bubbles in the mass of the electrolyte. However the predicted values were greater than the experimental results. Hopenfield and Cole (17) found that the best correlation of experimental data was obtained when the electrolyte conductivity χ was evaluated at the temperature of the electrolyte as it was calculated to exit in the gap. Barsov et al. (32) considered the problem for a three dimensional electrode gap formed by a tool having a hemispherical leading edge, the temperature distribution for both sodium chloride electrolyte and sodium nitrate electrolyte being treated.

Barsov et al. assumed that the gap between the electrodes to be very small compared to the radius of the

leading edge of the tool, and hence the normal to the tool surface was taken to be the normal to the work surface in finding current density at a particular point on the work surface. This value of current density was used in forming the equation to predict the temperature distribution along the electrode gap. The temperature rise of the electrolyte due to stray current machining was not considered. The expressions they obtained can only be applied to predict the temperature distribution in the electrode gap formed by tools having one geometry only, namely tool electrodes with spherical leading edge.

To predict the temperature in the electrode gap formed by other tool geometries different formulae would have to be found and the assumption that the normal to tool surface is normal to the work boundary, on which their analysis was based would not be true in these cases. Therefore there is a need for a more general approach to the prediction of temperature distribution in the electrode gap.

3.2 GENERAL EQUATION AND ASSUMPTIONS

Consider the case of an electrolyte flowing in a narrow channel width 'b' formed by the gap between the electrodes (FIG. 3.1). It is assumed that the whole of the electrical energy supplied to the tool, work piece, electrolyte, system appears as heat. The amount of heat lost via tool and work piece being neglected as it is very small compared to that carried away by the electrolyte. For example the heat lost via the tool holder and the work

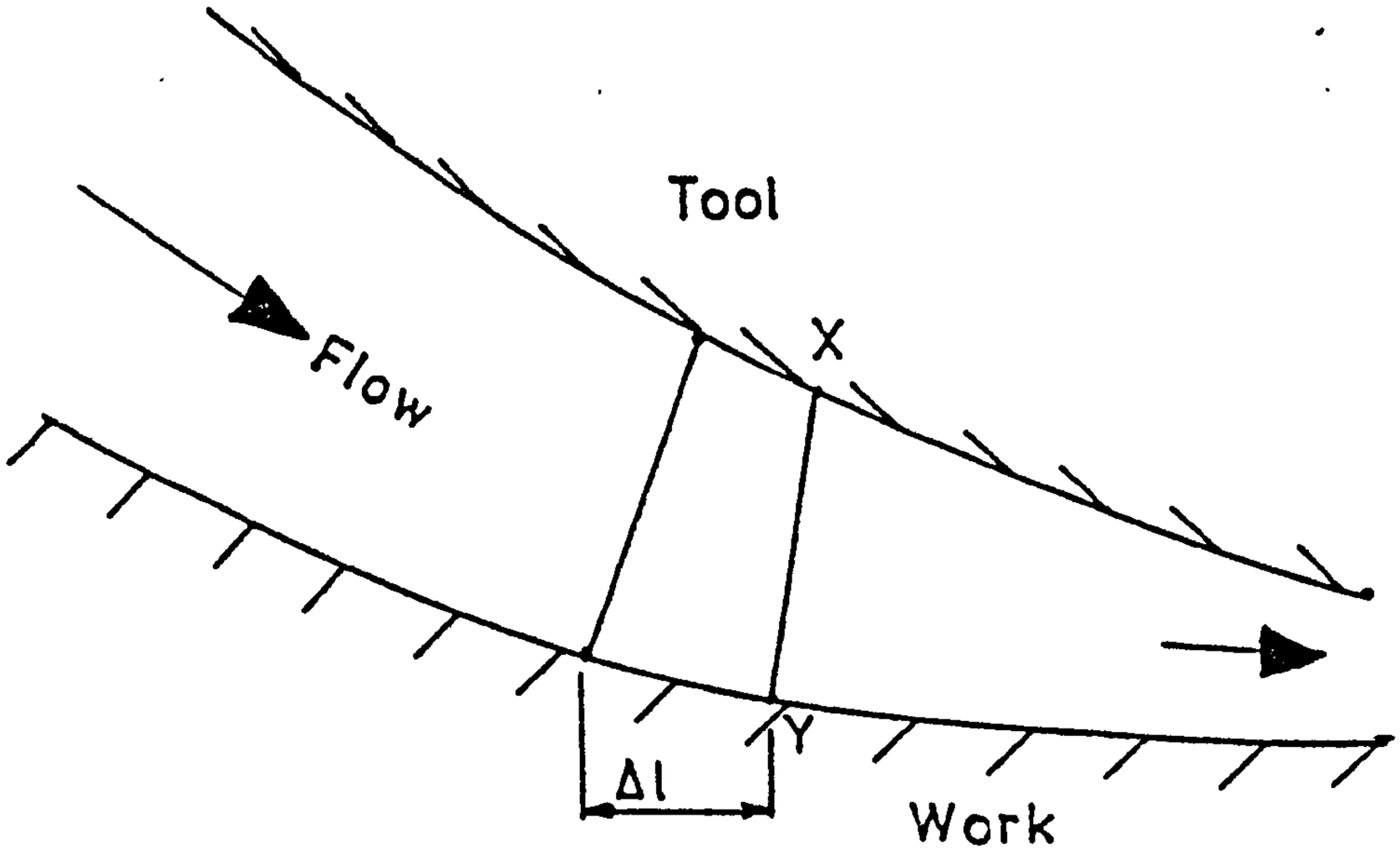

(FIG. 3.1)

holder FIG. (4 3) for the test run No.627 was approximately 4% of the machining power under steady machining conditions.

To make the calculations simple the effect of gas bubbles has been omitted in the flow calculations, and the electrolyte is considered as an incompressible fluid. If 'J' is the current density, at the anode over the area (ΔA)(= ($\Delta \ell$) x b), assuming the current density to be constant over the differential area (ΔA), the power used in machining area ΔA is given by

$$\Delta W = V \times J \times (\Delta A) \qquad (3.3)$$

where V is the applied voltage between the two electrodes.

The small part of V which accounts for the reversible electrode potentials does not contribute to the heating as it is a measure of the energy required to change the chemical form of the reactants. If (ΔT) is the increase in temperature of the electrolyte when it passes through the surface XY, assuming the electrolyte to be sufficiently well mixed by turbulence to be at a constant temperature at all points of the XY surface and also assuming that the surface XY does not change during the small time interval, the power used in machining the area (ΔA) can also be expressed as

$$\Delta W = (q_\ell) \times C \times (P_\ell) \times \Delta T \qquad (3.4)$$

where

(q_ℓ) is the volumetric flow rate of the electrolyte

C is the specific heat, and

(P_ℓ) is the density of the electrolyte.

Combining equation (3.3) and equation (3.4) increase in temperature (ΔT) is given by

$$T = \frac{V \times J \times (\Delta A)}{(q_\ell) \times C \times (P_\ell)} \qquad (3.5)$$

3.3 TEMPERATURE DISTRIBUTION IN THE GAP BETWEEN TWO PLANE PARALLEL ELECTRODES

In this case the gap between the electrodes is everywhere equal to the equilibrium gap (h_e) which is

given by

$$h_e = \frac{(V_{sp}) \times (\chi_e) \times (V_l)}{f}$$

The current density has the same value all over the whole of the surface of the anode. The temperature increase is given by equation (3.5), on substitution of $\Delta_l \times b$ for ΔA and taking infinitesimal increments, hence replacing ΔT by dT and Δx by dx

$$dT = \frac{V \times J \times (dx) \times b}{(q_l) \times C \times (P_l)}$$

and on integrating over the length of the electrode

$$T = \frac{V \times J \times b}{(q_l) \times (C) \times (P_l)} L + K$$

where K is an integration constant and L the length of the electrode measured along the direction of electrolyte flow.

At the entrance to the electrode gap that is when L = 0, the temperature of the electrolyte has the value of that of the bulk electrolyte. Therefore the temperature of the electrolyte at any length 'L' from the leading edge is given by

$$T = \frac{V \times J \times b}{(q_l) \times C \times (P_l)} \times L + T_o \qquad (3.6)$$

To express T in known machining parameters, replacing the constant current density J by f/V_{sp}

$$T = \frac{V \times f \times b}{q_l \times C \times P_{(t)} \times V_{sp}} \times L + T_o \qquad (3.7)$$

Equation (3.7) predicts the temperature rise in the electrolyte in the electrode gap of plane parallel electrodes due to Joule heating under steady E.C.M.

For work shapes produced by complex tool geometries, formulation of an exact expression becomes hopelessly involved, since there is no general formula which predicts the current distribution over the work surface. However the numerical method detailed in Chapter II predicts very accurately the primary current distribution over the work surface, and these values of current density on the work surface could very well be used in calculating the temperature increase in the electrolyte passing between two neighbouring grid points on the work surface.

3.4 TEMPERATURE RISE IN THE ELECTROLYTE IN AXI-SYMMETRIC DIE SINKING

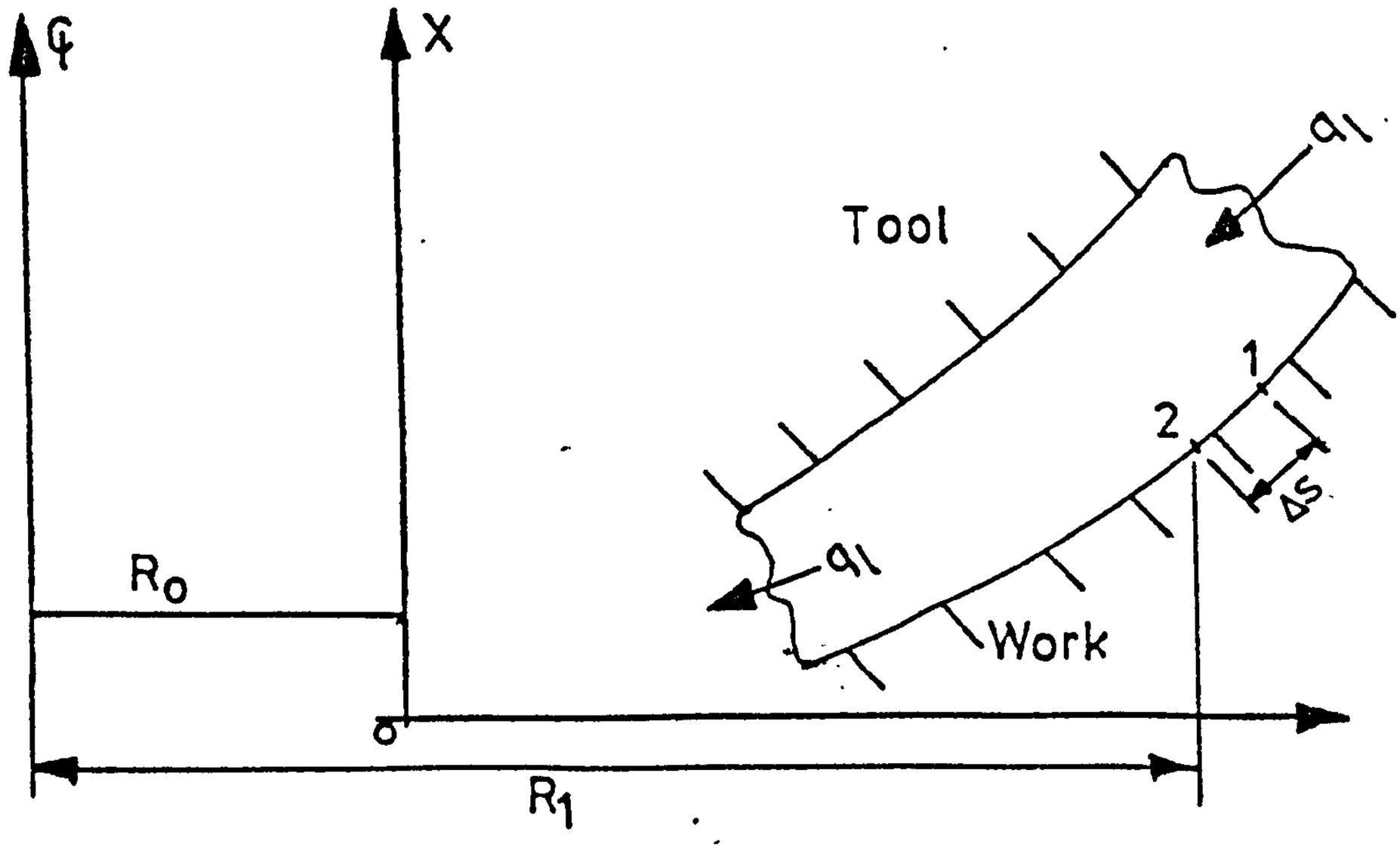

FIG. 3.2

With reference to FIG. (3.2), if ΔS is the arc length between two adjoining grid points 1 and 2 on the work surface, and $(\partial\phi/\partial N)_1$ and $(\partial\phi/\partial N)_2$ are the respective potential gradients at points 1 and 2 under steady machining conditions, since points 1 and 2 are chosen very close to each other the current reaching the ring area can be approximated to

$$2 \times \pi \times R1 \times \frac{(\partial\phi/\partial N)_1 + (\partial\phi/\partial N)_2}{2} \times \chi \times \Delta S$$

where R1 is the length from the symmetrical axis to the elemental length ΔS under consideration FIG. (3.2) substituting this expression for $J \times \Delta A$ in equation 3.5

$$\Delta T = \frac{V \times (\partial\phi/\partial N)_1 + (\partial\phi/\partial N)_2 \times \chi \times \Delta S \times \pi \times R1}{q \times C \times P} \qquad (3.8)$$

If the co-ordinate of points 1 and 2 are (x_1, y_1) and (x_2, y_2), the approximate expression for ΔS by Pythagoras is

$$\Delta S = \sqrt{(x_1 - x_2)^2 + (y_1 - y_2)^2} \qquad (3.9)$$

and R1 can be approximated to

$$R1 = RO + (x_1 + x_2)/2 \qquad (3.10)$$

on substitution for R1 and ΔS in equation (3.8), T the temperature rise of the electrolyte when passing point2 on the work surface is given by

$$\Delta T = \frac{\pi \times \{RO + (x_1 + x_2)\} \times V \times \{(\partial\phi/\partial N)_1 + (\partial\phi/\partial N)_2\} \times k \times \sqrt{(x-x_2)^2+(y_1-y_2)^2}}{q \times C \times \rho} \quad (3.11)$$

Knowing the temperature of the electrolyte at the inlet to machining cell, which was normally taken as the temperature of the bulk electrolyte, the temperature at any point on the work surface is given by

$$T = T_o + \sum \Delta T$$

where T_o is the temperature of the incoming electrolyte, $\sum \Delta T$ being the accumulated differential increase in temperature of the electrolyte calculated using equation (3.11) as it passes each grid point on the calculated work surface starting from the grid point on the work surface where the potential gradient is least. Apart from this the method considers the temperature rise due to stray current distribution over the work surface which protrude beyond the uninsulated part of the leading edge of the tool. Since the main program for determining the equilibrium work shape calculate normal potential gradients at each grid point, the amount of extra work and computation time involved in the prediction of temperature distribution is small.

CHAPTER IV

EXPERIMENTAL RIG AND ANCILLARY EQUIPMENT

4.1 ELECTRO-CHEMICAL MACHINE

A photograph of the machine used Fig. (4.1) shows a drilling tool used and a stainless steel specimen in position. The machine was one part of a three head electrochemical machine bought by the University from Rolls Royce Ltd.

The machine head was movable only in a vertical direction. Rapid traverse up or down for tool installation, work piece positioning etc. was accomplished by disengaging the clutch from the driven gear and by turning a hand wheel in an appropriate direction.

Automatic controlled feed of the tool or the work piece (depending on which of the two electrodes was connected to the machine head) was provided via a screw driven by an electric motor which was coupled to 1400:1 reduction gearbox. Any feed rate from 0.1 mm per sec. to 8 mm per sec. was possible. The maximum possible ram feed was approximately 580 mm and this was very much reduced depending on lengths of the tool holder and the work piece holder.

4.1.1 The Power Supply

The D.C. electrical power supply for machining was taken from two hexaphase rectifier sets supplied by a manually operated variable transformer. The output voltage from the two rectifiers could be preset to a maximum of 32V at 250 amps or 16 volts at 500 amps by using them in series or parallel. To prevent overloading

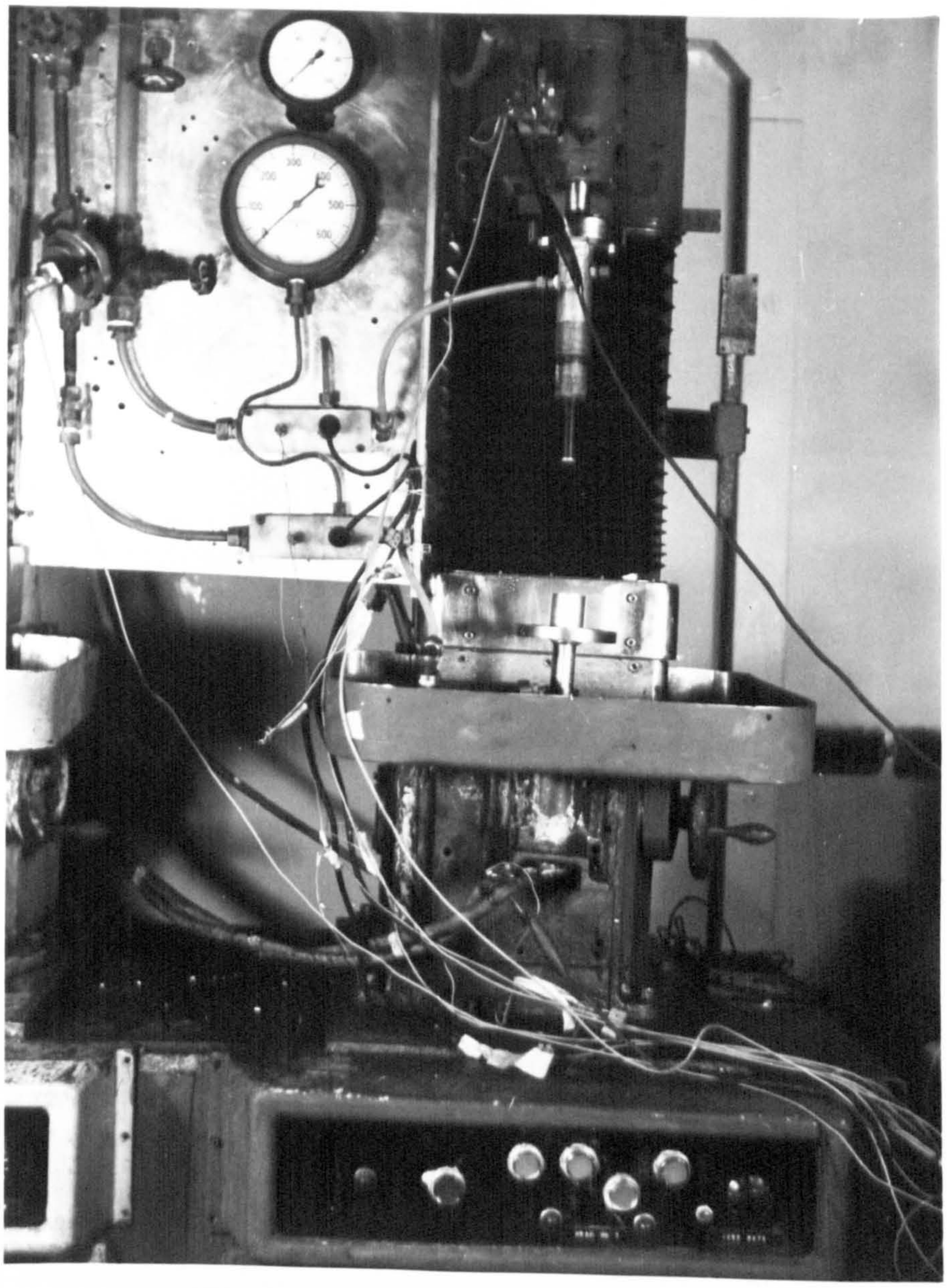

ELECTRO-CHEMICAL MACHINE

FIG. (4.1)

of the rectifier and tool damage due to severe sparking in the working gap, the maximum machining current could be limited to a desired value with the aid of a contact ammeter, which switched off the power drawn from the rectifier exceeded the preset level.

4.1.2 The Electrolyte System

A schematic diagram of the experimental machine Fig. (4.2) shows the electrolyte flow system. The electrolyte was stored in Polypropylene tanks which had a capacity of about 0.25 m^3. A 'MONO' pump (type SH32) was used to drive the electrolyte through the cell. The pump was driven by a 1.1 KW motor and was capable of attaining delivery pressures up to 600 KN m^{-2} and a maximum flow rate of 30 x 10^{-5} $m^3 s^{-1}$. At the outlet from the pump a coarse filter was fitted which prevented large particles of dirt and rubber particles which broke away from the stator of the pump entering the cell.

The common arrangement of the main pipe to the cell and a by pass valve was used to control the pressure and amount of electrolyte entering the cell. The valve which was placed in the exit pipe from the cell was used to control back pressure during machining.

The electrolyte was heated to the required temperature by dipping electric heaters. Temperature of the electrolyte was controlled during test runs by passing cold water from a tap through a cooling coil inside the tank containing bulk electrolyte. By controlling the amount of cold water through coil the temperature of the

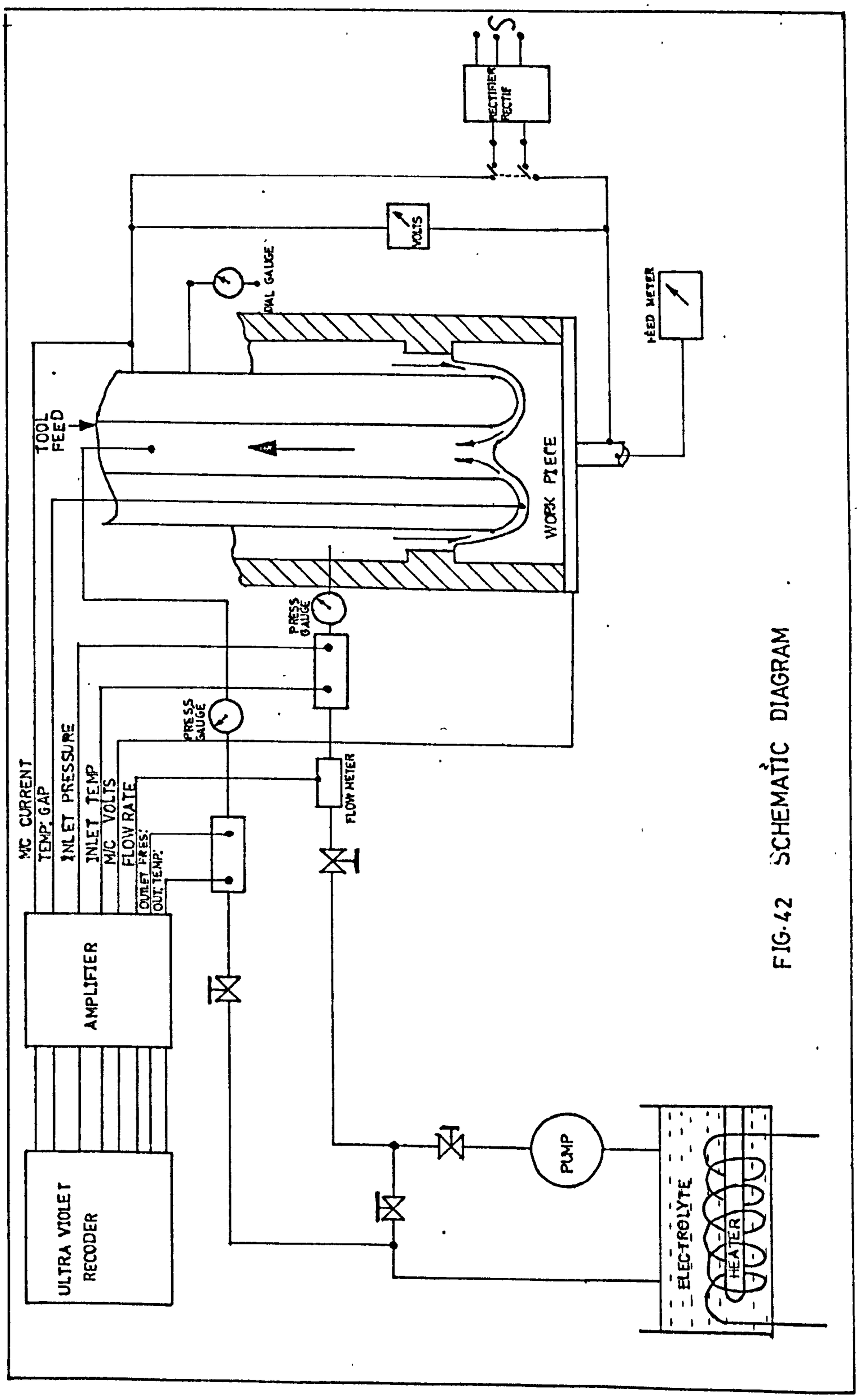

FIG. 42 SCHEMATIC DIAGRAM

E.C.M CELL ASSEMBLY

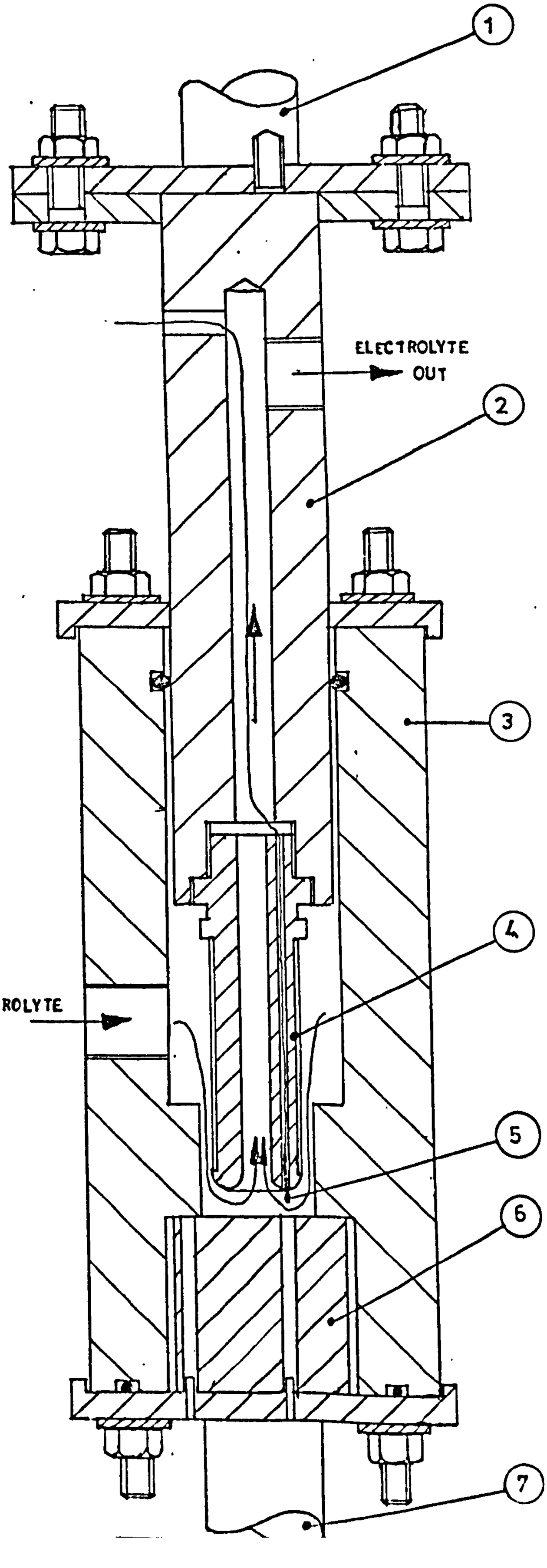

ITEM	DESCRIPTION
1	CONNECTOR TO M/C HEAD
2	TOOL HOLDER
3	M/C CELL
4	TOOL
5	THERMISTOR
6	WORK PIECE
7	CONNEC TO M/C BASE

FIG.4.3

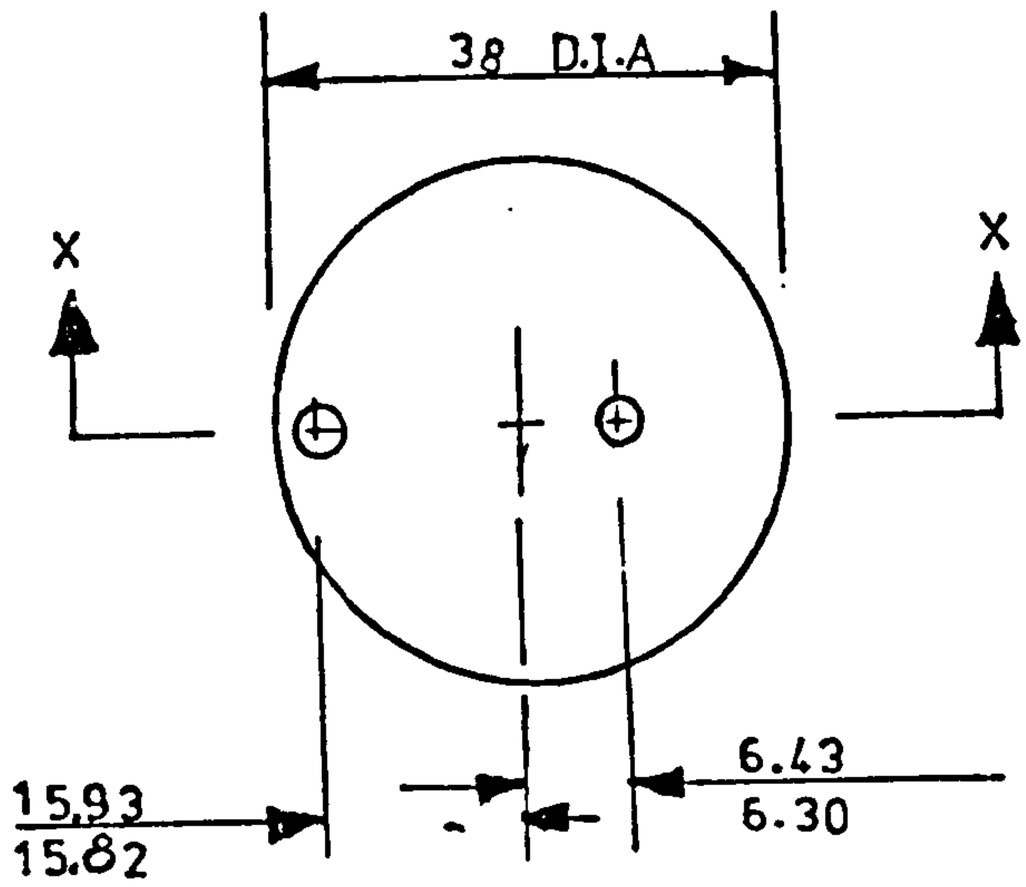

ALL DIMENSIONS IN MM

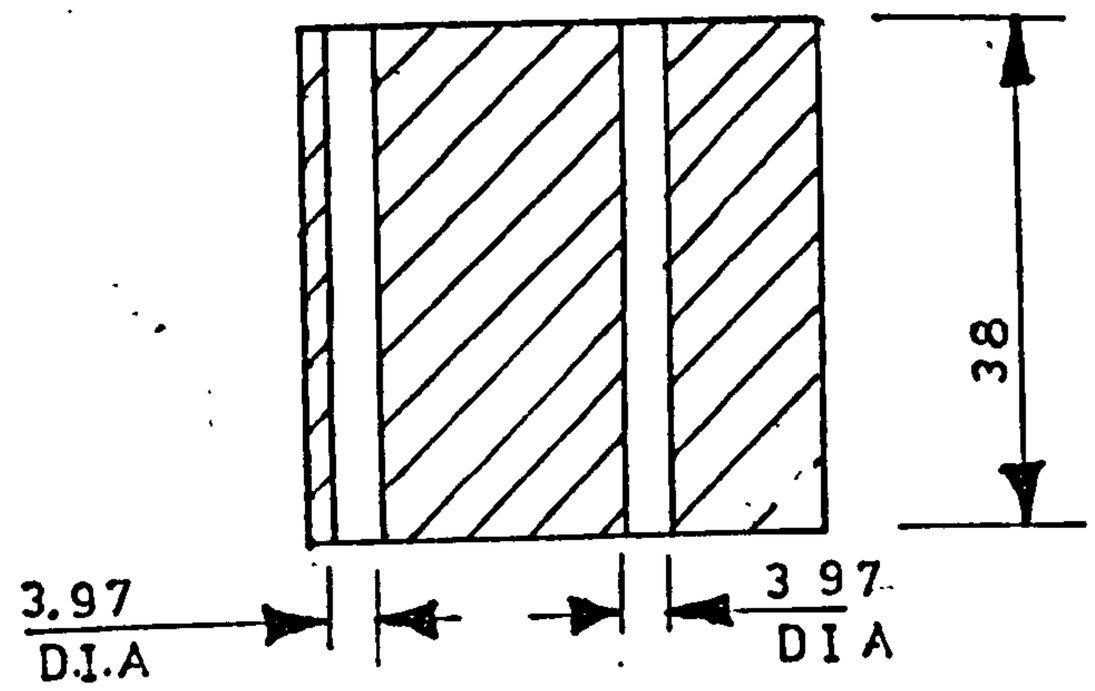

SECTION X-X

SPECIMEN

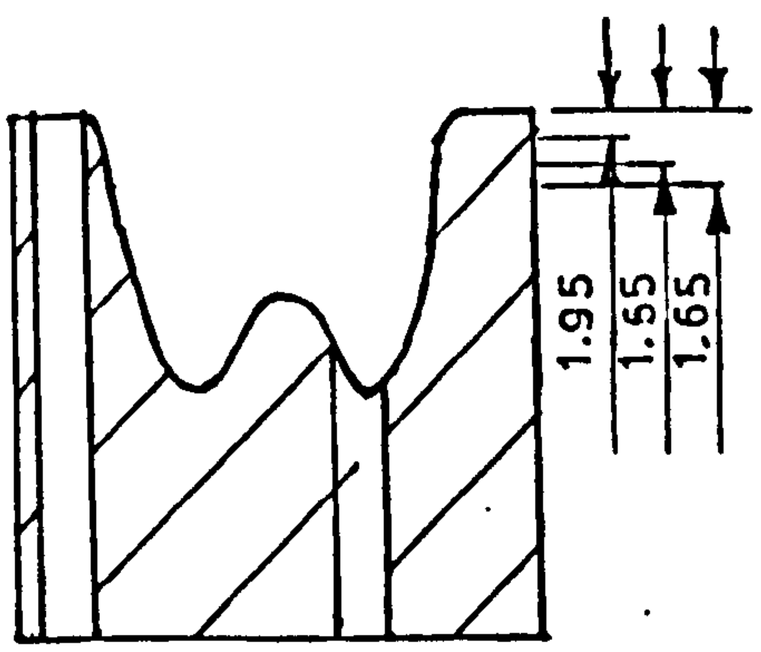

SECTION OF THE MACHINED SPECIMEN SHOWING POSITIONS WHERE THE DIAMETERS OF THE HOLE WERE MEASURED

FIG. 4.4

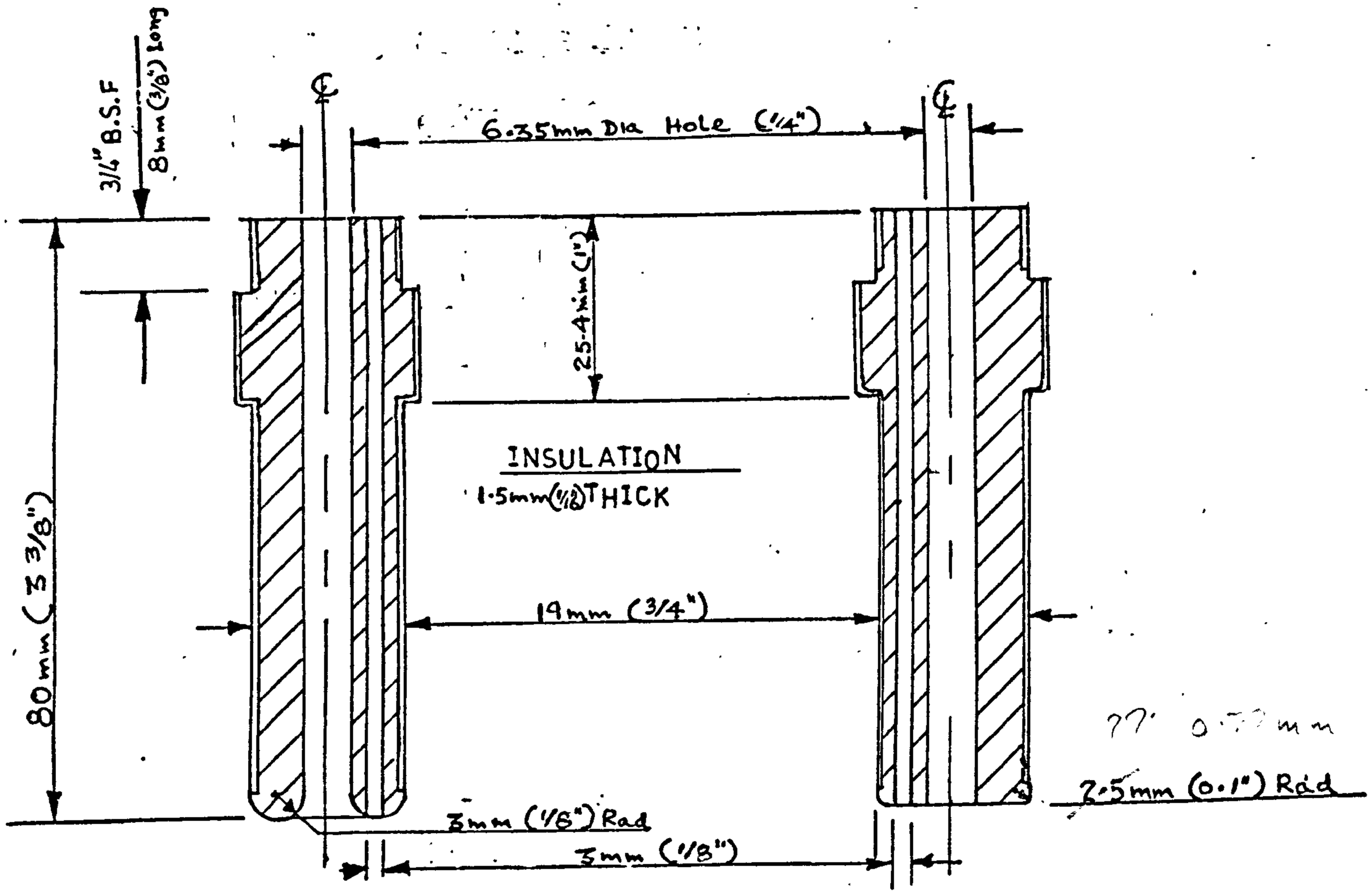

SECTION X-X

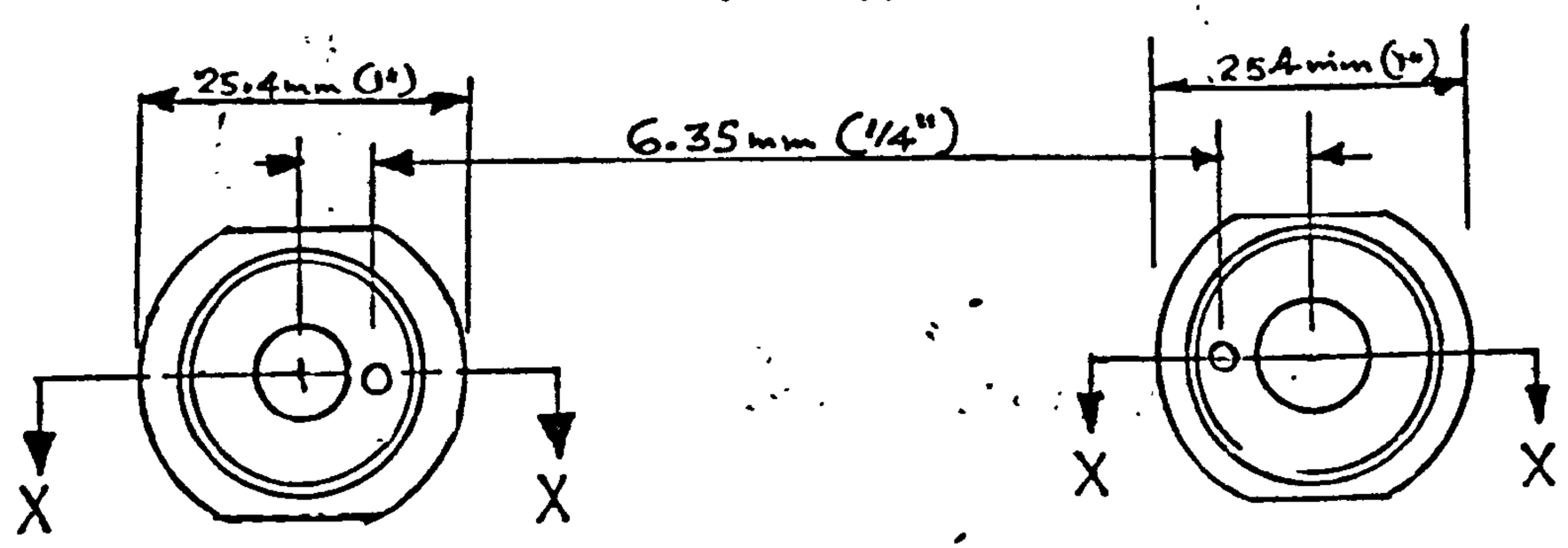

ECM DRILLING TOOLS
SHOWING NOMINAL DIMENSIONS

FIG.45

electrolyte was kept within ± 1°C of the desired value.

4.2 ECM CELL

Fig. (4.3) shows a drawing of the ECM cell. The tubular cell wall was machined from a Tufnol tube (3). An 'O' ring inserted in a recess on the small bore side of the cell prevented any electrolyte leaking from the tool holder side. The depth of the larger bore at the opposite end was such that when the cell was clamped in position by the four tie rods the work piece was held firmly on the work piece holder plate making a good electrical contact. An 'O' ring in the bottom face of the Tufnol tube prevented any electrolyte leaking. Thus the cell was completely leak proof during test runs.

The tool holder consisted of two parts, the shank (2) machined out of brass into which the tool was screwed and a stainless steel flange which was fixed to a similar flange on the machine ram (1) by four bolts. By using slots in the machine flange it was possible to orientate the tool holder assembly so that the thermistor in the tool was exactly opposite a pre-drilled hole in the work piece. This hole in the work piece was necessary to prevent the thermistor ramming on to the work piece during setting up the cell and during machining.

The work piece holder had a ridged circular base to accommodate the base of the Tufnol cell, and was welded on to a stainless steel bar (7) which was held in a fixture to the machine frame. Two dowel pins on the circular

base were used to locate the work piece in position.

4.3 SPECIMENS

Specimens were made out of austenitic stainless steel bars (B.S. EN58J) Fig. (4.4), of diameter 38 mm and of length 38 mm. Two small holes were drilled through the specimen for locating pins. One of these holes was alined with the thermistor in the tool and both used for location.

4.4 ECM DRILLING TOOLS

Two geometries of tools were used in drilling tests as shown in Fig. (4.5). The tools machined from brass bar, were threaded at the end to screw into the tool holder. The leading edge of tool (a) was rounded to give the rib a semi circular shape in section. The leading edge of tool (b) was machined to give the rib a flat leading surface and a small (0.75 mm) radius at the corner Fig. (4.6). A small hole of diameter 2 mm was drilled through the centre of the rib to accommodate the thermistor assembly which was used to measure the temperature of the electrolyte in the electrode gap. The drilled hole at the centre was for electrolyte flow.

To prevent stray machining, the sides of the tool had to be electrically insulated. Two types of insulating material were used.

1. Araldite AV 121 mixed with hardener HY 951 in appropriate proportions was applied to the outer surface of the tool and cured in an oven at $70^{o}C$ for 4 hours. The tool was then turned on a lathe to obtain the

required size.

2. A Nylon Coating was used as insulation, The leading edge of the tool was masked and the tool was heated to a temperature of 350^{o} - 400^{o}C in an oven. The tool was then held in a stream of nylon powder which gave an even coating all over unmasked surfaces.

Both coatings were satisfactory during the test runs but the nylon coating appeared to have a better life over the araldite.

4.4.1 Temperature Measurement

The temperatures of the electrolyte at inlet to the cell at outlet from the cell and in the gap between tool and work piece during machining were monitored by miniature glass bead thermistors (Mullard VA3706) incorporated in electrical bridge circuits. Details of the electrical bridge circuits are given in Appendix (A1). The glass bead thermistors were mounted in brass adaptors which screwed into the pipe lines for inlet and outlet temperature measurement. The thermistor which was used to measure the temperature of the electrolyte in the electrode gap was positioned in the small hole drilled through the centre of the rib of the tool so that only the glass bead protruded from the leading edge of the tool. Since the thermistor was located in the middle of the rib, the temperature recorded by this thermistor was the temperature of the electrolyte as it passes the frontal equilibrium gap region of the inter electrode space.

Considerable difficulty was experienced in preventing the electrolyte coming into contact with the bare leads of the thermistors. These wires had to be insulated from each other and from the electrolyte. The insulating material had to withstand the corrosiveness and high pressure of the electrolyte. Initially Araldite AV121 and hardener HY951 was used to coat the bare wires and cured according to manufacturers instructions. The prepared thermistors were then placed in the base of the adaptors and the space was filled with the same Araldite and cured to give strength and rigidity. But this method was not successful, as at high pressures electrolyte leaked through cracks in the insulation making contact with the wires. The two leads of the thermistor and electrolyte formed a cell whose voltage distorted the trace from the ultraviolet recorder.

In another attempt to overcome the leakage problem thermistors were placed inside drawn glass tubes. The tubes were filled with Araldite CY219 and hardener HY219 mixed in appropriate proportions together with accelerator DY219, which was allowed to set at room temperature. Thermistors assembled in this way failed to operate successfully as the glass tube cracked due to the different expansions of araldite and glass at elevated temperatures (40 - 55^{o}C), letting electrolyte in which made contact with thermistor leads. Several other different ways of sealing such as varnishing the leads, using silicon rubber, fusing P.V.C. sleeves on to the bare

thermistor leads were tried out, but did not provide an answer to the leaking problem of the electrolyte. Eventually a method used by the Civil Engineering Department gave termistor probes with a reasonable life. A general purpose araldite AV100 and hardener HV100 was used. First the extension wires were soldered and cleaned as before, and equal amounts of HV100 and AV100 were mixed with some trichloroethaline. This made a less viscous mixture which was easily applied to the wires of the thermistors. The solvent evaporated quickly and left a thin coating of resin which was cured at room temperature for 24 hours. A further coating of araldite was applied and cured in an oven at a temperature of 70°C. to provide the necessary strength. Thermistors prepared in this manner were then set in the brass adaptors as before. The thermistor for mounting in the tool, for the recording of temperature in the electrode gap was insulated in the same way and then forced into a small flexible plastic tube. This was positioned in the tool so that only the sensing bead of the thermistor protruded from the leading surface of the tool. Thermistors prepared in this manner operated successfully for about 10 test runs.

4.4.2 Pressure Measurement

To record fluctuation in inlet and outlet pressures of the electrolyte Bell and Howell pressure transducers type 4-366 were installed at inlet and outlet ports of the cell.

The transducers have an all welded case of Armco 17-4PH stainless steel. The diaphragm which senses the pressure was capable of withstanding a wide variety of corrosive fluids at all pressure changes.

The transducers works on a strain gauge bridge principle. With an applied voltage of 10V DC a linear output up to 40 mV for the nominal range is obtained. Transducers of nominal ranges 34.48×10^5 N/m^2 and 17.24×10^5 N/m^2 were used for input and outlet pressures respectively.

4.4.3 Machining Current Measurement

To record the machining current a 50 mV 500 amp shunt was connected to the end of the negative lead of the power supply cable at the tool end of the ECM cell. The output from the 50 mV shunt was fed into the U.V. recorder.

4.4.4 Machining Voltage

To record the cell voltage, i.e. the voltage drop across the tool holder and the work holder, the voltage across the electrodes was fed into the U.V. recorder.

4.4.5 Flow Measurement

A Rhodes flow transmitter model R.T. was used on the high pressure side of the cell to record electrolyte flow rate into the cell although the makers of this instrument recommend insertion in the low pressure side. However the electrolyte which flows out from the cell

contains liberated gasses such as hydrogen which would affect the meter reading.

The flow transmitter consists of a paddle which causes a reed switch to open and close each revolution. The Rhodes model PA flow meter supplied with the transmitter converts pulses from the reed switch to a non-linear recording on a 1 mA moving coil meter. A U.V. recorder galvanometer with a suitable matching circuit was used in series with the moving coil meter to provide a permanent record of flow.

4.4.6 Tool Feed Rate Measurement

To record tool feed rate similar circuitry to that of flow recording was used. A small 'propellor' with four mild steel blades at right angles to each other was fixed to the shaft of the feed motor of the E.C. machine. The blades moved through a gap between a permanent magnet and a reed switch from which an analogue output was obtained in the same way as with the flow meter. The feed rate was kept constant for each experiment and so was not recorded on the U.V. recorder.

For each machining parameter the traces from the U.V. recorder obtained as explained above were calibrated and scales were made to read directly the recorded machining parameters during each test run.

CHAPTER V

EXPERIMENTAL WORK

5.1 PURPOSE OF EXPERIMENTAL WORK

Blind hole electrochemical drilling tests were carried out to compare how accurately the work profile and the overcut were predicted by the mathematical model considering only the primary current distribution.

Test specimens were made out of EN58J stainless steel Fig. (5.1) which was chosen because it is a readily available chromium nickel alloy which presents some difficulties for conventional machining. Both sodium chloride and sodium nitrate electrolytes were chosen since both of these electrolytes are widely used in industry, apart from this sodium chloride electrolyte exhibits about 100% current efficiency but sodium nitrate is inefficient Konig (10). Therefore the machined work profile obtained using sodium chloride electrolyte should closely resemble the mathematical Primary Current Model but there could be a discrepancy with sodium nitrate. Of the passivating electrolytes sodium nitrate electrolyte is the most widely used industrially. The purpose of using this electrolyte is to compare its performance with that of sodium chloride electrolyte and hence to determine whether efficiency and polarization are actually important shaping parameters in practice.

5.2 PREPARATION OF ELECTROLYTE

The electrolytes were prepared using commercial grade salts dissolved in tap water. The concentrations were measured and adjusted using specific gravity readings

AUSTENTIC STAINLESS STEEL WITH MOLYBDENUM SIMILAR SPECIFICATIONS:- BRITISH EN58J, AMERICAN I.S.I 316, GERMAN S.E.L. 4436

Sp. Gravity 7.98

EN58J Composition Percentage by weight		Spectographic Analysis Composition Percentage by Weight
CARBON	0.07 max.	0.06
SILICON	0.20/1.0	0.42
MANGANESE	0.50/2.0	1.47
CHROMIUM	16.50/18.50	17.5
NICKEL	10.0/13.0	10.5
MOLYBDENUM	2.25/3.0	2.3
IRON	REST	REST
SULPHUR	0.030 max.	0.024
PHOSPHOROUS	0.045 max.	0.033

FIG. 5.1

and appropriate nomograms Appendix (A5). It was found necessary to take care in assessing that all of the salt in the tank was actually in solution otherwise the concentration rose during machining.

5.3 PREPARATION OF MACHINING CELL

The two drilled holes in the specimen for the locating dowels were deburred with a file. The specimen was then washed thoroughly, dried and weighed, and then located on the dowels on the work holder. The feed motor clutch was disengaged and the tool was manually fed downwards until the gap between the tool and the top surface of the workpiece was a few millimeters. The positions of both tool holder and the work holder were adjusted until the bead of the thermistor was located exactly opposite the pre-drilled hole in the workpiece.

To set the initial machining gap a multimeter was connected across the cell. To make sure the specimen was properly set the tool was slowly fed downwards till it pressed the specimen hard against the work holder. The tool was then moved up and fed to the workpiece slowly till it made contact which was shown on the multimeter by a full scale deflection on the Ohm scale. The reading on a dial indicator which was used to measure the amount of tool feed was noted. In order to place the Tufnol Cell which acts as the pressure chamber in position the tool assembley was moved up to the highest point. The cell was carefully placed over the work holder, the tool assembly was fed down into the cell and the cell was clamped in position by

bolting it on to the work holder Fig. (4.4). Knowing the reading of the dial indicator when the tool touched the workpiece, the initial gap was set for 0.38 mm.

5.4 OPERATION OF THE MACHINE

After the tool position with respect to the work-piece, had been determined the multimeter was connected to read the Cell voltage and the direct current switch was closed to connect the rectifier with the machining cell but the power was not switched on at this stage. The pump motor was switched on and the inflow valve was opened slowly until sufficient flow was obtained through the cell indicated by the flow rate meter. The machined head was manually readjusted so that the initial machining gap was 0.38 mm. The clutch was engaged, both the machining current rectifier switch and the tool feed motor switch were closed simultaneously. The voltage from the rectifier set was adjusted to give the required cell voltage. Machining was continued for about 10 mm of the tool feed.

During machining the flow rate of the electrolyte dropped sharply. The by-pass valve was gradually closed to give a back pressure of 138 KN/m^2 and the inlet valve was opened to obtain at least sufficient electrolyte flow into the cell to prevent machining failure. By experience this was found to be at least 5 ℓ/mm. The temperature of the electrolyte at the inlet to the machining cell, the temperature of the electrolyte at the outlet from the machining cell and the temperature of the electrolyte in

the machining gap were recorded using an ultraviolet recorder during the entire test run. The machining parameters such as cell voltage, machining current, tool feed rate, forward pressure and back pressure were also recorded.

5.5 INITIAL TEST RUNS AND MODIFICATIONS

To find any faults in the system and establish the capacity of the machine some initial tests were essential. It was decided to carry out the first few runs with sodium nitrate electrolyte, since the maximum tool feed velocity determined using sodium nitrate electrolyte is generally lower than that obtained for sodium chloride electrolyte for the same machining parameters.

Examination of the recorded information of first few test trials revealed that a large number of small scale sparks occurred during the test runs. Occurrence of sparks was shown on the chart as sudden jumps in the machining current trace, even though the rectifier contact ammeter was preset to trigger off when the machining current exceeded a lower value than reached by the peaks. The short period of high current during sparking was not sufficient to switch off the machine.

Inspection of the machined surface showed uneven machining. This was attributed to particles of dirt in the electrolytic system settling on the machining surface during the test run. These dirt particles were impurities from the salt itself and also disintegrated parts of the rubber starter of the mono pump. In some cases these

rubber parts stuck on to the machining surface forming an insulated barrier between the tool electrode and the work electrode which prevented further machining of that particular area. This caused the tool to ram on to the work surface with the result of a severe spark which did trigger the contact ammeter cut out. In some instances the tool was severely damaged and had to be replaced by a new one. To prevent dirt and particles of the rubber starter entering the cell a filter unit was fitted at the outlet from the pump. This unit contained a hollow cylindrical wire gauze element which was capable of giving a relatively dirt free electrolyte. The pressure loss due to the introduction of the filtering unit was as much as 100 KN/m^2 at the flow rates used. Examination of the surface of a specimen machined after the installation of the filter unit showed that the bottom surface was marked with striations. These were attributed to electrolyte starvation in these regions during machining. Chickamori et al (I9) has stated that during ECM negative pressure zones can occur in the electrode gap which prevents machining in these areas. A way of reducing this is to apply some back pressure by throttling the outlet of the cell. As the application of back pressure reduces the available pressure head for electrolyte flow to the machining cell a compromise has to be reached. A value of 138 KN/m^2 was used for all test runs. This back pressure was maintained from the start to finish of each test run by manually controlling the valve at the outlet

of the machining cell as necessary.

Two tool geometries were used during the tests, these were

(a) A tool having a toroidal leading edge, and

(b) A tool having a flat leading edge,

with a small corner radius which were shown in Fig. (4.6).

5.6 EQUILIBRIUM GAP MEASUREMENT

The machine was stopped at the end of the test run. The reading on the dial indicator which was used to measure the amount of tool feed was noted. The multimeter which was connected across the ECM cell to read the machining voltage was switched on to a milliampere scale. The electrolyte in the electrode gap, tool and the workpiece formed a cell whose current was sufficient to give a large deflection on the multimeter. The tool was then slowly fed downwards until the meter showed a sudden fall in current due to the tool coming into contact with the workpiece. The reading on the dial indicator was noted, the difference between the two readings gave the size of the equilibrium gap. This way of checking the contact between the tool and the workpiece was found to be more reliable than checking for the continuity as the tool comes to contact with the workpiece with the multimeter on a resistance range.

5.7 DETERMINATION OF THE DIAMETER OF THE DRILLED HOLE

To measure the overcut of the electrochemically drilled specimens, diameters of the drilled holes were

measured using a Universal Measuring Machine Model number MU-214B manufactured by Societe Genevose d'Instruments de Physiqe of Switzerland. This instrument was capable of reading dimensions of a specimen to $\pm$ 0.0005 mm. For measurement of diameters of the drilled holes the 'Feeler Microscope' facility was used. The microscope which was provided with a 4-station indexing collar for rotating it accurately through 90^{o} indicates the relative positions of the probe which was fitted with a spherical-ended feeler of 2 mm diameter. In use the probe exerted a force of approximately 6 grams. The specimen whose diameter was to be determined was set on the table and secured in position with plasticine. The feeler was brought down inside the drilled hole to the desired depth at which the diameter was to be determined. The table was then moved so that the feeler came into contact with the machined surface. Looking in the eye piece the reversing point of the probe was determined when the table was transversed. The position of the table was taken using the reading on microscope of the longitudinal scale. The same operation was repeated on the opposite face of the drilled hole. Care was taken not to ram the feeler against the pip of the specimen which was at the middle of the hole. Knowing the diameter of the spherical end of the feeler the required diameter of the drilled specimen was determined. The diameter of the drilled specimen was measured at three depths Fig. (4.5), which were 1.95 mm, 3.2 mm, and 4.85 mm respectively from the

top surface. Most of the specimens drilled using sodium chloride electrolyte at a voltage of 16 or 20 and some of the specimens drilled using sodium nitrate electrolyte at 20 volts had their machined surfaces pitted badly. In these cases the Universal Measuring Machine was too sensitive for the measurement of the diameter and so a Vernier Calliper was used.

5.8 TRACING THE WORK PROFILE

In order to check the accuracy of the theoretical model in predicting the profile of the electrochemically machined surface, it was necessary to reproduce the profile of the drilled hole obtained by sectioning it through the symmetrical axis. To obtain a magnified picture of a sectioned specimen, a Nikon Profile projector Model 5A was used. The image of the specimen was obtained on the ground glass screen, the magnifying ratios being held accurate over the whole area of the image.

5.8.1 Preparation of the Specimen

Sectioning a stainless steel specimen to give a burr free profile on a diameter of a drilled cavity is not easy. The drilled hole was not always positioned at the centre of the specimen. Moreover the position of the cavity changed each time the tool holder had to be dismantled to insert new thermistors. However as the gap thermistor was located exactly opposite a locating hole, a section of the specimen through the plane formed by the locating holes gave a profile either on a diameter

or very close to it.

After the specimen had been milled to expose the cavity profile, the boundary of the electrochemically drilled surface had to be deburred. This resulted in giving a deformed projected outline of the profile which was amplified by the magnification used in obtaining the projected profile. To overcome the above problem and to minimize the machining time involved in sectioning specimens the shapes of the drilled holes were cast in 'Dental' plaster.

The surface of the drilled hole which was to be cast was thinly greased to ease removing the plaster cast. Excess plaster was poured to form a ridge on the top surface which could be used to pull the cast out when it was set and ready. Initially only a few specimens were cast but as the method was very successful, all specimens were eventually cast in this manner to obtain the required profile. When using a plaster cast transmitted illumination was used to project the profile in the plane formed by the two locating holes. As the cases were not sectioned, the projected profile was automatically a diameter when focused to give the largest shadow.

The projected profiles were permanently recorded by tracing manually on to tracing paper. All tracings were made to 20:1 magnification in order to get the whole outline of the profile on A4 size paper. First the tool profile and the computed work profile were traced on to the paper which was placed on the

screen of the profile projector so that the axis of the tool was in coincidence with a vertical grid line of the screen Fig. (5.6). The casting was set on the stage of the projector so that the plane formed by locating holes was more or less parallel to the stage and was secured in that position with plasticine. The plaster cast was moved until the points on the profile at depth 1.95 mm, 3.2 mm and 4.85 mm from the top were located at respective measured diameter from the axis, Section (5.7). This ensured that the traced profile was the true machined profile relative to tool position.

CHAPTER VI

ANALYSIS OF EXPERIMENTAL RESULTS

6.1 DRILLING TEST RESULTS

The drilling tests were described in Chapter 5.

6.1.1 Metal removal rates

The average equilibrium volumetric metal removal rate for the work piece material (EN58J) when using both electrolytes sodium chloride and sodium nitrate electrolyte was calculated from the product of the tool feed rate and the area of cross-section of the electrochemically drilled hole in the specimen. The theoretical volumetric removable rates cannot be computed with certainty because the actual dissolution reactions are not known beyond doubt. As the metal removal rate varied with tool feed rate being a function of current density, and kind of electrolyte (NaCl; $NaNO_3$), the two variables were plotted against each other to find their functional relationship, Fig. 6.1, Fig. 6.2. The average current density was calculated by dividing the current at steady state machining by the area of cross-section of the machined hole.

6.1.2 Specific volumetric metal removal rate

Fig. 6.1 and Fig. 6.2 show the plots of average current density at steady state ECM vs tool feed rate for NaCl and $NaNO_3$ electrolytes. Within the experimental range of current density used, the feed rate showed a linear relationship with current density for both NaCl and $NaNO_3$. This result would be expected from the work

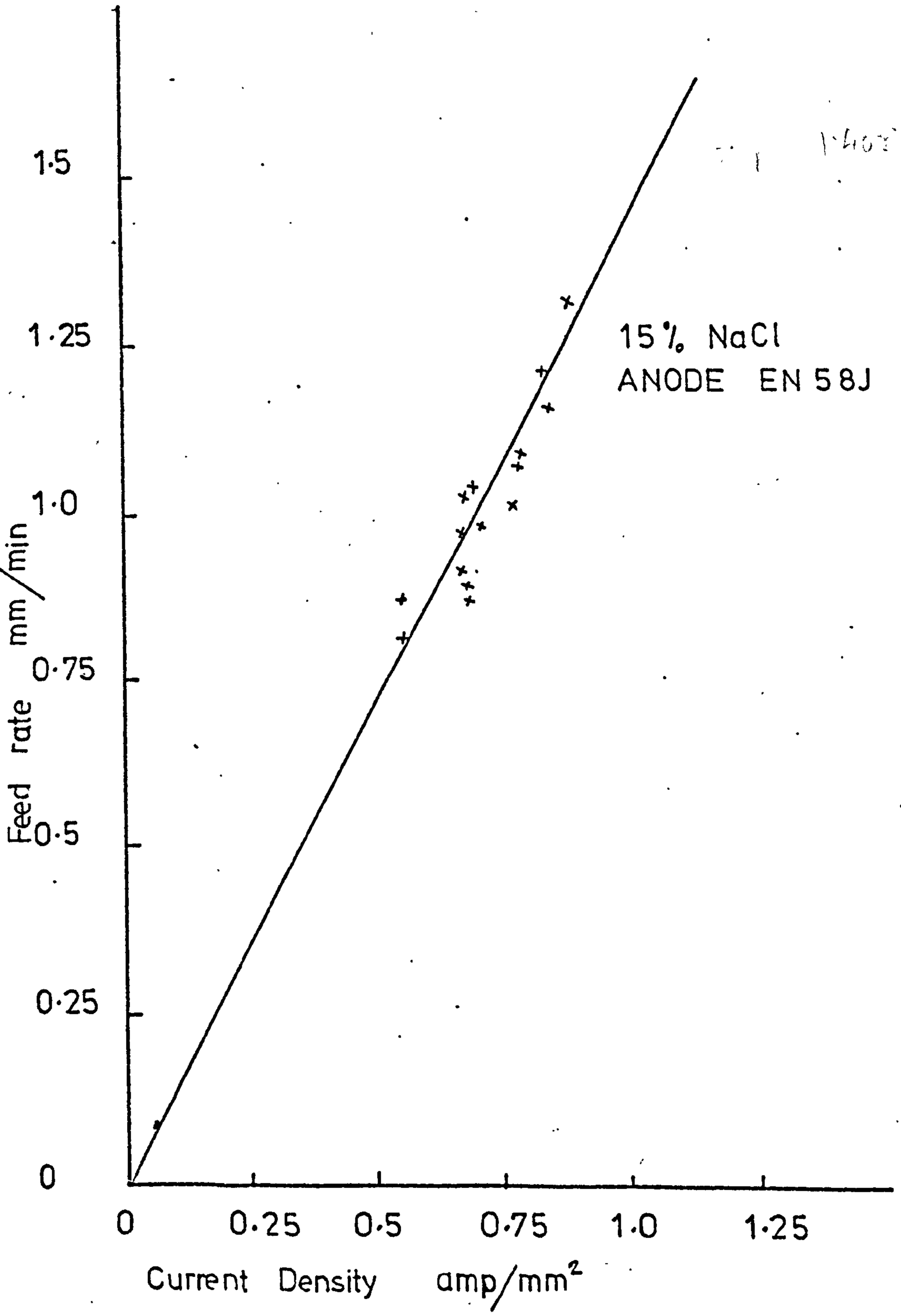
1·5
1·25
1·0
0·75
0·5
0·25
0
Feed rate mm/min
0
0·25
0·5
0·75
1·0
1·25
Current Density amp/mm²
15% NaCl
ANODE EN 58J

FIG 6.1

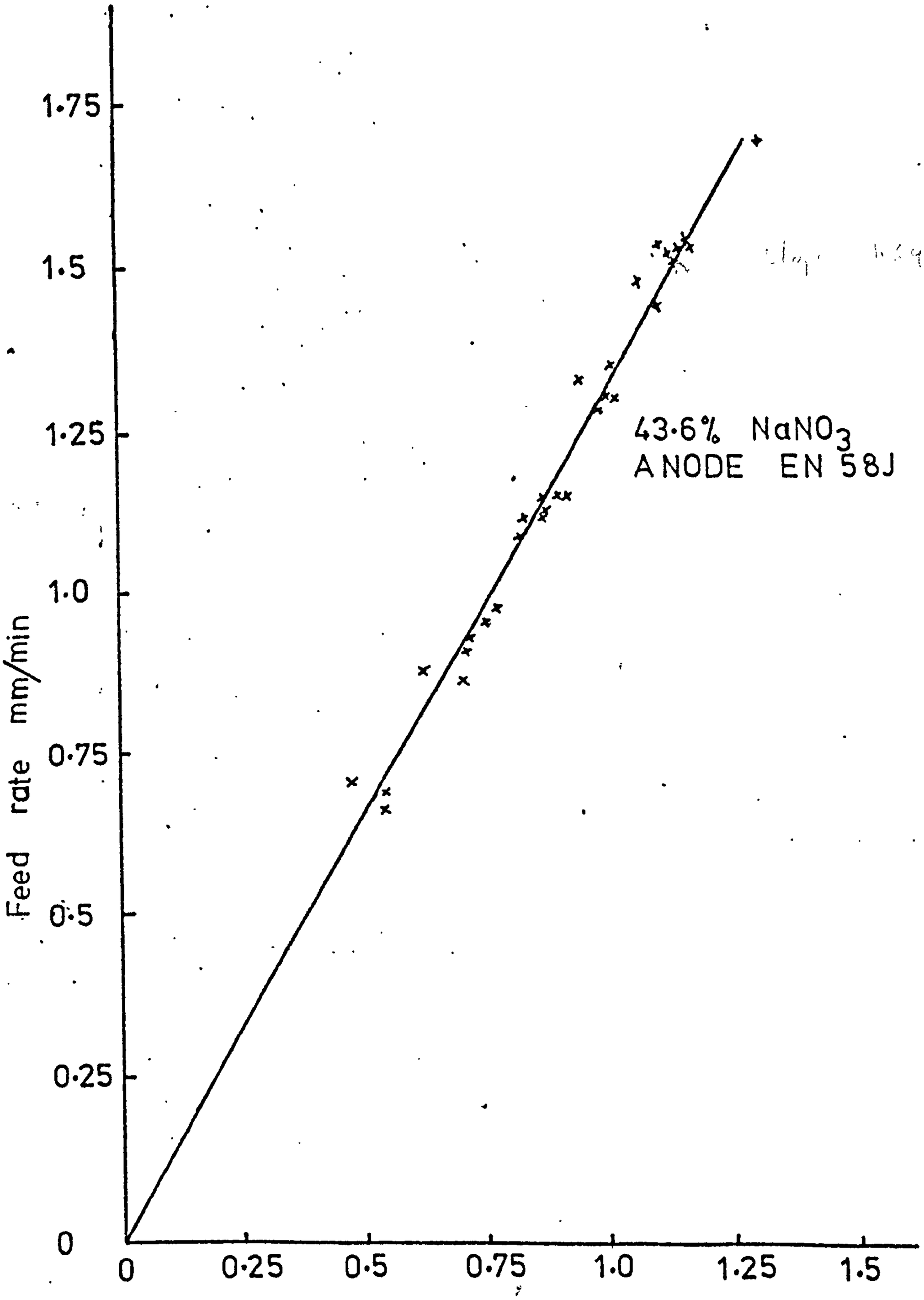
1·75
1·5
1·25
1·0
0·75
0·5
0·25
0
mm/min
Feed rate
0
0·25
0·5
0·75
1·0
1·25
1·5
Current Density amp/mm²
43·6% NaNO3
ANODE EN 58J

FIG 6.2

of Konig (17) and Muzaffamuddin (33) for NaCl as both showed that dissolution current efficiency remained approximately constant. However, for $NaNO_3$ both these authors showed that efficiency increased non linearly with current density starting from low values $\simeq$ 0.2 at low current densities. However, the present results correlate well with these authors' results over the limited range involved. As shown by Brasor et al. (32) , Konig (10) with low salt concentrations, the feed rate vs current curve for sodium nitrate does not pass through the origin but makes a finite intercept on the metal removal rate axis (tool feed rate), which becomes smaller with the increase in salt concentration. In the present experiments a high concentration was used and the curve passes through the origin.

The gradients of the graphs, Fig. 6.1 and Fig. 6.2 which is $\frac{\text{metal removal rate}}{\text{current density}}$ is the specific volumetric metal removal rate of anode material for the particular electrode electrolyte combination. The values of specific metal removal rates obtained from graphs Fig. 6.1 and Fig. 6.2 were 0.02408 mm/Amp.Sec. for sodium chloride electrolyte and 0.02187 mm/Amp.sec. for 43.6% sodium nitrate electrolyte. One should expect such close values for both electrolytes because of high salt concentration in sodium nitrate electrolyte. König (10) machining a similar stainless steel obtained a value of 0.033 mm/Amp.sec. for sodium chloride electrolyte and 0.0216 mm/Amp.sec. for 20% sodium nitrate electrolyte. Barsor et al. (32) obtained a value

of 0.034 mm/Amp.sec for both electrolytes independent of concentration of sodium nitrate electrolyte. These discrepancies could be explained by differences in composition of stainless steel machined by individual authors and the purity of the electrolyte used. For example, Chikamori et al. (19) has shown that presence of small amounts of sodium chloride in sodium nitrate electrolyte alters the machining properties of sodium nitrate. As clearly explained by Larsson (5) the theoretical calculation of specific metal removal rates is uncertain.

Because of this uncertainty the empirical values of specific volumetric metal removal rates obtained in the drilling tests were used in obtaining the erosion vectors at nodal points along the work surface in the theoretical model.

6.1.3 Current Efficiency

Current efficiency is defined as the ratio of actual metal rate to the theoretical removal rate. It has been well established that with passivating electrolytes such as $NaNO_3$ or $NaClO_3$, current efficiency changes with current density giving lower current efficiencies at lower current densities. A good electrolyte should have higher current efficiencies at higher current densities and lower current efficiencies at lower current density areas. Also it is easier to achieve good dimensional control of the work piece.

It is a well known fact that NaCl electrolyte

machines at 100% current efficiency or more. The different values of current efficiencies found by Cuthbertson and Turner, (34) Mao, (4) may be due to incorrect calculations of theoretical metal removal rates as explained by Larsson. (5) The current efficiency when using $NaNO_3$ electrolyte is greatly influenced by the salt concentration, the solution temperature and the current density. (10) Since current density is different at different points over the work surface, it was necessary for the present work to find the form of relationship between current density and current efficiency when using $NaNO_3$ electrolyte. In order to find current efficiency it was necessary to have a theoretical value of specific metal removal rate as a standard for comparison. Because of the difficulty of evaluating a true theoretical rate, a value of 1.42 grams/amp.min was taken for EN58J so that the efficiency was numerically the same as Königs (10) efficiency for the same current density. The actual metal removal rate was found by the product of the area of cross-section of the drilled hole by the corresponding tool feed rate.

The curve obtained for current efficiency 'η' vs current density 'J' is shown in Fig. 6.3. The part of the curve represented by the continuous line represents that area covered by experimental results. The rest of the curve has been obtained from the much wider range of results obtained by König (10,33)and Muzaffaruddin.
At higher current densities the curve was parallel to the

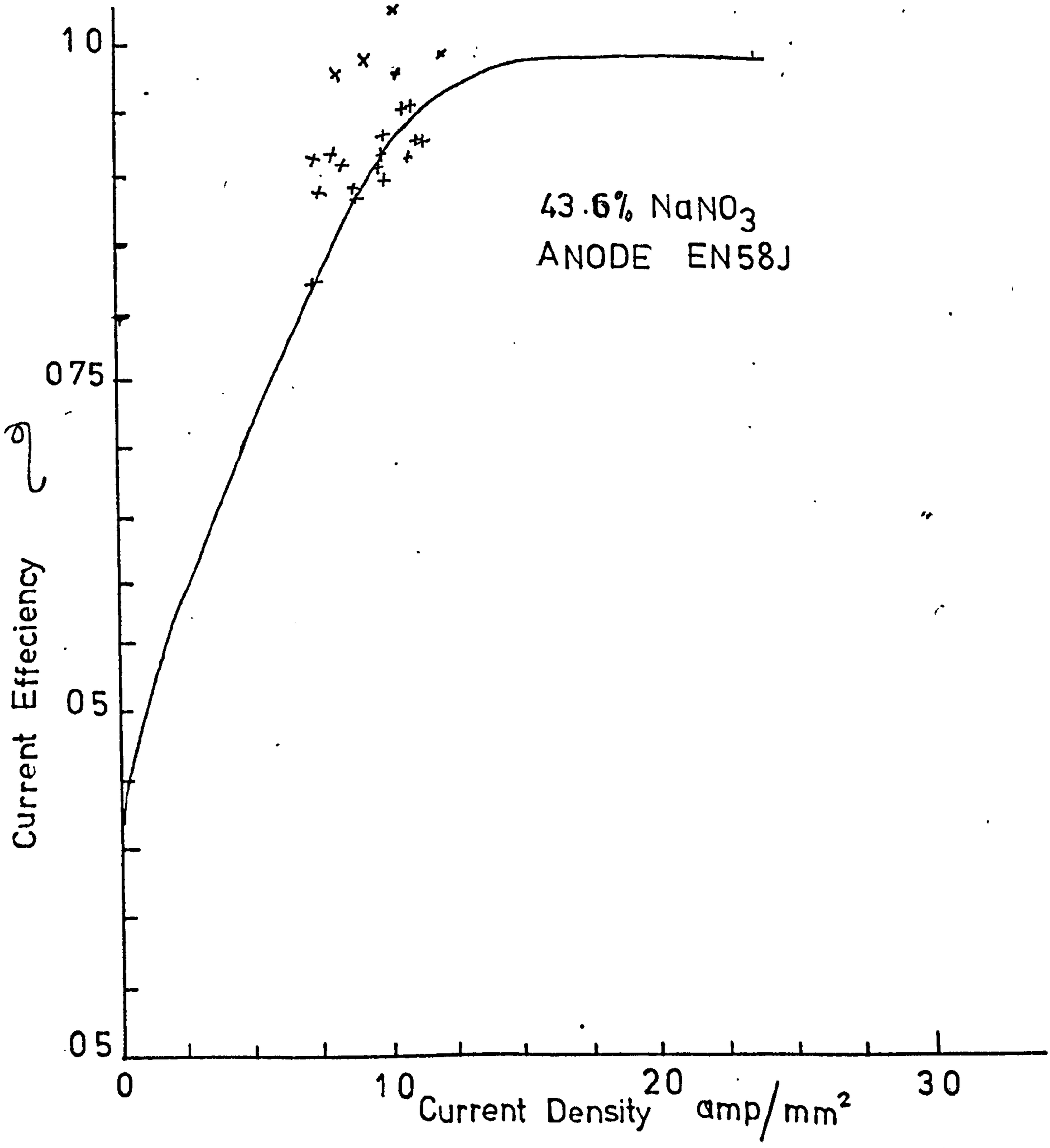
10
075
05
05
0
10
20
30
Current Effeciency η
Current Density amp/mm²
43.6% NaNO3
ANODE EN58J

FIG 6.3

current density axis giving constant value for 'η' above 2.6 amp/mm^2.

The curve for current efficiency Fig. (6.3) obtained was best represented by the algebraic expressions obtained by least square polynomials giving

$$\eta = 0.45834 + 0.577117 \times 'J' - 0.11525 \times J^2$$

for current densities ranging from zero up to 1.2 amp/mm^2 and

$$\eta = 0.002785 \times J + 0.974413$$

for current densities above 1.2 amps/mm^2 where J is the local current density.

6.1.4 Orthogonal Equilibrium Gap

The frontal equilibrium gap or the orthogonal equilibrium gap is the fundamental dimension in E.C.M., its importance being discussed in section 1.8.1. Fig. 6.4 shows the variation in orthogonal equilibrium gap calculated from the basic formula 1.11 against feed rate for both NaCl electrolyte and $NaNO_3$ electrolyte at cell voltage of 16 volts for temperatures 40^{o}C and 55^{o}C.

From these graphs it was evident that at the average machining current densities encountered in the drilling test runs the theoretical orthogonal equilibrium gaps for both the electrolytes were the same. But at lower current densities the gaps deviated by a small amount but this was considered negligible. Indeed the concentrations of 15%

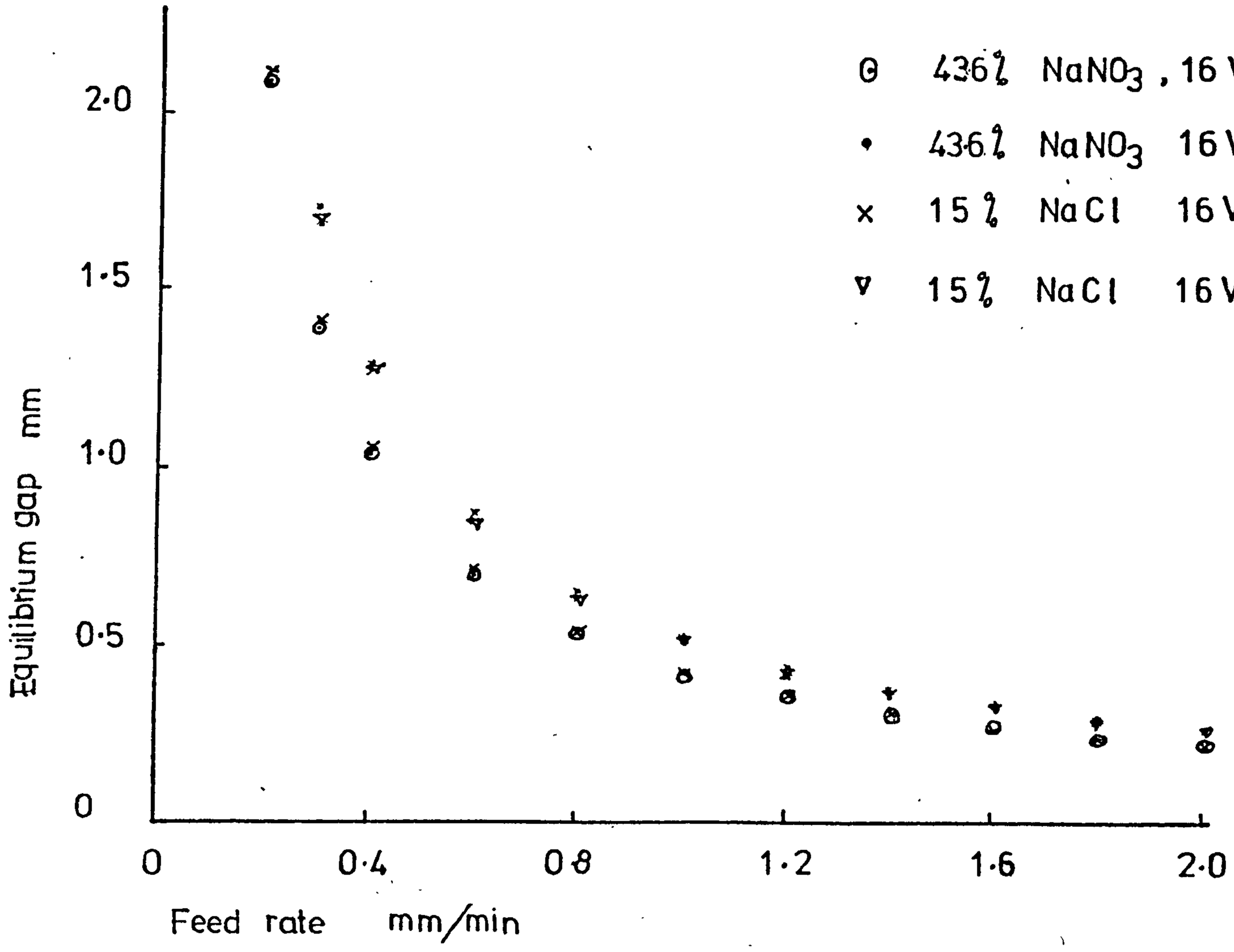
θ 43·6% NaNO3 , 16 VOLTS, 40°C
• 43·6% NaNO3 16 VOLTS, 55°C
× 15% NaCl 16 VOLTS, 40°C
▽ 15% NaCl 16 VOLTS, 55°C
Equilibrium gap mm
2·0
1·5
1·0
0·5
0
0
0·4
0·8
1·2
1·6
2·0
Feed rate mm/min

FIG 6.4

(w/w) for NaCl electrolyte and 43.6% (w/w) for $NaNO_3$ electrolyte used in drilling test runs were chosen to give similar gaps. Further to this the frontal equilibrium gap diminished asymptotically with increase in feed rate and the change in these gap dimensions above feed rate 1.6mm/min were very small. This was one of the reasons for the difficulties encountered in measuring the frontal equilibrium gap at higher feed rates described in section 5.6. With increase in temperature the gap increased, due to increased conductivity. However, for both electrolytes the difference in increased gap size for the same machining parameters was negligible.

Figs. 6.5 to 6.10 show the relationship between equilibrium gap and feed rate assessed in various ways for the sodium chloride and sodium nitrate solutions at three different voltages for the hemispherical tool and two voltages for the straight edge tool section 5.6. The solid line represents the relationship from equation 1.11. Experimental points are shown which indicate the gap measured by closing the tool into the work piece at the end of each experiment. The size of the plaster model taken of each cavity, with respect to the known tool movement gave another value while that predicted by the computer model is also shown.

The equilibrium gaps calculated using equation 1.11 gave slightly bigger gap sizes than those obtained by the computer model. Nilson (35) found that his theoretical model also gave smaller equilibrium gaps than those

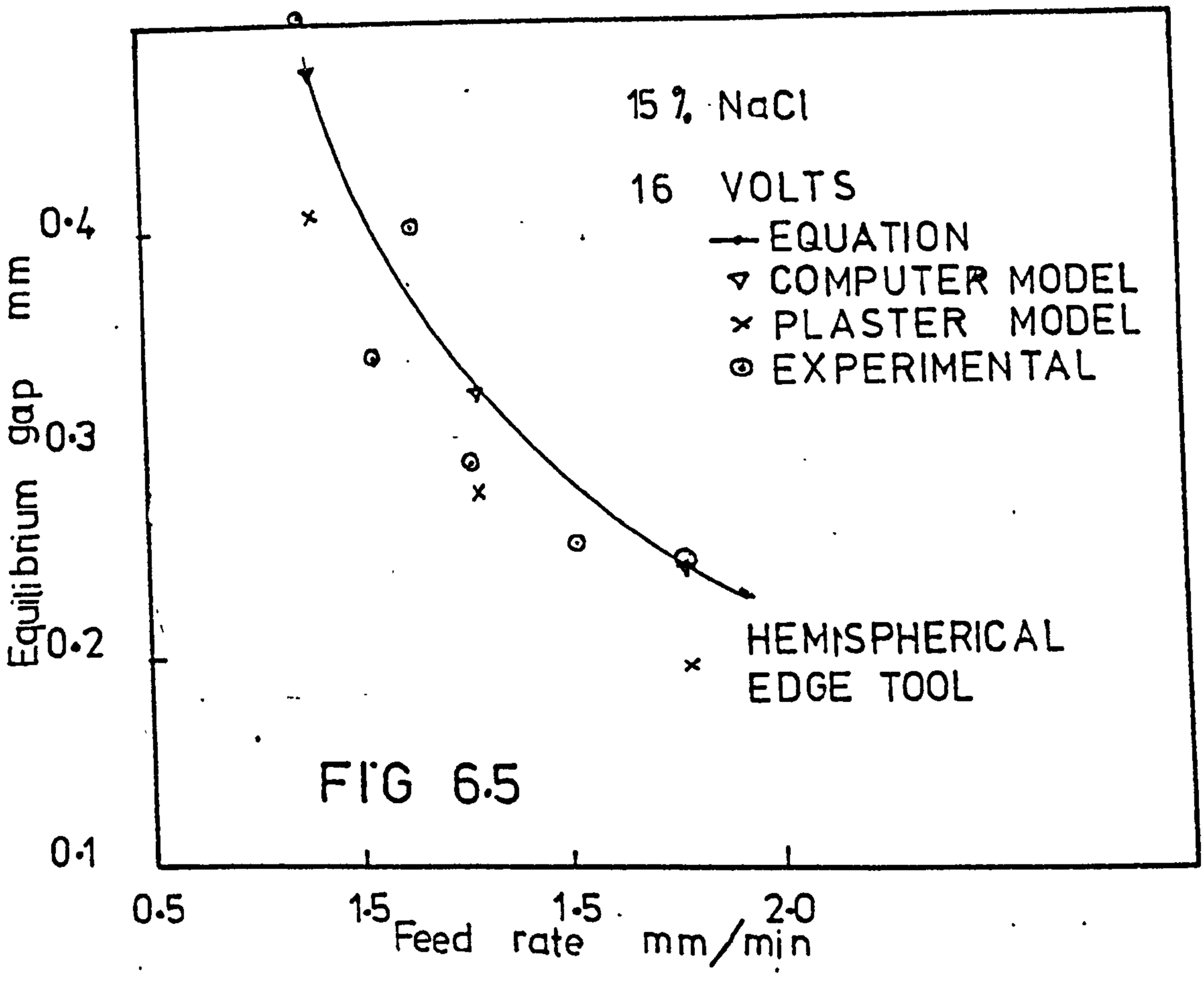
15 % NaCl
16 VOLTS
EQUATION
COMPUTER MODEL
PLASTER MODEL
EXPERIMENTAL
HEMISPHERICAL EDGE TOOL
Equilibrium gap mm
0·4
0·3
0·2
0·1
0·5
1·5
1·5
2·0
Feed rate mm/min

FIG 6.5

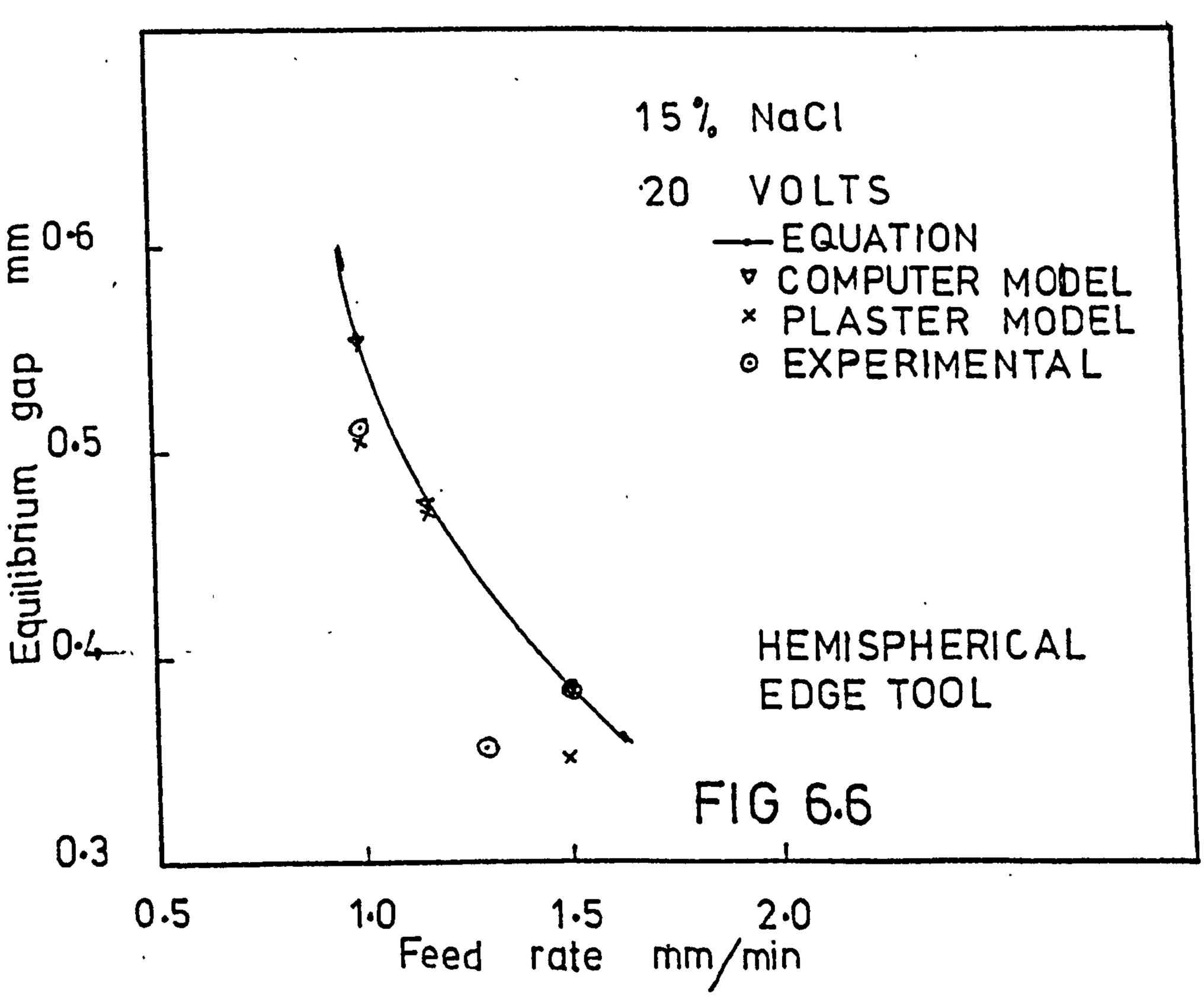
15 % NaCl
20 VOLTS
EQUATION
COMPUTER MODEL
PLASTER MODEL
EXPERIMENTAL
HEMISPHERICAL EDGE TOOL
Equilibrium gap mm
0·6
0·5
0·4
0·3
0·5
1·0
1·5
2·0
Feed rate mm/min

FIG 6.6

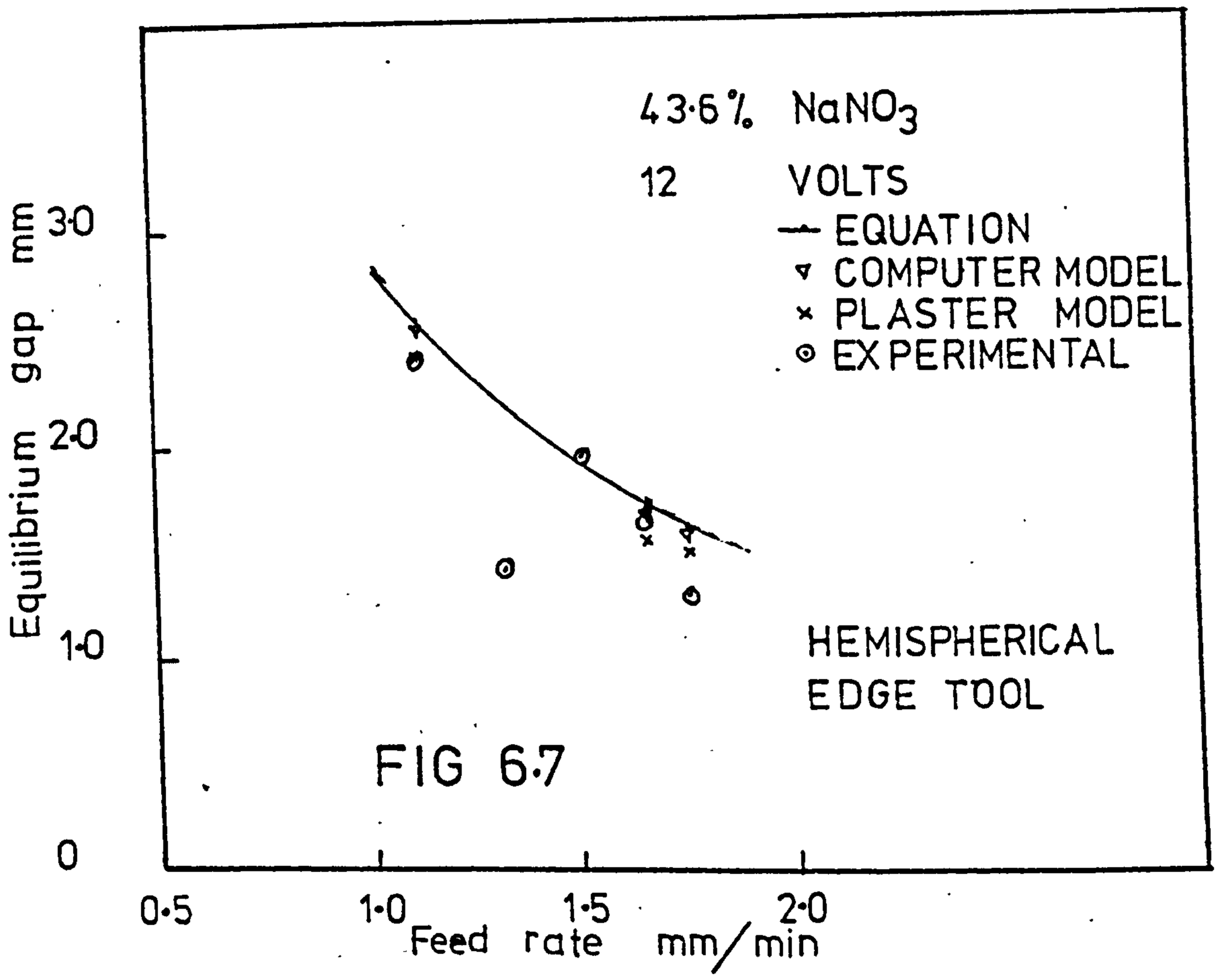
43·6 % NaNO3
12 VOLTS
— EQUATION
▿ COMPUTER MODEL
× PLASTER MODEL
⊙ EXPERIMENTAL
HEMISPHERICAL
EDGE TOOL
Equilibrium gap mm
3·0
2·0
1·0
0
0·5
1·0
1·5
2·0
Feed rate mm/min

FIG 6.7

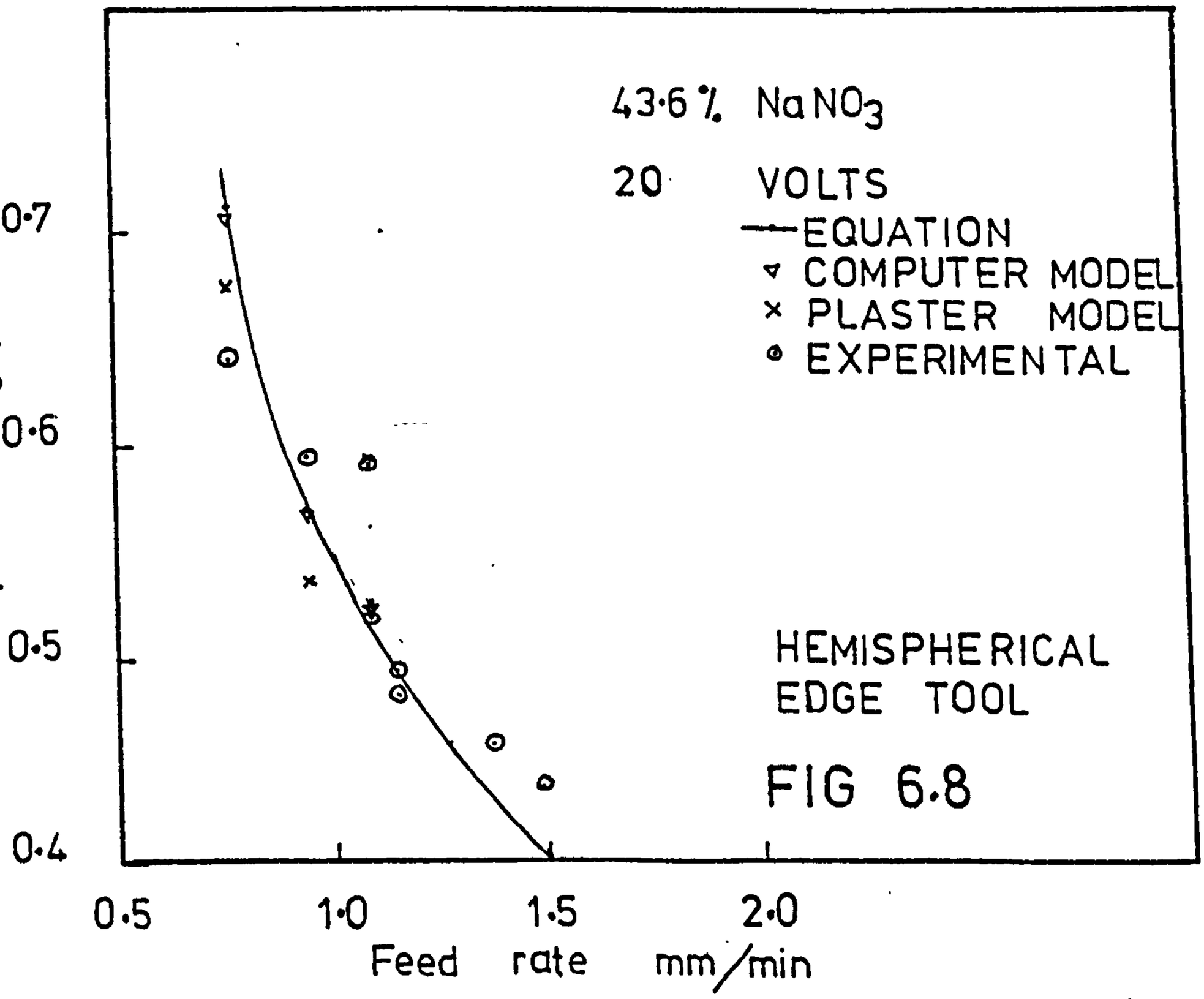
43·6 % NaNO3
20 VOLTS
— EQUATION
▿ COMPUTER MODEL
× PLASTER MODEL
⊙ EXPERIMENTAL
HEMISPHERICAL
EDGE TOOL
Equilibrium gap mm
0·7
0·6
0·5
0·4
0·5
1·0
1·5
2·0
Feed rate mm/min

FIG 6.8

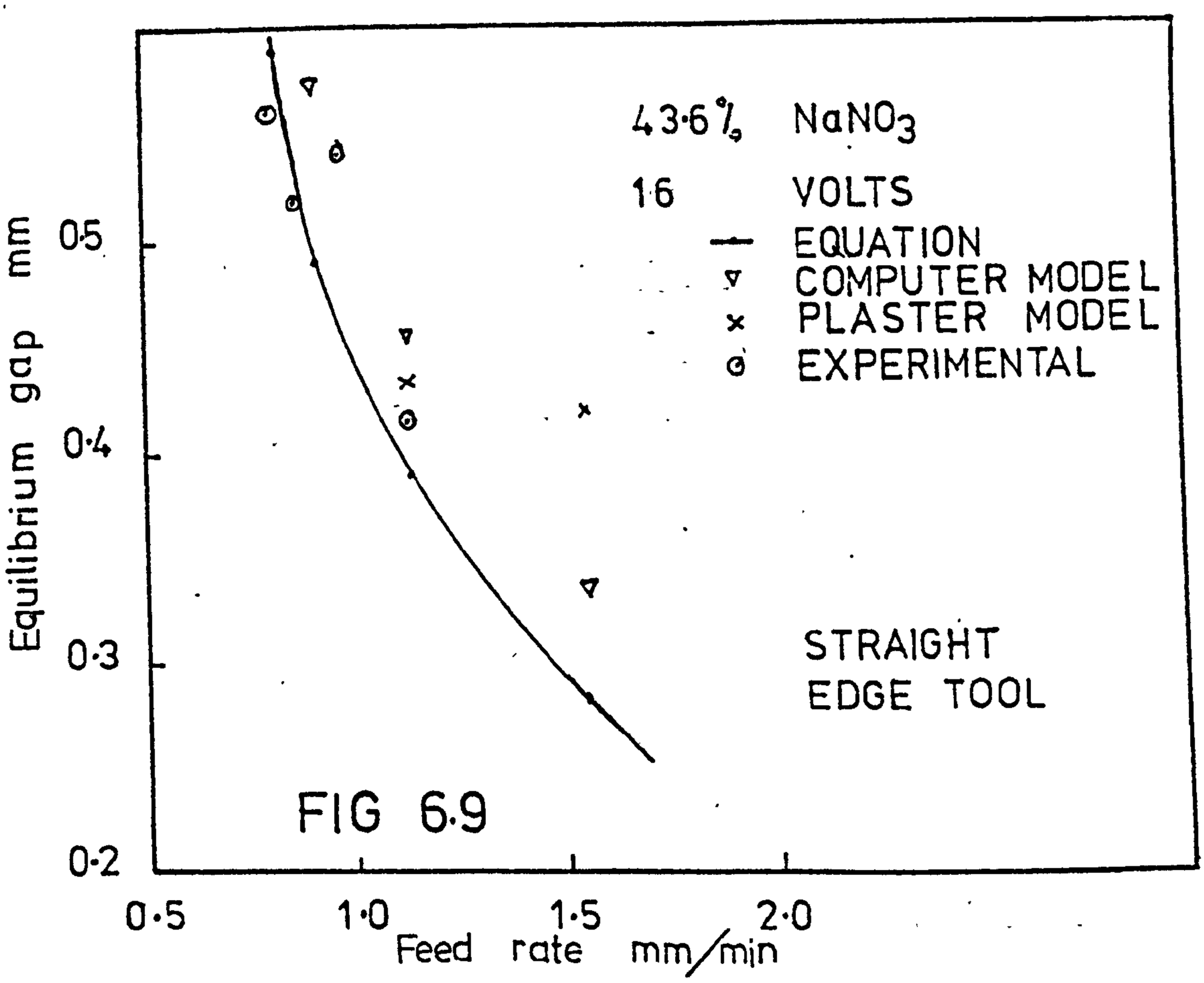

FIG 6.9

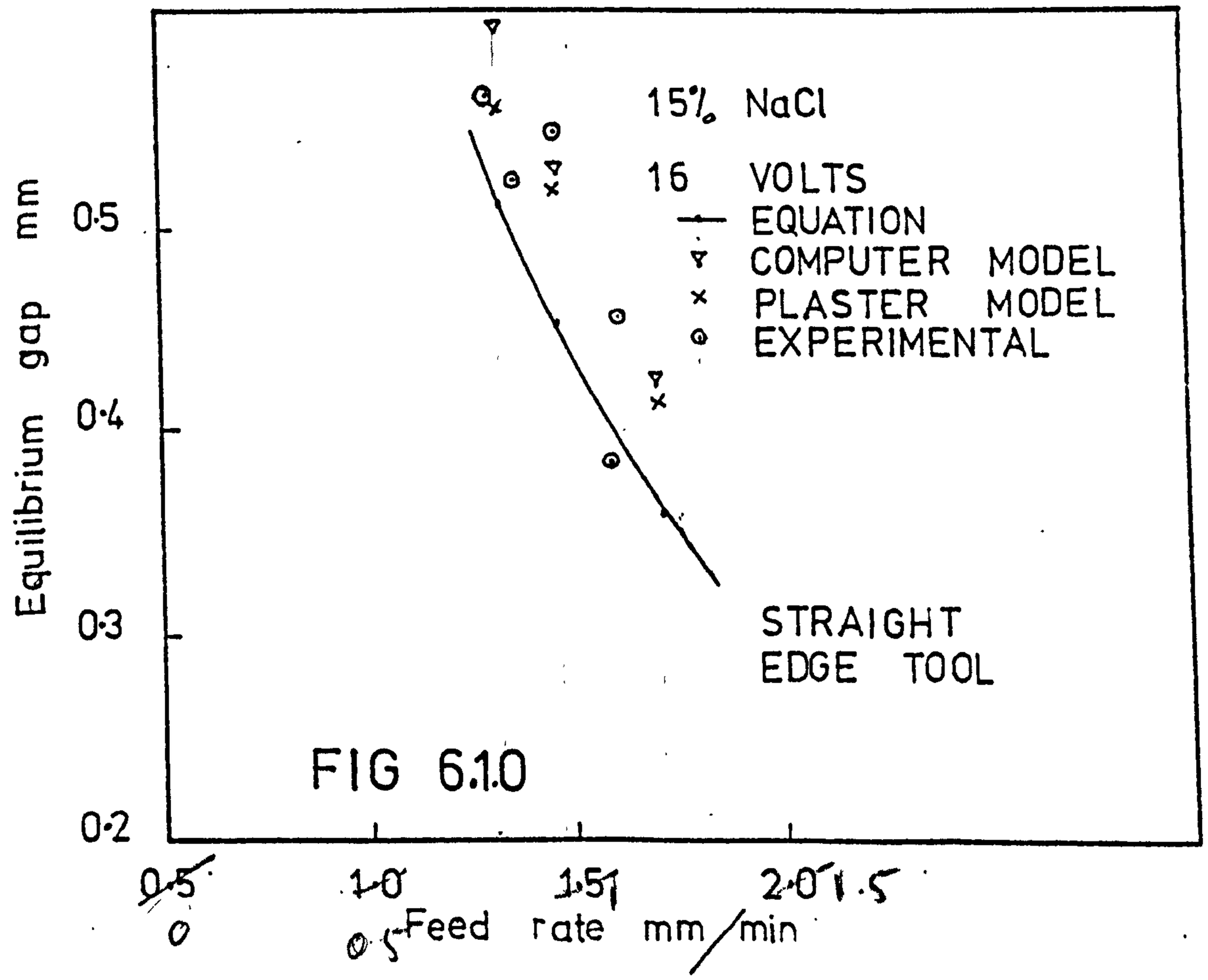

FIG 6.10

predicted by the equation 1.11 but the difference was insignificant. This very close correlation between the gaps predicted by the computer model and that by the basic equation 1.11 was due to similar current distribution, in the region concerned. Because of the larger radius of the leading edge of the tool, current distribution in the gap opposite the leading edge is nearly orthogonal, such a distribution of current was of course assumed in derivation of equation 1.11.

The experimentally measured equilibrium gaps showed slight scatter about the theoretical curve, but the general distribution of points showed that most points lie below the theoretical curve except in the case of straight leading edge tool which is dealt in a later stage. The maximum deviation of experimentally obtained gap from the theoretical curve was 0.07 mm Fig. 6.8. However, a gap obtained machining under identical conditions and the corresponding gap obtained from the plaster model shows that this was due to experimental error. The scatter of experimental results were mainly due to the difficulties experienced in measuring this gap which was detailed in section 5.6.

The equilibrium gaps obtained by tracing plaster models of electrochemically machined holes relative corresponding tool positions were in better agreement with those predicted theoretically than obtained by direct measurement.

This was mainly due to elimination of difficulties experienced in experimental measurement explained earlier.

In all cases the theoretically predicted equilibrium gaps for 2.5 volts over potential plus reversible potential, were slightly higher than those obtained by tracing plaster models.

At first sight this suggests that the assumed over potential was incorrect, but the computer plots of work profiles Figs. 6.16 to 6.33 show that the discrepancy was not constant. The use of a fixed over potential at 2.5V or any other value, can therefore only be an approximation. Tafel's equation 1.2 for polarization shows that polarization voltages are higher at high current densities; concentration and other types of polarization follow a similar trend. Since the area where the equilibrium gap was measured was one of high current density, the contribution of over potential as well as the fixed reversible potential, appears to have some significance.

6.1.5 Over Cut

Unlike the case of the orthogonal equilibrium gap there was no general mathematical or empirical formula to predict the maximum transverse gap between electrodes, which is commonly known as the overcut. Apart from electrochemical factors, the geometry of the tool also influences the magnitude of the side gap, due to the fact that the current distribution in the inter electrode gap depends on the leading edge of the tool geometry.

The curves obtained by plotting maximum transverse electrode gaps vs tool feed rates are displayed in Figs. 6.11 to 6.15. All predicted results showed good agreement

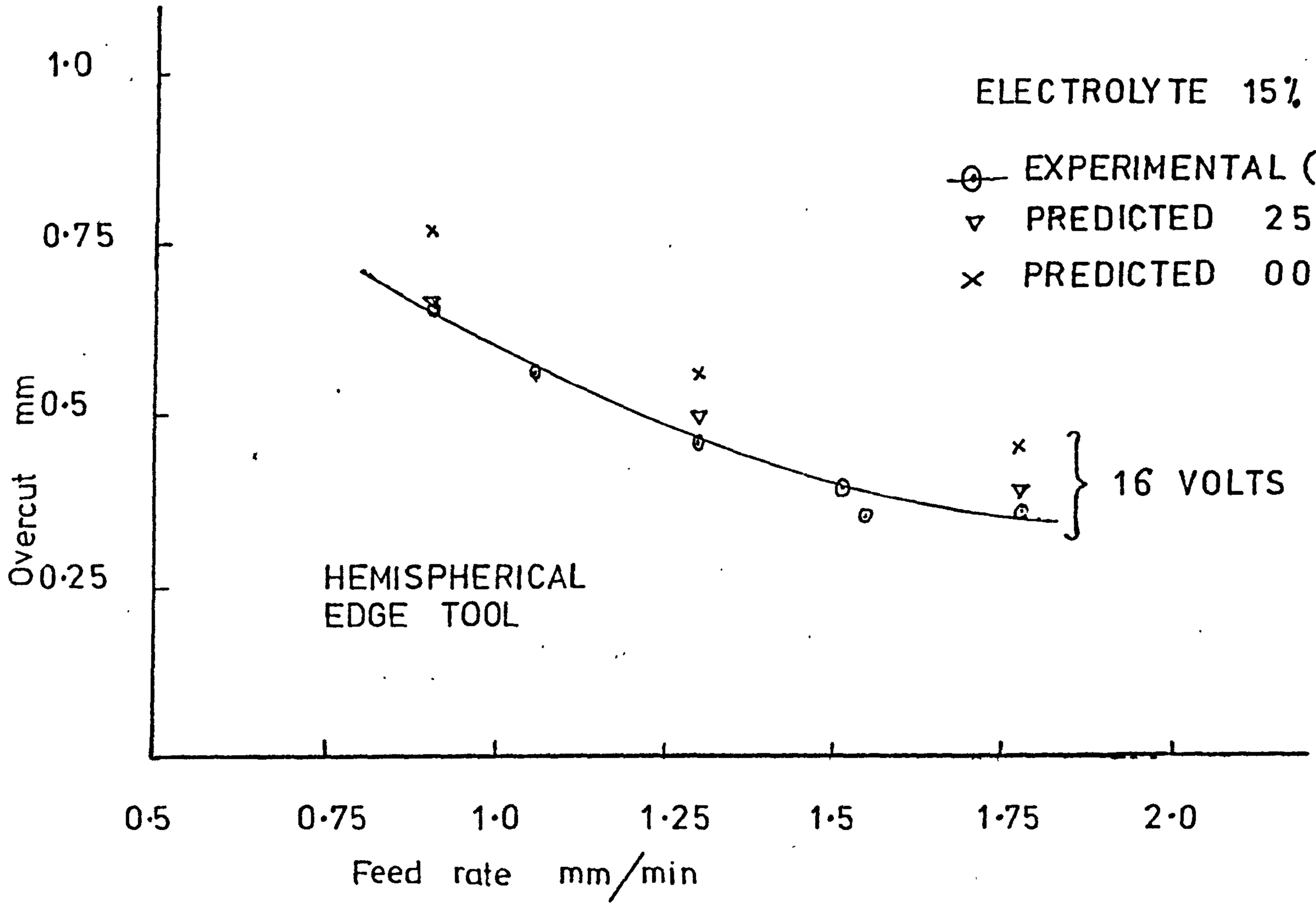
ELECTROLYTE 15% NaCl
EXPERIMENTAL (PLASTER MODEL)
PREDICTED 25 OVER POT
PREDICTED 00 OVER POT
16 VOLTS
HEMISPHERICAL
EDGE TOOL
Overcut mm
1·0
0·75
0·5
0·25
0·5
0·75
1·0
1·25
1·5
1·75
2·0
Feed rate mm/min

FIG 6·11

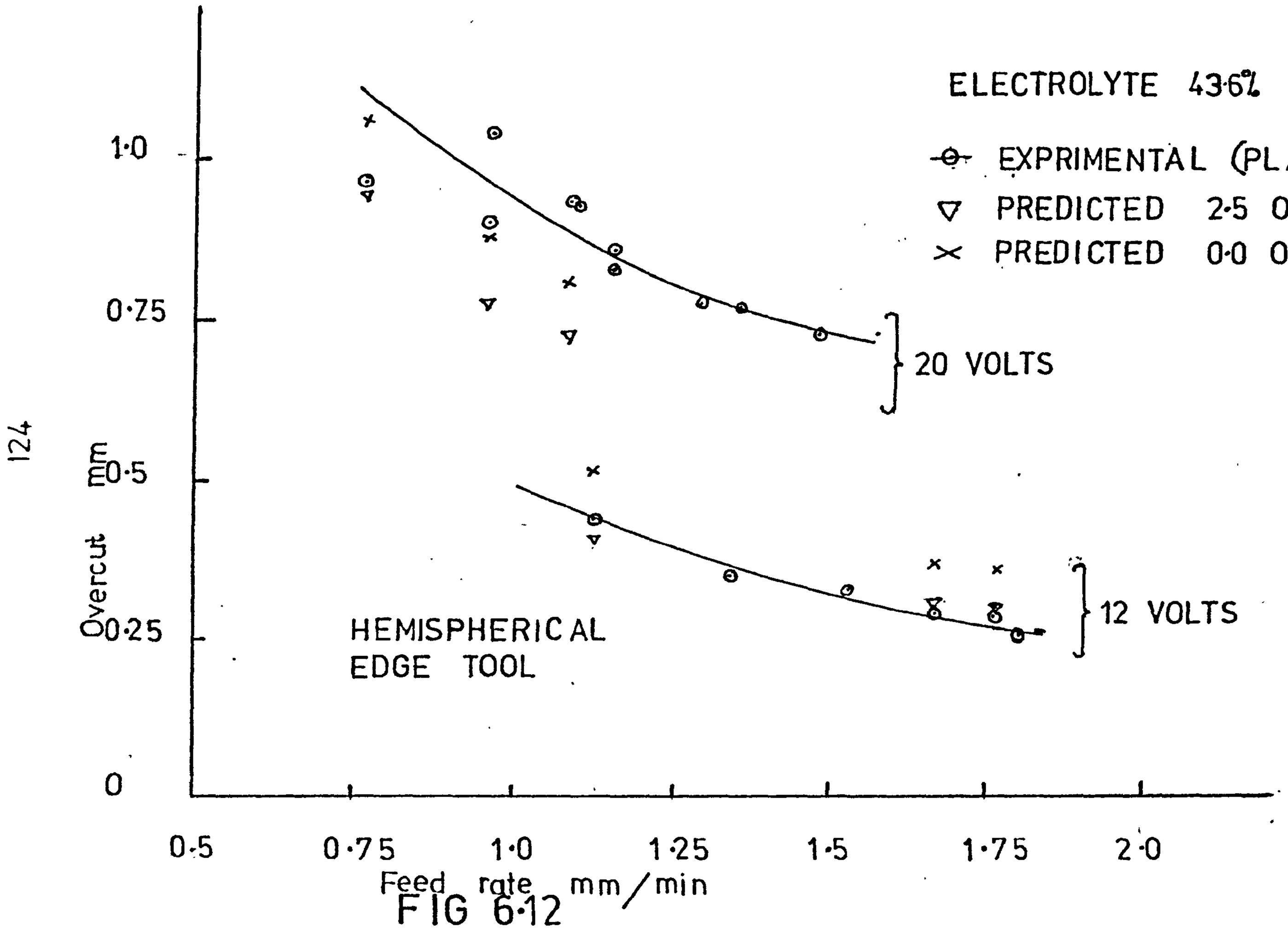
ELECTROLYTE 43·6% NaNO3
EXPRIMENTAL (PLASTER MODEL)
PREDICTED 2·5 OVER POT
PREDICTED 0·0 OVER POT
20 VOLTS
12 VOLTS
HEMISPHERICAL
EDGE TOOL
Overcut mm
1·0
0·75
0·5
0·25
0
0·5
0·75
1·0
1·25
1·5
1·75
2·0
Feed rate mm/min

FIG 6·12

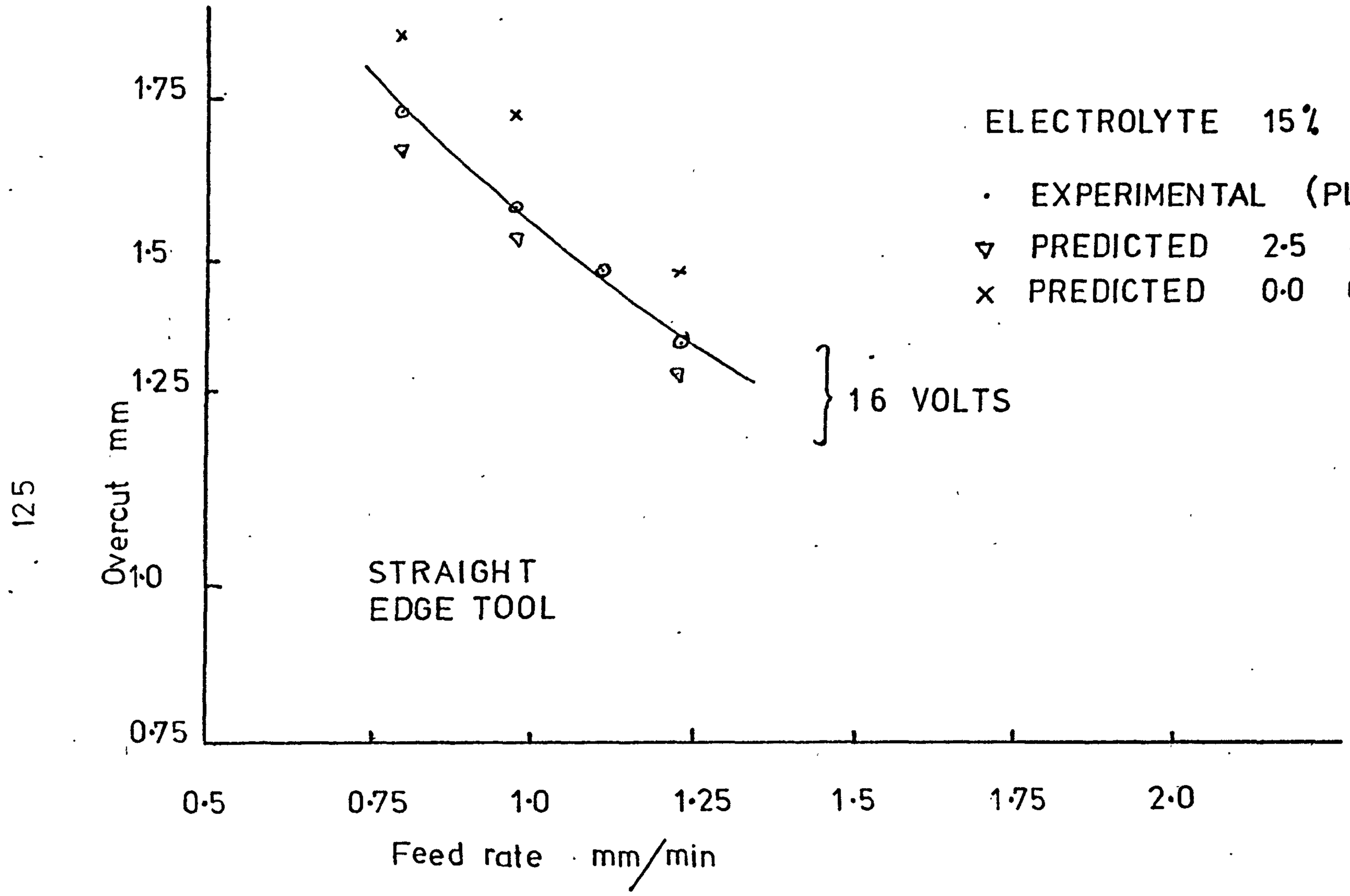
ELECTROLYTE 15% NaCl
· EXPERIMENTAL (PLASTER MODEL)
▽ PREDICTED 2·5 OVER POT
× PREDICTED 0·0 OVER POT
16 VOLTS
STRAIGHT
EDGE TOOL
Overcut mm
1·75
1·5
1·25
1·0
0·75
0·5
0·75
1·0
1·25
1·5
1·75
2·0
Feed rate mm/min

FIG 6.14

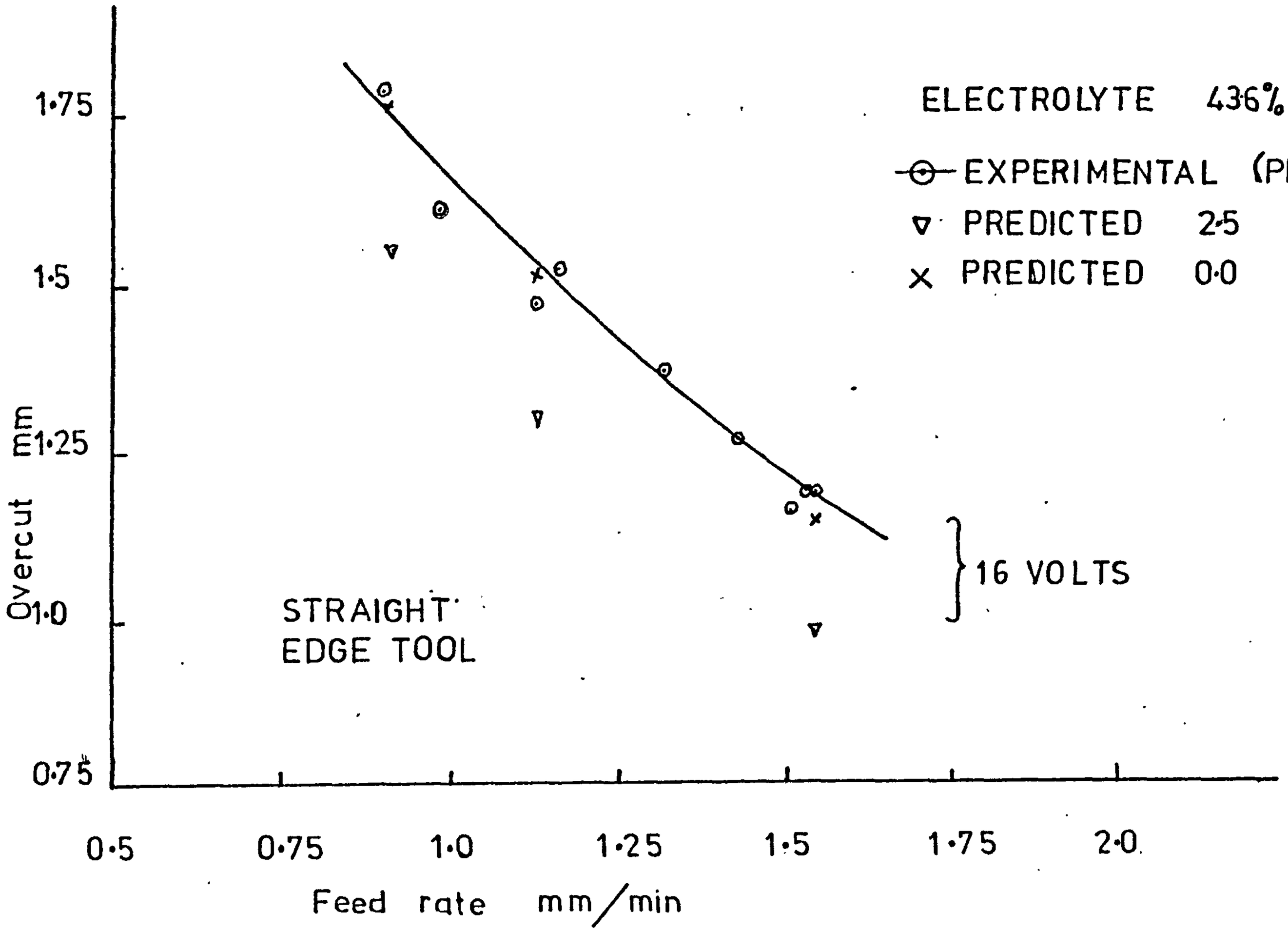
ELECTROLYTE 436% $NaNO_3$
EXPERIMENTAL (PLASTER MODEL)
PREDICTED 2·5 OVER POT
PREDICTED 0·0 OVER POT
16 VOLTS
STRAIGHT EDGE TOOL
Overcut
1·75
1·5
1·25
1·0
0·75
0·5
0·75
1·0
1·25
1·5
1·75
2·0
Feed rate mm/min

FIG 6.13

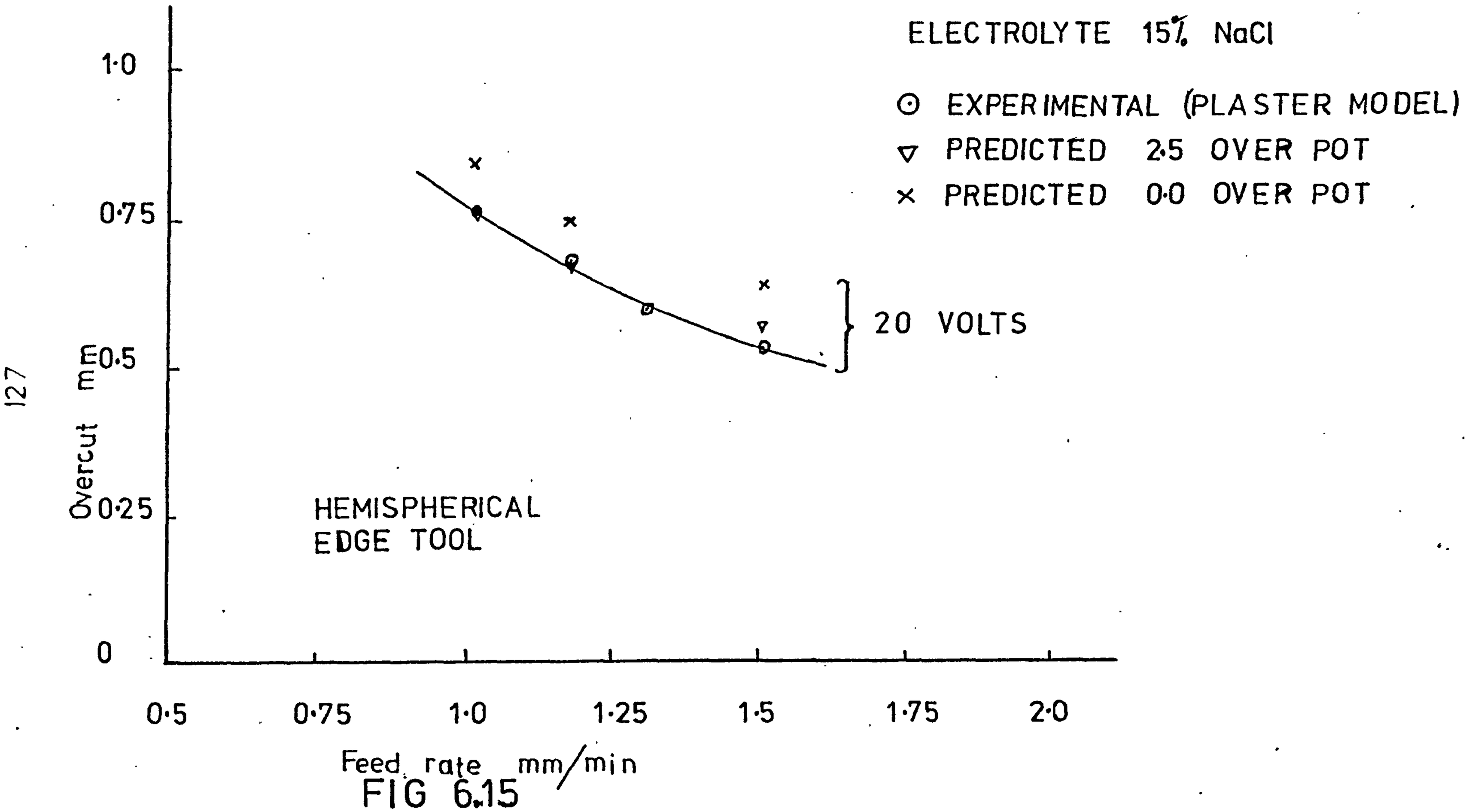
ELECTROLYTE 15% NaCl
⊙ EXPERIMENTAL (PLASTER MODEL)
▽ PREDICTED 2·5 OVER POT
× PREDICTED 0·0 OVER POT
20 VOLTS
HEMISPHERICAL
EDGE TOOL
Overcut 127 mm
1·0
0·75
0·5
0·25
0
0·5
0·75
1·0
1·25
1·5
1·75
2·0
Feed rate mm/min

FIG 6.15

with those obtained experimentally confirms the accuracy and applicability of the computer model. Moreover the assumption that overpotential and reversible potential could be accounted for by a single fixed value of overpotential in the model is justified as the fit was good enough for many purposes, over the whole range of feed rates and therefore current densities which were used. What is not quite so clear is the actual value to be used. In some cases, of the two values used for computation, 0.0V overpotential gave a good fit while in others 2.5 volts was better.

Experimental and theoretical curves were similar in form to hyperbolas. This should be expected since the overcut is a function of the frontal equilibrium gap. König(10) has shown that for a straight leading edge tool having small corner radius (below 3 mm) the overcut is a linear function of the frontal equilibrium gap and is given by equations 1.14 and 1.15.

Fig. 6.11 shows the overcut vs tool feed rate curves obtained, machining at 16 volts with 15% NaCl electrolyte. All experimental gaps were well below the theoretical curve obtained for 0.0V over potential, were in very good agreement with the curve for 2.5V over potential. The theoretical prediction at the tool feed rate of 0.9 mm/min was the same as the experimentally obtained gap at the same tool feed rate. But at higher tool feed rates the experimental curve for overcut gave a slightly larger value than that predicted by the curve for 2.5V over potential.

This slight discrepancy could be explained by a real increase in over potential with current density. Since high tool feed rates mean high current densities which in turn gives a high value for over potential the available voltage is reduced and so the gap is smaller than expected. Machining at a cell voltage of 20V showed the same effect, Fig. 6.15. The experimental values at higher feed rates were once more lower than those predicted by the curve for 2.5V over potential.

The curves obtained for overcut vs tool feed rate when machining with hemispherical leading edges tool at applied voltages of 12V and 20V using sodium nitrate electrolyte are shown in Fig. 6.12. The magnitude of the overcut when machining at 20V was almost double the value obtained at 12V for the same tool feed rate.

The experimental curve of overcut vs tool feed rate obtained at machining voltages of 20V gave larger values of overcut than those predicted by the computer model for 2.5V and 0.0V over potentials but were closer to the curve of 0.0V over potential. Even though the overcut of the specimen machined at the tool feed rate of 0.96 mm/min almost coincided with the theoretical prediction at 0.0V over potential, the general form of the experimental curve shows this was due to some experimental error. The curve obtained from the predicted values of overcut machining using $NaNO_3$ electrolyte at 12V cell voltage, 2.5V over potential showed very good agreement with experimental work, justifies the assumption of 2.5V over potential in this case. Larsson (5) has shown that when machining iron the

minimum applied potential required across the cell for machining to proceed was about 2.5V, which was the sum of the hydrogen over voltage and the effective over voltage at the anode.

Machining with straight leading edge tool Fig. 6.13, Fig. 6.14, gave a larger overcut than those predicted by the theoretical curve obtained at 2.5V over potential. With NaCl electrolyte the experimental points were midway between the two theoretical curves, but with $NaNO_3$ electrolyte the curve obtained at O.OV over potential showed good correlation. To summarize the use of an over potential of O.OV is too low for the NaCl tests while 2.5 volts is about right. With $NaNO_3$ O.O volts is about right while 2.5 volts is too high. This is an over simplification because the 12 volt tests with the $NaNO_3$ electrolyte gave better agreement with 2.5 volts. Also there is the expected trend which is just noticeable on the curves, that a higher over potential is required for correct prediction at higher feed rates, Fig. 6.16.

The discrepancies between predicted and actual over cut is unlikely to be due to the choice of over potential alone. There will also be a discrepancy due to change in dissolution rates at low current densities with the NaCl electrolyte and use of incorrect machining efficiencies obtained from the curve Fig. 6.3 in calculation of erosion rates at low current densities with $NaNO_3$ electrolyte. Muzaffaruddin (33) has shown that when machining EN58a stainless steel in 10% NaCl below a current density of

PREDICTED OVERCUT

Values of η Used in Prediction

App: Volt	Na Cl,		$Na NO_3$	
	$\eta = 0$	$\eta = 2.5$	$\eta = 0$	$\eta = 2.5$
	HEMISPHERICAL EDGE TOOL			
12V	-	-	Too High η too low	Crosses Expt Line. η about right too high at low feed too low at high feed
			Fig. (6.12)	
16V	Too High η too low	Little Low η little low	-	-
	Fig. (6.11)			
20V	Too High η too low	About Right High at High Feed η about right low at high feed	Low but in Scatter η too high?	Too Low η too high
	Fig. (6.15)		Fig. (6.12)	
	STRAIGHT EDGE TOOL			
12V	-	-	-	-
16V	Too High η too low	Too Low η too high	Good η right	Too Low η too high
	Fig. (6.14)		Fig. (6.13)	
20V	-	-	-	-
SUMMARY	η all too low	η quite near	η about right at mid tool feed rates	η too high at high tool feed rates

Fig. (6.16)

about 0.425 A/mm^2 specific metal removal rate corresponded to dissolution of the steel at valencies 3, 2, 2 for Chromium, Nickel and iron respectively. As the current density was increased dissolution of the steel showed mixed valencies and the specific metal removal rate fell to a value between dissolution rates obtained at valencies 3, 2, 2 and 6, 2, 3 for chromium, nickel and iron respectively. From the computer model of the present experiments theoretical current density on the work surface immediately opposite the point on the tool where the land width begins, when using $NaNO_3$ electrolyte was 16.9 Amp/mm^2 at a tool feed rate of 0.92 mm/min. This value of current density gradually dropped along the work surface to a value of 0.1058 amp/mm^2, where the overcut was measured. The developed mathematical model considered only the specific metal removal rate obtained from curve Fig. 6.3. This curve was constructed from average values of specific metal removal rates and current densities and so probably did not allow adequately for differing removal rates at very low current densities. The use of machining efficiencies predicted at low current densities in calculation of erosion rates were mainly responsible for predicted lower values of overcut with $NaNO_3$ electrolyte.

On the whole the predicted values of overcut using the mathematical model showed good correlation with experimental values.

6.2 COMPARISON OF THEORETICAL AND EXPERIMENTAL WORK PROFILES

The calculated and experimental records of work profiles relative to corresponding tool positions are shown in Figs. 6.17-6.34. The operating conditions of these test runs are also given. In all cases the continuous curve represents the outline of the work profile calculated for 2.5V over potential, the curve represented by the broken line is the work profile for 0.0V overpotential, and the curve represented by dots is the outline of the machined profile which was actually obtained at the given operating conditions. In reviewing the test results presented here it is apparent that the polynomial approximation method of solving Laplace equation for a free boundary problem consistently provided an excellent result even with a very coarse mesh. For example in the region opposite insulated part of the tool, the nodal arms have magnitudes varying from 0.3 to 1.6 orthogonal equilibrium gaps.

The correlation between the calculated and experimental work profiles was considered to be generally very satisfactory; justifying most of the assumptions which had been made during the development of the model. There are inevitably some differences between predicted and experimental profiles due to

(a) Simplification and assumptions involved in the model

(b) Inaccuracies in the numerical method used to solve the model, and

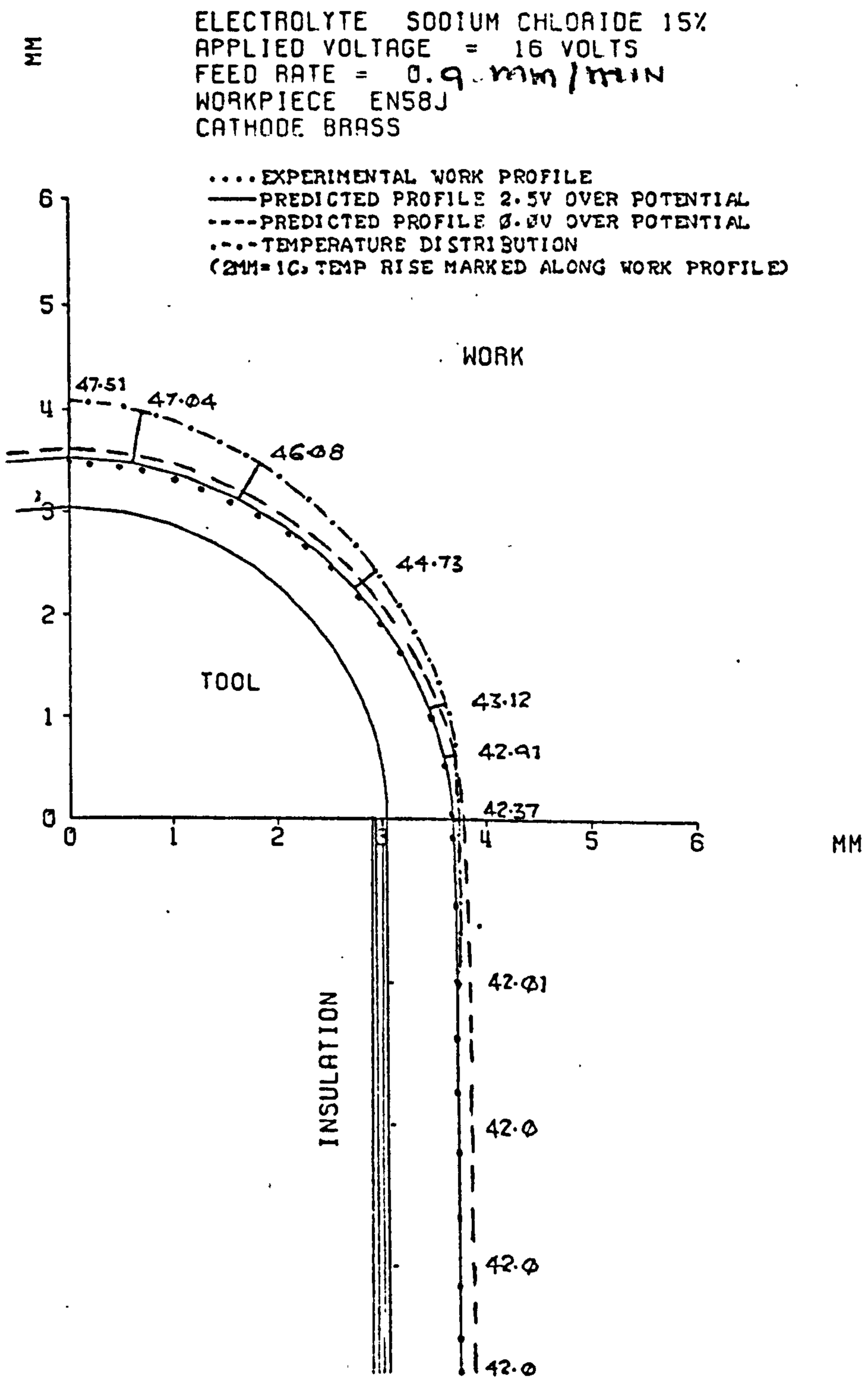
ELECTROLYTE SODIUM CHLORIDE 15%
APPLIED VOLTAGE = 16 VOLTS
FEED RATE = 0.9 mm/min
WORKPIECE EN58J
CATHODE BRASS
....EXPERIMENTAL WORK PROFILE
——PREDICTED PROFILE 2.5V OVER POTENTIAL
----PREDICTED PROFILE Ø.ØV OVER POTENTIAL
.-.-TEMPERATURE DISTRIBUTION
(2MM=1C, TEMP RISE MARKED ALONG WORK PROFILE)
WORK
TOOL
INSULATION
47.51
47.04
46.08
44.73
43.12
42.91
42.37
42.01
42.0
42.0
42.0
MM
MM
0
1
2
3
4
5
6

FIG.6.17

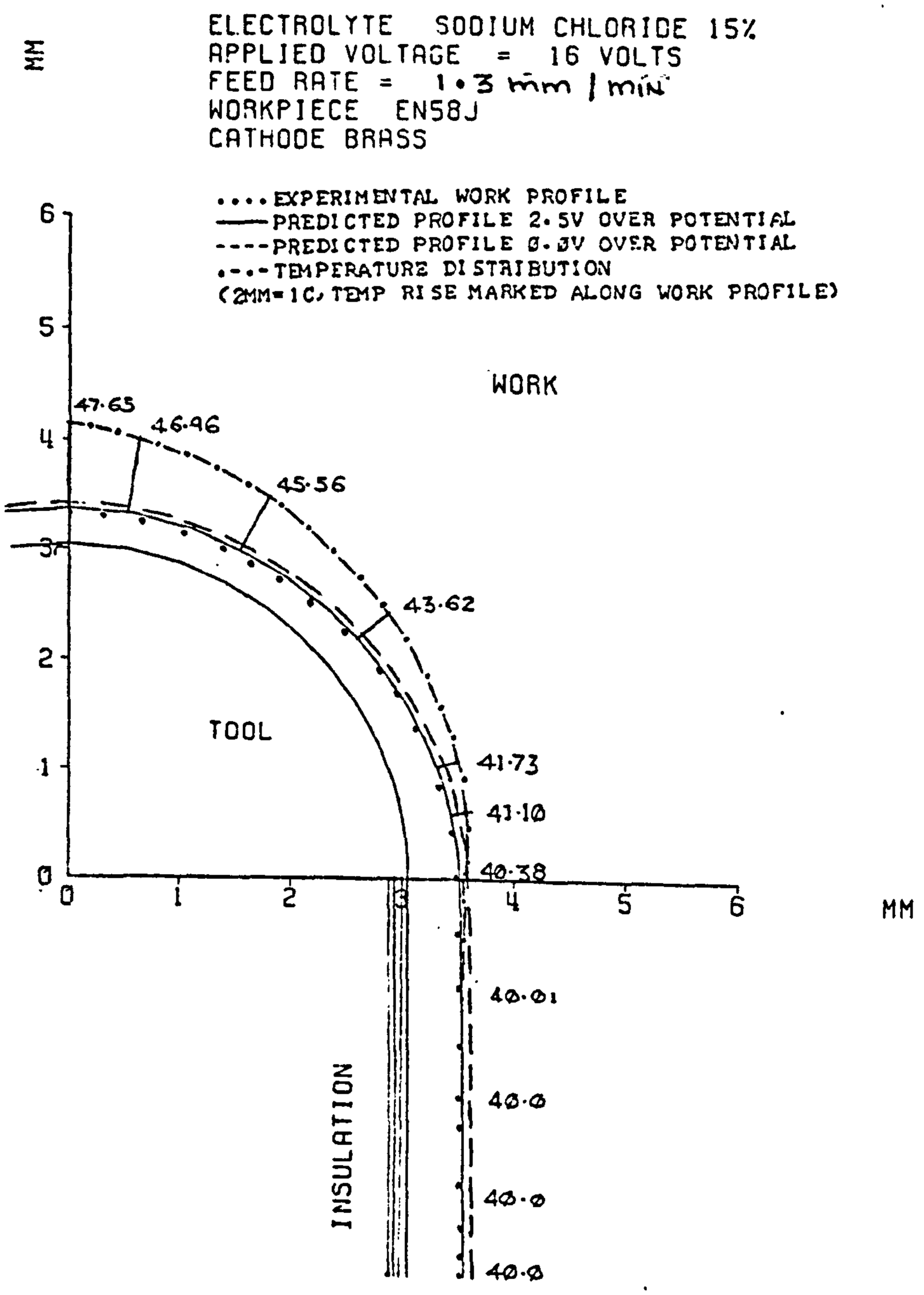
ELECTROLYTE SODIUM CHLORIDE 15%
APPLIED VOLTAGE = 16 VOLTS
FEED RATE = 1·3 mm / min
WORKPIECE EN58J
CATHODE BRASS
MM
····EXPERIMENTAL WORK PROFILE
——PREDICTED PROFILE 2·5V OVER POTENTIAL
----PREDICTED PROFILE 0·5V OVER POTENTIAL
·-·-TEMPERATURE DISTRIBUTION
(2MM=1C, TEMP RISE MARKED ALONG WORK PROFILE)
WORK
47·65
46·96
45·56
43·62
41·73
41·10
40·38
40·01
40·0
40·0
40·0
TOOL
INSULATION
0
1
2
3
4
5
6
MM

FIG. 6.18

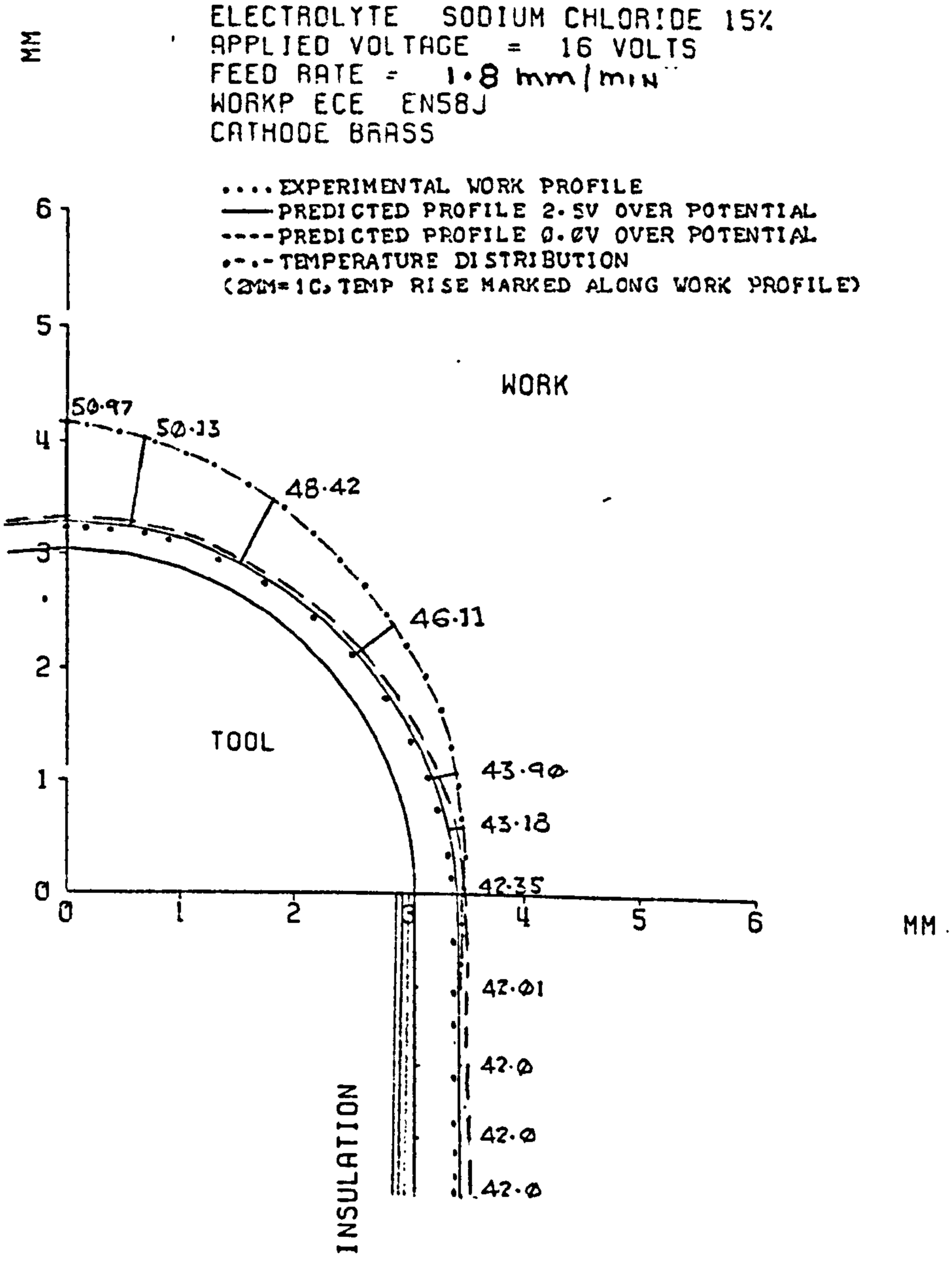
ELECTROLYTE SODIUM CHLORIDE 15%
APPLIED VOLTAGE = 16 VOLTS
FEED RATE = 1·8 mm/min
WORKP ECE EN58J
CATHODE BRASS
....EXPERIMENTAL WORK PROFILE
——PREDICTED PROFILE 2·5V OVER POTENTIAL
----PREDICTED PROFILE 0·0V OVER POTENTIAL
•-•-TEMPERATURE DISTRIBUTION
(2MM=1C, TEMP RISE MARKED ALONG WORK PROFILE)
MM
WORK
TOOL
INSULATION
50·97
50·13
48·42
46·11
43·90
43·18
42·35
42·01
42·0
42·0
42·0
0
1
2
3
4
5
6
MM.

FIG. 6.19

ELECTROLYTE SODIUM CHLORIDE 15%
APPLIED VOLTAGE = 20 VOLTS
FEED RATE = 1.02 mm/min
WORKPIECE EN58J
CATHODE BRASS

....EXPERIMENTAL WORK PROFILE
——PREDICTED PROFILE 2.5V OVER POTENTIAL
----PREDICTED PROFILE Ø.ØV OVER POTENTIAL
.-.-TEMPERATURE DISTRIBUTION
(2MM=1C. TEMP RISE MARKED ALONG WORK PROFILE)

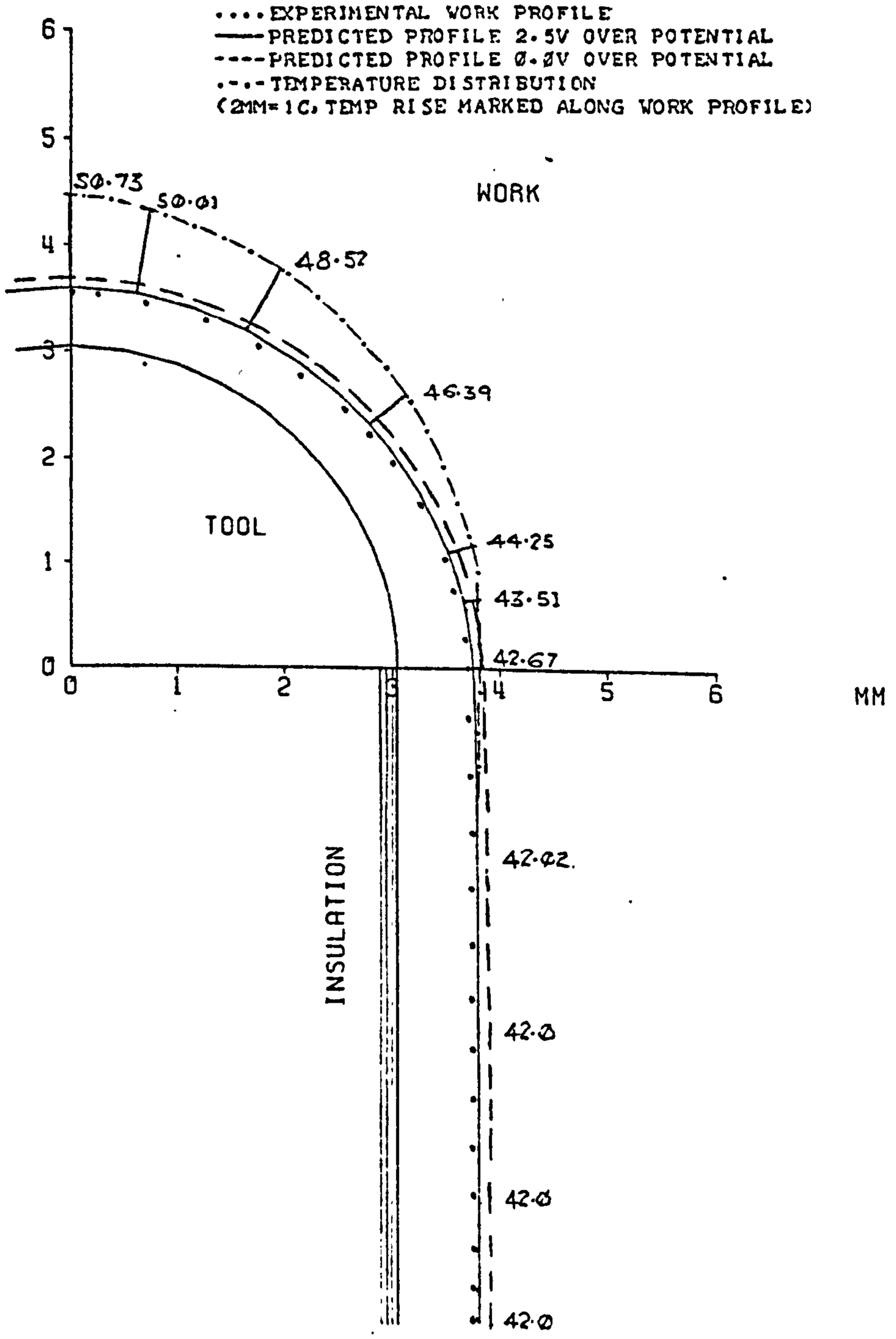

Fig 2

FIG.6.20

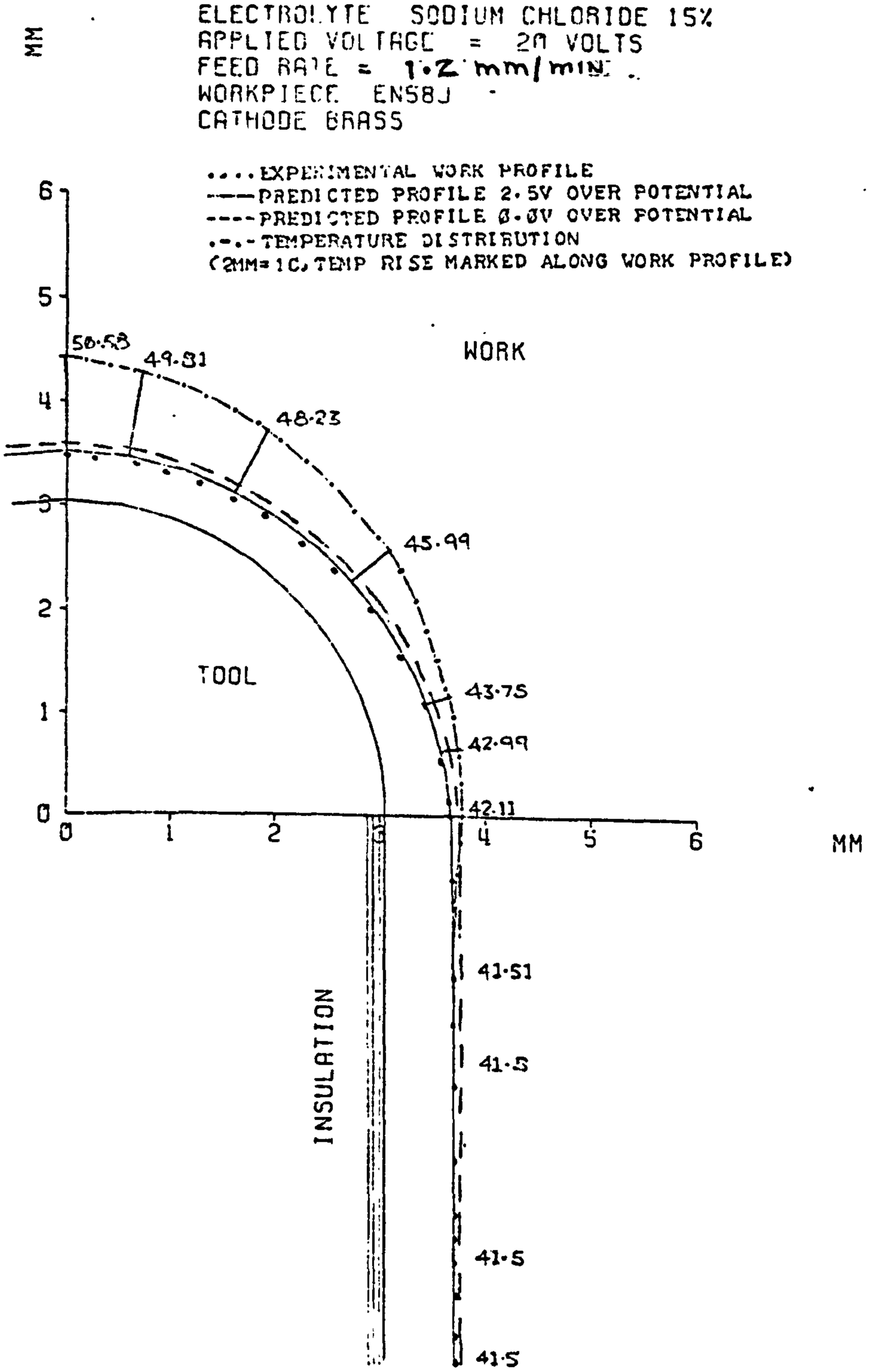
ELECTROLYTE SODIUM CHLORIDE 15%
APPLIED VOLTAGE = 20 VOLTS
FEED RATE = 1.2 mm/min
WORKPIECE EN58J
CATHODE BRASS
....EXPERIMENTAL WORK PROFILE
——PREDICTED PROFILE 2.5V OVER POTENTIAL
----PREDICTED PROFILE 0.0V OVER POTENTIAL
.-.-TEMPERATURE DISTRIBUTION
(2MM=1C, TEMP RISE MARKED ALONG WORK PROFILE)
MM
WORK
TOOL
INSULATION
50.58
49.31
48.23
45.99
43.75
42.99
42.11
41.51
41.5
41.5
41.5
0
1
2
3
4
5
6

FIG.6.21

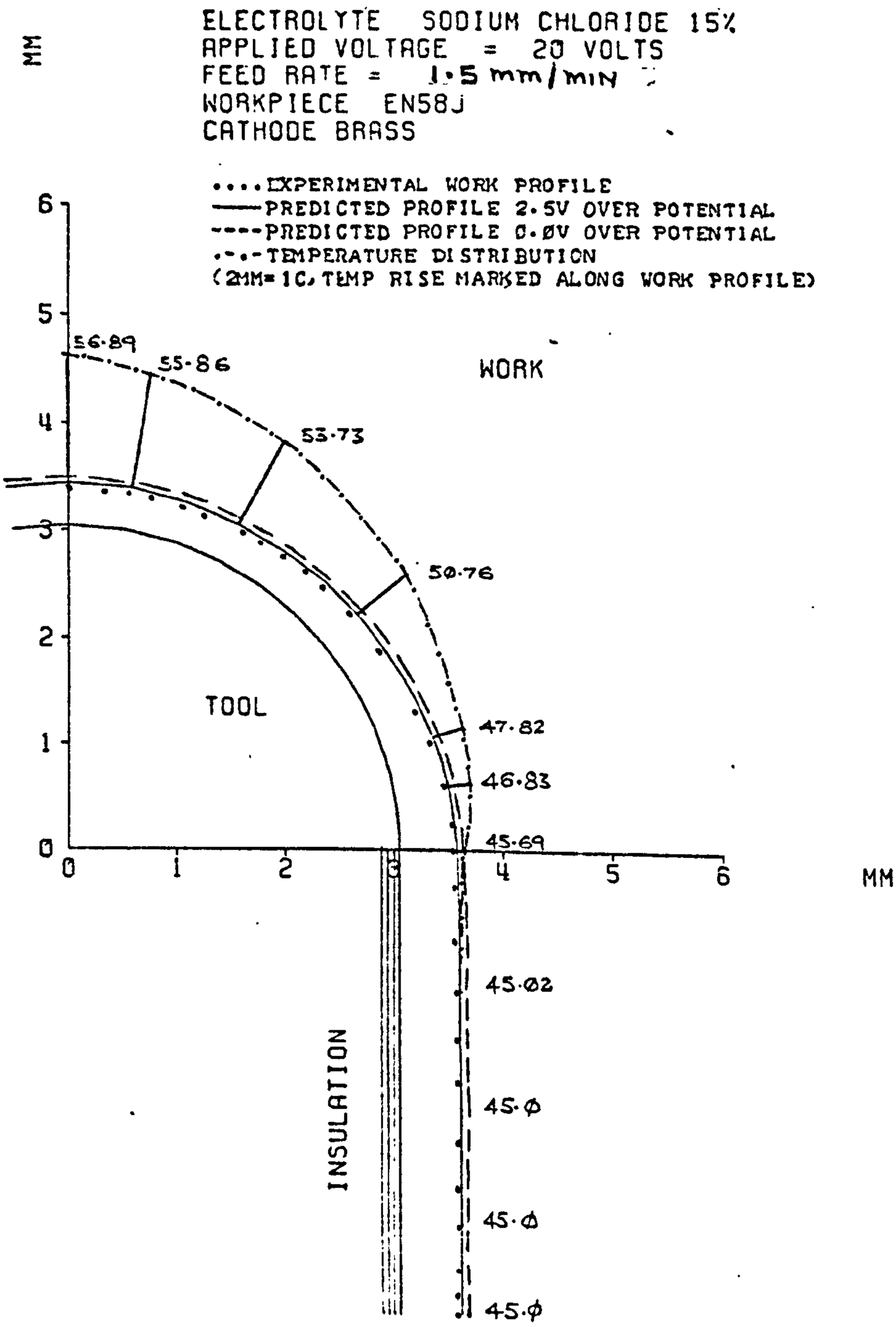
ELECTROLYTE SODIUM CHLORIDE 15%
APPLIED VOLTAGE = 20 VOLTS
FEED RATE = 1·5 mm/min
WORKPIECE EN58J
CATHODE BRASS
MM
····EXPERIMENTAL WORK PROFILE
——PREDICTED PROFILE 2·5V OVER POTENTIAL
----PREDICTED PROFILE 0·ØV OVER POTENTIAL
·-·-TEMPERATURE DISTRIBUTION
(2MM=1C, TEMP RISE MARKED ALONG WORK PROFILE)
WORK
TOOL
INSULATION
56·89
55·86
53·73
50·76
47·82
46·83
45·69
45·02
45·Ø
45·Ø
45·Ø
0
1
2
3
4
5
6
MM

FIG.6.22

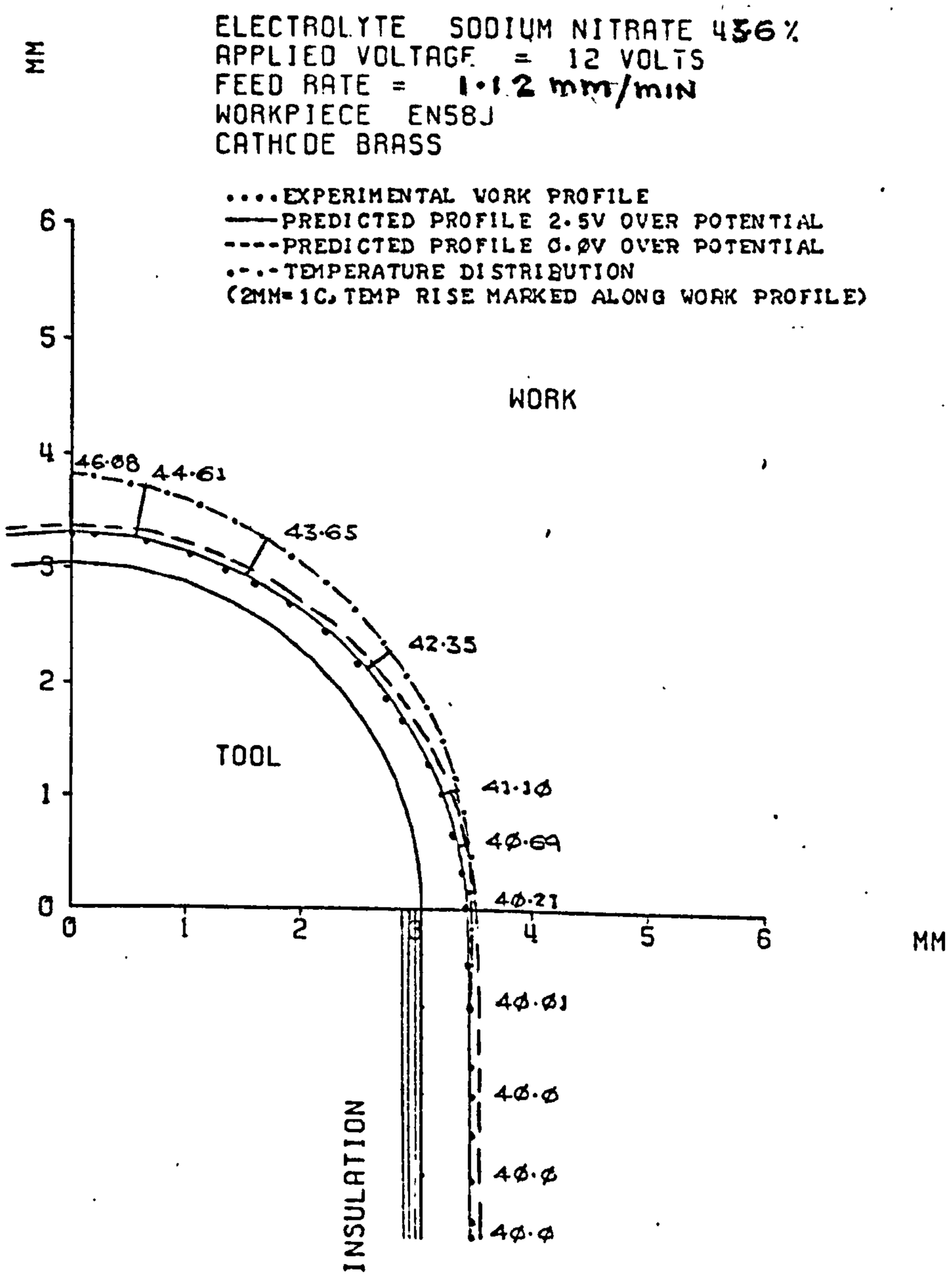
ELECTROLYTE SODIUM NITRATE 456 %
APPLIED VOLTAGE = 12 VOLTS
FEED RATE = 1·12 mm/min
WORKPIECE EN58J
CATHODE BRASS
····EXPERIMENTAL WORK PROFILE
——PREDICTED PROFILE 2·5V OVER POTENTIAL
----PREDICTED PROFILE 0·ØV OVER POTENTIAL
•-•-TEMPERATURE DISTRIBUTION
(2MM=1C, TEMP RISE MARKED ALONG WORK PROFILE)
WORK
TOOL
INSULATION
46·68
44·61
43·65
42·35
41·1Ø
4Ø·69
4Ø·21
4Ø·Ø1
4Ø·Ø
4Ø·Ø
4Ø·Ø
0
1
2
3
4
5
6
MM

FIG. 6.23

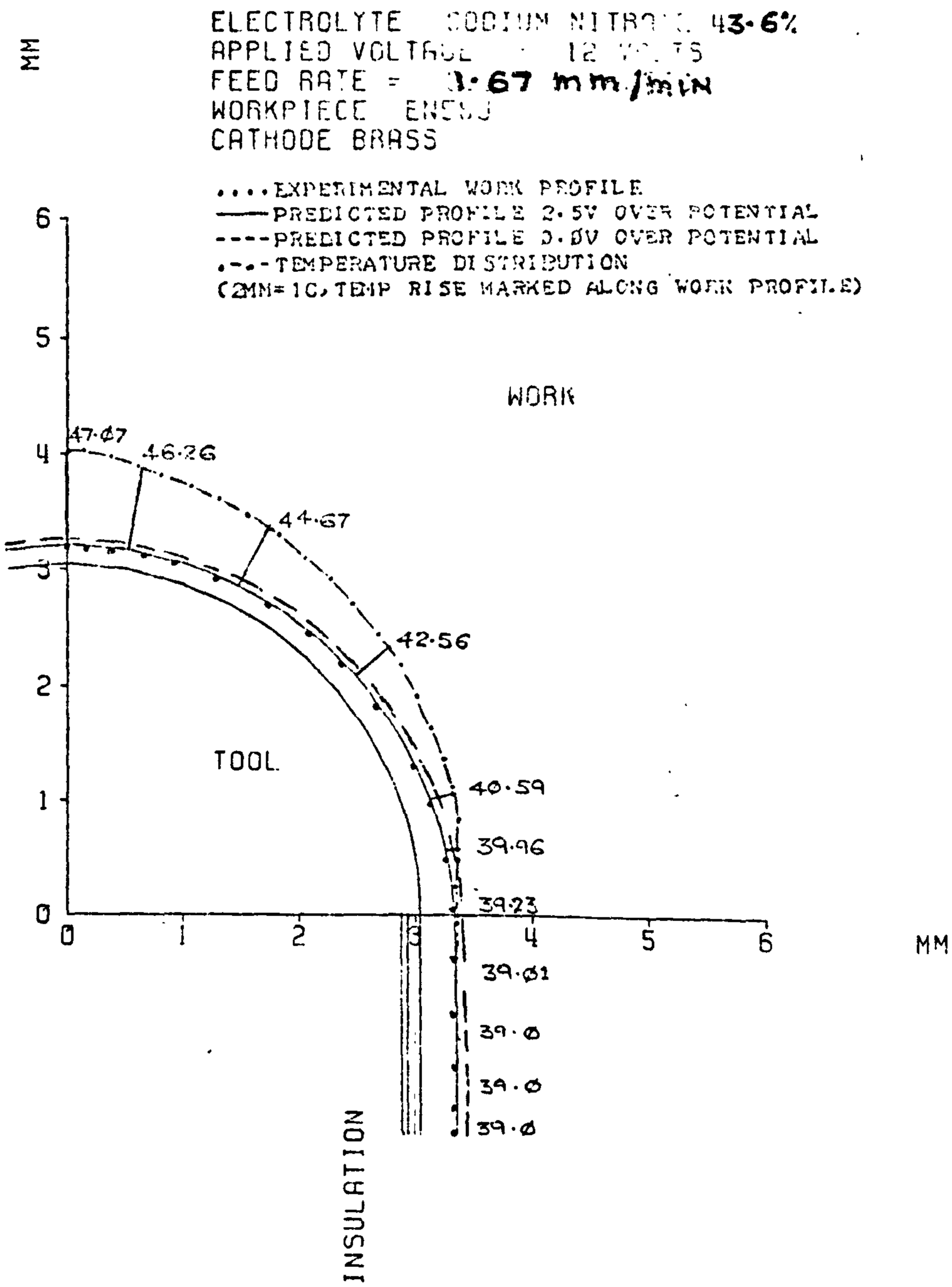
ELECTROLYTE SODIUM NITRATE 43·6%
APPLIED VOLTAGE 12 VOLTS
FEED RATE = 1·67 mm/min
WORKPIECE ENEDJ
CATHODE BRASS
....EXPERIMENTAL WORK PROFILE
——PREDICTED PROFILE 2·5V OVER POTENTIAL
----PREDICTED PROFILE 3·ØV OVER POTENTIAL
.-.-TEMPERATURE DISTRIBUTION
(2MM=1C, TEMP RISE MARKED ALONG WORK PROFILE)
WORK
TOOL
INSULATION
47·47
46·26
44·67
42·56
40·59
39·96
39·23
39·Ø1
39·Ø
39·Ø
39·Ø
MM
MM
0
1
2
3
4
5
6

FIG. 6.24

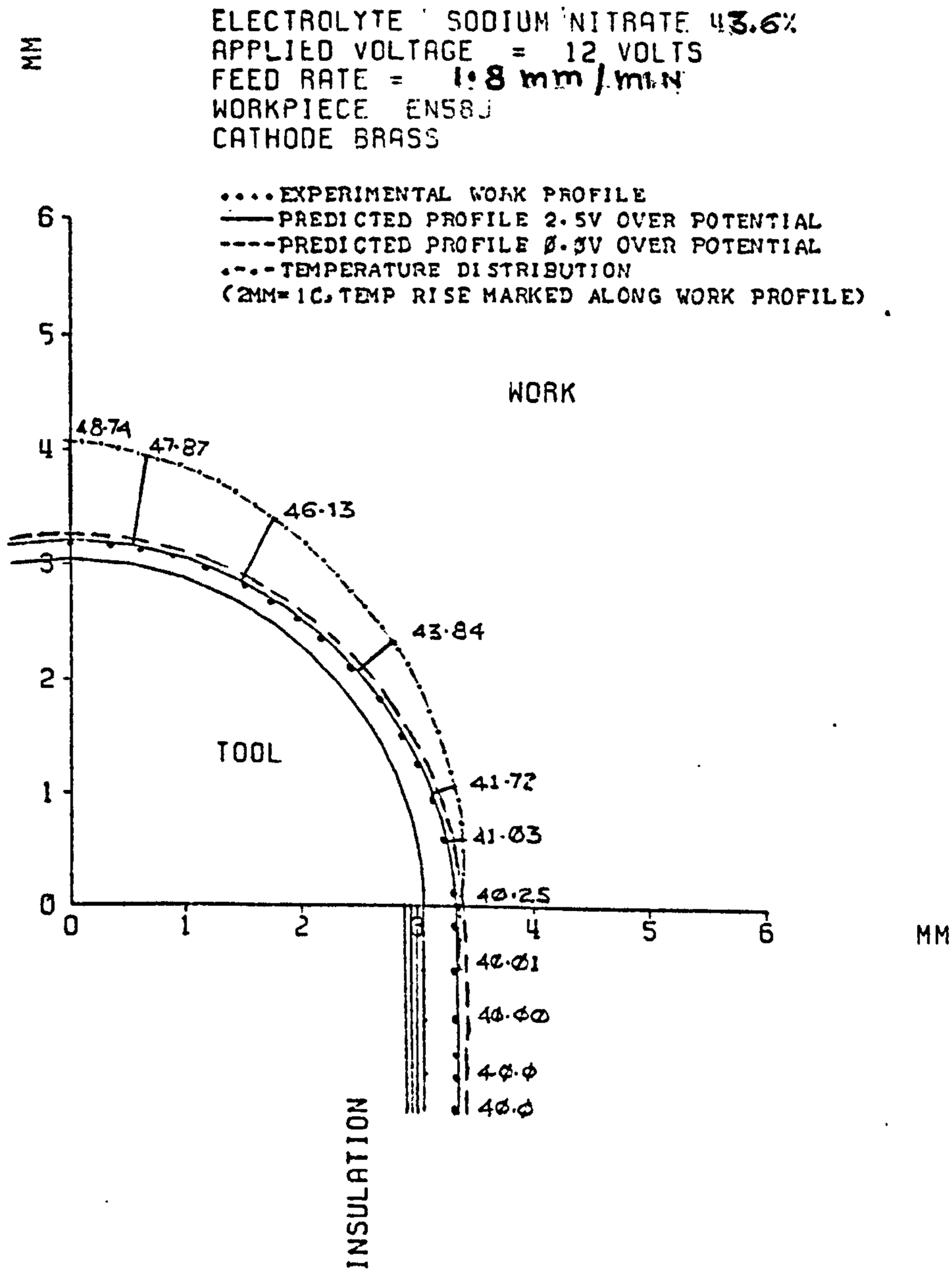
ELECTROLYTE SODIUM NITRATE 43.6%
APPLIED VOLTAGE = 12 VOLTS
FEED RATE = 1.8 mm/min
WORKPIECE EN58J
CATHODE BRASS
....EXPERIMENTAL WORK PROFILE
——PREDICTED PROFILE 2.5V OVER POTENTIAL
----PREDICTED PROFILE Ø.ØV OVER POTENTIAL
•-•-TEMPERATURE DISTRIBUTION
(2MM=1C, TEMP RISE MARKED ALONG WORK PROFILE)
WORK
TOOL
INSULATION
48.74
47.87
46.13
43.84
41.72
41.03
40.25
40.01
40.00
40.0
40.0
MM
MM
0
1
2
3
4
5
6

FIG. 6.25

MM.

ELECTROLYTE SODIUM NITRATE 43 6%
APPLIED VOLTAGE = 20.0 VOLTS
FEED RATE = 0·77mm / min
WORKPIECE EN58
CATHODE BRASS

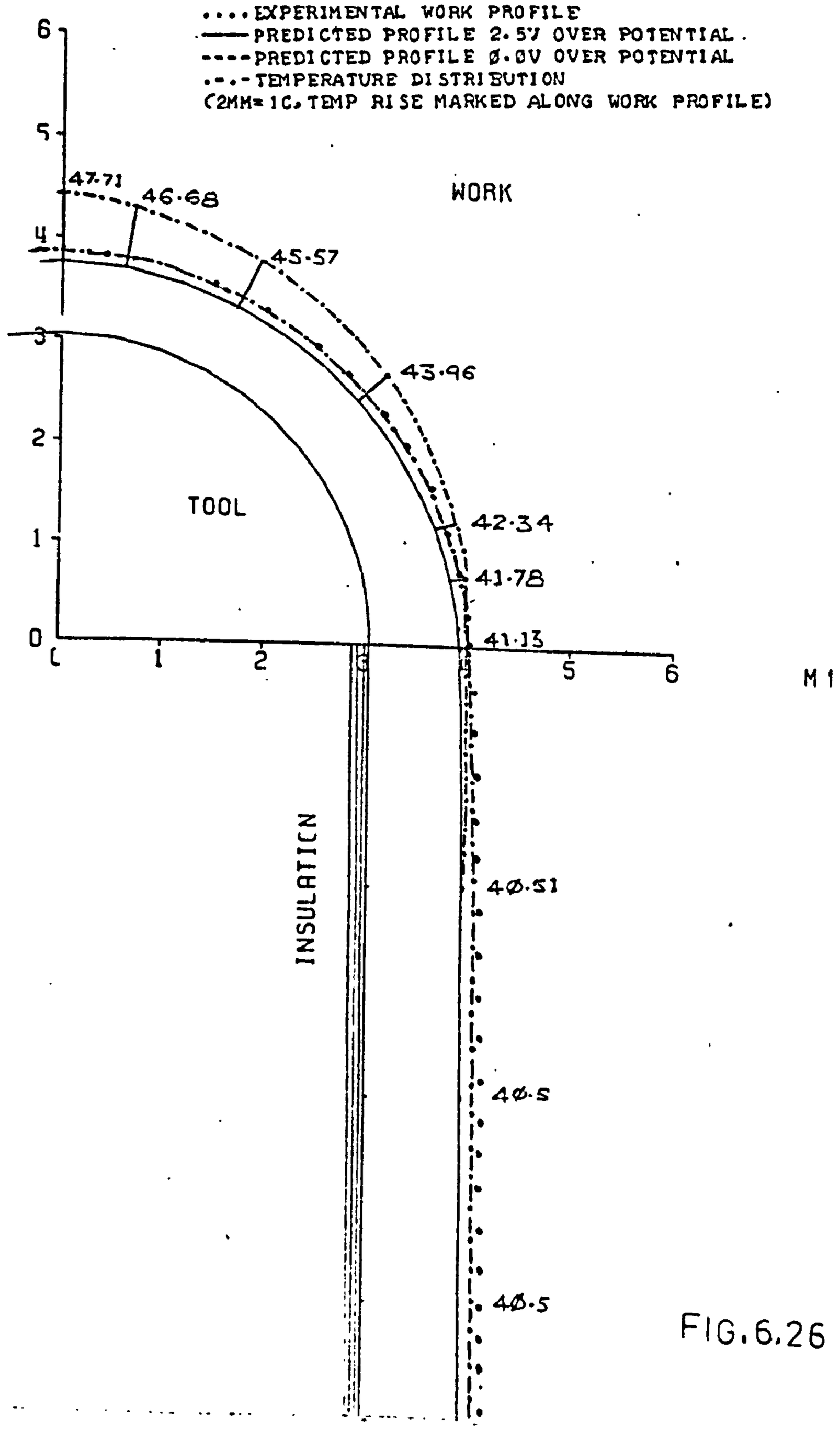

FIG.6.26

ELECTROLYTE SODIUM NITRATE 43.6%
APPLIED VOLTAGE = 20.0 VOLTS
FEED RATE = 0.96 mm/min
WORKPIECE EN58J
CATHODE BRASS

....EXPERIMENTAL WORK PROFILE
——PREDICTED PROFILE 2.5V OVER POTENTIAL
----PREDICTED PROFILE 0.0V OVER POTENTIAL
.-.-TEMPERATURE DISTRIBUTION
(2MM=1C. TEMP RISE MARKED ALONG WORK PROFILE)

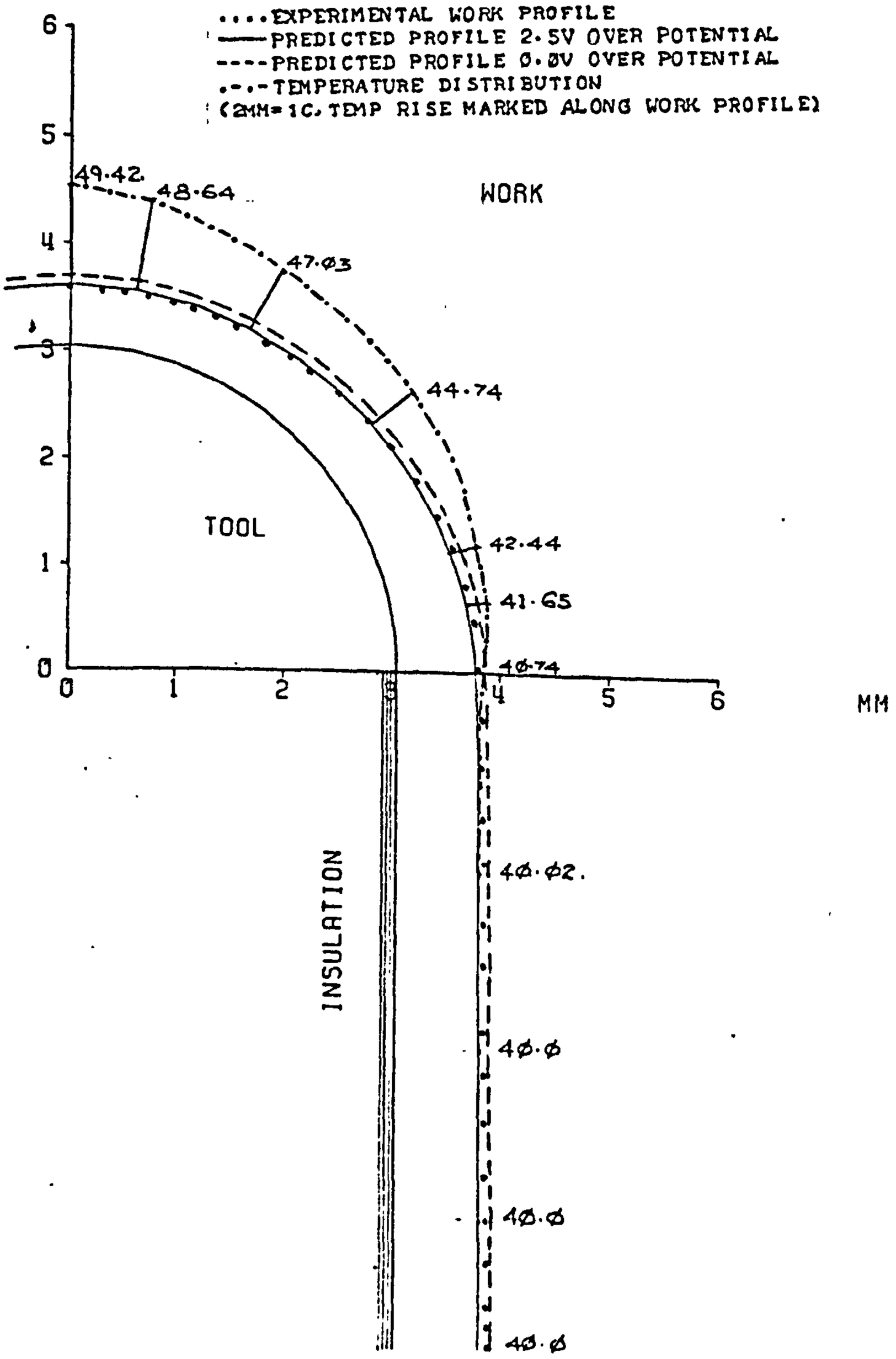

FIG. 6.27

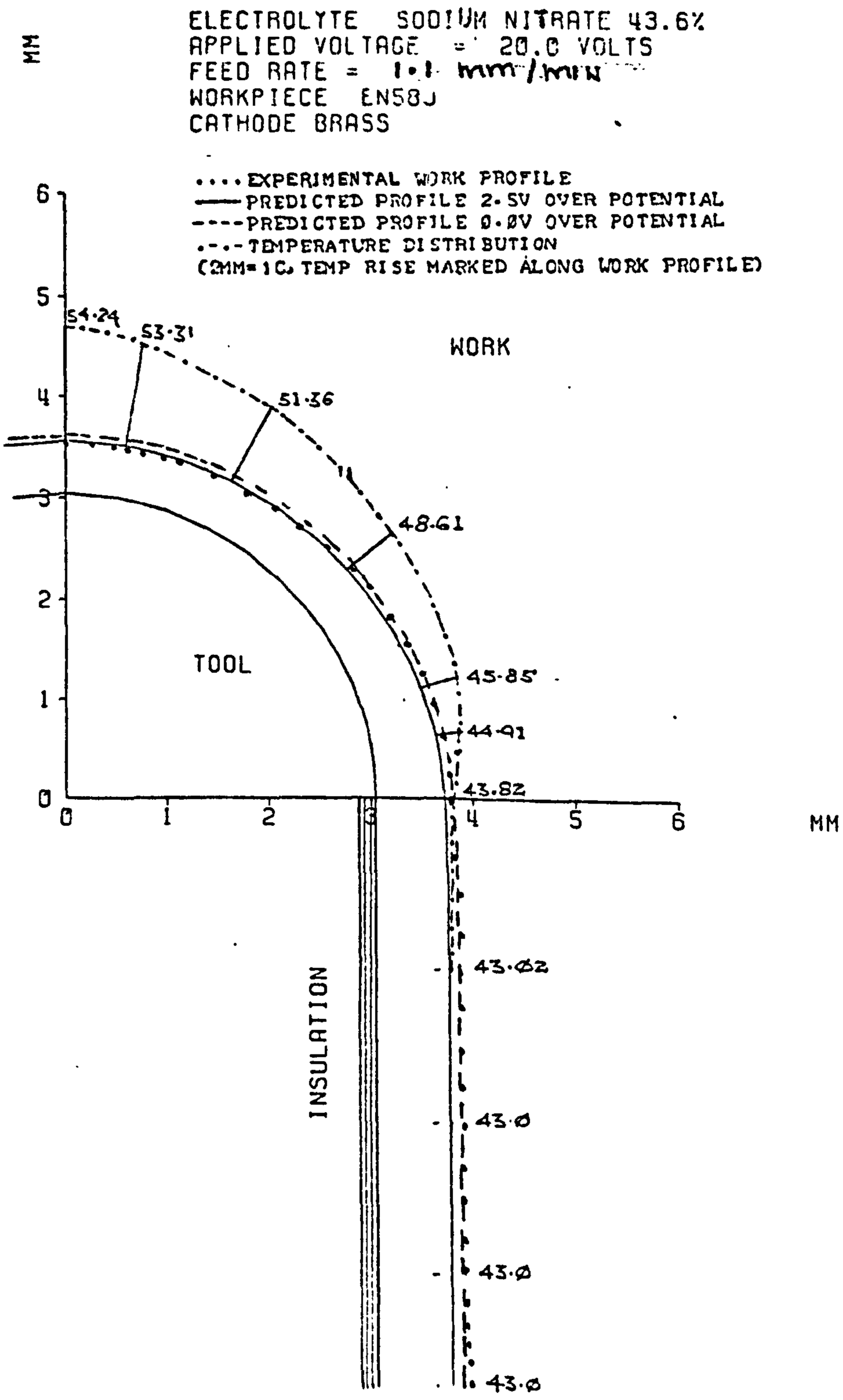
ELECTROLYTE SODIUM NITRATE 43.6%
APPLIED VOLTAGE = 20.0 VOLTS
FEED RATE = 1.1 mm/min
WORKPIECE EN58J
CATHODE BRASS
....EXPERIMENTAL WORK PROFILE
——PREDICTED PROFILE 2.5V OVER POTENTIAL
----PREDICTED PROFILE 0.0V OVER POTENTIAL
.-.-TEMPERATURE DISTRIBUTION
(2MM=1C. TEMP RISE MARKED ALONG WORK PROFILE)
WORK
TOOL
INSULATION
54.24
53.31
51.36
48.61
45.85
44.91
43.82
43.02
43.0
43.0
43.0
MM
0
1
2
3
4
5
6

FIG.6.28

ELECTROLYTE . SODIUM CHLORIDE 15%
APPLIED VOLTAGE = 16.0 VOLTS
FEED RATE = 0.8 mm/min
WORKPIECE EN58J
CATHODE BRASS

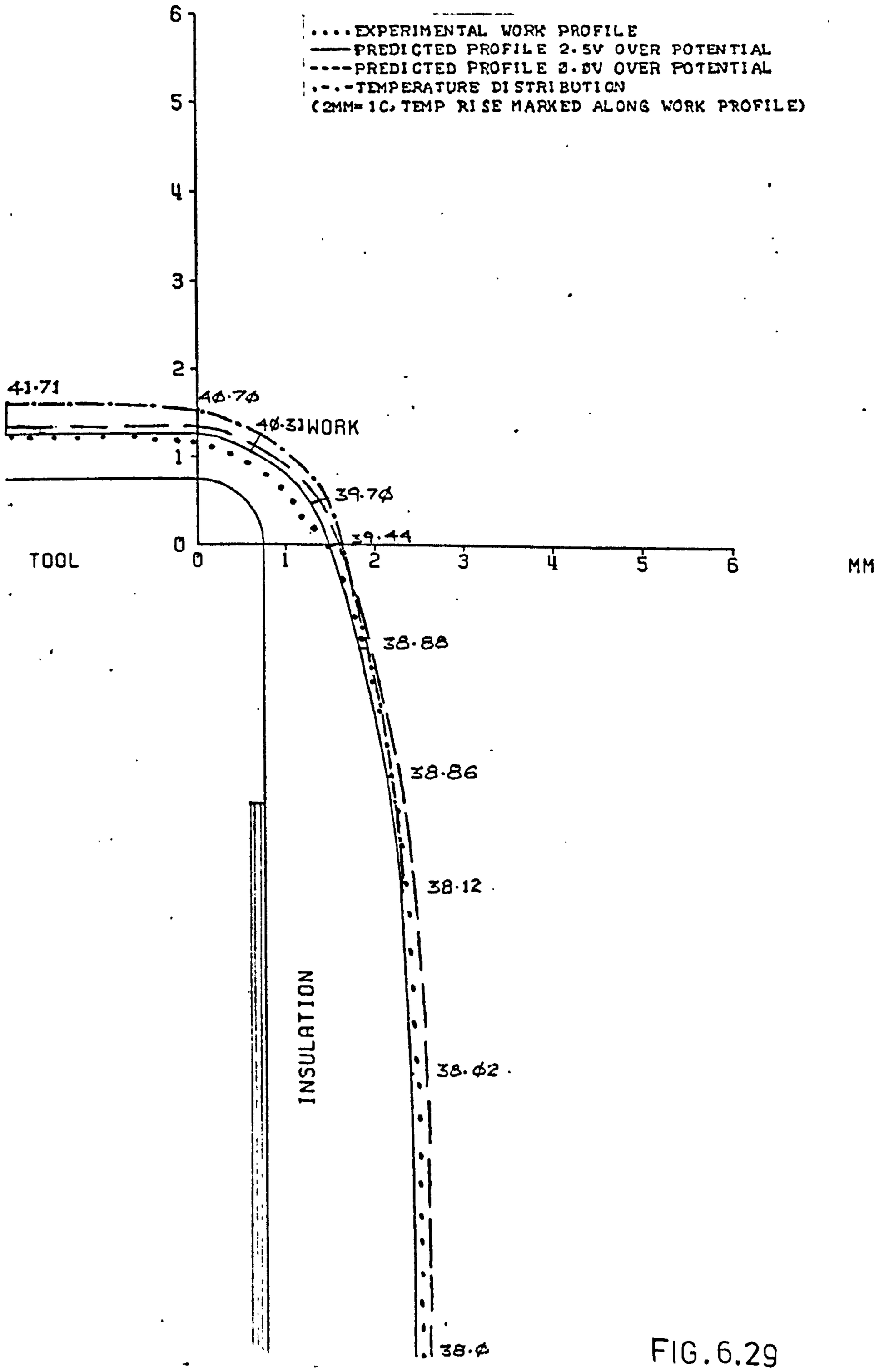

FIG. 6.29

ELECTROLYTE SODIUM CHLORIDE 15%
APPLIED VOLTAGE = 16.0 VOLTS
FEED RATE = 0.98 mm/min
WORKPIECE EN58J
CATHODE BRASS

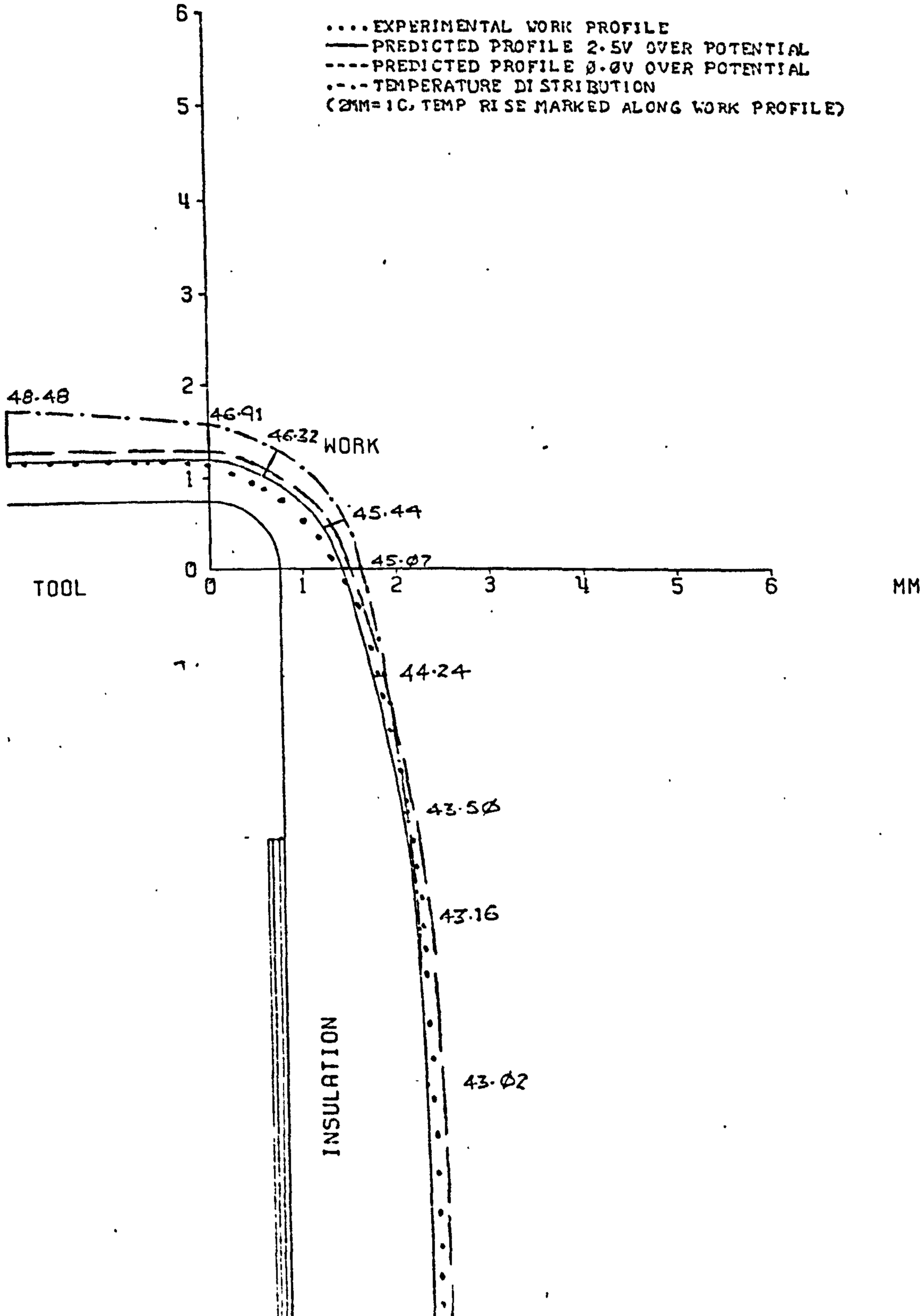

....EXPERIMENTAL WORK PROFILE
——PREDICTED PROFILE 2.5V OVER POTENTIAL
----PREDICTED PROFILE 0.0V OVER POTENTIAL
.-.-TEMPERATURE DISTRIBUTION
(2MM=1C. TEMP RISE MARKED ALONG WORK PROFILE)

FIG.6.30

ELECTROLYTE SODIUM CHLORIDE 15%
APPLIED VOLTAGE = 16.0 VOLTS
FEED RATE = 1.22 mm/min
WORKPIECE EN58J
CATHODE BRASS

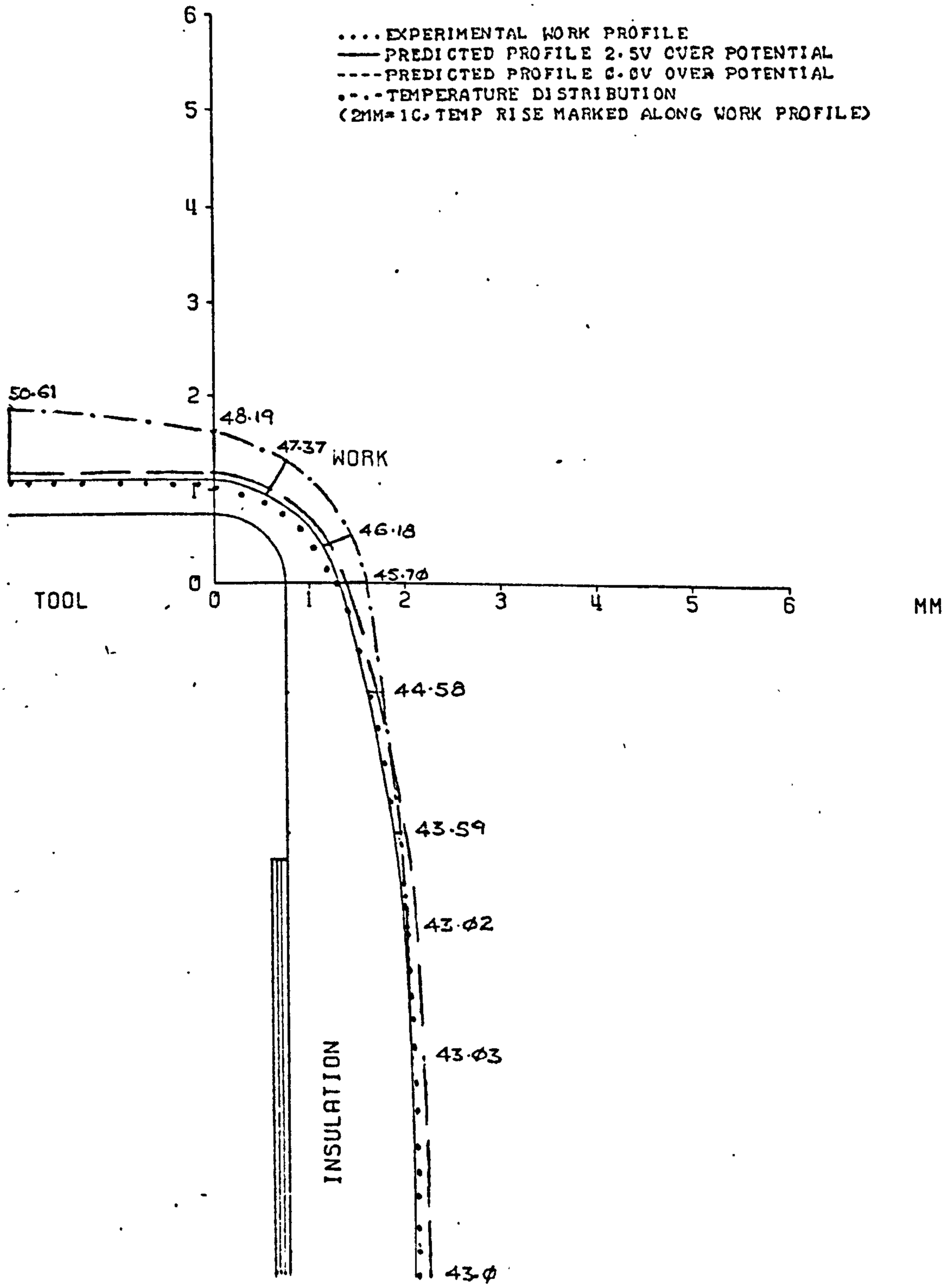

FIG. 6.31

Fig 9

ELECTROLYTE SODIUM NITRATE 43.6%
APPLIED VOLTAGE = 16.0 VOLTS
FEED RATE = 0.92 mm/min
WORKPIECE EN58J
CATHODE BRASS

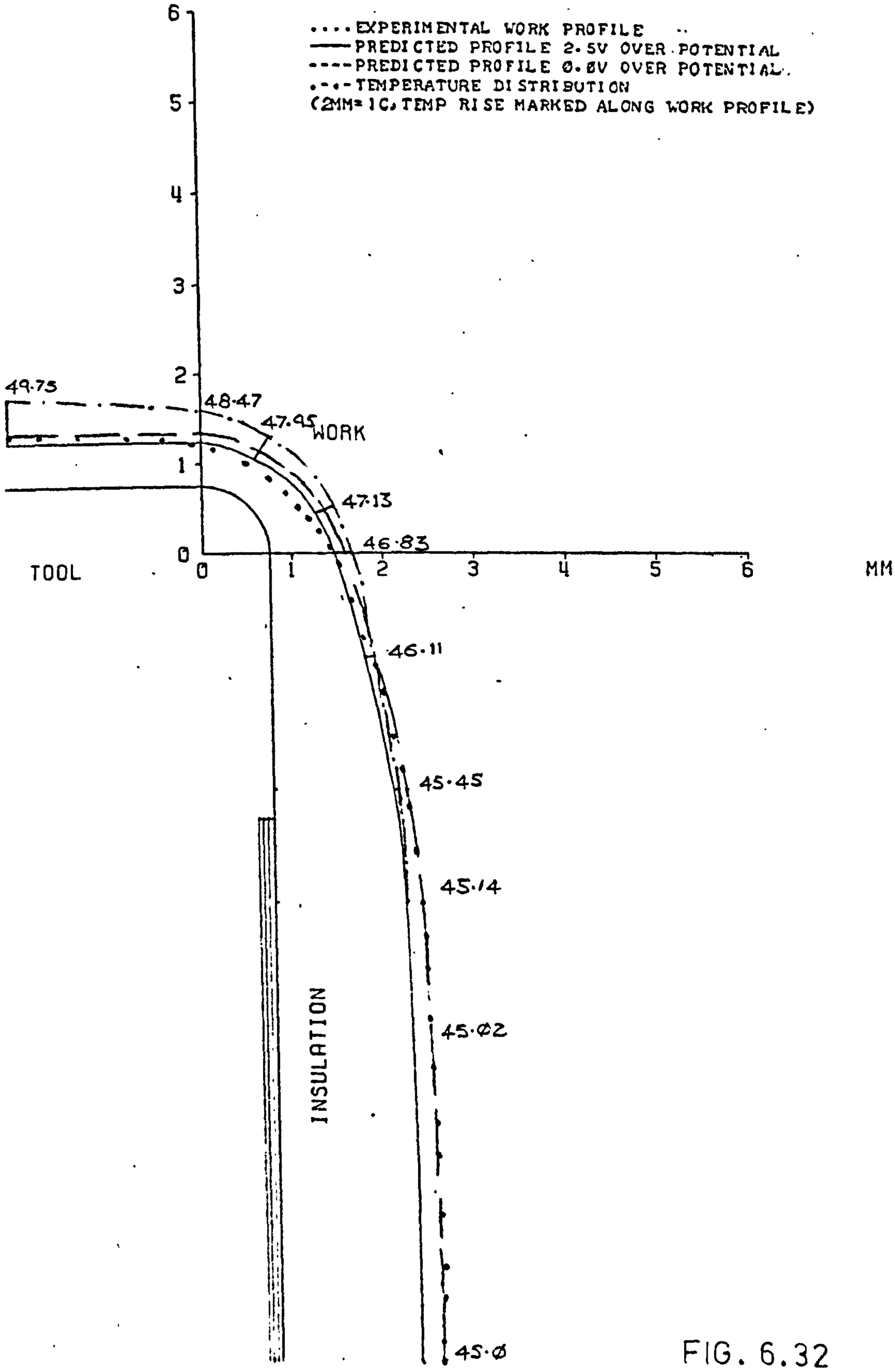

FIG. 6.32

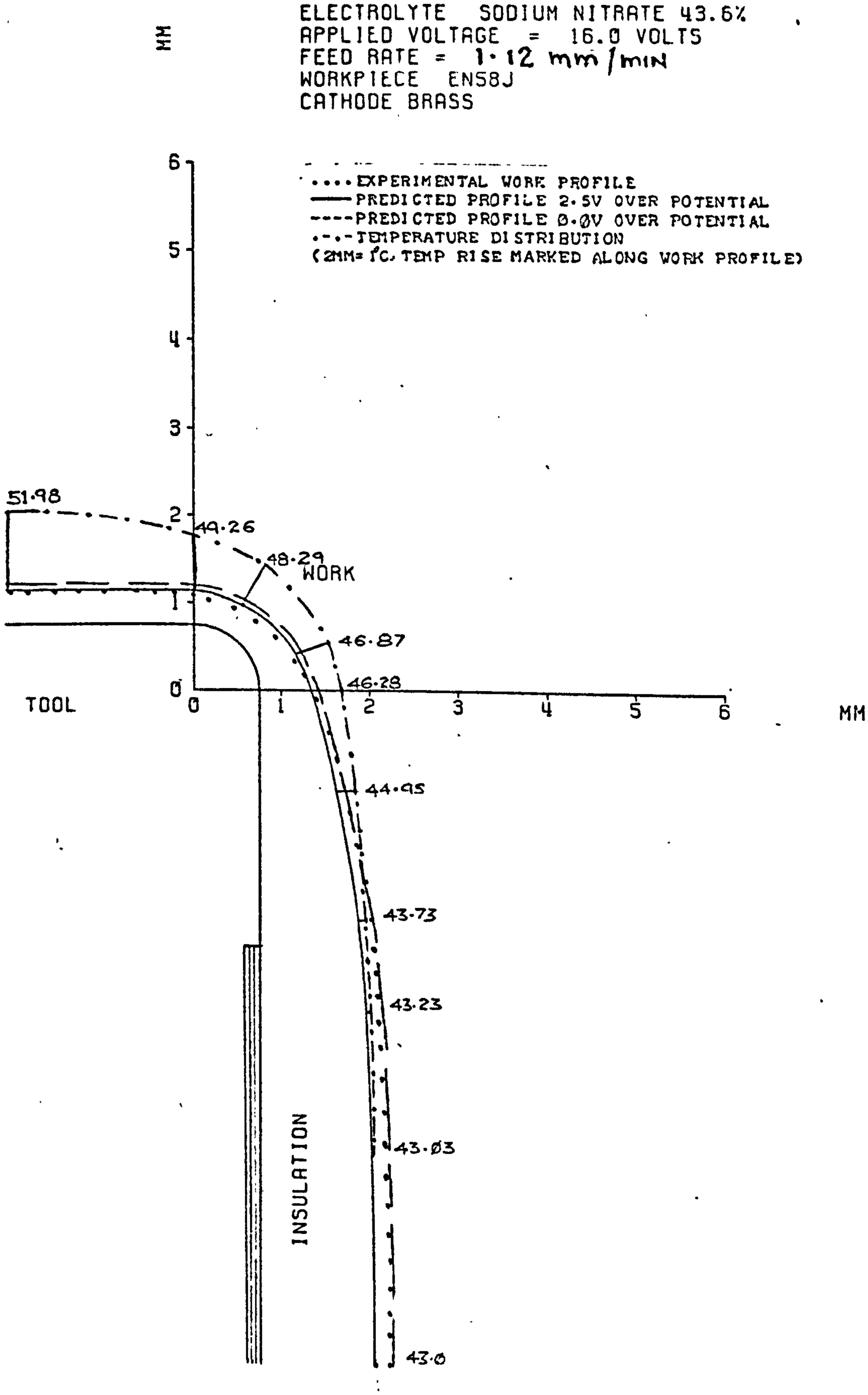
ELECTROLYTE SODIUM NITRATE 43.6%
APPLIED VOLTAGE = 16.0 VOLTS
FEED RATE = 1·12 mm/min
WORKPIECE EN58J
CATHODE BRASS
MM
····EXPERIMENTAL WORK PROFILE
——PREDICTED PROFILE 2·5V OVER POTENTIAL
----PREDICTED PROFILE 0·0V OVER POTENTIAL
·-·-TEMPERATURE DISTRIBUTION
(2MM= 1°C. TEMP RISE MARKED ALONG WORK PROFILE)
51·98
49·26
48·29
WORK
46·87
46·28
44·95
43·73
43·23
43·03
43·0
TOOL
INSULATION
0
1
2
3
4
5
6
MM

FIG. 6.33

ELECTROLYTE SODIUM NITRATE 43.6%
APPLIED VOLTAGE = 16.0 VOLTS
FEED RATE = 1.55 mm/min
WORKPIECE EN58J
CATHODE BRASS

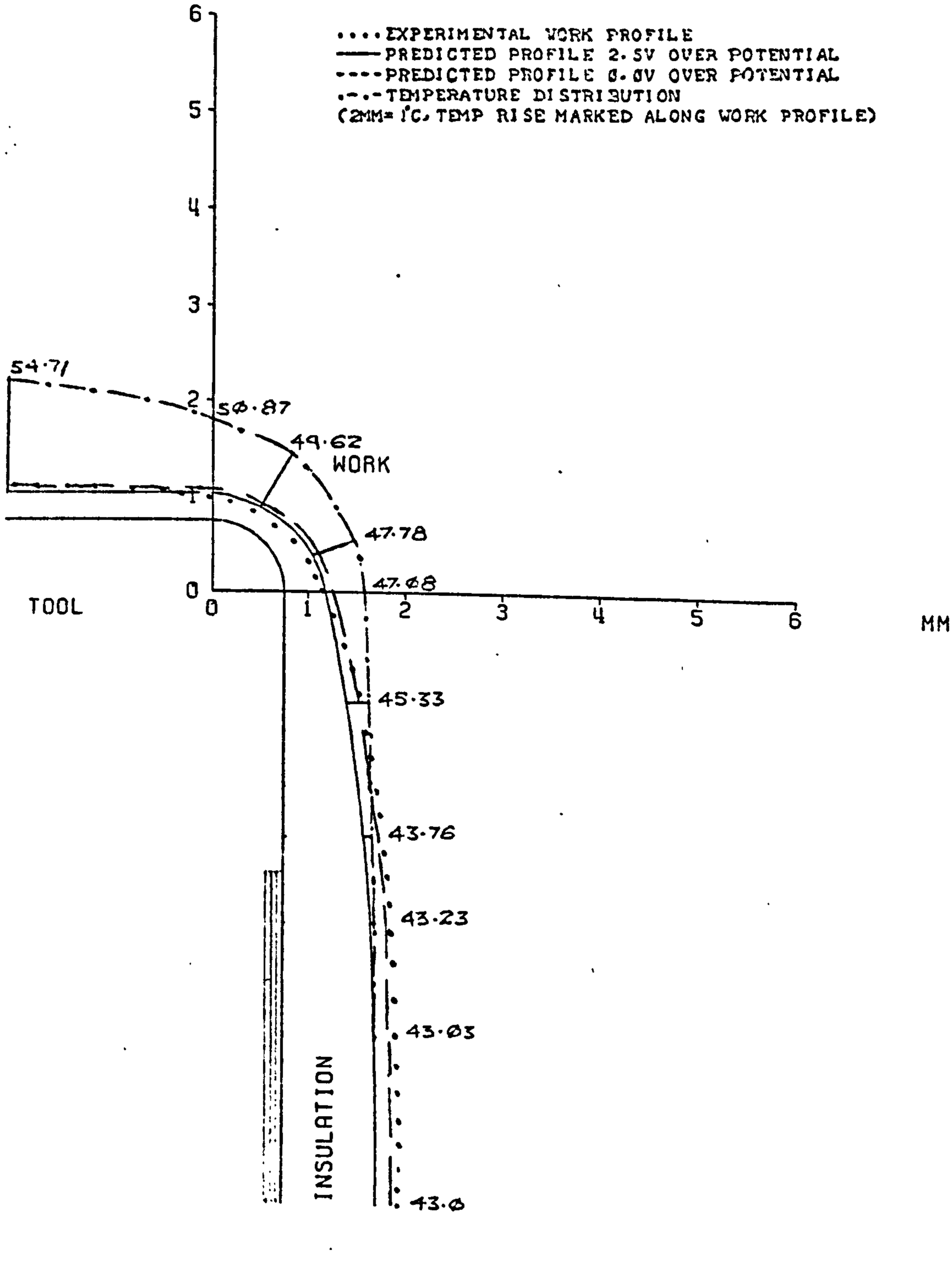

....EXPERIMENTAL WORK PROFILE
——PREDICTED PROFILE 2.5V OVER POTENTIAL
----PREDICTED PROFILE 6.0V OVER POTENTIAL
.-.-TEMPERATURE DISTRIBUTION
(2MM= 1°C. TEMP RISE MARKED ALONG WORK PROFILE)

FIG. 6.34

(c) Experimental errors.

Before reasoning out what caused these discrepancies, it should be worthwhile at this stage to give an account of general comparison between predicted and experimental profiles.

6.2.1 Machining with Hemispherical Leading Edge Tool

All experimental profiles obtained, machining with the hemispherical leading edge tool showed a smaller orthogonal equilibrium gap than those predicted by the developed mathematical model and these gaps were slightly smaller than the equilibrium gaps predicted by the simple equation 1.11. The predicted work profiles resembled very closely the experimental work profiles. All machined surfaces obtained with sodium chloride electrolyte showed that the theoretical predictions obtained at 2.5V over-potential were better representations of the work profile than those obtained at O.OV overpotential, other machining parameters being kept the same. However with sodium nitrate electrolyte experimental profiles obtained machining at 12V applied cell voltage were nearer to the theoretical predictions at 2.5V overpotential. Machining at 20V applied cell voltage, profiles were nearer to the predicted for O.OV overpotential. Thus bearing out for the whole profile the pattern which was observed for the overcut alone.

6.2.2 Machining with Straight Leading Edge Tool

The predicted profiles obtained for machining with straight leading edge tool were not such a good representation of the experimental profiles, as in the case of hemispherical leading edge tool. The predicted equilibrium gaps at 2.5V overpotential for both sodium chloride electrolyte and sodium nitrate electrolyte were smaller than the actual gap size. The machined profiles had a steeper curvature starting from the region where the equilibrium gap was measured up to the region opposite the land width of the tool work profile gave a region with smaller gaps than those predicted.

In the remaining region the curvature of the experimental profile was less steep and gave larger final gap than that predicted at 2.5V overpotential.

6.2.3 Surface Defects

Apart from deviation of predicted work profiles from corresponding experimental profiles, the surfaces of the machined profiles showed some surface defects which are enumerated below.

Machining with 15% w/w NaCl Electrolyte

a) Straight leading edge tool applied cell voltage 16V. The surfaces of all the machined specimens were very badly pitted indicating preferential machining. The peaks were brightly polished and the valleys showed agressive etching.

b) Hemispherical leading edge tool, cell voltage 16V. The walls of the machined holes were smooth. The region opposite the hemispherical leading edge was brightly polished.

c) Hemispherical leading edge tool, cell voltage 20V. The walls of the machined holes were badly pitted as in the case (a). Nevertheless, the regions opposite the leading edge were brightly polished.

Machining with 43.6% w/w $NaNO_3$ Electrolyte

a) Straight leading edge tool, cell voltage 16V. All machined surfaces were smooth. The base of the drilled specimen and the region of the work surface opposite the corner radius of the tool were brightly polished.

b) Hemispherical leading edge tool, cell voltage 12V. All machined surfaces were smooth. The regions of the work surfaces opposite the leading edge of the tool were bright and also showed slight striation marks.

c) Hemispherical leading edge tool, cell voltage 20V. Surfaces were similar to that obtained machining at 12V, but the striation marks were more pronounced opposite the leading edge of the tool.

6.3 TEMPERATURE DISTRIBUTION

The temperature increase of the electrolyte due to joule heating increases the conductivity of the electrolyte due to increased mobility of the ionic species. Since the

temperature of the electrolyte is different along the work profile, the change in conductivity due to this temperature increase will also vary. This affects the shaping performance but also the adverse rise in temperature could result in machining failure due to electrolyte boiling.

6.3.1 Theoretical Temperature Distribution

The temperature increase along the work profile due to joule heating as predicted by the equation 3.11 is displayed in Figs. 6.17 to 6.34. The computed temperature rise of the electrolyte is shown as a vector along the corresponding transverse lines of the mesh. It is evident from these figures, that most of the heating of the electrolyte occurred in the high current density region of the electrode gap. The heating of the electrolyte opposite the insulated part of the tool was negligible due to very low electrical energy input into the electrolyte in this region.

6.3.2 Correlation of Experimental and Predicted Gap Temperatures

Figs. 6.35 to 6.38 show the plots of temperature increase in the interelectrode gap recorded using thermistor circuits described in Appendix A2, and those obtained from the computer model, plotted against feed rate. Since the electrolyte flow rate varied with each test run, a direct plot of temperature increase against flow rate would be

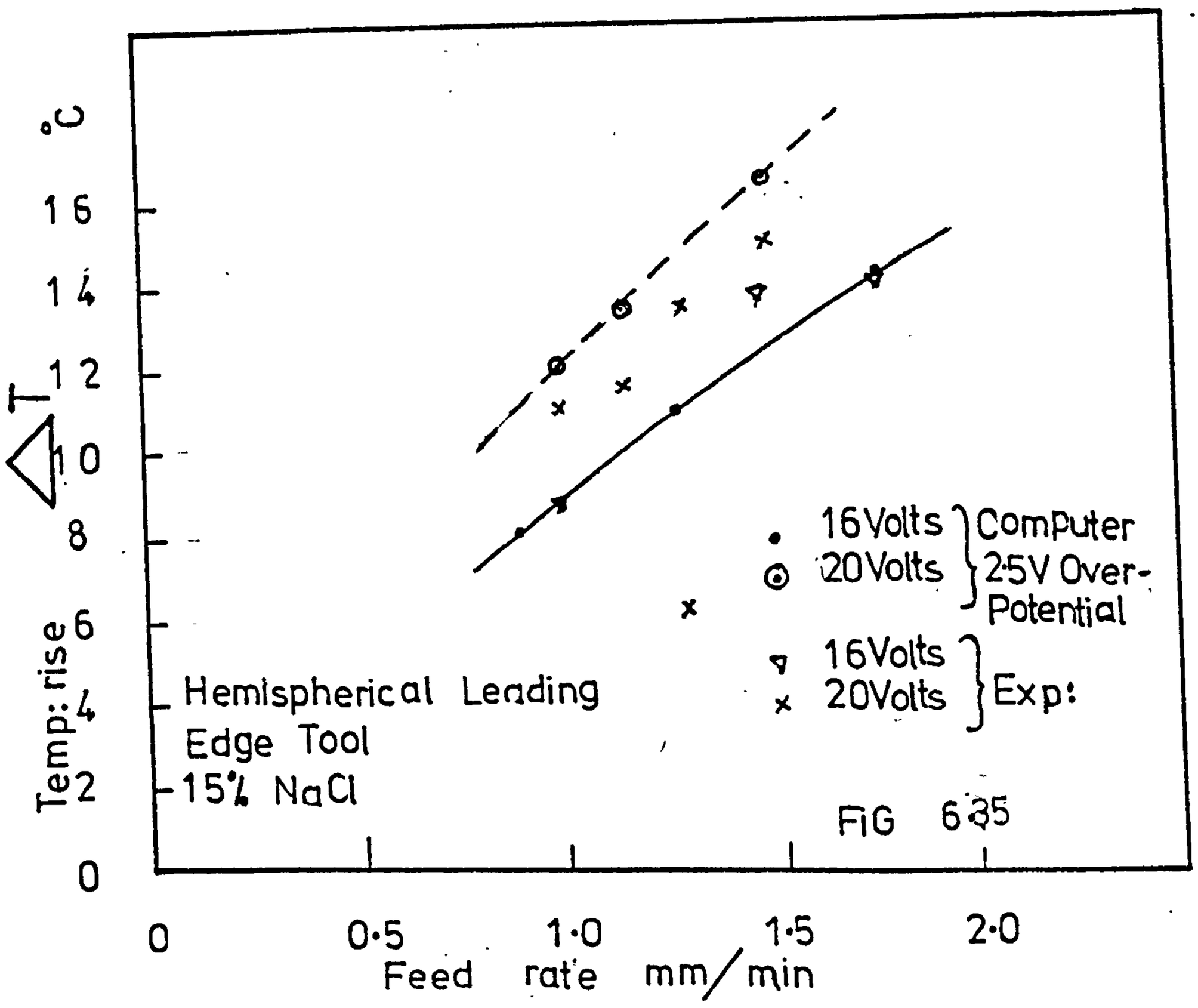

FIG 6·35

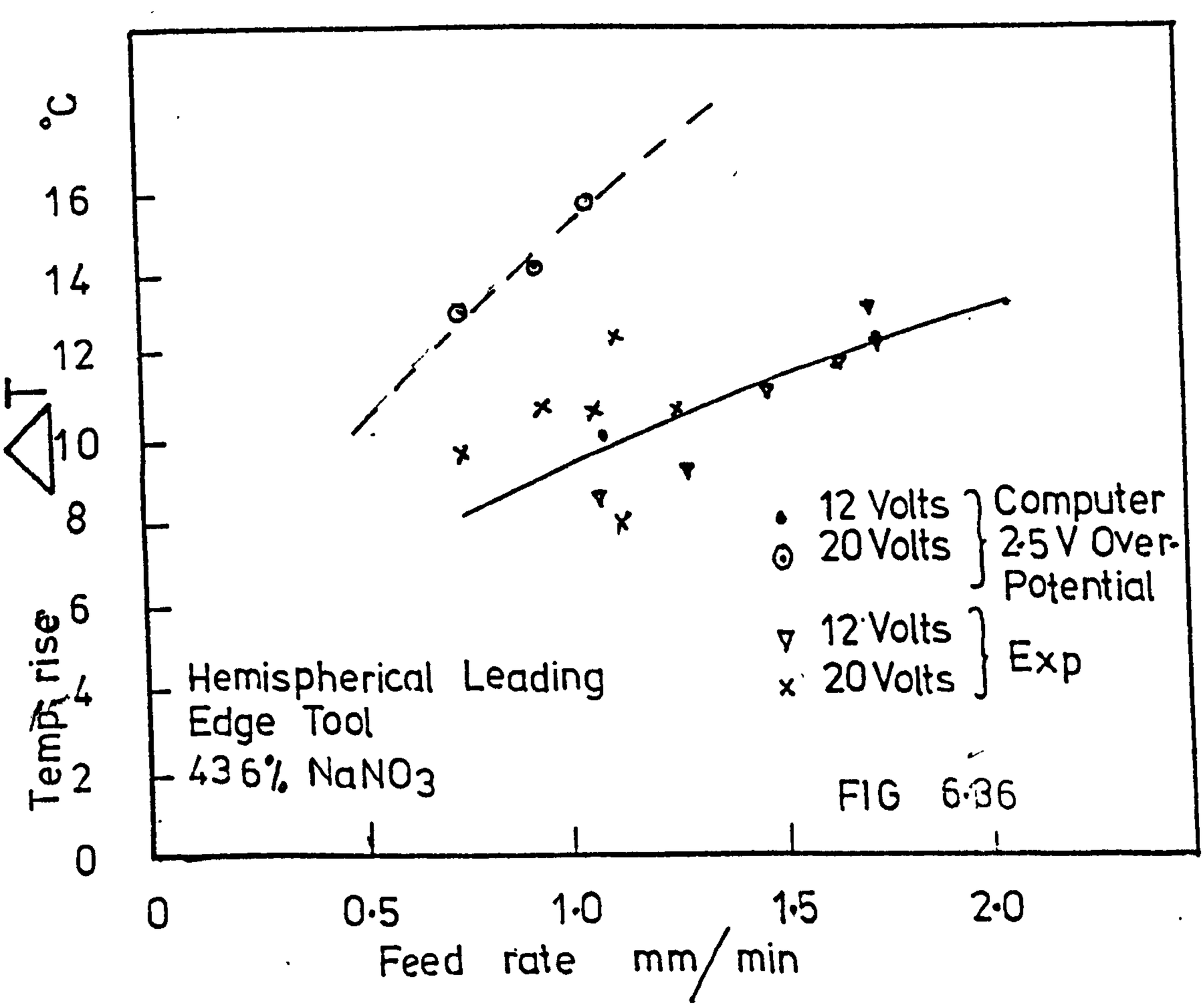

FIG 6·36

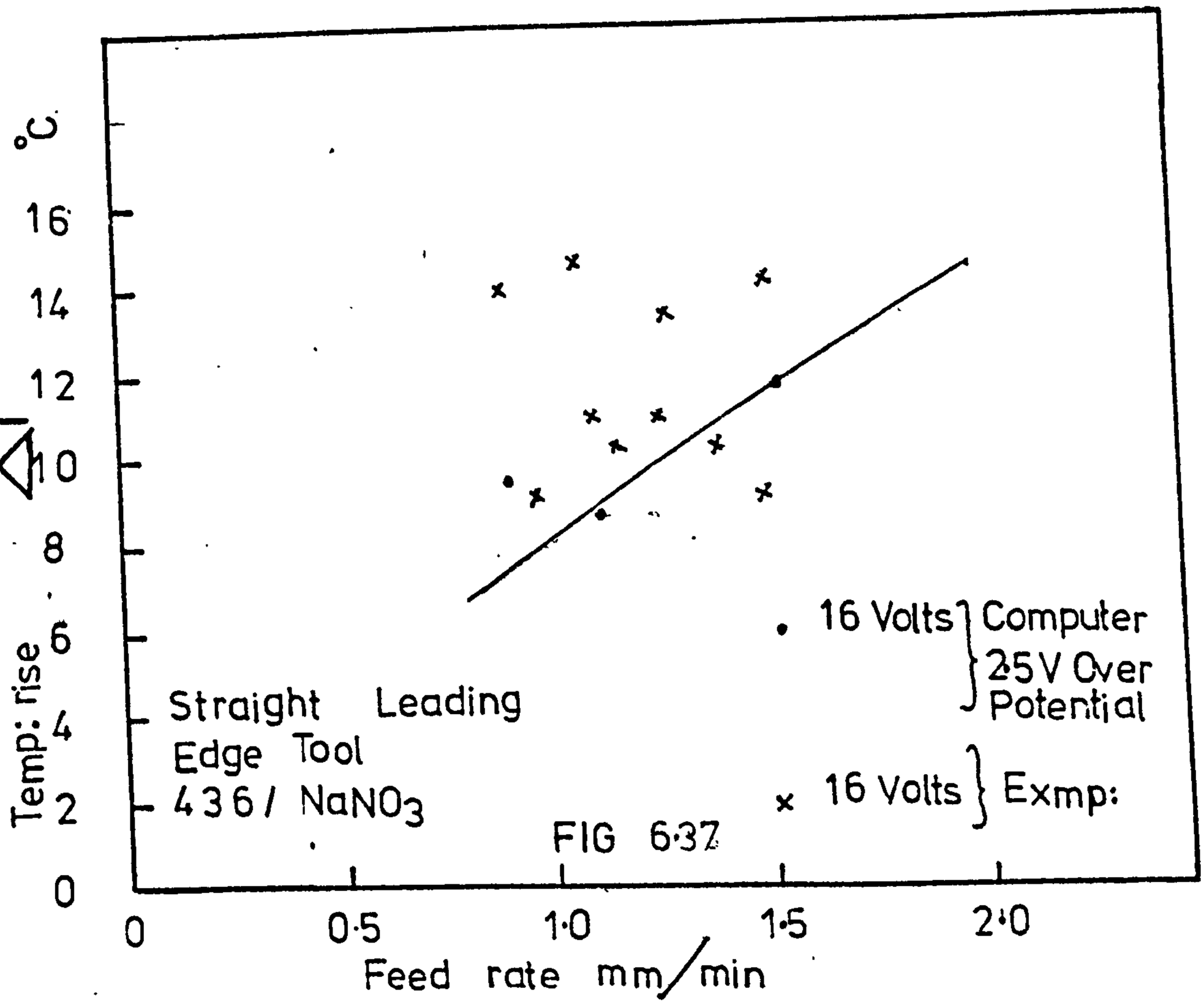

FIG 6·37

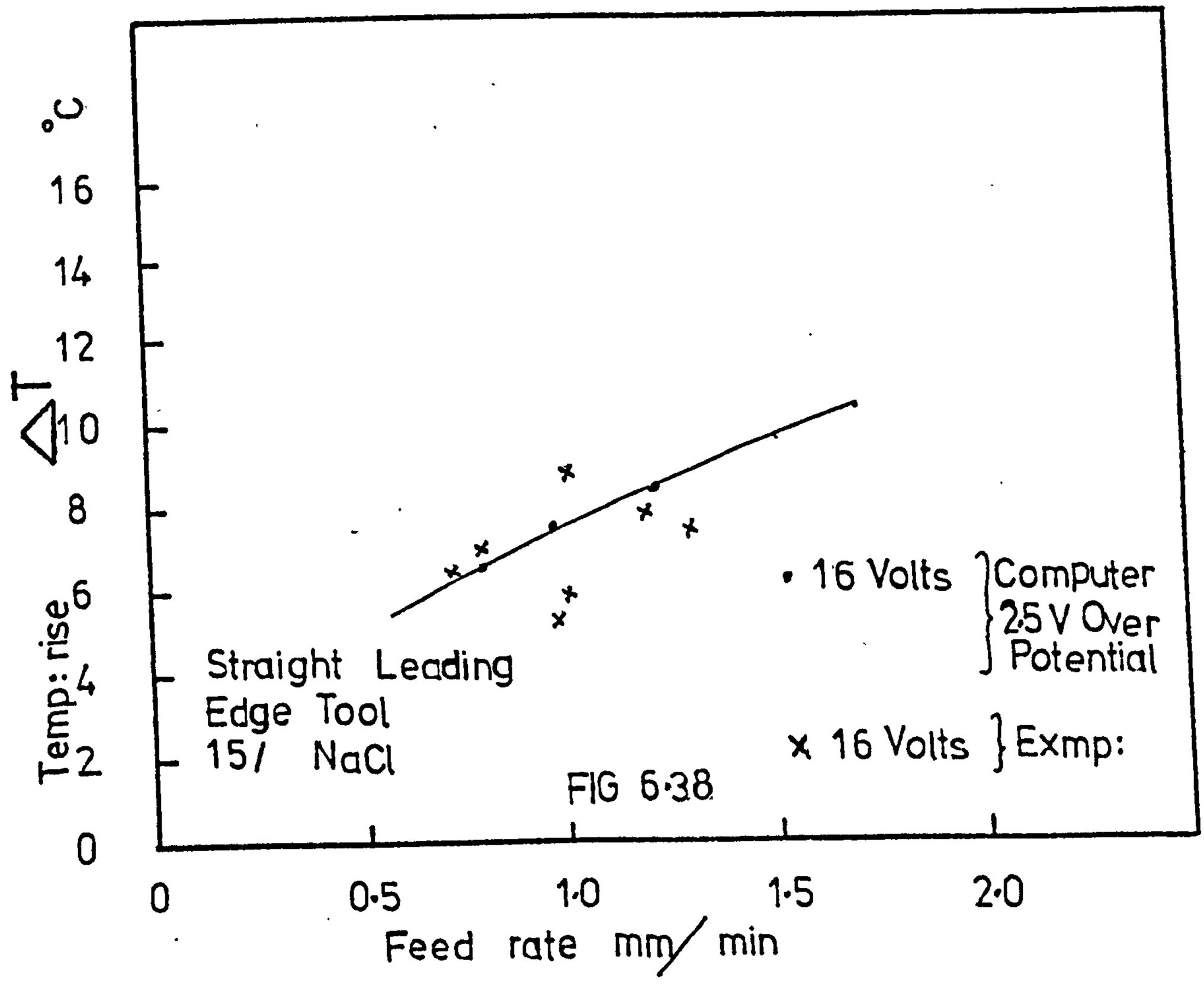

FIG 6·38

meaningless, and such a plot does not indicate any physical phenomenon. The temperature increases shown in Figs. 6.35 to 6.38 were calculated assuming electrolyte flow of 5 liters per minute rather than the actual flow rate, which varied slightly about this value with each test run.

The experimental results compared well with those obtained from the computer model considering that the actual flow rates were not used. It is very significant that the temperature rise increased with tool feed rate, i.e. with increase in current density. Also the temperature rise increased with an increase in cell voltage. The actual and calculated temperature increase for the $NaNO_3$ electrolyte for the same tool feed rate and cell voltage was higher than that of NaCl electrolyte; this is due to low specific heat of $NaNO_3$ electrolyte. The specific heat of 43.6% $NaNO_3$ electrolyte and 15% NaCl electrolyte being $2.97\ kJ\ kg^{-1}\ ^{\circ}K^{-1}$ and $3.58\ kJ\ kg^{-1}\ ^{\circ}K^{-1}$, respectively.

The trend of all experimental points obtained, machining with the hemispherical leading edge tool showed that the computer predicted results were an overestimate with both NaCl and $NaNO_3$ electrolyte machining at 20V. However one should expect this sort of error. In compilation of the theoretical model the heat lost to the surroundings via the tool holder and the work holder was neglected. Apart from this the thermistor which was installed in the tool electrode measured the mid stream temperature of the electrolyte. This temperature differs from the temperatures of the neighbouring layers of the

electrolyte. The temperature of the electrolyte adjoining the cathode will be greater due to the reduction of area available for passage of current not only due to the curved electrode but also due to the liberated gas bubbles. Clark (22) using plane parallel electrodes found that the temperature measured at the outlet from the machining cell to be lower than the temperature measured at adjacent to the cathode. This is due to the mixing of the electrolyte at the outlet from the machining cell, the electrolyte near the cathode which is a mixture of gas and pure electrolyte will be at a higher temperature than those layers with less or no gas mixed. The mixing of electrolyte gives an average temperature which will be higher than the mid stream temperature of the electrolyte. The temperature computed by the theoretical model is the average temperature of the electrolyte across the gap and not the mid stream temperature as measured by the thermistor. Machining at 16 volts with NaCl and 12 volts with $NaNO_3$ the computer predicted results were closer to the experimentally measured gap temperatures. This may be due to the fact that at lower frontal gaps encountered machining at these voltages than at 20V, the bead of the thermistor which sensed the temperature covered most of the frontal gap giving an average temperature of the electrolyte layers across the gap.

The low predicted gap temperature obtained when machining with $NaNO_3$ electrolyte using a straight edge

tool were mainly due to predicted smaller machined diameters. Since the smaller predicted shapes require less energy input than the larger experimental shapes, for the same electrolyte flow, the temperature increase with the experimental machining should be larger than the corresponding predicted values.

CHAPTER VII

DISCUSSION

7.1 INTRODUCTION

The simulation model which was described in chapter 2, solves the direct free boundary problem. The developed computer program reads from data cards the tool geometry, machining parameters and electrolyte properties, and predicts the unique equilibrium work profile and the temperature distribution of the electrolyte over the work surface. This computer program can also be utilized to predict the intermediate positions of the work profile.

The extent to which the model could satisfactorily predict the steady state electrochemically machined work profile and the factors which limit the accuracy of the model has been obtained by comparing its predictions with experimental results. The many assumptions made during the development of the computer model being justified where the correlation was satisfactory. Discrepancies between the analytical and the experimental results indicate where further improvements to the model are required. One way of improving the model would be to make arbitrary adjustments, for example by using some form of empirical coefficients for the modification of gaps between electrodes to produce a better predicted work profile but this would tend to obscure the real cause of these discrepancies and the effort involved in developing this model would be lost. As there is no single criterion to judge the overall validity of the model, the discussion is based on the extent of the agreement between predicted and experimental work piece shapes obtained for

certain representative values of 'tool feed rate', 'machining voltage', 'overvoltage', machining efficiency' etc.

7.2 ELECTROCHEMICAL ASSUMPTIONS

The mathematical model predicts only the primary current distribution and does not take into consideration the influence of the following factors in machining performance.

(a) the change of overpotential with current density.

(b) possible changes in valency with current density although such changes should be accounted for by the efficiency correction.

(c) changes in electrolyte conductivity due to heating effect and gas evolution.

The uninsulated surfaces of the electrodes were considered as equipotential surfaces, even though this is true the polarization which is usually an unknown function of the current density ensures that the layer just adjoining the electrodes is not an equipotential surface. Klingert, Lynn and Tobias (26) using a standard finite difference approach calculated the current distribution in an 'L' shaped region considering both linear and Tafel polarization. In electroplating once the current distribution is evaluated, the deposition performance can be predicted; further prediction of current distribution will not be necessary, since the shape of the electrodes are not changed significantly during the process. In

ECM however the work piece shape is altered consistently and the current distribution is changed and the extra calculation in finding the distribution many times for non-equipotential surfaces is prohibitive. Again since the electrodes are in close proximity the polarization of both electrodes has to be considered.

This effect of polarization can be seen for both sets of test results obtained with the hemispherical leading edge tool and straight leading edge tool. With the hemispherical leading edge the electrode gap directly opposite the leading edge was smaller than that predicted by assuming 2.5V overpotential; with the straight leading edge tool the gap opposite the small corner radius of the tool was much smaller than that predicted at 2.5V over-potential. To explain the overpotential effect consider a current flux 'i' flowing at section in the inter-electrode gap. To maintain this current the applied voltage should have a magnitude V volts given by

$$V = (E_c - E_a) + \eta_a + \eta_{conc} + \eta_r + iR$$

where E_c and E_a are the reversible electrode potentials at the cathode and the anode respectively, η_a, η_{conc} and η_r are activation, concentration and resistance overpotentials and iR the ohmic drop across the electrode gap. In practice it has not been possible to measure overpotential satisfactorily for electrochemical machining conditions but it may be safely assumed that higher the current density the larger will be the value of over-

potential thus the available potential for driving current through the ohmic resistance of the solution will be reduced by this amount. In the theoretical model the assumed 2.5V overpotential which represents the algebraic sum of E_c, E_a, η_a, η_{conc} and η_r appears to be an underestimate in the high current density regions such as opposite the leading edge of the tool, opposite the corner radius. Since the available voltage for ECM was reduced by this increased amount of overpotential and since the applied cell voltage was constant, the only way of maintaining steady state machining was by reduction of the gap in the high current density areas.

7.3 MACHINING RATES AND EFFICIENCY

The accuracy of the mathematical model depends on the accuracy of the erosion vector, used to calculate the amount of shift of a nodal point on the work surface. Since the erosion vector was found by the product of local current density and specific volumetric metal removal rate, the actual metal removal rate at different current densities should be known. The difficulties encountered in finding the actual metal removal for a given current density are given in (5), and is reviewed in Chapter I. For steels such as EN58J many valency combinations of dissolution can be found to give a theoretical metal removal rate which is closer to the experimental one. In both cases of 15. % sodium chloride and 43.6% sodium nitrate, the specific metal removal rate obtained from

experimental data corresponded to dissolution valencies of 6 and 2 for chromium and nickel. Iron corresponded to dissolution at mixed valencies of 2 and 3. Iron and chromium which are found in alloyed steel have stable ions for more than one valency. There is evidence that the constituents of steel dissolves at different valencies at different current densities. Mazaffaruddin's (33) experimental results showed that when machining stainless steel EN58a in 10% NaCl, below a current density of about $1A/mm^2$ the dissolution of steel corresponded to valencies of 3, 2 and 2 for chromium, nickel and iron, but with further increase in current density the metal removal rate varied abruptly and the dissolution corresponded to mixed valencies of 3 and 6 for chromium. Another explanation of observed rates is with very high current densities encountered in ECM existence of side reactions is a definite possibility. Part of the current passing across the anode interface might well be used in producing oxygen. Even though it was assumed in calculation of theoretical work profiles that NaCl is 100% efficient, there is evidence (36) that efficiency is dependent on current density and electrolyte flow rate.

Cuthbertson and Turner (36) machining Nimonic 80 in saturated NaCl, found that the current efficiency decreased from 82% at 15.5 Amp/cm^2 to 76% at 46.5 Amp/cm^2. Increasing electrolyte flow velocity from 1.26 meter/sec to 2.85 meter/sec the current efficiency was observed to increase slightly from 74% to 76%. The average

current densities encountered machining with NaCl ranged from 50 Amp/cm^2 to about 100 Amp/cm^2. A typical flow rate was about 5 meter/sec. However, a decrease in current efficiency with an increase in current density for mild steel machined in 2 molar and 4 molar NaCl electrolyte has been reported by Mao, (4) the current efficiency which was 99% at 26 Amp/cm^2 reduced to 94% at 62 Amp/cm^2. For nickel-chromium alloy machined in $NaClO_3$, $NaNO_3$, $NaNO_2$, Na_2SO_4 and $Na_2Cr_2O_7$ electrolytes increase in current efficiency with current density has been reported by König. (10) The part of the least squares curve obtained from experimental results Fig. 6.3 showed a similar trend. The efficiency changed from 82.5% at 75 Amp/cm^2 to 97.5% at 125 Amp/cm^2. Similar results were also observed by Mao (37) for mild steel machined in $NaClO_3$, $NaClO_4$ and $NaNO_3$ electrolytes. Mao (37) suggests this effect is largely due to an iron oxide film formed on the anode surface. The oxide film which forms at the anode acts as a barrier which hinders the mobility of reaction products, thereby reducing the metal removal rate. The magnitude of this reduction depends on the thickness of the film and with diminished metal removal, part of the current is used in liberating oxygen. Mao (37) suggests that as the current density is increased the thickness of the film decreases and so metal removal is increased. Chikamori and Ito (38) also reported that the current efficiency for mild steel machined in $NaNO_3$ solution increases with increasing current density.

7.4 EFFECT OF ELECTROLYTE HEATING AND FLOW RATE ON SHAPING PERFORMANCE

There are many ways in which solution temperature affects gap processes. The conductivity is the most important property of an electrolyte when predicting shaping performance. The electrolyte conductivity is determined by the mobilities of the ionic species present and their concentrations. An Increase in temperature, increases the mobility of the ionic species and results in increased conductivity. Apart from this, a temperature increase also speeds up the electrode reactions, that is reduces the overvoltages required. The solubility of the reaction products increases and the pressure required to force electrolyte through the gap at the desired rate is reduced due to a lower viscosity of the electrolyte at elevated temperatures. The average increase in temperature of the electrolyte opposite the leading edge of the tool was about $10^{o}C$. The increase in conductivity of a 43.6% $NaNO_3$ electrolyte for this temperature rise is 16% and for 15 .% NaCl electrolyte is 13.8% of the conductivities at $40^{o}C$. The corresponding increase in orthogonal gap will be of the same order since this gap is directly proportional to the conductivity, equation 1.11. However, these changes are quite insignificant compared with size of the frontal gap. However, a higher temperature rise could lead to significant variations in electrode gap giving a work profile which would not be acceptable. Limitation of tool feed rate due to

electrolyte boiling is proposed in Ref. (5,22) . The gas evolved during machining usually reduces the effective conductivity. Under steady-state machining conditions, these changes in conductivity due to heating and gas are compensated by a corresponding change in the inter-electrode gap, so that the steady state local current density does not vary along the anode surface. Since most of the gas was evolved in the high current density area, which was opposite the leading edge of the tool the electrode gap in this region should be smaller than that predicted by the computer program, neglecting the effect of gas bubbles. The good agreement of the experimental and predicted work profiles in this region indicates that the effect of gas bubbleswas not great. This implies that the volume occupied by these bubbles should be small. Photographic studies of the process by Landolt et al.(39) has revealed that the size of individual bubbles decreased with increase flow velocity. Baxter's (40) work also verifies the above claim. The variation of the inter-electrode gap of a drilled specimen was analogous to a convergent-divergent duct having a maximum cross-sectional area opposite the leading edge of the tool. This ensures that the electrolyte velocity in this region is greatest. At higher flow velocities large bubbles break into a number of small bubbles. High turbulence in this region ensures bubbles are thoroughly mixed in the electrolyte. Thus the effect on effective conductivity was not adverse. This was apparent from

close agreement of predicted and experimental work profiles in this region. The same argument should apply for the work profiles obtained machining with the straight edge tool, but the slight deviation of the predicted results were also influenced by an erroneous assumption in the computation of current distribution opposite leading edge of the tool. This error is discussed in paragraph 7.6.2.

In order to find the effect of flow rate on current efficiency, the flow rate at steady state machining was changed abruptly by opening or closing the valve which let the electrolyte into the machining cell. The back pressure was maintained the same throughout these changes. From Fig. 6.38, which shows the curves of flow rate, inlet pressure, outlet pressure and steady state machining current, it was apparent that the electrolyte flow rate of the orders used in test runs has no effect on the steady state machining current, which means that the current efficiency was independent of flow rate. König (7) also reports that the flow rate has no direct influence on current efficiency apart from the effect caused by the change in electrolyte temperature. As all the test runs were done in reverse flow, the dead machining zone, explained by Dietz, Gunther, Otto, (41) which is that part of the anode completely covered by liberated gas preventing further machining, does not effect the wall of the machined hole. Even if a dead machining zone exists it would have formed adjacent to the pip of the machined hole.

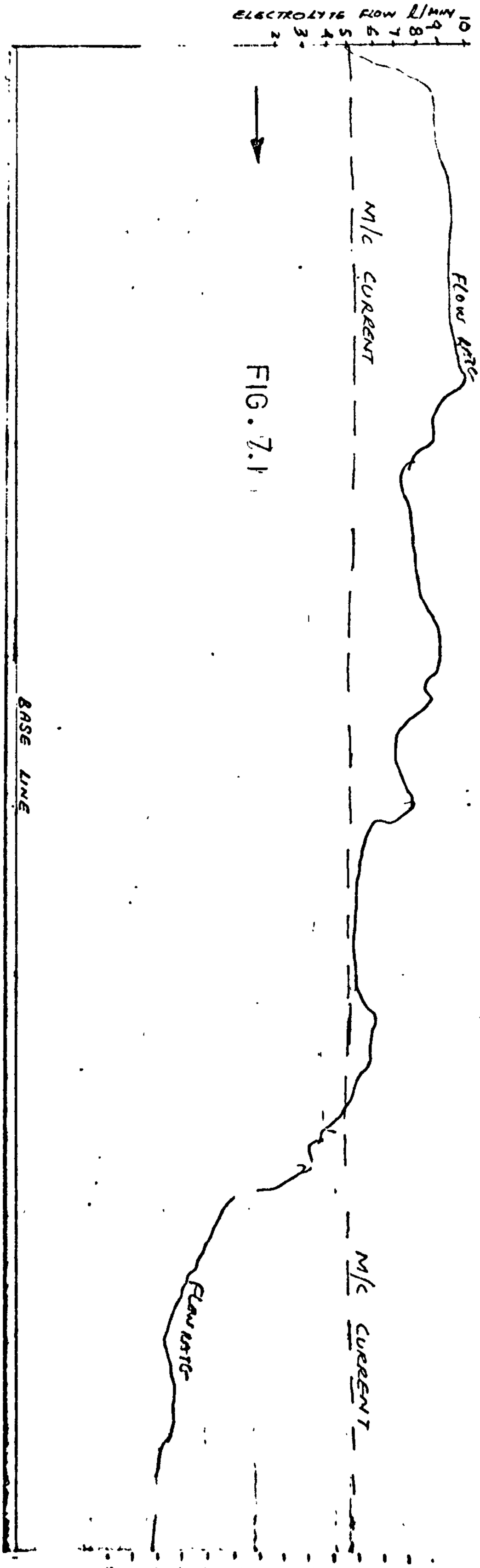
ELECTROLYTE FLOW L/MIN
2 3 4 5 6 7 8 9 10
FLOW RATE
M/C CURRENT
- 200
- 225
- 250 AMPS
- 275
- 300 IN
- 325 CURRENT
- 375
- 400 M/C
- 425
- 450
- 500
BASE LINE

FIG. 7.1

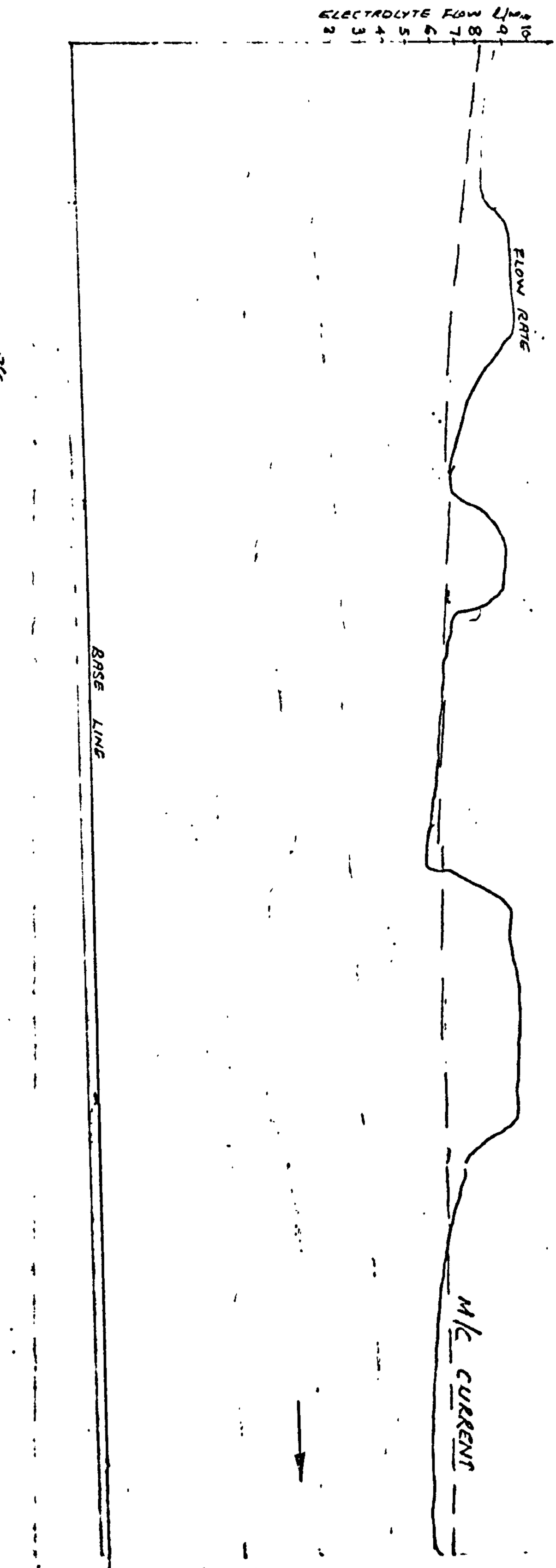
ELECTROLYTE FLOW L/MIN
2 3 4 5 6 7 8 9 10
FLOW RATE
M/C CURRENT
- 200
- 225
- 250 AMPS
- 275
- 300 IN
- 325 CURRENT
- 375
- 400 M/C
- 425
- 450
- 500
BASE LINE

7.5 DISCUSSION ON SURFACE DEFECTS

The occurrence of aggressive pitting on the surface which was observed on the specimens machined with NaCl electrolyte, section 6.2.3, is explained by Hoar, Mears and Rothwell, (42) in terms of surface film of varying ionic conductivity. The cationic conductivity of the surface film was thought to be intensified by the inclusion of anions. The anions would travel into the film under the applied potential field, the smallest anion going through the film with least resistance. Hence Cl^- is usually found to be more aggressive than the NO_3^-. At the first instant the entry of ions would be in the region of film corresponding to grain boundary, disarrayed or impurity zones of the metal. Once anions are in the film, it would become more conductive in that region, encouraging entry of further anions from the electrolyte to the film and cations to the electrolyte. The process would then become autocatalytic and a pit would develop in that region of the metal due to the passage of cations through the film into the solution. The reason for the peaks of overlapping pits being usually polished was explained by assuming that there would be an anion contaminated compact film of high cation conductivity on the pit surface.

Muzaffaruddin, (33) also found pitting on drilled EN58a specimen using 10% NaCl at a cell voltage of 10V. He explained that the effect was due to activation control dissolution of the work piece.

The striation marks or flow marks found on the bottom face of the specimens machined with $NaNO_3$ electrolyte, section 6.2.3, appear to be due to a cavitation effect. With NaCl electrolyte pitting and etching was too aggressive for the cavitation marks to be noticed. Chikamori, Ito, Sakurai, (19) found that with circular electrodes negative pressure zones exist when machining at gaps ranging between 0.1 mm and 0.9 mm, and employing flow rate between 5 ℓ/m and 30 ℓ/m. Meda et al. (43) also found streaks on the bottom of the machined surface at high flow rates. The equilibrium gaps and flow rates employed in the work described here were within those limits mentioned above.

7.6 INACCURACY OF THE MATHEMATICAL MODEL IN SHAPE PREDICTION

Apart from the simplified assumptions made regarding electrochemistry of ECM, there are errors in the mathematical model, which may or may not aggravate or compensate for the simplified electrochemical assumptions in shape prediction. In the case of electrochemistry in principle the errors could be avoided by having a clear knowledge of the process, but with the numerical method some errors are inherent.

7.6.1 Truncation Errors

The potential 'Ø' inside the region was assumed to be a polynomial of co-ordinates of the neighbouring points where 'Ø' was defined as

$$\emptyset = Ax^2 + By^2 + Cx + Dy + E$$

The validity of 'Ø' defined above in predicting the potential distribution is given in Appendix 3 . Even though this equation was very satisfactory in predicting the potential distribution in the Laplace region considered, it may not be the exact function which yields the true distribution. This would undoubtedly give rise to errors which are almost impossible to rectify. The comparison of this method with a known analytical solution of a field however gives confidence.

7.6.2 Boundary Condition Errors

The solution of Laplace equation for the potential distribution requires a closed region of known boundary conditions. The region chosen and the boundary conditions are presented in Fig. 2.16.

Conducting Boundaries:-

Since the work described here deals in finding how well the primary current distribution predicts the equilibrium work profile, the uninsulated parts of tool boundary (BG) and the work boundary (EF) were assumed to be equipotential surfaces. In reality this is not true. The deviation due to polarization effects were discussed earlier.

Boundary BE:-

The assumption that the boundary 'OA' is a line of constant current is true only in the case of hemispherical

leading edge tool due to the geometrical symmetry of the section considered about an axis parallel to the feed direction. However, with the straight leading edge tool this assumption is not strictly true, and was an over simplification. It was assumed that the orthogonal equilibrium gap distance was equal to 'BE'. Also assumed was that over the flat leading part of the cathode, the gap between the electrodes remains constant having the same magnitude as the orthogonal equilibrium gap. From the experimental profiles obtained Figs. 6.29 - 6.34 it was clearly seen that the work profile opposite the straight leading edge of the tool had a small curvature giving much smaller gap for 'OA' than the predicted gap. Due to this improper assumption the potential distribution in the vicinity of 'OA', of the region was in error. This was evident from the larger predicted gap around 'OA' for the straight leading edge tool.

Insulated Boundaries:-

Within the applied cell voltages (0 - 20 V), the assumption that no current flux passes through the insulated boundary (GC) is valid.

Boundary CF:-

This boundary which was located 10 orthogonal equilibrium gaps down the insulated part of the tool was considered to be a line of zero current. This was a good representation of the actual current distribution encountered in ECM. Theoretically speaking 'BC' has to

be located at a distance infinitely far down the insulated boundary of the tool, but however, the potential difference between two consecutive transverse mesh lines in this region decays rapidly and at about 10 orthogonal equilibrium gaps down the insulated region the difference in potential becomes negligible. Thus the error on the work profile due to this assumption was insignificant. This was evident from the experimental profiles obtained using NaCl electrolyte which showed good correlation in the region opposite the insulated boundary of the tool. With $NaNO_3$ electrolyte, the assumed current efficiency factor masked the accuracy of the predicted profiles opposite the insulated region.

7.6.3 Numerical Errors

Errors which are difficult to eliminate may be generated from the numeral procedure of the method of solution of the Laplace equation. For example errors may have been induced from rounding off the potential values at each grid point. Error is also introduced by the numerical integration method which calculates the amount of shift of nodal points on the work boundary along a radial direction. Further errors may derive from the least square polynomial approximation method which fixes a curve through neighbouring points on the work boundary, taking four boundary nodal points at a time.

7.6.4 Method of Convergency

Iteration procedure involves computing by how much a nodal point on the work boundary should be shifted along a transverse grid line with respect to the proceding electrode gap along a corresponding grid line. The movement of the nodal points were initiated from the nodal point on the work profile which was directly opposite the leading edge of the tool (the point on the work profile which gave the orthogonal equilibrium gap). The equilibrium work profile was supposed to attain when the largest shift at any point on the work boundary was less than a small fraction of the orthogonal equilibrium gap. However, this way of achieving the equilibrium work shape could give rise to a larger or smaller work profile than the expected one due to under correction or over correction of the shift of nodal points. The amount of correction in each iteration depends on the potential distribution, hence on the geometry of the tool. It is always advisable to find the amount of correction needed for each tool geometry used. This could be easily obtained from few initial runs of the program with different correction factors. Whether a free boundary problem has a solution, and whether this is unique is an extremely difficult mathematical problem (44). Cryer (44) and Tipton, (11) have also employed a similar convergency criterion to obtain a free boundary solution. So in practice convergency has been achieved for ECM problems.

CHAPTER VIII

CONCLUSIONS AND RECOMMENDATIONS FOR FURTHER STUDY

8.1 CONCLUSIONS

A mathematical model was developed to simulate the two dimensional electrochemical machining process considering only the primary current distribution. The computer program written to evaluate the model ran successfully. The shapes predicted by the model were generally in good agreement with experiment. The closeness of fit has been used to test the validity of certain assumptions.

Frontal Equilibrium Gap

A trace obtained from an optical projection of a plaster model of the cavity of the drilled hole provided more consistent values of equilibrium gap than those obtained by closing the electrode gap in the ECM cell. Both computer predicted values and the values obtained using the simple equation for gap were close to the equilibrium gaps obtained from the plaster models. Slightly deviated gap values predicted by the computer models for test with the straight leading edge were due to an incorrect assumption of a boundary condition i.e. that a parallel face would be produced by the straight edge.

Electrode Potentials and Overpotentials

The use of a fixed value for the sum of electrode potentials and overpotentials i.e. independent of current density, was found to give satisfactory shape prediction

so long as the correct value was chosen. A value of 0.0 volts was found to be too low for the NaCl tests while 2.5 volts was about right. With $NaNO_3$ 0.0 volts was about right while 2.5 volts was too high. However tests carried at 12V with $NaNO_3$ electrolyte gave better agreement with 2.5 volts.

Temperature of the Electrolyte in the Electrode Gap

The theoretical temperature prediction showed that temperature rise increases with tool feed rate, i.e. with increase in current density, also increased with increase in cell voltage. The predicted temperature opposite the leading edge of the tool was slightly higher than the experimental value for the reasons given in Chapter VI. The temperature increase with NaCl was lower than that of $NaNO_3$ electrolyte for identical machining parameters.

In general good correlation of experimental and predicted results indicates that the primary current distribution predictions are adequate for steels such as EN58J machining with NaCl or $NaNO_3$ electrolytes.

8.2 RECOMMENDATIONS FOR FURTHER STUDY

Polarization Effects

The developed model does not take into consideration the polarization effects except for the assumed over voltages. It may be that the polarization effects have no adverse effect on the primary current distribution

when machining EN58J with NaCl or $NaNO_3$, but metals such as alloyed titanium exhibit significant polarization effects (3,35,45) which could alter the primary current distribution significantly. Allowance for this secondary current distribution is not provided in the developed model and so if this model were employed to predict the work profile of, for example, a titanium alloy it might yield an incorrect work shape beyond acceptable limits of tolerance. Therefore it is recommended that further investigation is necessary to include polarization effects.

Variable Conductivity

Apart from the salt concentration the conductivity of the electrolyte depends on the temperature and the amount of liberated gas during machining. Due to these effects conductivity of the electrolyte will be different along the work profile and this will effect the local erosion rate. Although conductivity-temperature equations were used in the present work to calculate conductivity and the temperature of the electrolyte due to joule heating were also calculated. Correction for change in conductivity was not written into the program. Therefore it would be profitable to investigate this aspect for inclusion in the mathematical model, so that machining conditions with high temperature rises could be dealt with. The affect of gas bubbles would be more difficult to compensate for but the success of the present model with no correction indicates that a simple correcting assumption might be satisfactory.

APPENDICES

APPENDIX A1

DESIGN OF THERMISTOR CIRCUITS

A1.1 GENERAL

Thermistors are temperature sensitive semiconductor devices which change their resistance with temperature. Thermistors are available with either a positive or negative temperature coefficient. The second type of thermistors are widely used for thermometry having many advantages over conventional temperature sensors, e.g. they are comparatively small, robust and respond quickly. They are used in measuring temperatures within the range of $-100^{o}C$ to $+300^{o}C$. There are many versions available varying in size, configuration and nominal resistance covering a range from $2\,\Omega$ to $2M\,\Omega$ at $25^{o}C$. Since thermistors are temperature sensitive resistive devices, to be used as a thermometer they require an indicator, associated circuits and a power supply. Unlike common metal resistors, the resistance of the thermistor obeys a form of an exponential law; by careful circuit design thermistors can be used to indicate temperatures directly within a given range. The linearity of indication to temperature depends on the range of temperature measured. A range of temperature $\pm\ 10^{o}C$ about the mid range temperature being achieved relatively easily.

In selecting thermistors the level of power dissipation is very important as excessive internal heating can lead to errors in measurement. The temperature rise of a thermistor dur to self heating depends upon its size and mechanical configuration, and the medium in which it is operating. The dissipation constant of a thermistor is defined as the power required to raise the temperature of the thermistor by $1^{o}C$ in a given environment. In order to record rapid fluctuation in temperature, the time constant has to be low as possible. The time constant is defined as the time taken for temperature of the thermistor to change by a factor of (e-1)/e of the total temperature difference when temperature of the measuring medium is suddenly changed.

Both dissipation constant and time constant are considerably effected by different conditions of the medium in which temperatures are to be recorded.

For the Mullard VA3406 thermistor which was used to record variation in temperatures during electrochemical drilling tests described in Chapter V, the values of dissipation constant and thermal constant quoted by the manufacturers are 0.75 $mW/^{o}C$ and 12 sec respectively.

A1.2 BRIDGE CIRCUIT DESIGN

For temperature measurement it is normally desirable for the indicating or recording meter, to have a linear scale. The theory on which such a circuit is designed is given in references 46 and 47. The resistance

'RT' of a thermistor is given by the equation

$$(R_T) = A \exp B/T \qquad \ldots \qquad (A1.1)$$

where T = temperature of the thermistor in ^oK

B = characteristic temperature ^oK

A = constant.

Consider a thermistor of resistance (R_T) and source resistance (R_S) in a series network as shown in Fig. A1.1.

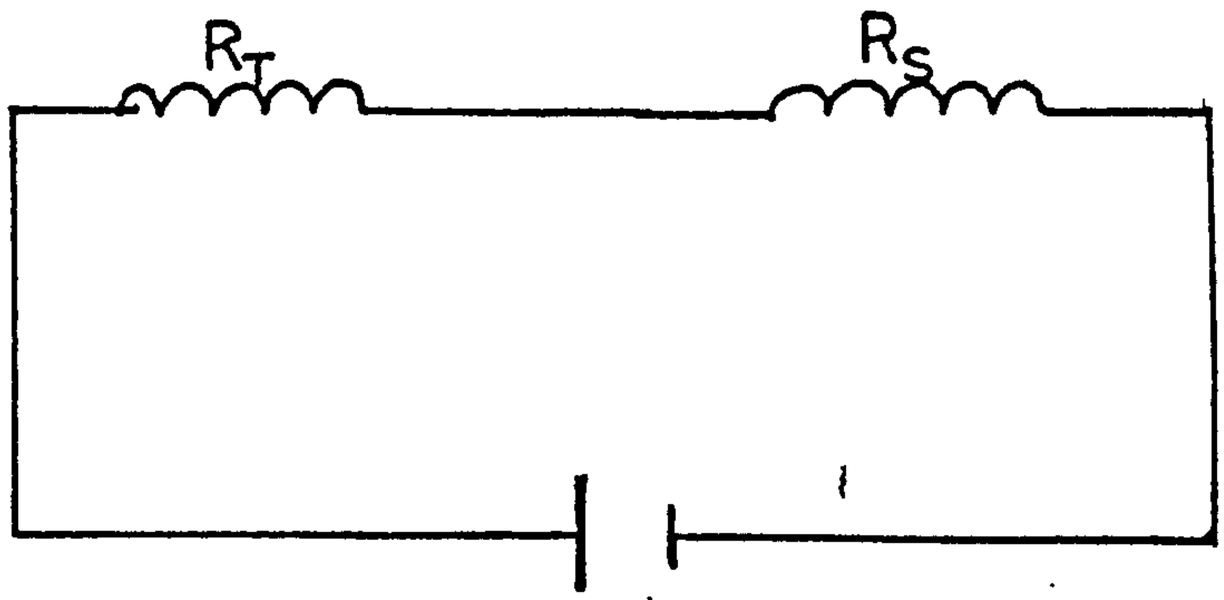

FIG. A1.1

Total resistance $R = (R_T) + (R_S)$

or total conductance $$S = \frac{(S_S) \times (S_T)}{(S_S) + (S_T)}$$

(S_S) = conductance of source

(S_T) = conductance of thermistor

On substitution for (S_T) from (A1.1)

$$S = \frac{e^{-B/T} \times (S_S)}{A((S_S) + e^{-B/T})} \qquad \ldots \qquad (A1.2)$$

S will change linearly about the point of inflection and the condition for the point of inflection is given by $\frac{d^2S}{dT^2} = 0$.

Therefore differentiating equation (A1.2) with respect to T and equating the numerator to zero the condition is

$$(A \times (S_S) + e^{-B/T})(B/T - 2) - \frac{2 \times B}{T} e^{-B/T} = 0$$

From which

$$(S_S) = (S_T) \frac{(B + 2T)}{(B - 2T)}$$

or in resistance terms

$$(R_S) = (R_T) \frac{(B - 2T)}{(B + 2T)} \quad \ldots \quad (A1.3)$$

That is for linearity about the temperature T the source resistance should have the value given by equation (A1.3) which is a function of temperature. For most cases a reasonable linearity could be achieved over a range of $\pm$ 10^{o}C about the mid range temperature T.

Incorporating a thermistor in a series resistive network as explained above and using the potential drop across the thermistor or current through the circuit as a measure of temperature will give temperature readings on a confined scale which is difficult to read. Usual practice is to use thermistors in a bridge circuit Fig. (A1.2). The out of balance voltage due to resistance change is fed into a recording meter or an indicating instrument after suitable amplification.

For maximum efficiency with respect to change of voltage across the thermistor due to temperature rise, most of the current change that occurs through the thermistor

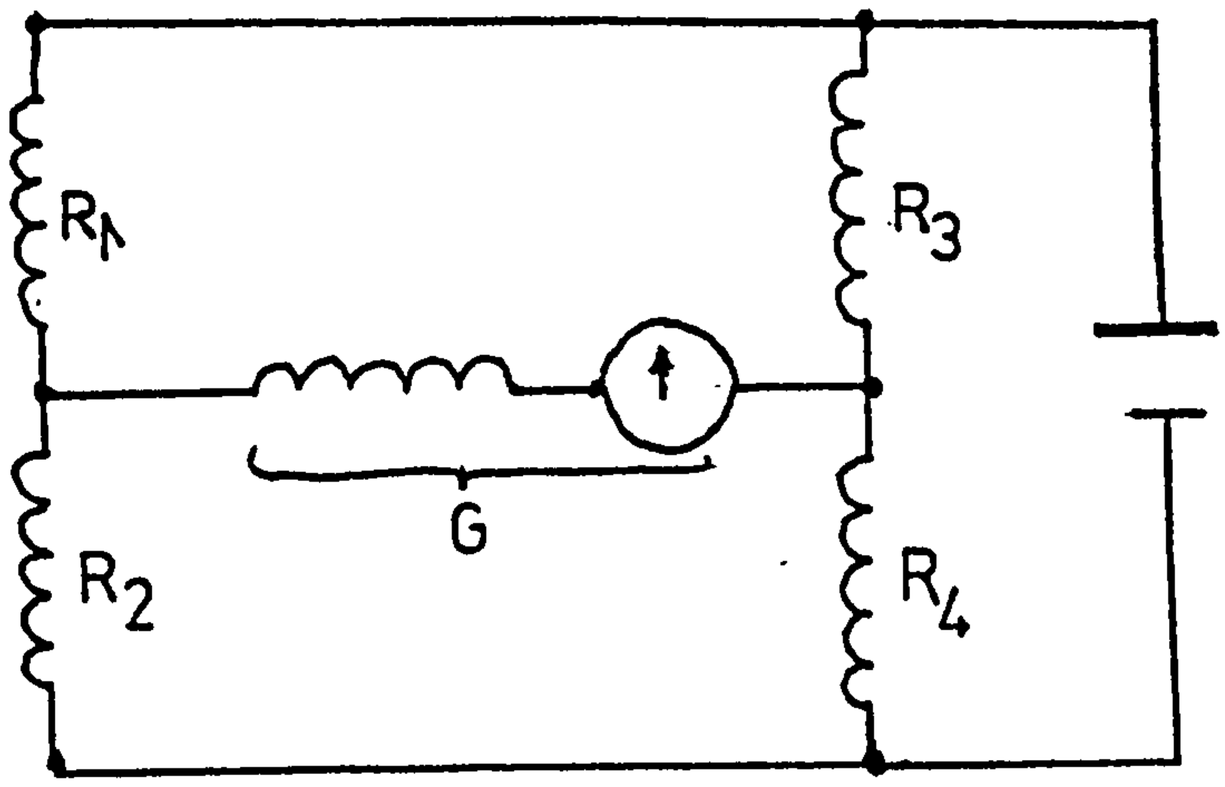

FIG. (A1.2)

should occur through the recording meter. One way to achieve this condition is to make resistance (R_3) comparatively larger than thermistor resistance (R_4), such that the half bridge comprising arm (R_3) and the thermistor tend to operate in a constant current mode. For linearity about the balance temperature, the source resistance must have the value given by equation (A1.3). Therefore the resistance of the arms (R_1), (R_2) and the indicator G must be accordingly selected. A thermistor bridge circuit will have the approximately correct source resistance if the bridge arms were comprised of the resistances given below .

$$R_1 = \frac{R_T}{R_b} \times G$$

$$R_3 = 10 \times R_T$$

$$R_2 = G/10$$

$$R_4 = R$$

$$G = (R_T)^2 \frac{(B - 2T)}{(B + 2T)}$$

Where R is the resistance of the thermistor at any given temperature. R_T the resistance at mid-range temperature, R_b resistance at balance temperature.

The thermistor bridge circuit and the associated circuitry used to amplify the output signal to the U.V. recorder is shown in Fig. A1.3. The values of the components shown in the diagram produced a relatively linear output signal for the temperature range of the thermistor between 30^oC - 60^oC - 90^oC.

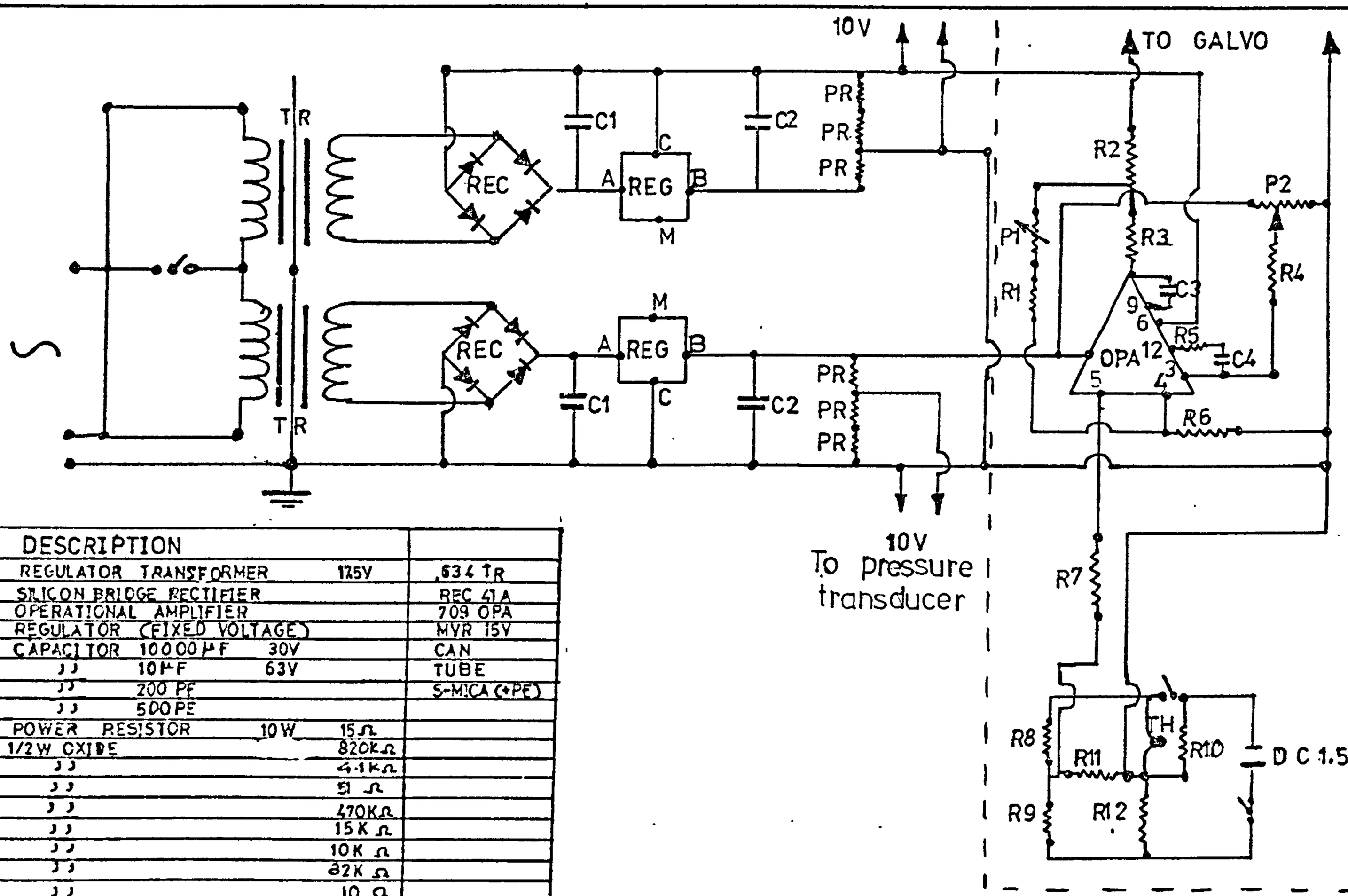

ITEM	DESCRIPTION		
TR	REGULATOR TRANSFORMER	175V	.634 TR
REC	SILICON BRIDGE RECTIFIER		REC 41A
OPA	OPERATIONAL AMPLIFIER		709 OPA
REG	REGULATOR (FIXED VOLTAGE)		MVR 15V
C1	CAPACITOR 10000 µF	30V	CAN
C2	" 10 µF	63V	TUBE
C3	" 200 PF		S-MICA (+PE)
C4	" 500 PE		
P	POWER RESISTOR	10W 15 Ω	
R1	1/2W OXIDE	820K Ω	
R2	"	4.1K Ω	
R3	"	51 Ω	
R4	"	470K Ω	
R5	"	15K Ω	
R6	"	10K Ω	
R7	"	82K Ω	
R8	"	10 Ω	
R9	"	30 Ω	
R10	"	8K Ω	
R11	"	36K Ω	
R12	"	27K Ω	
P1	VARIBLE RESISTOR	250K Ω	MOULDED +Ω
P2	"	100K Ω	MOULDED VC+Ω
TH	THERMISTOR MULLARD TYPE		VA 3406

FIG. A.1.3 Amplifier Unit

APPENDIX A2

CALIBRATION AND MATCHING CIRCUITS

The output voltages, from the pressure transducers, from the thermistor circuits which were used to monitor the temperature of the electrolyte, from the electrolyte flow rate meter, from the shunt which was used to record the machining current and the cell voltage were fed into U-V recorder via matching circuits.

A2.1 MIRROR GALVANOMETERS AND DAMPING

The mirror galvanometers of the U-V recorder are electromechanical transducers which accept electrical energy and transform it into mechanical energy, the mirror is rotated so that the light beam is moved laterally in proportion to the input signal. In order to use a galvanometer to record a true representation of the input signal it is necessary that frequency response is flat over the operating range. If there were no proper damping in the system the response would rise steeply at the resonant frequencies and if used to record wave forms containing such frequencies or harmonics, there would be both amplitude and phase distortion. In most systems a damping of 64% of the critical being used which has become universally accepted for the majority uses. Damping in the system is also necessary to control two other characteristics the phase angle relationship and step frequency response.

The galvanometers are of two types

1. Low-frequency type galvanometers where the effective damping resistance is the combination of the coil resistance and the external damping resistance which gives the damping of 64% critical. Hence it is important that the correct damping resistance is used and that it is equal to the resistance of the driving source.

2. High-frequency type galvanometers where the damping is obtained by the surrounding of the suspension by a silicone fluid. The viscosity fluid is chosen to provide the correct damping ratio.

A2.2 INPUT CIRCUIT PARAMETER

When the driving source resistance is not the same as the required specified damping resistance an appropriate network has to be provided to obtain the optimum 64% critical damping. In any application the source impedance must be considered in obtaining proper damping. If the source impedance is low a series resistance R_d is used to obtain proper damping Fig. A2.1 .

When the source resistance is high a shunt resistance is used to obtain proper damping, Fig. A2.2 .

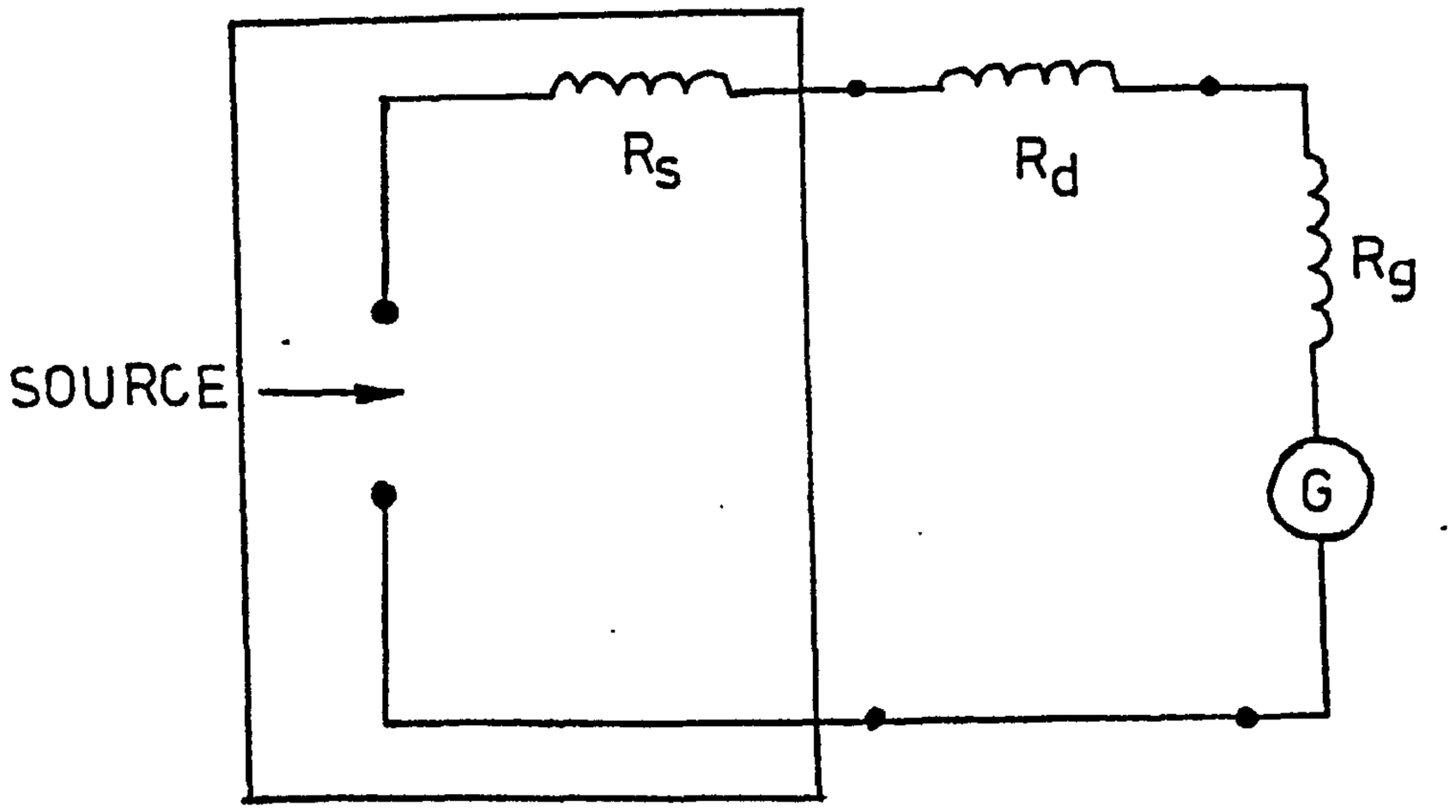

FIG. A2.1

R_S - source resistance

R_d - series resistance

R_g - galvanometer resistance

R_D - damping resistance

$$R_d = R_D - R_S$$

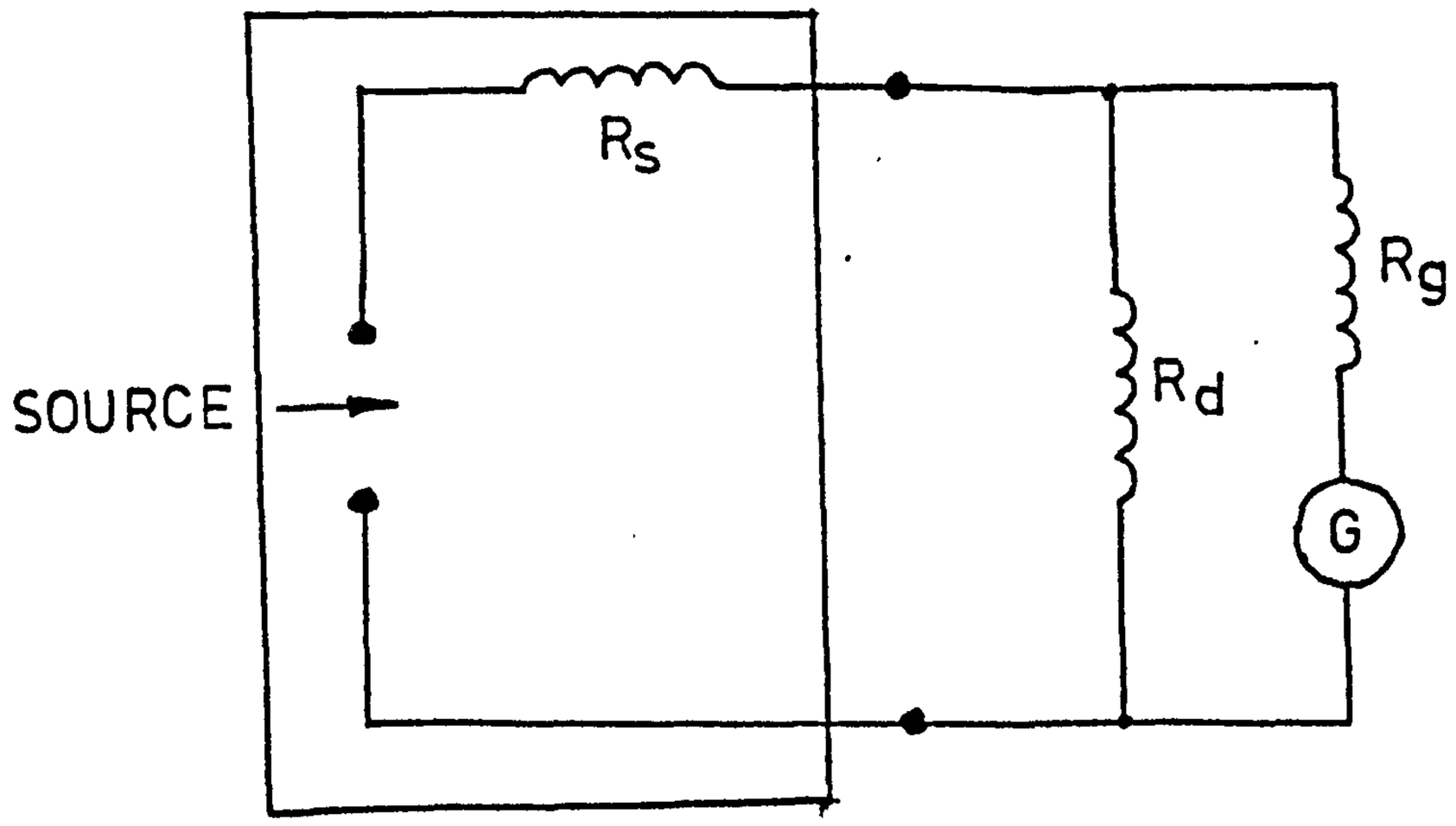

FIG. A2.2

$$R_d = \frac{R_S \times R_D}{R_S - R_D}$$

A2.3 CALIBRATION AND MATCHING CIRCUITS

A2.3.1 Inlet and Outlet Pressure

The pressure transducers were calibrated against a precision Borden gauge using a hydraulic pump to simulate the pressure exerted by the electrolyte. The output signal from transducers were fed via matching circuits Fig. A2.3 to the U.V. recorder to obtain a permanent trace. Knowing the displacement of the light spot reflected by the mirror galvanometer on the recording paper for corresponding pressures, read from the Borden gauge a scale was made to read directly the pressures from the trace obtained from the U.V. recorder during drilling test runs.

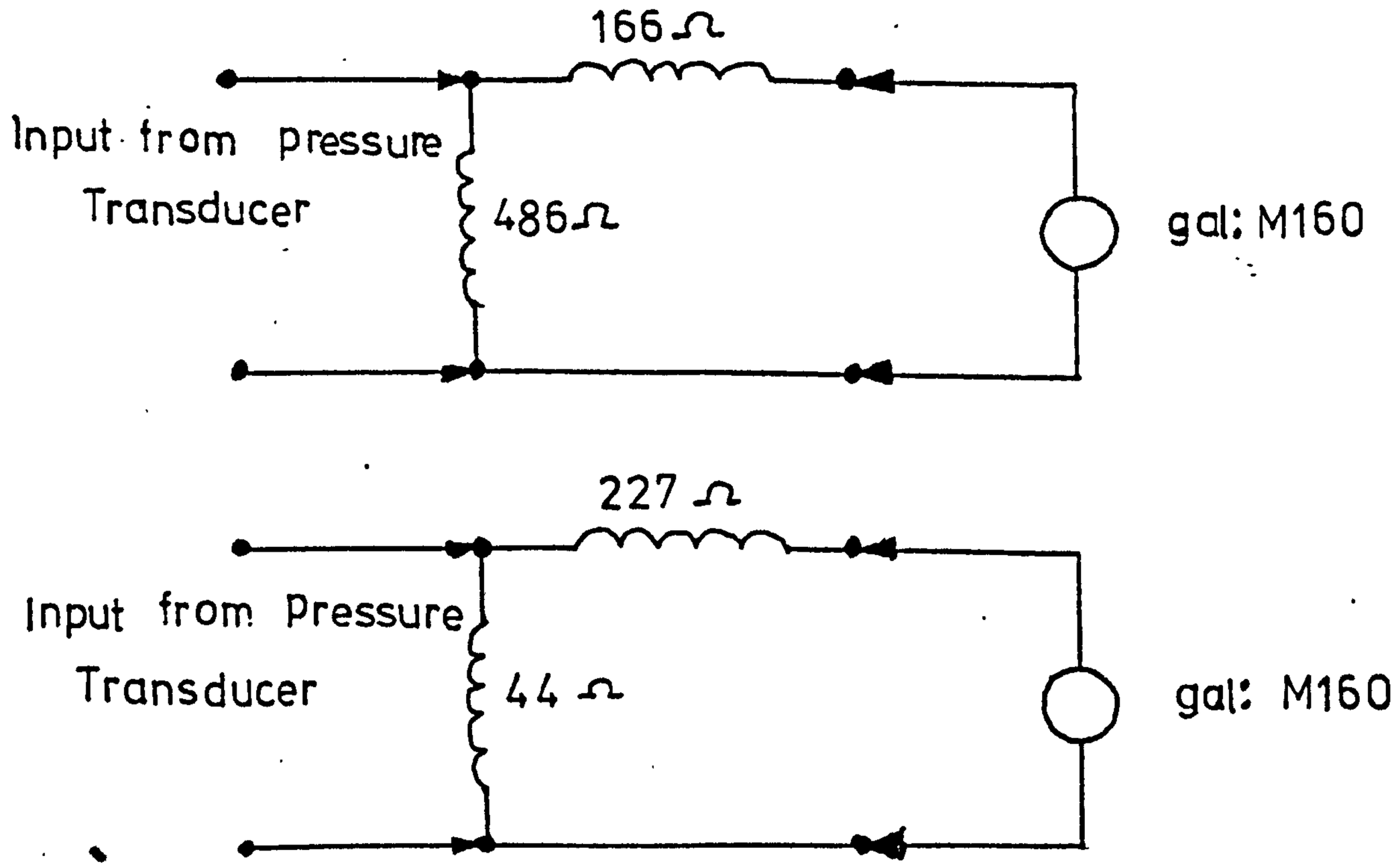

FIG. A2.3

A2.3.2 Machining Current

To calibrate the trace obtained from the U.V. recorder and to obtain a scale which reads machining current direct from the trace, current to the U.V. recorder from 50 mV shunt was simulated using a circuit similar to that shown in Fig. A2.4..

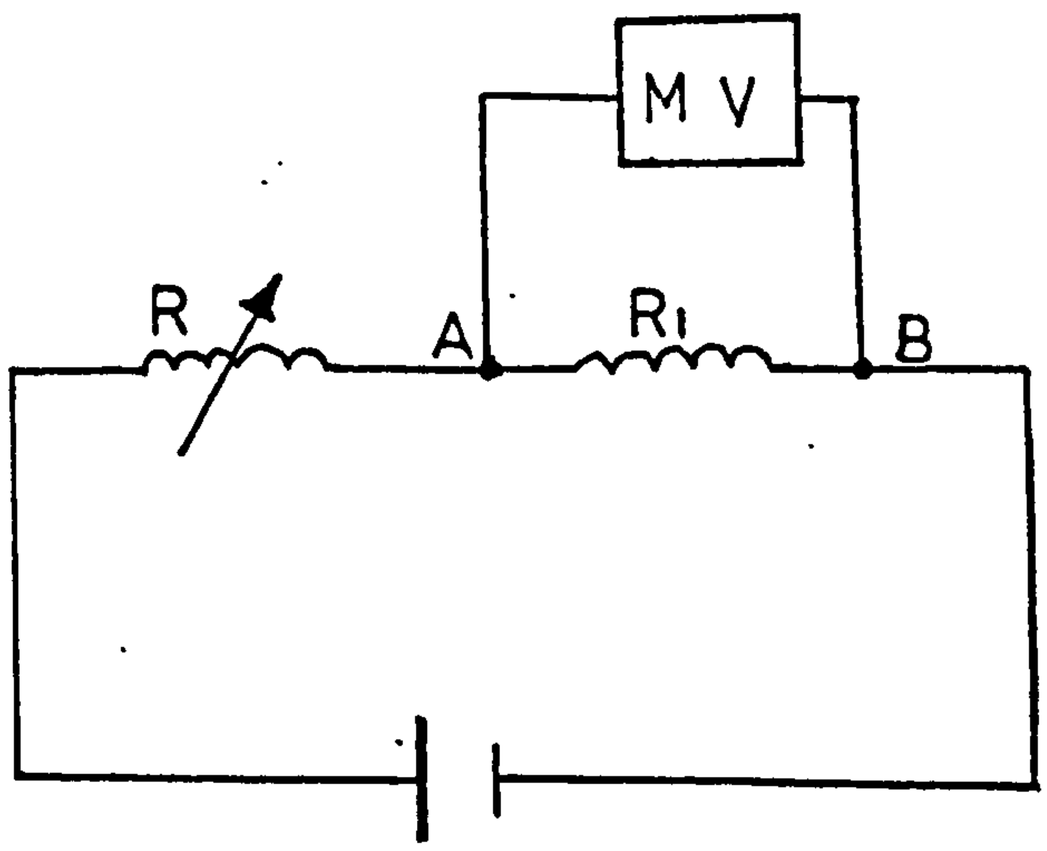

Fig. A2.4

A resistor R_1 and variable resistor R was connected to a U2 battery. Potential drop across R_1 was fed into the U.V. recorder via a matching circuit Fig. A2.5 , the magnitude of this voltage was measured directly using a mV meter. By varying R, potential drop across R_1 was varied from zero at open circuit to a maximum of 50 mV (in 5 mV increments) which corresponds to the output from the shunt when machining. A scale was prepared for reading the machining current directly from the traces obtained.

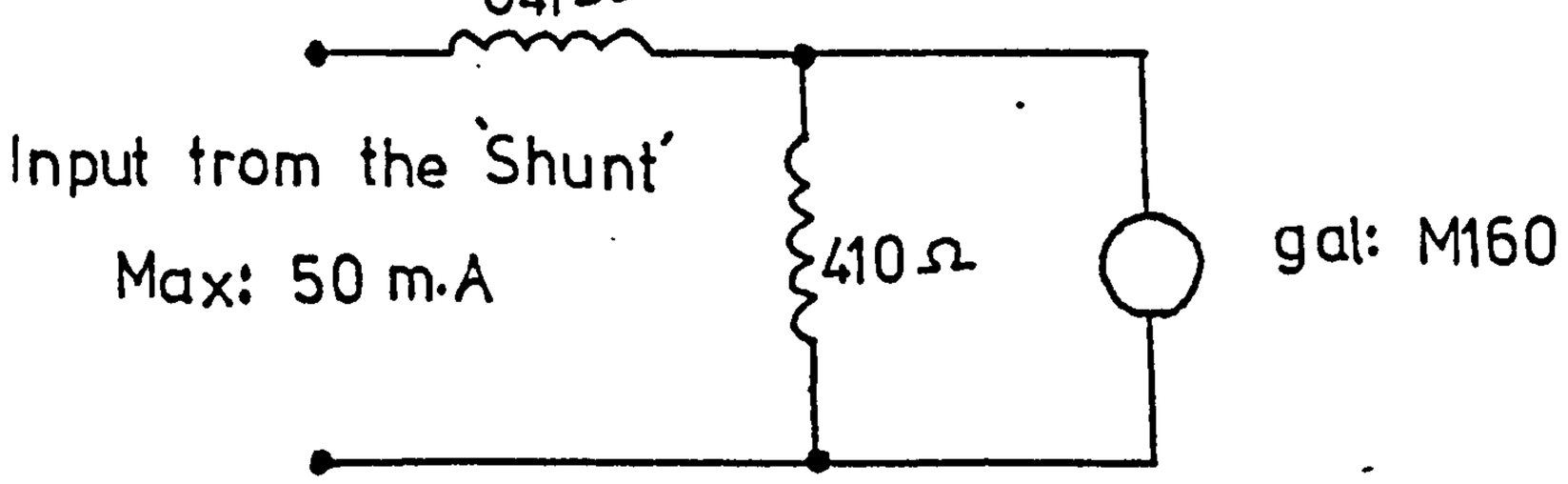

FIG. A2.5

A2.3.3 Machining Voltage

To produce a calibration scale, a similar technique to that of machining current simulation was used, but in this case a Farnel power supply unit was used as the source. Fig. A2.6 shows the matching circuit used to give a 10 cm displacement on the recording paper.

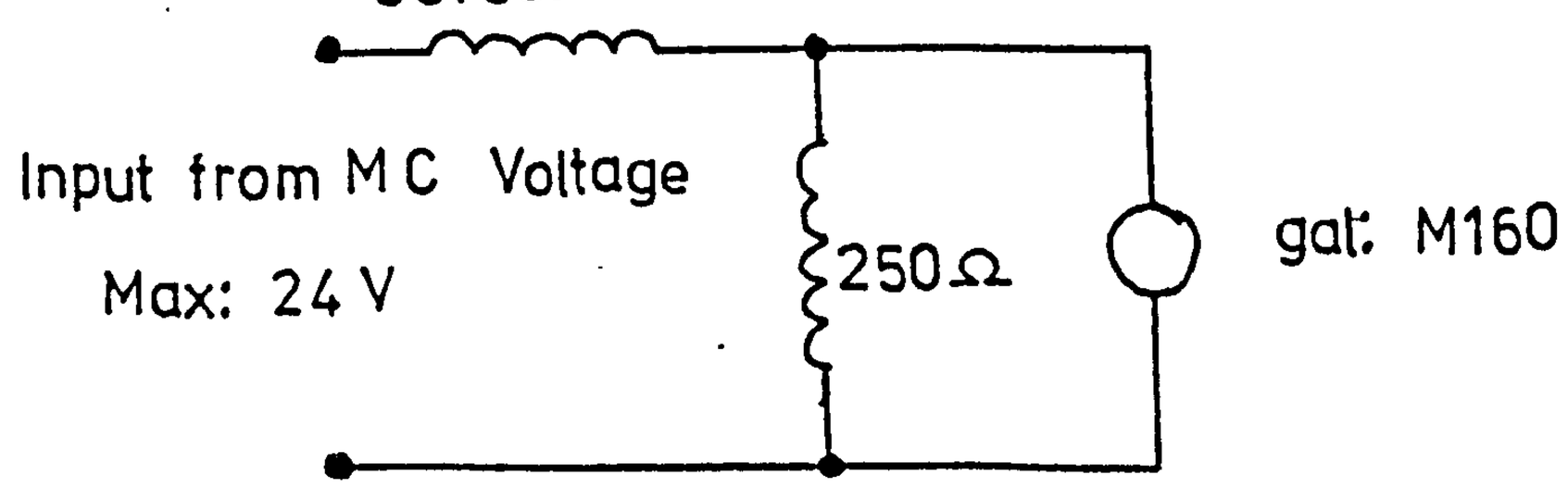

FIG. A2.6

A2.3.4 Electrolyte Flow Rate

The flow transmitter consists of a paddle wheel which causes a reed switch to open and close each revolution. The Rhodes model PA flow meter supplied with the transmitter converts pulses from the reed switch to a non-linear recording on a 1 mA moving coil meter. Calibration was done by measuring the flow through the flow meter for a constant meter reading for a given time. A U.V. recorder galvanometer with suitable matching circuit Fig. A2.7 was used in series with the moving coil meter of the indicator to provide a permanent record of flow.

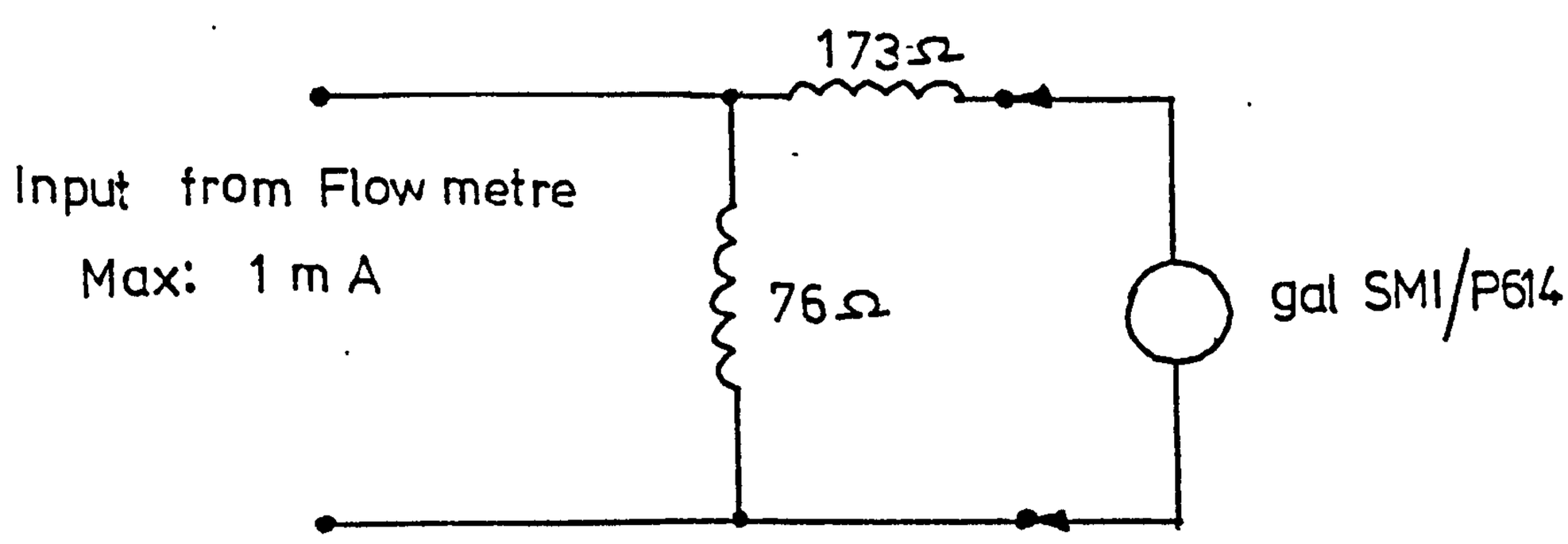

FIG. A2.7

A2.3.5 Temperature of the Electrolyte

In order to calibrate mounted thermistors, these were connected to an electrical bridge circuit shown in Fig. Al.4. The beads of the thermistor were completely immersed in a water bath which was continually stirred during heating. The temperature of the water bath was

measured using mercury in a glass thermometer. The out of balance voltage from the bridge circuit due to the resistance change in the thermistor corresponding to temperature of the water bath was fed into the U.V. recorder via matching circuit Fig. A2.8 . The circuits were designed to give a relatively linear trace in the region of 30^{o} - 90^{o}C. The amplifier circuit gave signal of 8.65 volts at 90^{o}C, to obtain a 12 cm deflection over the range. A resistance of 2020 Ω had to be used in series with galvanometer.

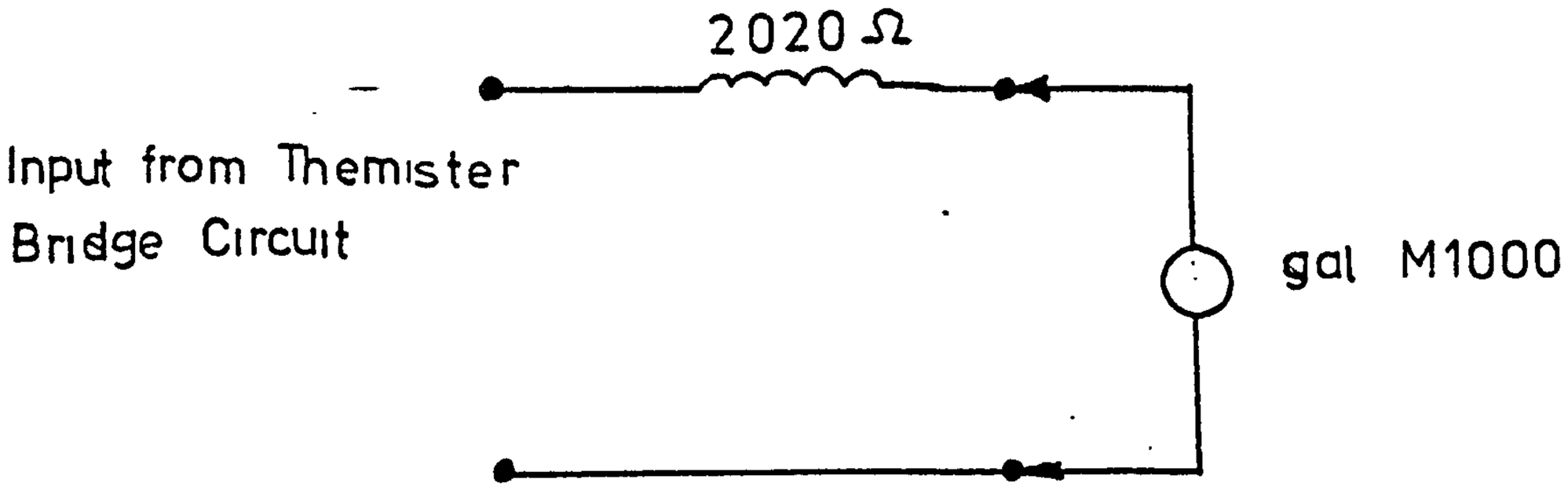

FIG. A.2.8

APPENDIX A3

POTENTIAL DISTRIBUTION IN THE REGION BOUNDED BY TWO CONCENTRIC CHARGE CIRCLES

A3.1 Formulation of the Difference Scheme

Detailed account of the formulation of the difference scheme using equation (2.12) is given in section (2.9.1). The difference scheme for the potential distribution defined by equation (2.11) is obtained in a similar manner.

The potential $\emptyset$ at a grid point is given by

$$\emptyset = Ax^3 + By^3 + Cx^2y + Dy^2x + Ex^2 + Fy^2 + Gx + Hy + J \quad \ldots (2.11)$$

Then

$$\frac{\partial \emptyset}{\partial x} = 3Ax^3 + 2Xxy + Dy^2 + 2Ex + G \quad (A3.1)$$

$$\frac{\partial^2 \emptyset}{\partial x^2} = 6Ax + 2Cy + 2E \quad (A3.2)$$

$$\frac{\partial \emptyset}{\partial y} = 3By^2 + Cx^2 + 2Dyx + 2Fy + H \quad (A3.3)$$

$$\frac{\partial^2 \emptyset}{\partial y^2} = 6By + 2Dx + 2F \quad (A3.4)$$

$$\therefore \nabla^2 \emptyset = 6Ax + 2Cy + 2E + 6By + 2Dx + F = 0$$

Boundary conditions where the potential gradient is zero (symmetric boundaries such as LM, ON FIG A3.1 or similar boundaries where there is no current flow across the boundary is given by equating equations (A3.1) or (A3.3) to zero. Since in the local co-ordinate system the point under consideration has co-ordinate x=0, y=0,

$$\nabla^2 \emptyset = 2E + F = 0$$

Boundary conditions

$$\frac{\partial \phi}{\partial x} = 0, \text{ is } G = 0$$

and

$$\frac{\partial \phi}{\partial y} = 0, \text{ is } H = 0$$

In application of equation (2.11) in prediction of potential distribution these functions were extracted from the solution of the nine simultaneous equations similar to that of equation (2.17) which were formed for the nine grid points. The origin of the local co-ordinate system was taken as the grid point under consideration.

A3.2 SETTING UP THE GRID

The symmetry of the problem requires only to consider a segment of the region as shown.

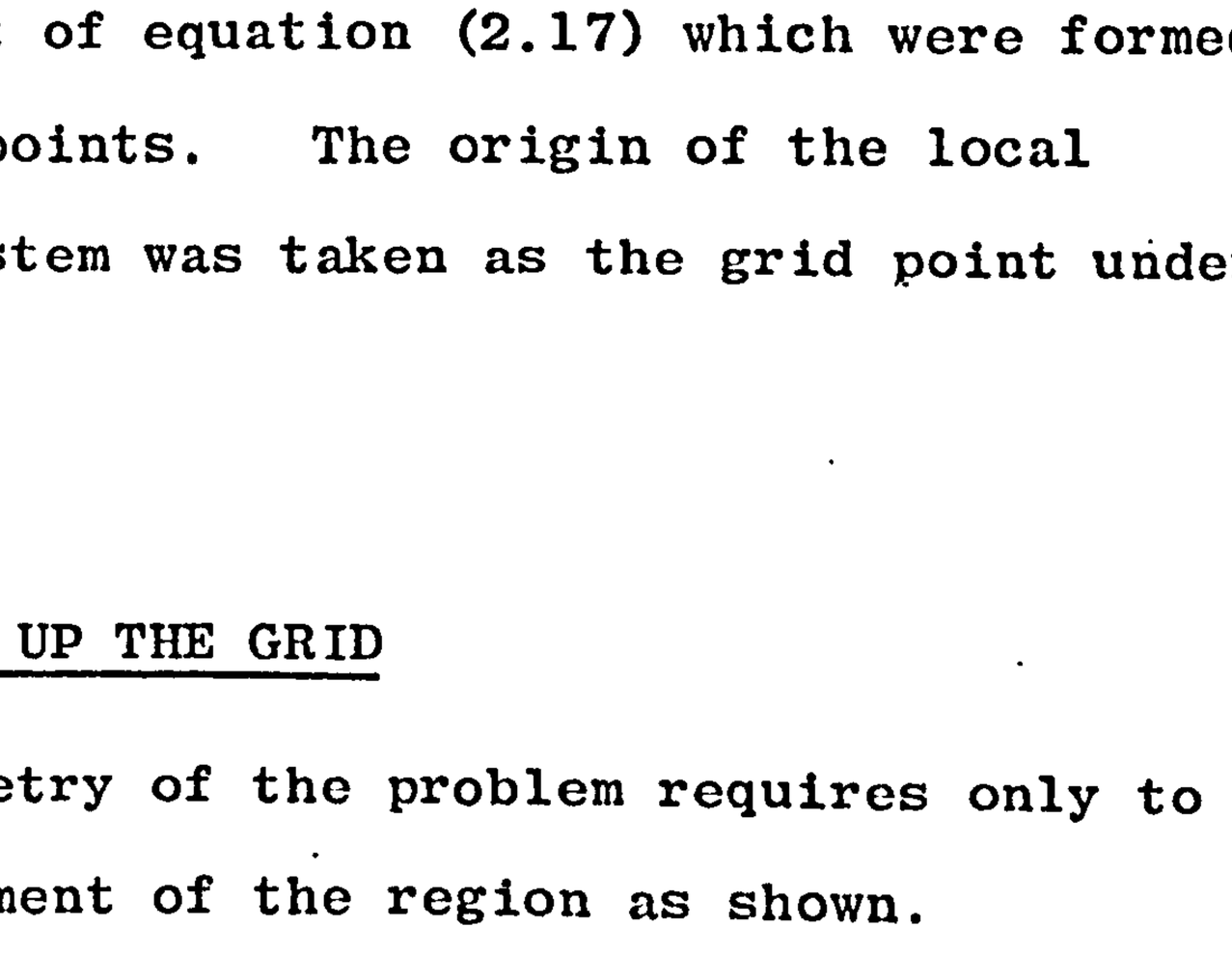

FIGURE A3.1

The boundary condition being $\frac{\partial \phi}{\partial \theta} = 0$, along LM and ON, $\phi = 0$, and 12 along LO and MN respectively. Since the actual prediction of the electrochemically machined profile involves a mesh with a large number of nodal points, it was thought to be better to use a larger mesh covering a semicircular region FIG. 3.2 . An advantage of this is that the boundary condition $\frac{\partial \phi}{\partial \theta} = 0$, becomes $\frac{\partial \phi}{\partial x} = 0$.

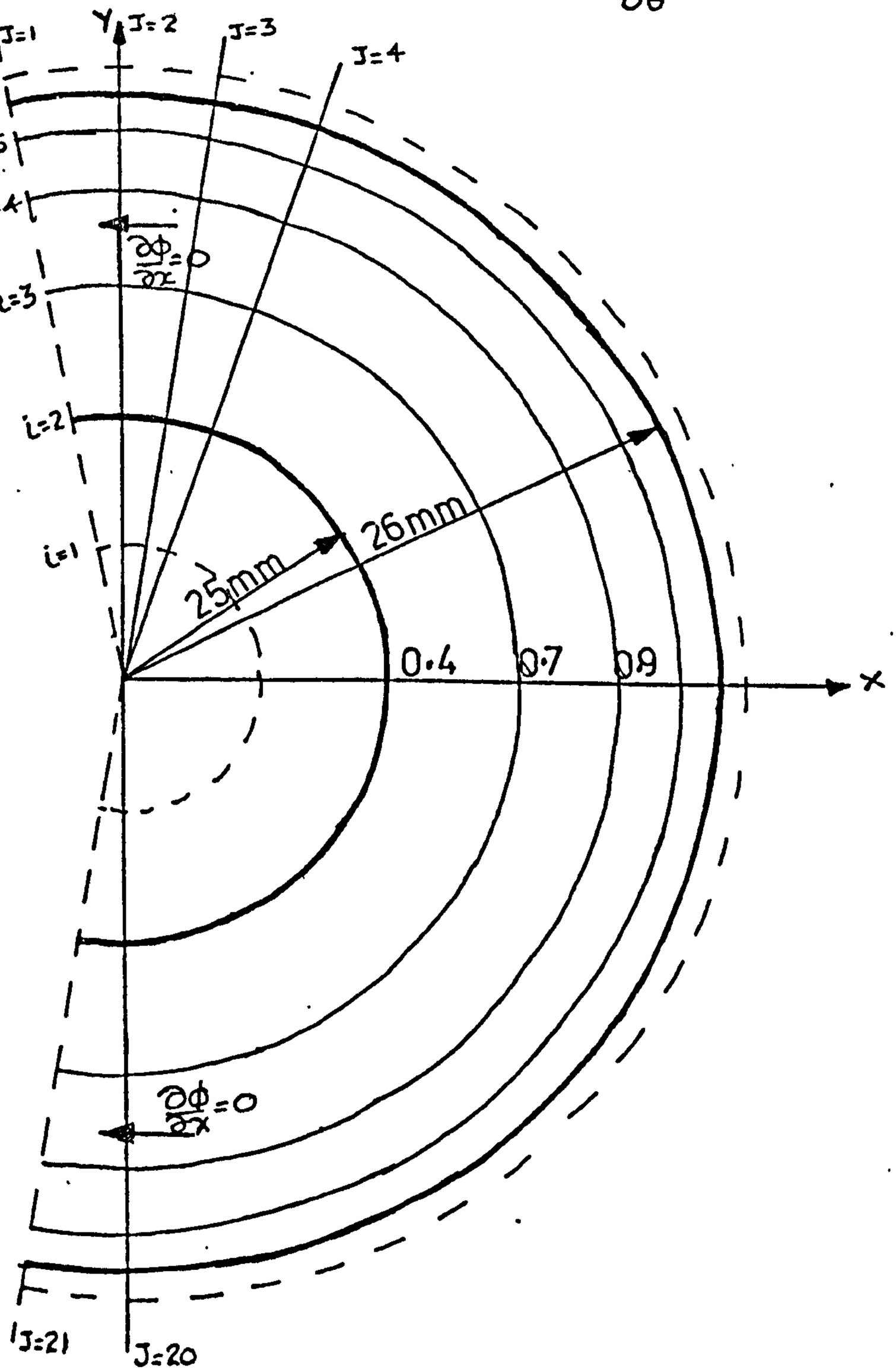

FIGURE A3.2

The gap between the two surfaces was divided into four by parts in the proportions 0.4:0.3:0.1 by longitudinal lines which in this case were concentric rings positioned at 0.4, 0.7, and 0.9 of the gap from the inner surface (i lines). The region was subdivided into small segments by transverse radial lines (J lines) at equal intervals of 10^{o}. Intersections of 'J lines' and 'i lines' formed the mesh. For the boundaries where $\frac{\partial \phi}{\partial x} = 0$, Image grid points were constructed and were treated in the same manner as an internal point. The listing of the computer program used shows the details of the procedure.

APPENDIX 4

COMPUTER PROGRAMS

4.1 Electrochemical Machining Simulation Program

The mathematical sequences and the general structure of the computer model are described in Chapter II. A block diagram of program, which describes the function of each subroutine is shown in Fig. A4.1. The program can be run in any computer with 250 k bytes core store that offers a FORTRAN IV compiler. A complete listing of the computer program is given here. Comment cards have been inserted to define the main variables used and to explain each step in the program.

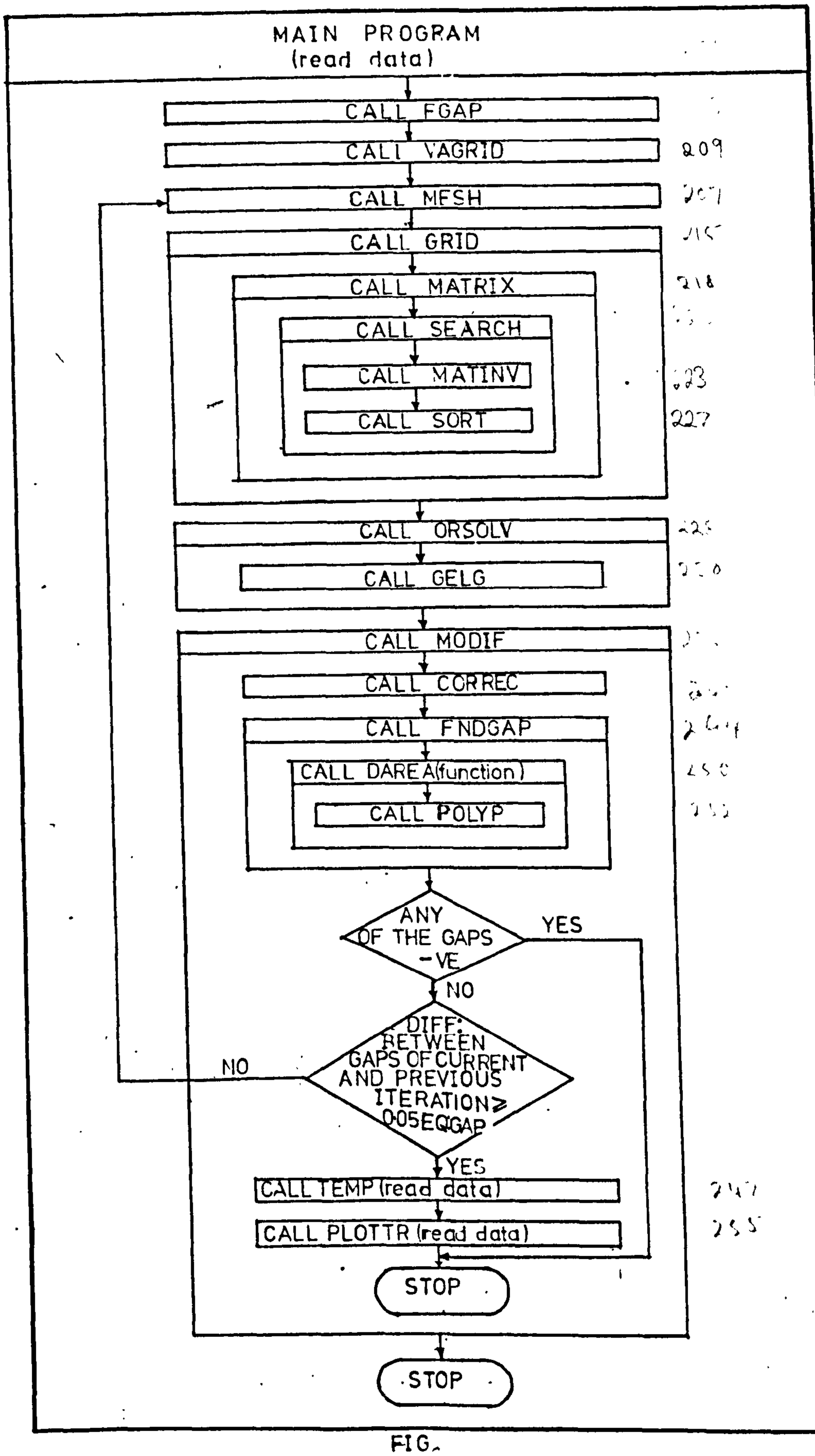

FIG.

FLOW

FLOW CHART OF THE COMPUTER PROGRAM FOR THE PREDICTION OF ELECTROCHEMICALLY MACHINED PROFILE

```
C
C     ..................................................
C     .                                                .
C     .     ECM SYSTEM SIMULATION PROGRAM              .
C     .                                                .
C     .                                                .
C                        MAIN PROGRAM
C
C     ..................................................
C       ALL DIMENSIONAL VARIABLES ARE SPECIFIED BY ()
C     ..................................................
C
C        THIS PROGRAM CONSIDERS CYLINDRICAL TOOLS WITH
C        HEMISPHERICAL LEADING EDGES OR STRAIGHT
C        LEADING EDGES WITH CORNER RADIUS WITH OR
C        WITHOUT LAND WIDTH.
C        CONSIDERS BOTH SODIUM CHLORIDE ELECTROLYTE AND
C        SODIUM NITRATE ELECTROLYTE AND ELECTRODE
C        POTENTIALS.
C
C     ..................................................
C       DEFINITION OF VARIABLES IN DIMENSION AND COMMON
C     ..................................................
C     XIS     DIMENSION OF THE SECTION OF THE STRAIGHT
C             LEADING EDGE OF THE TOOL.
C     RO      CORNER RADIUS OR RADIUS OF THE LEADING
C             EDGE OF THE TOOL.
C     XNLH    DIMENSION OF THE LANDWIDTH OF THE TOOL.
```

```
C          NRAD     NUMBER OF RADIAL LINES (J LINES).
C          NLH      NUMBER OF TRANSVERSE LINES WHIICH DIVIDES
C                   THE LANDWIDTH OF THE TOOL TO FORM THE
C                   MESH.
C          NHOR     NUMBER OF LINES PARREL TO X AXIS (J LINES).
C          NIL      NUMBER OF POINTS TAKEN ON A TRANSVERSE
C                   LINE TO FORM THE MESH.
C          NTOT     TOTAL NUMBER OF 'J' LINES.
C          NILM1    NIL-1
C          NILM2    NIL-2
C          NTOTM1   NTOT-1
C          NTOTM2   NTOT-2
C          X( )     ABSCISSA OF NODAL POINTS.
C          Y( )     ORDINATE OF NODAL POINTS.
C          VOLTS    APPLIED CELL VOLTAGE.
C          CONDUC   CONDUCTIVITY OF THE ELECTROLYTE.
C          VSP      SPECIFIC VOLUMETRIC METAL REMOVAL RATE.
C          DVOLTS   ELECTRODE POTENTIAL OF THE SYSTEM.
C          NANO3    SODIUM NITRATE ELECTROLYTE (IF NANO3=1).
C          NACL     SODIUM CHLORIDE ELECTROLYTE (IF NACL=1).
C          TEMPIN   TEMPERATURE OF THE ELECTROLYTE AT INLET.
C          CONC     CONCENTRATION OF THE ELECTROLYTE.
C          HE       ORTHOGONAL EQUILIBRIUM GAP.
C          PI       CONSTANT 360 DEGREES IN RADIANS.
C          THETA( )ANGLE MADE BY RADIAL LINES WITH THE
C                   VERTICAL IN RADIANS MEASURED IN CLOCKWISE
C                   DIRECTION.
C          ALPHA( )THETA IN DEGREES.
```

```
C     -  R( )    -RADIAL DISTANCE FROM NODAL POINTS ON THE
C                 WORK SURFACETO THE ORIGIN.
C          ICODE() CODING OF THE BOUNDARY AND INNER POINTS
C                  OF THE REGION ACCORDING TO BOUNDARY
C                  CONDITIONS.
C          IFLAG   WARNING TO SHOW WHETHER THE 5 BY 5
C                  MATRICES ARE SINGULAR,IF SINGULAR STOPS
C                  THE PROGRAM.
C          B( , )  MATRIX FORMED FOR THE SOLUTION OF THE SET
C                  OF DIFFERENCE EQUATIONS.
C          VOLTS( )POTENTIAL AT EACH MESH POINT.
C          PHI( )  POTENTIAL AT EACH MESH POINT.
C          DXDY( ) INVERSE GRADIENT AT NODAL POINTS ON THE
C                  WORK SURFACE.
C          DRDTH( )SLOPE OF THE WORK PROFILE AT NODAL POINTS
C                  IN POLAR COORDINATES.
C          DPHIDN()NORMAL POTENTIAL GRADIENT.
C          XP( )   ABSCISSA OF TOOL PROFILE.
C          YP( )   ORDINATE OF TOOL PROFILE.
C          DH( )   CHANGE IN GAPS AFTER EACH ITERATION ALONG
C                  TRANSVERSE LINES.
C          GAP( )  GAPS BETWEEN THE ELECTRODES ALONG
C                  TRANSVERSE LINES AFTER EACH ITERATION.
C          GAPO( ) GAPS OF PREVIOUS ITERATION.
C          XW( )   ABSCISSA OF THE EQUILIBRIUM WORK SURFACE.
C          YW( )   ORDINATE OF THE EQUILIBRIUM WORK SURFACE.
C          ..........................................
```

```
      COMMON/CONTRL/NRAD,NLH,NIL,NILM1,NILM2,NTOT,NTOTM1,
     1NTOTM2,XIS,XNLH,RO,NIN
      COMMON X(350),Y(350),B(190,190),VOLTS,VOLT(190),
     1PHI(190),ICODE(4),GAP(50),IFLAG,THETA(50),XP(50),
     2YP(50),DH(50),YYI(50),DRDTH(50),DXDY(50),ALPHA(50),
     3R(50),PI,SLOPE(50),GAPO(50),XW(50),YW(50),CONDUC,VSP
     4,HE,DPHIDN(50),DVOLTS,FEED,NANO3,NACL,TEMPIN,CONC
C
      READ (5,12) XIS,XNLH,RO,NRAD,NLH,NIN,NIL
      READ (5,15) VOLTS,DVOLTS,VSP,FEED
      WRITE (6,16) XIS,XNLH,RO,NRAD,NLH,NIN,NIL
      WRITE (6,17) VOLTS,DVOLTS,VSP,FEED
      READ (5,5) NANO3,NACL,TEMPIN,CONC
      WRITE (6,6) NANO3,NACL,TEMPIN,CONC
      PI=3.1415926
      CALL FGAP
      IRET=0
      NILM1=NIL-1
      NILM2=NIL-2
      NTOT=NRAD+NLH+NIN
      NTOTM1=NTOT-1
      NTOTM2=NTOT-2
      NP=NTOTM2*NILM2
      CALLVAGRID (2,1.0)
      CALL MESH
    8 IRET=IRET+1
      WRITE (6,500) IRET
------------------------------------------------------------
  500 FORMAT (5X,'IRET=',I5)
```

```
      IF (IRET.GE.25) GO TO 9
603   CALL GRID (NP)
      IF (IFLAG.EQ.1) GO TO 9
      CALL ORSOLV(NUM,NP)
601   DO 1 I=1,NTOT
      GAPO(I)=GAP(I)
1     CONTINUE
14    CALL MODIF (DTHETA,IRET)
      GO TO 8
C
C        DESCRIPTION OF FORMAT STATEMENTS
C
12    FORMAT (3F12.6,5I5)
15    FORMAT (4F12.6)
16    FORMAT (/,3X,3F12.6,4I6,/)
17    FORMAT (/,3X,4F12.6,/)
5      FORMAT (2I1,2F12.6)
6     FORMAT (/,3X,'NANO3=',I2,'NACL=',I2,3X,'TEMPIN=',
     1F12.6,3X,'CONC=',F12.6)
9     STOP
      END
```

```
C     ..................................................
C
C     SUBROUTINE FGAP
C
C     PURPOSE
C        TO FIND THE THEORETICAL ORTHOGANAL GAP.
C        TO CONVERT ALL DIMENSIONS AND MACHINING
C           PARAMETERS IN TERMS OF THIS DIMENSION.
C
C     USAGE
C        CALL FGAP.
C     REMARKS
C        LOGICAL PROGRAM.
C
C     METHOD
C        ORTHOGONAL EQUILIBRIUM GAP IS CALCULATED USING
C        THE EQUATION H=(VOLTS-DVOLTS)*CONDUC*VSP/FEED
C
C     SUBROUTINES ANDFUNCTION SUBPROGRAMS REQUIRED
C        NONE.
C
C     ..................................................
C
      SUBROUTINE FGAP
      COMMON/CONTRL/NRAD,NLH,NIL,NILM1,NILM2,NTOT,
     1NTOTM2,XIS,XNLH,PO,NIN
      COMMON X(350),Y(350),B(190,190),VOLTS,VOLT(190),
     1PHI(190),ICODE(4),GAP(50),IFLAG,THETA(50),XP(50),
```

```
     2YP(50),DH(50),YYI(50),DRDTH(50),DXDY(50),ALPHA(50),
     3P(50),PI,SLOPE(50),GAPO(50),XW(50),YW(50),CONDUC,VSP
     4,HE,DPHIDN(50),DVOLTS,FEED,NANO3,NACL,TEMPIN,CONC
C
      IF (NACL.EQ.1) GO TO 2
      IF (NANO3.EQ.1) GO TO 3
3     CONDUC=(0.00385*TEMPIN+0.000233*CONC-0.026)/10.0
      GO TO 4
2     CONDUC=(0.003*TEMPIN+0.000783*CONC-0.0205)/10.0
C
4     HE=(VOLTS-DVOLTS)*CONDUC*VSP/FEED
6     RO=RO/HE
      FEED=FEED/HE
      VSP=VSP/(HE**3)
      WRITE (6,5)RO,FEED,VSP,HE
5     FORMAT (/,3X,4F12.6)
      RETURN
      END
```

MESH

```
C     ..................................................
C
C          PURPOSE
C             TO FORM THE MESH IN THE REGION BOUNDED BY THE
C             TOOL BOUNDARY AND THE WORK BOUNDARY .
C
C          USAGE
C             CALL MESH
```

```
C
C       REMARKS
C           LOGICAL PROGRAM.
C           THE MESH CAN BE CHANGED AT WILL BY CHANGING
C           THE BLOCK DATA.
C
C       SUBROUTINES AND FUNCTION SUBPROGRAMS REQUIRED
C           NONE
C
C       METHOD
C           THE TOOL BOUNDARY COORDINATES AND THE WORK
C           BOUNDARY COORDINATES WERE INPUT TO THE PROGRAM.
C           THE GAP BETWEEN THE ELECTRODES ALONG
C           TRANSVERSE LINES WERE DIVIDED ACCORDING TO
C           BLOCK DATA GIVING REQUIRED MESH.
C
C     ..................................................
C
      SUBROUTINE MESH
      COMMON/CONTRL/NRAD,NLH,NIL,NILM1,NILM2,NTOT,
     1NTOTM2,XIS,XNLH,RO,NIN
      COMMON X(350),Y(350),B(190,190),VOLTS,VOLT(190),
     1PHI(190),ICODE(4),GAP(50),IFLAG,THETA(50),XP(50),
     2YP(50),DH(50),YYI(50),DRDTH(50),DXDY(50),ALPHA(50),
     3R(50),PI,SLOPE(50),GAPO(50),XW(50),YW(50),CONDUC,VSP
     4,HE,DPHIDN(50),DVOLTS,FEED,NANO3,NACL,TEMPIN,CONC
      DIMENSION PROPM(7)
      DATA PROPM/-0.4,0.0,0.4,0.7,0.9,1.0,1.1/
      DO 1 J=1,NTOT
```

```
      IJT=(J-1)*NIL+2
      IJWP=(J-1)*NIL+NIL-1
      DO 1 I=1,NIL
      IJ=(J-1)*NIL+I
      X(IJ)=X(IJT)+PROPM(I)*(X(IJWP)-X(IJT))
1     Y(IJ)=Y(IJT)+PROPM(I)*(Y(IJWP)-Y(IJT))
      RETURN
      END
C
C     ..........
C     SUBROUTINE VAGRID
C
C     PURPOSE
C        TO LOCATE THE TOOL BOUNDARY AND THE INTIAL
C        WORK BOUNDARY.
C        TO FIND THE INTIAL GAP BETWEEN THE TOOL AND
C        WORK BOUNDARIES ACCROSS CORRESPONDING POINTS
C        ON THE TOOL AND WORK BOUNDARIES.
C
C     USAGE
C        CALL VAGRID (NEXP,CB)
C
C     DESCRIPTION OF PARAMETERS
C        NEXP - THE EXPONENT IN WHICH THE GAP IS
C        RADIALLY DIVIDED.
C        CB - ORDINATE OF THE CENTRE OF THE RADIUSED
C           SECTION OF THE GUESSED WORK PROFILE.
C
```

```
C       REMARKS
C          TOOL GEOMETRY AND WOK PROFILE GEOMETRY IS READ
C          THE MAIN PROGRAM.
C
C     ..................................................
      COMMON/CONTRL/NRAD,NLH,NIL,NILM1,NILM2,NTOT,NTOTM1,
     1NTOTM2,XIS,XNLH,RO,NIN

      COMMON X(350),Y(350),B(190,190),VOLTS,VOLT(190),
     1PHI(190),ICODE(4),GAP(50),IFLAG,THETA(50),XP(50),
     2YP(50),DH(50),YYI(50),DRDTH(50),DXDY(50),ALPHA(50),
     3R(50),PI,SLOPE(50),GAPO(50),XW(50),YW(50),CONDUC,VSP
     4,HE,DPHIDN(50),DVOLTS,FEED,NANO3,NACL,TEMPIN,CONC
C
C          CALCULATION OF ANGLES OF RADIAL LINES.
C
      NRADP1=NRAD+1
      NRH=NRAD+NLH
      NRHP1=NRH+1
      DO 1 J=2,NRAD
      XX=FLOAT(J-2)/FLOAT(NRAD-2)
      JT=NRAD-J+2
      THETA(JT)=PI*(1.0-XX)/2.0
      ALPHA(JT)=THETA(JT)*180.0/PI
1     CONTINUE
C
C          MIRROR RADIAL LINES.
C
      THETA(1)=-THETA(3)
```

```
      ALPHA(1)=-ALPHA(3)
      IF (XIS.EQ.0.0) GO TO 10
C
C          CALCULATION OF 'Y' COORDINATES OF TRANSVERSE
C             LINES UP TO WHERE THE INSULATION BEGINS.
C
C        CALCULATION OF 'Y' COORDINATES OF TRANSVERSE LINES
      DO 2 J=NRADP1,NRH
      XX=FLOAT(J-(NRADP1-1))/FLOAT(NRH-NRAD)
      DO 2 I=1,NIL
      IJ=(J-1)*NIL+I
    2 Y(IJ)=-XNLH*XX
C
C
C
   10 DO 3 J=NRHP1,NTOTM1
      XX=FLOAT(J-(NRHP1-1))/FLOAT(NTOTM1-NRH)
      DO 3 I=1,NIL
      IJ=(J-1)*NIL+I
    3 Y(IJ)=-XNLH-NIN*(XX**NEXP)
C
C          CALCULATION OF MIRROR POINTSFOR THE LAST
C          TRANSVERSE LINE.
C
      DO 4 I=1,NIL
      IJ1=NTOTM1*NIL+I
      IJ2=(NTOTM1-1)*NIL+I
      IJ3=(NTOTM1-2)*NIL+I
```

```
4       Y(IJ1)=2.0*Y(IJ2)-Y(IJ3)
        WRITE (6,300)
C
C           COORDINATES OF THE TOOL POINTS 'RADIAL LINES',
C
        DO 5 J=1,NRAD
        IJ=(J-1)*NIL+2
        X(IJ)=RO*SIN(THETA(J))
        Y(IJ)=RO*COS(THETA(J))
5       CONTINUE
C
C           COORDINATES OF THE TOOL POINTS 'VERTICAL REGION'.
C
        DO 6 J=NRADP1,NTOT
        IJ=(J-1)*NIL+2
6       X(IJ)=RO
C
C           COORDINATES OF THE WORK PROFILE UP TO 'X' AXIS.
C           ASSUMED WORK PROFILE A CIRCULAR ARC OF RADIUS 'RW'
C           AND WHOSE CENTRE IS OFFSET BY THE AMOUNT 'CB'.
C
        RW=RO+1.0+CB
        DO 7 J=2,NRAD
        IJ=(J-1)*NIL+NIL-1
        IF (J.EQ.2) GO TO 20
        IF (J.EQ.NRAD) GO TO 30
        AP =(1.0+(1.0/TAN(THETA(J)))**2)
        BP=2.0*(1.0/TAN(THETA(J)))*CB
```

```
      CP=CB**2-RW**2
      X(IJ)=(-BP+SQRT(BP**2-4.0*AP*CP))/(2.0*AP)
      Y(IJ)=X(IJ)/TAN(THETA(J))
7     CONTINUE
20    X(IJ)=0.0
      Y(IJ)=RO+1.0
      GO TO 7
30    X(IJ)=SQRT(RW**2-CB**2)
      Y(IJ)=0.0
C
C        FIRST MIRROR POINT ON WORK PROFILE.
C
      JL1=NILM1
      JL3=2*NIL+NILM1
      X(JL1)=-X(JL3)
      Y(JL1)=Y(JL3)
C
C          GAP BETWEEN THE TOOL AND WORK PROFILES
C
      DO 8 J=1,NRAD
      IJWP=(J-1)*NIL+NILM1
      R(J)=SQRT(X(IJWP)**2+Y(IJWP)**2)
8     GAP(J)=R(J)-RO
C
C          'X' COORDINATES OF THE WORK PROFILE ASSUMED WORK PROFILE
C        PARABOLA OF THE FORM Y=A*X**2+B.
C
      IJWR=(NRAD-1)*NIL+NILM1
```

```
      AX=-0.5
      BX=-AX*X(IJWR)**2
      DO 9 J=NRADP1,NTOT
      IJ=(J-1)*NIL+NILM1
      X(IJ)=SQRT((Y(IJ)-BX)/AX)
C
C        GAP BETWEEN THE TOOL AND THE WORK PROFILE.
      GAP(J)=X(IJ)-RO
    9 CONTINUE
C
C        CALCULATION OF EXTRA 'R(J)' AND THETA(J) TO BE
C        USED IN FUNCTION DAREA.
C
      NRADP1=NRAD+1
      NRADP4=NRAD+4
      DO 11 J=NRADP1,NRADP4
      IJWP=(J-1)*NIL+NILM1
      R(J)=SQRT(X(IJWP)**2+Y(IJWP)**2)
      THETA(J)=PI/2.0+ATAN(ABS(Y(IJWP)/X(IJWP)))
      ALPHA(J)=(THETA(J)*180.0)/PI
   11 CONTINUE
C
C        COORDINATES OF THE TOOL BOUNDARY TO BE USED IN
C        THE SUBROUTINE PLOTTR.
C
      DO 12 J=2,NTOT
      IJ=(J-1)*NIL+2
      XP(J)=X(IJ)*HE
      YP(J)=Y(IJ)*HE
```

```
12      CONTINUE
        XP(1)=-XIS
        YP(1)=RO*HE
        RETURN
        END

C
C       ..................................................
C
C       SUBROUTINE GRID
C
C       PURPOSE
C          TO CODE THE MESH POINTS ACCORDING TO BOUNDARY
C          CONDITIONS.
C          TO SELECT MESH POINTS TO FORM THE DIFFERENCE
C             EQUATIONS.
C             TO FORM THE POSITION MATRIX FROM THE FIVE
C             POINTS SELECTED.
C
C       USAGE
C          CALL GRID (NP)
C
C       DESCRIPTION OF PARAMETERS
C             NP     - NUMBER OF MESH POINTS.
C
C       REMARKS
C          LOGICAL PROGRAM.
C
```

```
C          SUBROUTINES AND FUNCTION SUBPROGRAMS REQURIED
C             1)SUBROUTINE MATRIX.
C
C          ..........................................
C
      SUBROUTINE GRID (NP)
      DIMENSION II(5),JJ(5),XX(5),YY(5),IHELP(5)
       COMMON/CONTRL/NRAD,NLH,NIL,NILM1,NILM2,NTOT,
     1NTOTM2,XIS,XNLH,RO,NIN
       COMMON X(350),Y(350),B(190,190),VOLTS,VOLT(190),
     1PHI(190),ICODE(4),GAP(50),IFLAG,THETA(50),XP(50),
     2YP(50),DH(50),YYI(50),DRDTH(50),DXDY(50),ALPHA(50),
     3R(50),PI,SLOPE(50),GAPO(50),XW(50),YW(50),CONDUC,VSP
     4,HE,DPHIDN(50),DVOLTS,FEED,NANO3,NACL,TEMPIN,CONC
       NSRH=NRAD+NLH
      DO 1 J=1,NTOTM2
      DO 1 I=1,NILM2
      DO 10 ICO=1,4
1C    ICODE(ICO)=0.0
      IP1=I+1
      IM1=I-1
      JP1=J+1
      JM1=J-1
      INDEXO=(J*NIL)+(I+1)
C
C          CODING MESH POINTS.
C
      IF (IM1.LT.1.AND.J.LE.(NSRH-1)) ICODE(4)=1
      IF (IP1.GT.NILM2) ICODE(4)=1
```

```
      IF (JM1.LT.1) ICODE(2)=1
      IF (JP1.GT.NTOTM2) ICODE(3)=1
      IF (IM1.LT.1.AND.J.GT.(NSRH-1)) ICODE(1)=1
      II(1)=I
      JJ(1)=J
      II(2)=IP1
      JJ(2)=J
      II(3)=IM1
      JJ(3)=J
      II(4)=I
      JJ(4)=JM1
      II(5)=I
      JJ(5)=JP1
      IF (IM1.LT.1.AND.J.LE.(NSRH-1)) II(3)=3
      IF(IP1.GT.NILM2) II(2)=NILM2-2
      KANS=(J-1)*NILM2+I
      DO 2 K=1,5
      INDEX=(JJ(K)*NIL)+(II(K)+1)
C
C        COORDINATES WITH RESPECT TO LOCAL ORIGIN.
C
      XX(K)=X(INDEX)-X(INDEXO)
      YY(K)=Y(INDEX)-Y(INDEXO)
      IHELP(K)=((JJ(K)-1)*NILM2)+II(K)
       IF (JJ(K).GT.NTOTM2.OR.JJ(K).LT.1.OR.II(K).GT.NILM2.
     1OR.II(K).LT.1) IHELP(K)=0
2      CONTINUE
       NP=NTOTM2*NILM2
       XX(K)=X(INDEX)-X(INDEXO);
C
```

```
C       CALLING SUBROUTINE MATRIX WHICH FORMS THE 5 BY5
C       POSITION MATRIX.
C
        CALL MATRIX (XX,YY,KANS,IHELP,J,NP)
1       CONTINUE
        RETURN
        END
C
C       .....
C
C       SUBROUTINE MATRIX
C
C       PURPOSE
C          TO FORM 5 BY 5 MATRIX FROM SELECTED MESH
C          POINTS IN SUBROUTINE GRID TO FORMTHE SET OF
C          EQUATION FOR THE WHOLE REGION.
C
C          USAGE
C             CALL MATRIX (XX,YY,K,IHELP,J,NP)
C
C          DESCRIPTION OF PARAMETERS
C             XX    'X' COORDINATE WITH RESPECT TO LOCAL
C             COORDINATE AXIS
C
C          YY    'Y' COORDINATE WITH RESPECT TO LOCAL
C          COORDINATE AXIS.
C          K     COUNTER FOR GRID POINTS.
C          IHELP COUNTER TO CHECK WHETHER THE GRID POINT
C          IS INSIDE THE LAPLACE REGION.
C          J     COUNTER FOR TRANSVERSE LINES.
C          NP    NUMBER OF GRID POINTS.
```

```
C
C          REMARKS
C              FROM THE LOCAL COORDINATES FORMS 5 BY 5
C              MATRICES OF THE FORM,
C
C                     XX(1)**2  YY(1)**2  XX(1)  YY(1)  1
C                     XX(2)**2  YY(2)**2  XX(2)  YY(2)  1
C                     XX(3)**2  YY(3)**2  XX(3)  YY(3)  1
C                     XX(4)**2  YY(4)**2  XX(4)  YY(4)  1
C                     XX(5)**2  YY(5)**2  XX(5)  YY(5)  1
C
C                FOR EACH GRID POINT OF THE REGION.
C
C          SUBROUTINES AND FUNCTION SUBPROGRAMS REQUIRED
C              1) SUBROUTINE SEARCH
C
C              .....
C
      SUBROUTINE MATRIX (XX,YY,K,IHELP,J,NP)
      DIMENSION A(5,5),IHELP(5),XX(5),YY(5)
      COMMON X(350),Y(350),B(190,190),VOLTS,VOLT(190),
     1PHI(190),ICODE(4),GAP(50),IFLAG,THETA(50),XP(50),
     2YP(50),DH(50),YYI(50),DRDTH(50),DXDY(50),ALPHA(50),
     3R(50),PI,SLOPE(50),GAPO(50),XW(50),YW(50),CONDUC,VSP
     4,HE,DPHIDN(50),DVOLTS,FEED,NANO3,NACL,TEMPIN,CONC
C
C                FORMATION OF THE 5 BY 5 MATRIX
C
```

```
      DO  1  M=1,5
      A(M,1)=XX(M)**2
      A(M,2)=YY(M)**2
      A(M,3)=XX(M)
      A(M,4)=YY(M)
      A(M,5)=1.0
1     CONTINUE
C
C           CALLING SUBROUTINE SEARCH
C
2 0   CALL SEARCH (A,K,IHELP,J,NP)
      DO 2 L=1,NP
2     B(K,L)=PHI(L)
3 0 0 RETURN
      END
C
C     ..................................................
C
C     SUBROUTINE SEARCH
C
C     PURPOSE
C        TO INVERT 5 BY 5 POSITON MATRICES FORMED BY
C     SUBROUTINE MATRIX.
C     TO SELECT THE REQUIRED COMBINATION OF COLOUMNS
C     OR ROWS FOR EACH MESH POINT ACCORDING TO
C     BOUNDARY CONDITIONS.
```

```
C
C          USAGE
C              CALL SEARCH (A,K,IHELP,J,NP)
C
C          DESCRIPTION OF PARAMETERS
C              A      - INPUT 5 BY 5 MATRIX.
C              K      - COUNTER FOR MESH POINTS.
C              IHELP  - COUNTER USED TO CHECK WHETHER THE MESH
C              POINT IS INSIDE THE REGION.
C              J      - COUNTER FOR TRANSVERSE LINES (J LINES).
C              NP     -  NUMBER OF MESH POINTS.
C
C          REMARKS
C              LOGICAL PROGRAM.
C
C          SUBROUTINES AND FUNCTION SUBPROGRAMS REQUIRED
C
C              1)SUBROUTINE MATINV (FROM R.H.PENNINGTON
C              INTRODUCTORY COMPUTER METHODS AND NUMERICAL
C              ANALYSIS) 2) SUBROUTINE SORT.
C
C     ..................................................
C
      SUBROUTINE SEARCH (A,K,IHELP,J,NP)
      DIMENSION A(5,5),IHELP(5),D(5),L(5),M(5),AT(5,5),
     1C(5,5)
      COMMON/CONTRL/NRAD,NLH,NIL,NILM1,NILM2,NTOT,
     1NTOTM2,XIS,XNLH,RO,NIN
```

```
      COMMON X(350),Y(350),B(190,190),VOLTS,VOLT(190),
     1PHI(190),ICODE(4),GAP(50),IFLAT,WHSTA(50),XP(50),
     2YP(50),DH(50),YYI(50),DRDTH(50),DXDY(50),ALPHA(50),
     3R(50),PI,SLOPE(50),GAPO(50),XW(50),YW(50),CONDUC,VSP
     4,HE,DPHIDN(50),DVOLTS,FEED,NANO3,NACL,TEMPIN,CONC
      DO 24 I7=1,5
      DO 24 I8=1,5
24    AT(I7,I8)=A(I7,I8)
C
C           CALLING SUBROUTINE TO INVERT 5 BY 5 MATRICES.
C
      CALL MATINV (AT,5,10,A,IFLAG,K)
11    DO 20 I=1,NP
20    PHI(I)=0.0
      DO 10 ICO=1,3
      IF (ICODE(ICO).EQ.0) GO TO 10
      IF (ICODE(1).EQ.1) CALL SORT (A,3,2,1)
      IF (ICODE(2).EQ.1) CALL SORT (A,4,5,1)
      IF (ICODE(3).EQ.1) CALL SORT (A,5,4,1)
10    CONTINUE
      DO 30 N=1,5
      LPOS=IHELP(N)
      IF(LPOS.EQ.0) GO TO 30
      PHI(LPOS)=A(1,N)+A(2,N)
      IF (ICODE(4).EQ.1) PHI(LPOS)=A(5,N)
30    CONTINUE
      RETURN
      END
```

```
C
C     ..................................................
C
C     SUBROUTINE MATINV
C
C     PURPOSE
C        TO INVERT 5 BY 5 MATRICES FORMED BY SUBROUTINE
C        MATRIX.
C
C     USAGE
C        CALL MATINV (AA,N,N2,AINV,IFLAG,KANS)
C
C     DESCRIPTION OF PARAMETERS
C        AA      -THE MATRIX TO BE INVERTED.
C        N       -NUMBER OF ROWS OF THE SQUARE MATRIX.
C        N2      - 2*N.
C        AINV    -INVERTED MATRIX.
C        IFLAG   -WARNING IF AA IS SINGULAR.
C        KANS    -SHOWS THE POSITION OF THE MATRIX IN
C                 THE REGION.
C
C     REMARKS
C        CONSIDERS ONLY 5 BY 5 MATRICES FOR INVERTION
C        AS DIMENSIONED.
C
C     METHOD
C        INVERSION BY ELEMINATION PROCESS
C        REFER INTRODUCTORY COMPUTER METHODS AND NUMERICAL
C AL
C        NUMERICAL ANALYSIS BY R.H.PENNINGTON PAGE 323.
```

```
C
C          SUBROUTINES AND FUNCTION SUBPROGRAMS REQUIRED
C              NONE
C
C     ..................................................
C
      SUBROUTINE MATINV(AA,N,N2,AINV,IFLAG,KANS)
      DIMENSION AA(5,5),AINV(5,5),A(5,10),ID(3)
      IFLAG=0
      NN=N+1
      N2=2*N
      DO 200 I=1,N
      DO 200 J=1,N
  200 A(I,J)=AA(I,J)
      K=1
      DO 1 I=1,N
      DO 1 J=NN,N2
      A(I,J)=0
    1 CONTINUE
      DO 21 I=1,N
      A(I,N+I)=1
   21 ID(I)=I
    2 CONTINUE
      KK=K+1
      IS=K
      IT=K
      B=ABS(A(K,K))
      DO 3 I=K,N
      DO 3 J=K,N
```

```
      IF(ABS(A(I,J))-B)3,3,31
31    IS=I
      IT=J
      B=ABS(A(I,J))
3     CONTINUE
      IF(IS-K)4,4,41
41    DO 42 J=K,N2
      C=A(IS,J)
      A(IS,J)=A(K,J)
42    A(K,J)=C
4     CONTINUE
      IF(IT-K)5,5,51
51    IC=ID(K)
      ID(K)=ID(IT)
      ID(IT)=IC
      DO 52 I=1,N
      C=A(I,IT)
      A(I,IT)=A(I,K)
52    A(I,K)=C
5     CONTINUE
      IF(A(K,K))6,120,6
6     CONTINUE
      DO 7 J=KK,N2
      A(K,J)=A(K,J)/A(K,K)
      DO 7 I=KK,N
      W=A(I,K)*A(K,J)
      A(I,J)=A(I,J)-W
      IF(ABS(A(I,J))-.00001*ABS(W))71,7,7
71    A(I,J)=0
```

```
7       CONTINUE
        K=KK
        IF(K-N)2,81,120
81      IF(A(N,N))9,120,8
8       CONTINUE
        DO 9 J=NN,N2
        A(N,J)=A(N,J)/A(N,N)
9       CONTINUE
        N1=N-1
        DO 10 M=1,N1
        I=N-M
        II=I+1
        DO 10 K=II,N
        DO 10 J=NN,N2
        A(I,J)=A(I,J)-A(I,K)*A(K,J)
10      CONTINUE
        DO 11 I=1,N
        DO 11 J=1,N
        IF(ID(J)-I)11,111,11
111     DO 112 K=NN,N2
112     AINV(I,K-N)=A(J,K)
11      CONTINUE
        RETURN
120     WRITE(6,1000)KANS
        IFLAG=1
        RETURN
1000    FORMAT(I10,'MATRIX IS SINGULAR')
        END
```

```
C
C     ..................................................
C
C     SUBROUTINE SORT
C
C     PURPOSE
C        TO SELECT THE REQUIRED COMBINATION OF THE ROWS
C        OR COLUMNS TO FROM THE INVERTED MATRIX.
C
C     USAGE
C        CALL SORT (A,ICOL1,ICOL2,ISIGN)
C
C     DESCRIPTION OF PARAMETERS
C        A     THE 5 BY 5 INVERTED MATRIX OF THE MESH
C              POINT UNDER CONSIDERATION.
C        ICOL1    COLUMN '1' OF THE INVERTED MATRIX.
C        ICOL2    COLUMN '2' OF THE INVERTED MATRIX.
C        ISIGN=1
C
C     REMARKS
C        LOGICAL PROGRAM
C
C     ..................................................
C
      SUBROUTINE SORT (A,ICOL1,ICOL2,ISIGN)
      DIMENSION A(5,5)
      DO 1 I=1,5
      A(I,ICOL2)=A(I,ICOL1)+A(I,ICOL2)
      A(I,ICOL1)=0.0
1     CONTINUE
      RETURN
      END
```

```
C
C     ..................................................
C
C     SUBROUTINE ORSOLV
C
C     PURPOSE
C        TO FORM THE DIFFERENCE EQUATION FOR EACH MESH
C        POINT.
C        TO SOLVE THE SET OF EQUTION WHICH GIVES THE
C        POTENTIAL AT EACH GRID POINT.
C
C     USAGE
C        CALL ORSOLV.
C
C     REMARKS
C        LOGICAL PROGRAM.
C
C     SUBROUTINES AND FUNCTION SUBPROGRAMS REQUIRED
C        1) SUBROUTINE GELG (ROUTINE FROM THE IBM SSP).
C
C     ..................................................
C
      SUBROUTINE ORSOLV (NP)
      DIMENSION V(190)
      COMMON/CONTRL/NRAD,NLH,NIL,NILM1,NILM2,NTOT,
     1NTOTM2,XIS,XNLH,RO,NIN
      COMMON X(350),Y(350),B(190,190),VOLTS,VOLT(190),
     1PHI(190),ICODE(4),GAP(50),IFLAG,THETA(50),XP(50),
     2YP(50),DH(50),YYI(50),DRTH(50),DXDY(50),ALPHA(50),
```

```
     3R(50),PI,SLOPE(50),GAPO(50),XW(50),YW(50),CONDUC,VSP
     4,HE,DPHIDN(50),DVOLTS,FEED,NANO3,NACL,TEMPIN,CONC
C
C          CHECK FOR BOUNDARY POINTS.
C
      DO 20 I=1,NP
      I1=I/NILM2
      I2=I1*NILM2
      VOLT(I)=0.0
      IF (I.EQ.I2) VOLT(I)=VOLTS
20    CONTINUE
      DO 50 I=1,NP
30    V(I)=VOLT(I)
C
C          CALLING SUBROUTINE GELG WHICH SOLVES THE SET OF
C          SIMULTANEOUS EQUATIONS FOR THE WHOLE REGION.
C
      CALL GELG(V,P,NP,1,0.000001,IER)
      WRITE(6,601)IER
      DO 60 I=1,NP
60    VOLT(I)=V(I)
C
C          DESCRIPTION OF THE FORMAT STATEMENT.
C
601   FORMAT('    RETURN CODE FROM GELG=',I4)
      RETURN
      END
```

```
C
C     ..................................................
C
C        SUBROUTINE GELG
C
C        PURPOSE
C           TO SOLVE A GENERAL SYSTEM OF SIMULTANEOUS
C           LINEAR EQUATIONS.
C
C        USAGE
C           CALL GELG(R,A,M,N,EPS,IER)
C
C        DESCRIPTION OF PARAMETERS
C           R    THE M BY M MATRIX OF RIGHT HAND SIDES.
C                (DESTROYED) ON RETURN R CONTAINS THE
C                SOLUTION OF THE EQUATIONS.
C           A    THE M BY M COEFFICIENT MATRIX (DESTROYED)
C           M    THE NUMBER OF EQUATION IN THE SYSTEM.
C           N    THE NUMBER OF RIGHT HAND SIDE VECTORS.
C           EPS  AN INPUT CONSTANT WHICH IS USED AS
C                RELATIVE TOLERANCE FOR TEST ON LOSS OF
C                SIGNIFICANCE.
C           IER  RESULTING ERROR PARAMETER CODED AS FOLLOWS
C                IER=0    NO ERROR,
C                IER=-1   NO RESULT BECAUSE OF M LESS THAN
C                1 OR PIVOT ELEMENT AT ANY ELIMINATION
C                IS EQUAL TO ZERO.
C                IER=5    WARNING DUE TO POSSIBLELOSS OF
C                SIGNIFICANCE INDICATED AT ELIMINATION
```

```
C                STEP K+1,WHERE PIVOT ELEMENT WAS LESS THAN
C                OR EQUAL TO THE INTERNAL TOLERANCE EPS
C                TIMES ABSOLUTELY GREATEST ELEMENT OF
C              MATRIX A.
C
C           REMARKS
C              INPUT MATRICES R AND A ARE ASSUMED TO BE
C              STORED COLUMNWISE IN M*N RESP. M*M SUCCESSIVE
C              STORAGE LOCATIONS. ON RETURN SOLUTION MATRIX 'R'
C              IS STORED COLUMNWISE TOO. THE PROCEDURE GIVES
C              RESULT IF THE NUMBER OF EQUATIONS M IS GREATER
C              THAN 0 AND PIVOT ELEMENTS AT ALL ELIMINATION
C              STEPS ARE DIFFERENT FROM 0.HOWEVER, WARNING
C              IER=K IF GIVEN INDICATES POSSIBLE LOSS OF
C              SIGNIFICANCE. IN CASE OF A WELL SCALED MATRIX
C              A AND APPROPRIATE TOLERANCE EPS, IER=K MAY BE
C              INTERPRETED THAT MATRIX A HAS THE RANK K.
C              NO WARNING IS GIVEN IN CASE M=1.
C
C           SUBROUTINES AND FUNCTION SUBPROGRAMS REQUIRED
C              NONE
C
C           METHOD
C              SOLUTION IS DONE BY MEANS OF GAUSS-ELIMINATION
C              WITH COMPLETE PIVOTING.
C
C     ..................................................
```

```
C
      SUBROUTINE GELG(R,A,M,N,EPS,IER)
C
C
C
      DIMENSION A(1),R(1)
      IF(M)23,23,1
C
C     SEARCH FOR GREATEST ELEMENT IN MATRIX A.
    1 IER=0
      PIV=0.
      MM=M*M
      NM=N*M
      DO 3 L=1,MM
      TB=ABS(A(L))
      IF(TB-PIV)3,3,2
    2 PIV=TB
      I=L
    3 CONTINUE
      TOL=EPS*PIV
C
C        A(I) IS PIVOT ELEMENT .PIV CONTAINS THE ABSOLUTE
C        VALUE OF A(I).
C
C
C     START ELIMINATION LOOP.
      LST=1
      DO 17 K=1,M
C
```

```
C       TEST ON SINGULARITY
        IF(PIV)23,23,4
    4   IF(IER)7,5,7
    5   IF(PIV-TOL)6,6,7
    6   IER=K-1
    7   PIVI=1./A(I)
        J=(I-1)/M
        I=I-J*M-K
        J=J+1-K
C       I+K IS ROW-INDEX, J+K COLUMN-INDEX OF PIVOT ELEMENT.
C
C       PIVOT ROW REDUCTION AND ROW INTERCHANGE IN RIGHT
HAND SIDE R.
        DO 8 L=K,NM,M
        LL=L+I
        TB=PIVI*R(LL)
        R(LL)=R(L)
    8   R(L)=TB
C
C       IS ELIMINATION TERMINATED.
        IF(K-M)9,18,18
C
C       COLUMN INTERCHANGE IN MATRIX A.
    9   LEND=LST+M-K
        IF(J)12,12,10
   10   II=J*M
        DO 11 L=LST,LEND
        TB=A(L)
        LL=L+II
        A(L)=A(LL)
   11   A(LL)=TB
```

```
C
C       ROW INTERCHANGE AND PIVOT ROW REDUCTION IN MATRIX A.
   12 DO 13 L=LST,MM,M
      LL=L+I
      TB=PIVI*A(LL)
      A(LL)=A(L)
   13 A(L)=TB
C
C       SAVE COLUMN INTERCHANGE INFORMATION.
      A(LST)=J
C
C       ELEMENT REDUCTION AND NEXT PIVOT SEARCH.
      PIV=0.
      LST=LST+1
      J=0
      DO 16 II=LST,LEND
      PIVI=-A(II)
      IST=II+M
      J=J+1
      DO 15 L=IST,MM,M
      LL=L-J
      A(L)=A(L)+PIVI*A(LL)
      TB=ABS(A(L))
      IF(TB-PIV)15,15,14
   14 PIV=TB
      I=L
   15 CONTINUE
      DO 16 L=K,NM,M
      LL=L+J
   16 R(LL)=R(LL)+PIVI*R(L)
```

```
   17 LST=LST+M
C       END OF ELIMINATION LOOP.
C
C
C       BACK SUBSTITUTION AND BACK INTERCHANGE.
   18 IF(M-1)23,22,19
   19 IST=MN+M
      LST=M+1
      DO 21 I=2,M
      II=LST-I
      IST=IST-LST
      L=IST-M
      L=A(L)+.5
      DO 21 J=II,NM,M
      TB=R(J)
         LL=J
         DO 20 K=IST,MM,M
         LL=LL+1
   20    TB=TB-A(K)*R(LL)
         K=J+L
         R(J)=R(K)
   21    R(K)=TB
   22 RETURN
C
C
C       ERROR RETURN
   23 IER=-1
      RETURN
      END
```

```
C
C     ..................................................
C     SUBROUTINE MODIF
C
C     PURPOSE
C        TO MODIFY GAPS BETWEEN ELECTRODES AFTER EACH
C        ITERATION.
C        COMPARES THE GAPS OF THE CURRENT ITERATION
C        WITH THEPREVIOUS ITERATION, IF THE DIFFERENCE
C        BETWEEN ANY TWO CORRESPONDING GAPS IS LESS
C        THAN SOME GIVEN VALUE (SAYC.05 OF THE
C        EQUILIBRIUM GAP) THE WORK SHAPE IS TAKEN TO BE
C        THE EQUILIBRIUM WORK SHAPE.
C        IF ANY OF THE GAPS IS -VE, STOPS THE PROGRAM,
C        BECAUSE THE TOOL HAS MADE CONTACT WITH THE
C        WORK SURFACE.
C        WHEN THE EQUILIBRIUM WORK SHAPE IS ATTAINED
C        BOTH THE WORK BOUNDARY COORDINATES AND TOOL
C        BOUNDARY COORDINATES WERE PLOTTED TO SHOW THE
C        RELATIVE POSITIONS.
C
C     USAGE
C        CALL MODIF
C
C     REMARKS
C        LOGICAL PROGRAM
C
C     SUBROUTINES AND FUNCTION SUBPROGRAMS REQUIRED
C        1)SUBROUTINE CORREC 2)SUBROUTINE FNDGAP
```

```
C          3) SUBROUTINE PLOTTR.
C
C     ..................................................
C
      SUBROUTINE MODIF (IRET)
      DIMENSION GAM(4),DRD(4),YY(4),DXY(4)
      COMMON/CONTRL/NRAD,NLH,NIL,NILM1,NILM2,NTOT,
     1NTOTM2,XIS,XNLH,RO,NIN
       COMMON X(330),Y(350),B(190,190),VOLTS,VOLT(190),
     1PHI(190),ICODE(4),GAP(50),IFLAG,THETA(50),XP(50),
     2YP(30),DH(30),YYI(30),DRDTH(50),DXDY(30),ALPHA(50),
     3R(50),PI,SLOPE(30),GAPO(50),XW(50),YW(50),CONDUC,VSP
     4,HE,DPHIDN(50),DVOLTS,FEED,NANO3,NACL,TEMPIN,CONC
C
C          CALCULATION OF THE RADIAL POTENTIAL GRADIENT
C
      DO 1 J=2,NTOTM1
      II=(J-1)*NILM2
      DX=0.1*GAP(J)
      DPHIDR=(VOLT(II)-VOLT(II-1))/DX
C
C          CALLING SUBROUTINE CORREC WHICH APPLIES THE
C          EGUILIBRIUM MACHINING CONDITION.
C
      CALL CORREC (J,DPHIDR,EFF,IRET)
      IF (DRDTH(J).LE.0.0) DRDTH(J)=0.0
1     CONTINUE
      DRDTH(1)=-DRDTH(3)
      DRDTH(2)=0.0
      DXDY(NTOT)=DXDY(NTOTM1)
```

```
      DO 2 J=2,NTOTM1
      IS=1
      IF (J.GT.NRAD) IS=2
C
C        CALLING SUBROUTINE FNDGAP WHICH CALCULATES THE
C        CHANGE IN GAP LENGTHS ALONG TRANSVERSE LINES.
C
      CALL FNDGAP (J,IS)
2     CONTINUE
      JL1=NILM1
      JL3=2*NIL+NILM1
      THETA(1)=-THETA(3)
      GAP(1)=GAP(3)
      R(1)=R(3)
      X(JL1)=-X(JL3)
      Y(JL1)=Y(JL3)
      GAP(NTOT)=2.0*GAP(NTOTM1)-GAP(NTOTM2)
      THETA(NTOT)=PI/2.0
      JL=(NTOT-1)*NIL+NILM1
      JLM1=(NTOT-2)*NIL+NILM1
      X(JL)=X(JLM1)
C
C        CHECKING FOR CONVERGENCE
C
      DO 3 J=3,NTOTM1
      IF (ABS(GAP(J)-GAPO(J)).GT.0.05) GO TO 31
3     CONTINUE
      WRITE (6,200) (I,GAP(I),I=1,NTOT)
C
C        COORDINATES OF THE EQUILIBRIUM WORK PROFILE.
C
```

```
      DO 10 J=1,NTOT
      IJ=(J-1)*NIL+NILM1
      XW(J)=X(IJ)*HE
      YW(J)=Y(IJ)*HE
10    CONTINUE
C
C        NORMAL POTENTIAL GRADIENT OVER THE EQUILIBRIUM
C        WORK PROFILE.
C
      DO 4 J=2,NTOTM1
4     DPHIDN(J)=DPHIDN(J)/HE
      WRITE(6,100)
C
C        CALLING SUBROUTINE TEMP WHICH CALCULATES THE
C        TEMPERATURE DISTRIBUTION OVER THE WORK PROFILE.
C
      CALL TEMP
      WRITE (6,32) (XW(JX),YW(JX),JX=1,NTOT)
32    FORMAT (/,3X,10F10.4)
      WRITE (6,32) (DPHIDN(JX),JX=2,NTOTM1)
C
C        INTIALISING THE PLOTTING PROGRAMS
C
      CALL PLOTS ( 'B.NANAYAKKARA STRATHCLYDE',25,96)
      CALL PLOT (3.0,6.0,-3)
C
C        CALLING SUBROUTINE PLOTTR WHICH PLOTS THE
C        RELATIVE POSITIONS OF BOTH ELECTRODES.
C
```

```
      CALL PLOTTR  (XW,YW,XP,YP,40)
      CALL PLOT (0.0,0.0,999)
      STOP
C
C        CALLING SUBROUTINE MESH FOR ITERATION.
C
   31 CALL MESH
C
C          DESCRIPTION OF FORMAT STATEMENTS
C
  100 FORMAT(///,' CONVERGENCE WAS OBTAINED')
  200 FORMAT (5(4X,'GAP(',I2,')=',F9.6)/)
      RETURN
      END
C
C     ..................................................
C
C     SUBROUTINE CORREC
C
C     PURPOSE
C        TO FIND THE NORMAL POTENTIAL GRADIENT AT NODAL
C        POINTS ALONG THE WORK BOUNDARY.
C        TO APPLY THE EQUILIBRIUM MACHINING CONDITION
C           TO CORRECT THE WORK PROFILE.
C
C        USAGE
C           CALL CORREC (J,DPHIDR,IRET)
C
```

```
C       DESCRIPTION OF PRAMETERS
C          J    COUNTER FOR TRANSVERSE LINES.
C          DPHIDR RADIAL POTENTIAL GRADIENT.
C          IRET NUMBER OF ITERATION.
C
C       REMARKS
C          LOGICAL PROGRAM.
C
C       METHOD
C          FROM THE EROSION CONDITION,THE ANGLE BETWEEN
C          THE TANGENT TO THE SHOULD BE WORK PROFILE AND
C          THE -VE FEED DIRECTION WAS FOUND.
C          THE CORRESPONDING ANGLE OF THE GUESSED WORK
C          PROFILE WAS CORRECTED BY FORMULA
C
C       SUBROUTINES AND FUNCTON SUBPROGRAMS REQUIRED
C          NONE.
C
C       ..........................................
C
      SUBROUTINE CORREC (J,DPHIDR,EFF,IRET)
      COMMON/CONTRL/NRAD,NLH,NIL,NILM1,NILM2,NTOT,
     1NTOTM2,XIS,XNLH,RO,NIN
      COMMON X(350),Y(350),B(190,190),VOLTS,VOLT(190),
     1PHI(190),ICODE(4),GAP(50),IFLAG,THETA(50),XP(50),
     2YP(50),DH(50),YYI(50),DRDTH(50),DXDY(50),ALPHA(50),
     3R(50),PI,SLOPE(50),GAPO(50),XW(50),YW(50),CONDUC,VSP
     4,NE,DPHIDN(50),DVOLTS,FEED,NANO3,NACL,TEMPIN,CONC
      FAC=0.1
```

```
C
C          CALCULATION OF THE GRADIENT TO THE WORK SURFACE
C          AT NODAL POINTS.
C
      IF (J.EQ.2) AT=PI/2.0
      IF (J.EQ.2) GRAD=0.0
      IF (J.EQ.2) GO TO 10
      IWM1=(J-2)*NIL+NILM1
      IWP1=J*NIL+NILM1
      ADX=ABS(X(IWM1)-X(IWP1))
      GRAD=(Y(IWP1)-Y(IWM1))/(X(IWP1)-X(IWM1))
      SLOPE(J)=-1.0/GRAD
      IF (SLOPE(J).LE.0.0) SLOPE(J)=0.0
      AT=ATAN(SLOPE(J))
10    TANGLE=(PI/2.0)-AT
      IF (J.GT.(NRAD-1)) GO TO 100
      ANGLE=ABS(AT-(PI/2.0)+THETA(J))
      DPHIDN(J)=DPHIDR/COS(ANGLE)
      IF (J.EQ.2) DRDTH(J)=0.0
      IF (J.EQ.2) GO TO 130
      GO TO 20
100   DPHIDN(J)=DPHIDR/COS(AT)
C
C          THE ABOVE PROCEDURE CALCULATES THE NORMAL EROSION
C          VECTOR.
C
C
20    AGRAD=ABS(GRAD)
      IF (NANO3.EQ.1) GO TO 30
      GO TO 40
30    DPHID=DPHIDN(J)
```

```
C
C          ETTA THE MACHINING EFFICIENCY WHEN USING SODIUM
C          NITRATE ELECTROLYTE.
C
      IF (DPHID.LE.1.2) ETTA=0.45384+0.577117*DPHID
     1-0.11525*(DPHID*2)
      IF (DPHID.GT.1.2) ETTA=0.002785*DPHID+0.974413
      ERRATE=ETTA*VSP*DPHIDN(J)*CONDUC
      GO TO 50
   40 ERRATE =VSP*DPHIDN(J)*CONDUC
   50 XKALU=PI-TANGLE
C
C          TKANTI IS THE TANGENT OF THE ANGLE BETWEEN
C          EROSION VECTOR AND THE -VE TOOL FEED VECTOR.
C
      TKANTI=(ERRATE*SIN(XKALU))/(FEED+ERRATE*COS(XKALU))
      XKANTI=ATAN(TKANTI)
      IF (TKANTI.LT.0.0) XKANTI=PI+ATAN(TKANTI)
      CRAT=(1.0-FAC)*AT+FAC*XKANTI
      IF (CRAT.GE.PI/2.0) CRAT=PI/2.0
      DXCRAT=-TAN(PI/2.0-CRAT)
      DYCRAT=1.0/DXCRAT
      IF (J.GE.(NRAD-2)) DXDY(J)=DYCRAT
      IF (J.GT.(NRAD+3)) GO TO 130
      DRDTH(J)=(R(J)*(SIN(THETA(J))+DXCRAT*COS(THETA(J))))
     1/(COS(THETA(J))-DXCRAT*SIN(THETA(J)))
  130 RETURN
      END
```

```
C
C     ..................................................
C
C     SUBROUTINE FNDGAP
C
C     PURPOSE
C        TO FIND THE CHANGE IN GAPS BETWEEN TOOL AND
C        THE WORK PROFILE ALONG TRANSVERSE LINES AFTER
C        EACH ITERATION.
C
C     USAGE
C        CALL FNDGAP (J,ISEND)
C
C     DESCRIPTION OF PARAMETERS
C        J    COUNTER FOR TRANSVERSE LINES.
C        ISEND INTEGER WHICH SELECTS DIFFERENT PARTS OF
OF
C              THE PROGRAM IN CALCULATION THE CHANGE
C              IN GAP LENGTHS (DH).
C
C     REMARKS
C        LOGICAL PROGRAM.
C
C     METHOD
C        FOUR NEIGHBOURING POINTS WERE SECLECTED
C        STARTING WITH THE FIRST MIRROR POINT.
C        A POLYNOMIAL WAS FITTED TO THESE FOUR
C        NEIGHBOURING POINTS NUMERICAL INTEGRATION OF
C        THE EXPRESSION OF THE POLYNOMIAL BETWEEN
C        SECOND AND THIRD YIELDS THE AMOUNT BY WHICH
```

```
C          THE GAP AT THE THIRD NODAL POINT HAS TO BE
C          CORRECTED.
C
C     ..................................................
C
      SUBROUTINE FNDGAP (J,ISEND)
      DIMENSION GAM(4),DRD(4),YY(4),DXY(4)
       COMMON/CONTRL/NRAD,NLH,NIL,NILM1,NILM2,NTOT,
     1NTOTM2,XIS,XNLH,RO,NIN
       COMMON X(350),Y(350),B(190,190),VOLTS,VOLT(190),
     1PHI(190),ICODE(4),GAP(50),IFLAG,THETA(50),XP(50),
     2YP(50),DH(50),YYI(50),DRDTH(50),DXDY(50),ALPHA(50),
     3R(50),PI,SLOPE(50),GAPO(50),XW(50),YW(50),CONDUC,VSP
     4,HE,DPHIDN(50),DVOLTS,FEED,NANO3,NACL,TEMPIN,CONC
       READ (5,10) FACTOR
       IF (J.EQ.2.AND.NANO3.EQ.1) GO TO 7
       IF (J.EQ.2) GO TO 5
       GO TO (1,2),ISEND
 1     DO 3 I=1,4
       GAM(I)=THETA(J-3+I)
       DRD(I)=DRDTH(J-3+I)
 3     CONTINUE
       DH(J)=DAREA(GAM,DRD)
       R(J)=R(J-1)+DH(J)*FACTOR
       GO TO 6
 5     DH(J)=((VSP*DPHIDN(J)*CONDUC)-FEED)*0.1
 8     R(2)=R(2)+DH(2)
```

```
6       GAP(J)=R(J)-RO
        IJWP=(J-1)*NIL+NILM1
        X(IJWP)=R(J)*SIN(THETA(J))
        Y(IJWP)=R(J)*COS(THETA(J))
        RETURN
2       DO 4 I=1,4
        IJWP=(J-4+I)*NIL+NILM1
        YY(I)=Y(IJWP)
        DXY(I)=DXDY(J-3+I)
4       CONTINUE
        GO TO 9
7       DPHID=DPHIDN(J)*(HE**2)
C
C           ETTA THE MACHING EFFICIENCY WHEN USING SODIUM
C           NITRATE ELECTROLYTE.
C
        IF (DPHID.LE.1.2) ETTA=0.45834+0.577117*DPHID
       1-0.11525*(DPHID**2)
        IF (DPHID.GT.1.2) ETTA=0.002785*DPHID+0.974413
        ERRATE=ETTA*VSP*DPHIDN(J)*CONDUC
        DH(J)=((VSP*DPHIDN(J)*CONDUC*ETTA)-FEED)*0.1
        GO TO 8
9       DH(J)=DAREA(YY,DXY)
        IJWP=(J-1)*NIL+NILM1
        IJWM=(J-2)*NIL+NILM1
        X(IJWP)=X(IJWM)+DH(J)*FACTOR
        GAP(J)=X(IJWP)-RO
        R(J)=SQRT(X(IJWP)**2+Y(IJWP)**2)
```

```
C
C          DESCRIPTION OF THE FORMAT STATEMENT,
C
1C      FORMAT (F12.6)
        RETURN
        END

C
C       ..........................................
C       SUBROUTINE TEMP
C
C       PURPOSE
C          TO FIND THE OHMIC HEATING WHEN THE ELECTROLYTE
C          PASSES EACH NODAL POINT ON THE WORK SURFACE
C          AND TO CALCULATE THE RISE IN TEMPERATURE.
C
C       USAGE
C          CALL TEMP
C
C       REMARKS
C          ELECTROLYTE FLOW RATE, SPECIFIC GRAVITY OF THE
C          ELECTROLYTE, THE DISTANCE FROM THE SYMMETRICAL
C          AXIS OF THE TOOL TO THE CENTRE OF THE LEADING
C          RADIUSED EDGE AND THE SPECIFIC HEAT OF THE
C          ELECTROLYTE IS READ FROM A DATA CARD.
C
C       SUBROUTINE AND SUBPROGRAMS REQUIRED
C          NONE
```

```
C
C       METHOD
C           AVERAGE CURRENT IS CALCULATED BETWEEN TWO
C           CONSERCATIVE MESH POINTS ON THE WORK SURFACE.
C           ASSUMING THE TOTAL ELECTPAICAL ENERGY IS
C           CONVERTED IN TO HEAT AND WAS USED IN RAISING
C           THE TEMPERATURE OF THE ELECTROLYTE THE
C           TEMPERATURE OF THE ELECTROLYTE AS IT LEAVES
C           THE SECOND MESH POINT WAS CALCULATED.
C           STARTING FROM THE TEMPERATURE TO THE MACHINING
C           CELL,THE TEMPERATURE OF THE ELECTROLYTE AS IT
C           LEAVES EACH NODAL POINT WAS CALCULATED.
C
C     .....
C
      SUBROUTINE TEMP
      COMMON X(350),Y(350),B(190,190),VOLTS,VOLT(190),
     1PHI(190),ICODE(4),GAP(50),IFLAG,THETA(50),XP(50),
     2YP(50),DH(50),YYI(50),DRDTH(50),DXDY(50),ALPHA(50),
     3R(50),PI,SLOPE(50),GAPO(50),XW(50),YW(50),CONDUC,VSP
     4,HE,DPHIDN(50),DVOLTS,FEED,NANO3,NACL,TEMPIN,CONC
       READ (5,15) FLOW,ROWL,C,RA
      WRITE (6,20) FLOW,ROWL,C,RA
      T=TEMPIN
      CONDUC=CONDUC/HE
      DO 1 JJ=2,NTOTM2
      I1=41-JJ
      I2=I1-1
```

```
C
C       CALCULATION OF THE RING AREA OF THE WORK PROFILE
C       BETWEEN TWO NEIGHBOURING NODAL POINTS ON THE
C       WORK SURFACE.
C
      DS=SQRT((XW(I1)-XW(I2))**2+(YW(I1)-YW(I2))**2)
      DPHIDA=(DPHIDN(I1)+DPHIDN(I2))/2.0
       R1=(XW(I1)+XW(I2))/2.0+RA
       DT=R1*VOLTS*CONDUC*2.0*PI*DPHIDA*DS/(FLOW*1000.0*
     1ROWL*C/60.0)
C
C          INCREASE IN TEMPERATURE AS THE ELECTROLYTE PASSES
C          THE RING AREA OF THE WORK SURFACE.
C
       T=T+DT
      WRITE (6,10) JJ,DT,T,DS
1     CONTINUE
C
C          CALCULATING THE TEMPERATURE RISE IN THE STRAIGHT
C          LEADING EDGE. AREA 'DA'=AREA OF THE WORK PROFILE
C          OPPOSITE THE STRAIGHT LEADING EDGE OF THE TOOL.
C
      DA=PI*(RA**2-(RA-XIS)**2)
       DT=DA*VOLTS*CONDUC*DPHIDN(2)/(FLOW*1000.0*ROWL*C/
     160.0)
       T=T+DT
       WRITE (6,11) JJ,DT,T,DA
C
C               DESCRIPTION OF FORMAT STATEMENTS.
```

```
C
10    FORMAT (/,3X,'JJ=',I2,4X,'DT=',F12.6,'T=',F12.6,'DS=
     1',F12.6)
11    FORMAT (/,3X,'JJ=',I2,4X,HDT=',FUI.L,'T=',F12.6,'DA=
     1',F12.6)
15    FORMAT (5F12.6)
2C    FORMAT (/,3X,'***',3X,'FLOW=',F12.6,3X,'ROWL=',F12.6
     1,3X,'C=',F12.6,3X,'RA=',F12.6,'***')
      RETURN
      END

C
C     ..................................................
C
C          FUNCTION DAREA
C
C          PURPOSE
C             TO NUMERICALLY INTEGRATE THE FUNCTION FITTED
C          FOUR NEIGHBOURING POINTS ON THE WORK PROFILE.
C
C          USAGE
C
C             DH(J)=DAREA (X,Y)
C
C          DESCRIPTION OF PARAMETERS
C             DH    CHANGE IN GAP.
C             X     INPUT PARAMETER, ANGLE MADE BY THE RADIAL
C                   LINES WITH THE VERTICAL IN THE RADIUSED
```

```
C                SECTION OF THE TOOL OR 'Y' COORDINATE OF
C                THE STRAIGHT SECTION OF THE TOOL.
C          Y     (DELTAHR'/DELTA'THETA') IN THE RADIAL
C               SECTION OF THE TOOL OR (DELTA'X'/DELTA'Y')
C                IN THE STRAIGHT SECTION OF THE TOOL.
C
C        REMARKS
C           INPUT PARAMETERS ARE DENOTED BY X AND Y, OUTPUT
C           PARAMETER IS THE VALUE OF THE INTEGRAL BETWEEN
C           LIMITS GIVEN BY SECOND AND THIRD POINTS
C           SELECTED IN FITTING THE POLYNOMIAL.
C
C     SUBROUTINES AND FUNCTION SUBPROGRAMS REQUIRED
C          1) SUBROUTINE POLYAP
C
C        METHOD
C           CHANGE IN GAP IS FOUND BY SUBSTITUTION OF
C           VALUE OF THE FUNCTION CORRESPONDING TO X IN
C           THE INTEGRATED FUNCTION.
C
C     ..................................................
C
      FUNCTION DAREA (X,Y)
      DOUBLE PRECISION C(10)
      DIMENSION X(4),Y(4)
       CALL POLYAP (X,Y,3,4,C)
C
C         DAREA=VALUE OF THE INTEGRAL
```

```
C
      OAREA=C(1)*(X(3)-X(2))+C(2)*(X(3)**2-X(2)**2)/2.0
     1+C(3)*(X(3)**3-X(2)**3)/3.0+C(4)*(X(3)**4-X(2)**4)/4.0
      DAREA=OAREA
      RETURN
      END
C
C     ..................................................
C
C     SUBROUTINE POLYAP
C
C     PURPOSE
C        TO OBTAIN THE LEAST-SQUARE POLYNOMIAL FOR EACH
C        SET OF FOUR NEIGHBOURING POINTS SELECTED ON
C        THE WORK SURFACE.
C
C     USAGE
C        CALL POLYAP (X,Y,M,IPOINT,C)
C
C     DESCRIPTION OF PARAMETERS
C        X,Y  COORDINATES OF THE POINTS TO WHICH A
C             LEAST SQUARE POLYNOMIAL IS FITTED.
C        M    DEGREE OF THE REQUIRED POLYNOMIAL.
C        IPOINT NUMBER OF POINTS.
C        C    COEFFICIENTS OF THE POLYNOMIAL.
C
C     REMARKS
C        ALWAYS THE DEGREE OF THE POLYNOMIAL SHOULD BE
C        LESS THAN THE NUMBER OF POINTS.
```

```
C          AS DIMENSIONED WILL CONSIDER UP TO 50 POINTS
C        SUBROUTINES AND FUNCTION SUBPROGRAMS REQURIED
C           NONE.
C
C     ..................................................
C
      SUBROUTINE POLYAP(X,Y,M,IPOINT,C)
      DOUBLE PRECISION A(10,10),B(10),C(10),P(20),TEMP,
     1FACTOR,SUM
      DIMENSION X(50),Y(50)
      NUMBER=IPOINT-1
      MX2=M*2
      DO 13 I=1,MX2
      P(I)=0.0
      DO 13 J=1,NUMBER
   13 P(I)=P(I)+X(J)**I
      N=M+1
      DO 30 I=1,N
      DO 30 J=1,N
      K=I+J-2
      IF(K)29,29,28
   29 A(I,J)=P(K)
      GO TO 30
   29 A(1,1)=NUMBER
   30 CONTINUE
      B(1)=0.0
      DO 21 J=1,NUMBER
   21 B(1)=B(1)+Y(J)
      DO 22 I=2,N
```

```
      B(I)=0.0

      DO 22 J=1,NUMBER

22    B(I)=B(I)+Y(J)*X(J)**(I-1)
```

```
      NM1=N-1
      DO 300 K=1,NM1

      KP1=K+1

      L=K

      DO 400 I=KP1,N

      IF(DABS(A(I,K))-DABS(A(L,K)))400,400,401

401   L=I

400   CONTINUE

      IF(L-K)300,500,405

405   DO 410 J=K,N

      TEMP=A(K,J)

      A(K,J)=A(L,J)

410   A(L,J)=TEMP

      TEMP=B(K)

      B(K)=B(L)

      B(L)=TEMP

300   DO 300 I=KP1,N

      FACTOR=A(I,K)/A(K,K)

      A(I,K)=0.0

      DO 301 J=KP1,N

301   A(I,J)=A(I,J)-FACTOR*A(K,J)

300   B(I)=B(I)-FACTOR*B(K)

      C(N)=B(N)/A(N,N)

      I=NM1

710   IP1=I+1

      SUM=0.0

      DO 700 J=IP1,N
```

```
700     SUM=SUM+A(I,J)*C(J)
        C(I)=(P(I)-SUM)/A(I,I)
        I=I-1
        IF(I)800,800,710
300     CONTINUE
        RETURN
        END
C
C       ..................................................
C
C       SUBROUTINE PLOTTR
C
C       PURPOSE
C          TO PLOT THE RELATIVE POSITIONS OF THE ELECTRODES.
ES
C
C       USAGE
C          CALL PLOTTR (X1,Y1,X2,Y2,N)
C
C       DESCRIPTION OF PARAMETERS
C          X1,Y1   COORDINATES OF THE TOOL BOUNDARY.
C          X2,Y2   COORDINATES OF THE WORK BOUNDARY.
C          N       NUMBER OF NODAL POINTS ON EACH BOUNDARY.
C
C       REMARKS
C          THIS SUBROUTINE PROVIDES A STANDARD PROCEEDING
C          TO CALL THE UNIVERSITY GRAPH PLOTTER.
C         PLOTS BOTH TOOL ELECTRODE AND WORK ELECTRODE
C          SHOWING THEIR RELATIVE EQUILIBRIUM POSITIONS.
```

```
C          PRINTS MACHINING PARAMETERS WHICH WERE READ
C          FROM BLOCK DATA AND FROM A DATA CARD.
C          EMPLOYS ROUTINES PLOT, LINE,AND SYMBOL, WHICH
C          WERE STANDARD ROUTINES USED BY THE GRAPH
C          PLOTTER.
C          AS DIMENSIONED CONSIDERS 50 NODAL POINTS.
C
C     ..........
C
      SUBROUTINE PLOTTR  (X1,Y1,X2,Y2,N)
      DIMENSION X1(50),Y1(50),X2(50),Y2(50),TIT1(3),
     1TIT2(5),TIT3(3),TIT4(4),TIT5(4),TIT6(5),TIT7(5),
     2TIT8(5),T1(2),T2(2),TIT9(1),TIT10(1),TIT11(1),
     3TIT12(1),TIT13(3),C(6)
      DATA TIT1/'ELEC','TROL','YTE '/
      DATA TIT2/'APPL','IED ','VOLT','AGE ',' =   '/
      DATA TIT3/'FEED',' RAT','E = '/
      DATA TIT4/'WORK','PIEC','E  E','N5RJ'/
      DATA TIT5/'CATH','ODE ','BRAS','S   '/
      DATA TIT9/'TOOL'/
      DATA TIT10/'WORK'/
      DATA TIT11 /'  MM'/
      DATA TIT12/'  MM'/
      DATA TIT13 /'INSU','LATI','ON  '/
      DATA C/'1   ','2   ','3   ','4   ','5   ','6   '/
      DATA T1/'    ','    '/
      DATA T2/'    ','    '/
      X1(N+1)=0.0
      X1(N+2)=1.27
```

```
      Y1(N+1)=0.0
      Y1(N+2)=1.27
      X2(N+1)=0.0
      X2(N+2)=1.27
      Y2(N+1)=0.0
      Y2(N+2)=1.27
      READ(5,100) TIT6,TIT7,TIT8
      DIST=1.0/1.27
      CALL SYMBOL (-0.04,-0.2,0.12,'0    ',0.0,4)
      CALL PLOT (0.0,0.0,3)
      DO 1 I=1,6
      X=FLOAT(I)*DIST
      CALL PLOT (X,0.0,2)
      CALL PLOT (X,-0.05,2)
      CALL SYMBOL ((X-0.04),-0.2,0.12,C(I),0.0,4)
      CALL PLOT (X,0.0,3)
1     CONTINUE
C
      CALL SYMBOL (-0.2,-0.06,0.12,'0    ',0.0,4)
      CALL PLOT(0.0,0.0,3)
      DO 2 I=1,6
      Y=FLOAT(I)*DIST
      CALL PLOT (0.0,Y,2)
      CALL PLOT (-0.05,Y,2)
      CALL SYMBOL (-0.2,(Y-0.06),0.12,C(I),0.0,4)
      CALL PLOT (0.0,Y,3)
2     CONTINUE
      CALL PLOT (0.0,0.0,3)
      CALL LINE (X1,Y1,N,1,0,1)
      CALL LINE (X2,Y2,N,1,0,1)
```

```
      CALL SYMBOL (1.0,6.0,0.12,TIT1,0.0,12)
      CALL SYMBOL (2.6,6.0,0.12,TIT6,0.0,20)

      CALL SYMBOL (1.0,5.8,0.12,TIT2,0.0,20)
      CALL SYMBOL (3.4,5.8,0.12,TIT7,0.0,20)
      CALL SYMBOL (1.0,5.6,0.12,TIT3,0.0,12)
      CALL SYMBOL (2.6,5.6,0.12,TIT8,0.0,20)
      CALL SYMBOL (1.0,5.4,0.12,TIT4,0.0,16)
      CALL SYMBOL (1.0,5.2,0.12,TIT5,0.0,16)
      CALL SYMBOL (1.0,1.0,0.12,TIT9,0.0,4)
      CALL SYMBOL (3.0,3.5,0.12,TIT10,0.0,4)
      CALL SYMBOL (-0.2,5.5,0.12,TIT11,90.0,4)
      CALL SYMBOL (5.5,-0.2,0.12,TIT12,0.0,4)
      CALL SYMBOL (2.0,-2.5,0.12,TIT13,90.0,12)
      WRITE (6,200)
      RETURN
C
C          DESCRIPTION OF FORMAT STATEMENTS.
C
100   FORMAT(3(5A4))
200   FORMAT ( ' PLOT O.K')
      END
```

NOMOGRAM TO DETERMINE THE CONCENTRATION OF SODIUM CHLORATE SOLUTIONS

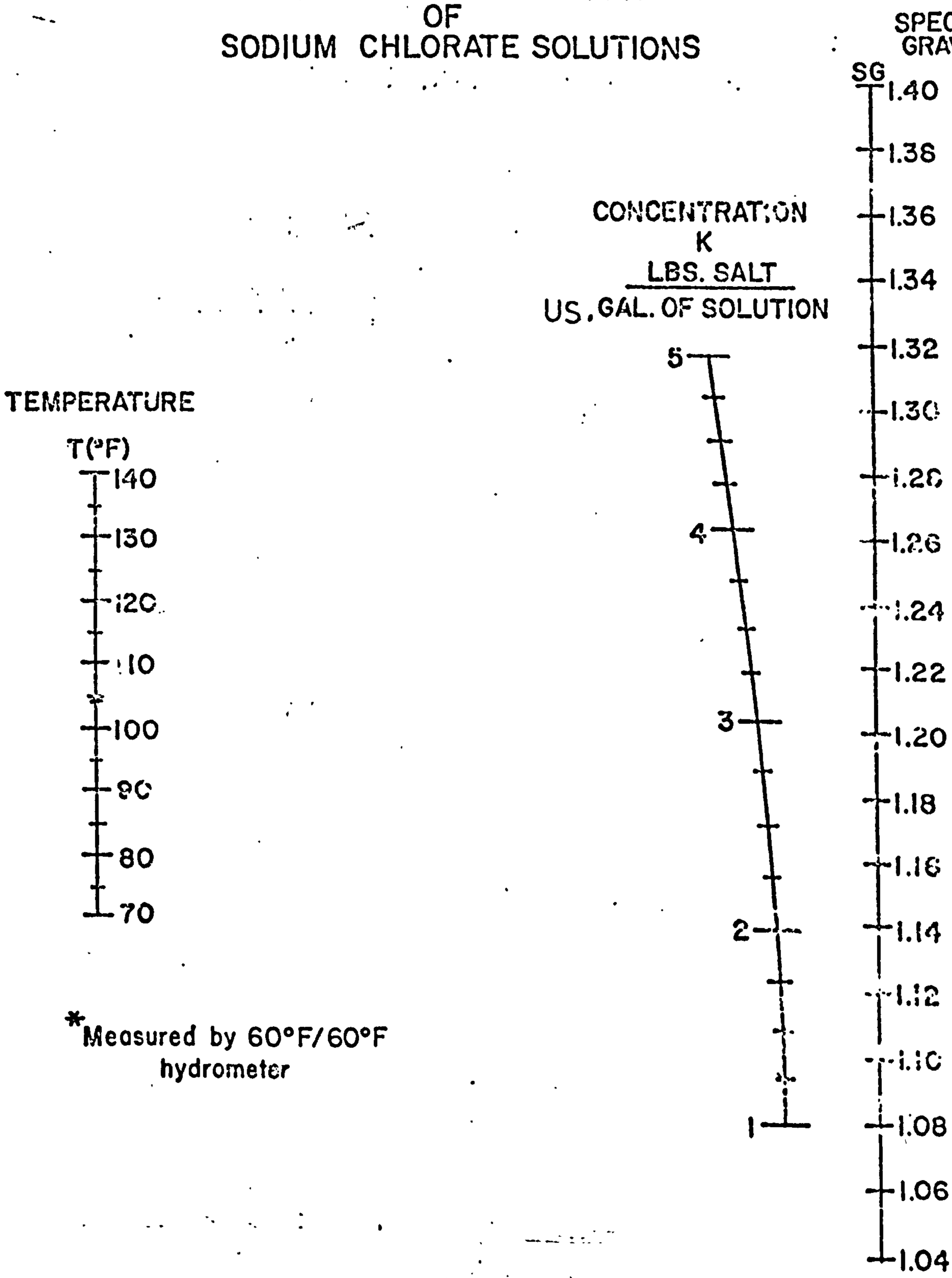

*Measured by 60°F/60°F hydrometer

NOMOGRAM TO DETERMINE THE CONCENTRATION OF SODIUM NITRATE SOLUTIONS

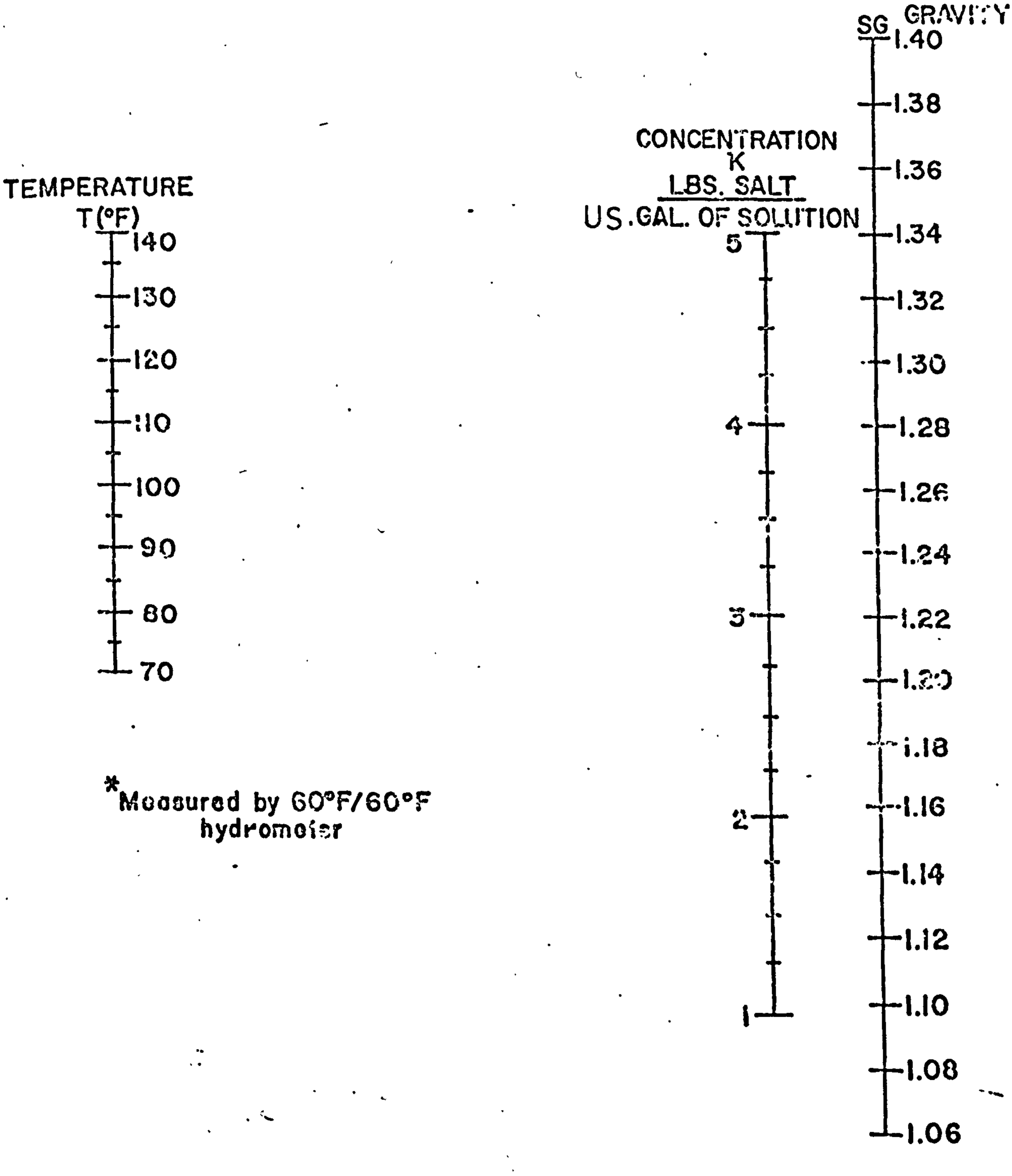

*Measured by 60°F/60°F hydrometer

REFERENCES

1. DEBARR, A.E., OLIVER, D.A., Electrochemical Machining ed. De Barr, A.E. and Oliver, D.A., Macdonald, London (1968).

2. BOCKRIS, J.O.M. and REDDY, A.K.N., Modern Electrochemistry, Vol. I, Plenum Press New York. (1970).

3. HOAR, T.P. 'Modern Aspects of Electrochemistry', Vol. II, ed. J.O.M. Bockris, Butterworths (1959).

4. MAO, K.W., J. Electrochemical Society Vol. 118, p.1876 (1971).

5. LARSSON, C.N., Ph.D. Thesis, Lancester College, Coventry (1968).

6. DAVIDSON, A.W., Encyclopedia of Electrochemistry. ed. Hampel, C.A., p.48 (1964).

7. KOICHI, S., ITO, S., "The Influence of Electrolyte Products on Electrolyte Flow Rate in Electrochemical Machining'. bull, Japan Soc. of Prec. Eng., Vol. 4, No. 3, (1970).

8. STRAUMANIS, M.E., 'Anodic Disintegration of Electrochemistry' ed. Hampel, C.A. (1964).

9. Metalcutting. P.E.R.A., report No. 145 (Sept. 1965).

10. KONIG, W., DEGENHARDT, H., 'The influence of process parameters and Tool Electrode Geometry on the Development of the Overcut in Electrochemical Machining with High Current Densities. Fundamental of Electrochemical Machining. ed. Faust, C.L. The Electrochemical Soc. incorporated (1971).

11. TIPTON, H., 'The Determination of the Shape of Tools for Use in Electrochemical Machining. M.T.I.R.A. Research Report No. 40.

12. COLLET, D.E., HEWSON BROWNE, R.C., WINDLE, D.W., A Complex Variable Approach to Electrochemical Machining Problems. J. of Engineering Mathematics Vol. 4, No. I, p.29. (1970).

13. KRYLOV, A.L., The Cauchy Problem for the Laplace Equation in the Theory of Electrochemical Metal Machining. Soviet Physics-Doklady, Vol. 13, No. I, p.15 (July 1968).

14. LEONG, K.K., M.Sc. Thesis, The University of Strathclyde, Glasgow, 1970.

15. WRIGHT, E.G., 'Graphical Field Plotting'. Field Analysis, ed. Vitkovitch, D. London (1966).

16. THORPE, J.F., ZERKLE, R.D., A Theoretical Analysis of the Equilibrium Sinking of Shallow Axially Symmetric Cavities by Electrochemical Machining. Fundamentals of Electrochemical Machining ed. Faust, C.L. The Electrochemical Machining Soc. Incorporated (1971).

17. HOPENFIELD, J., COLE, R.R., Electrochemical Machining Prediction and Correlation of Process Variables. J. of Engineering for Industry. Trans. of the ASME 460 (Nov. 1966).

18. TIPTON, H., WILSON, J.F., 'The Working Gap' ed. DE BARA, A.E., OLIVER, D.A. (1968) Macdonald London (1968).

19. CHIKAMORI, K., ITO, S., SAKURAI, F., 'Flow of Electrolyte in Electrochemical Die-Sinking. Bulletin of the Japan Soc. of Prec. Eng. Vol. 2, No. 4, p.318 (April 1968).

20. LOUTREL, S.P., COOK, N.H., 'High Rate Electrochemical Machining. Trans. ASME, J. Eng. for Industry. No. 73 - Prod 3. p.992 (Nov. 1973).

21. BHATTACHARYYA, A., SUR, B., SORKEL, S.K., 'Analysis for Optimum Parametric Combination in Electrochemical Machining. Annuls of the C.I.R.P. Vol. 22/1, p.59 (1973).

22. CLARK, W.G., Ph.D. Thesis, University of Strathclyde Glasgow (1974).

23. LAWRENSON, P.J., 'Numerical Methods in Field Analysis' ed. Vitkovitch, D. London (1966).

24. ARMS, R.J., and GATES, L.D., ZONDE, B., 'A Method of Block Iteration'. J. Soc. Indust. APPL. Math. Vol. 4, No. 4, (Dec. 1956).

25. PEACEMAN, D.W., and RACHFORD, H.H. Jr., 'The Numerical Solution of Parabolic and Elliptic Differential Equations'. J. Soc. Indust. Appl. Math. Vol. 3, No. 1, March (1955).

26. KLINGERT, J.A., LYNN, S., and TOBIAS, C.W., 'Evaluation of the Current Distribution in Electrode Systems by High Speed Digital Computers'. Electrochemica Acta, Vol. 9, p.297 (1964).

27. MOON, P., and SPENCER, D.E., 'Partial Differential Equations'. Massachussetts. (1969).

28. McCRACKEN, D.D. and WILLIAMS, S.D., 'Numerical Methods and FORTRAN Programing' John Wiley, New York. (1964).

29. FORSYTHE, G., and WASOW, R., 'Finite Difference Methods for Partial Differential Equations'. Wiley, New York (1960).

30. WOLOSEWICZ, R.M., 'ECM Electrolyte Properties'. Technical Paper, MR70-220, Soc. of Manufacturing Engineers, Michigan, U.S.A. (1970).

31. McGEOUGH, J.A. 'Principles of Electrochemical Machining', Chapman and Hall Ltd., London (1974).

32. BARSOV, M.D., HUMBS, H.J., LINDENLAUF, P., Temperaturverteilung in Arbeistsspalt beim Electrochemischen Senken, von Raumformen. Industrie-Anzeiger 96, ig, Nr. 20V. 8.3 (1974).

33. MUZAFFARUDDIN, K., Ph.D. Thesis, University of Strathclyde, Glasgow (1975).

34. NILSON, R.H., TSUEI, Y.G., 'Free Boundary Problem of ECM by Alternating-Field Technique on Inverted Plane' Journal of Computer Methods in Applied Mechanics and Engineering, Vol. 6, No. 3, p.265, 1975.

35. NILSON, R.H., TSUEI, Y.G., Free Boundary Problem for the Laplace Equation with Application to ECM Tool Design. ASME App. Mechanics Division. Paper No. 76-APM.6 (1975).

36. CUTHBERTSON, J.W., TURNER, T.S. 'Electrochemical Machining - A Study of the Effects of Some Variables'. The Journal of the Institution of Production Engineers. p.270. May 1966.

37. MAO, K.W., 'ECM Study in Closed-Cell System'. Journal of Electrochemical Soc. Vol. 118. p.1870, 1971.

38. CHIKAMORI, K., ITO, S., 'Electrolytic Dissolution of Mild Steel in High Current Density Region'

39. LANDOLT, D., MULLER, R.H., TOBIAS, C.W., 'Transport Process in ECM'. Fundamental of Electrochemical Machining ed. Faust, C.L. The Electrochemical Soc. Incorporated (1971).

40. BAXTER, A.C., FREER, H.E., and WILLENBRUCH, D.A., 'Photographic Studies of Evolved Gas during Electrochemical Machining.' First International Conference on Electrochemical Machining. Leicester University (March 1973).

41. DIETZ, H., GUNTHER, K.G., OTTO, K., 'Reproduction Accuracy with Electrochemical Machining'. Annal of the CIRP Vol. 22/1, p.61, (1973).

42. HOAR, T.P., MEAR, D.C., and ROTHWELL, G.P., Corrosion Science, Vol. 5, p.279 (1965).

43. MAEDA, S., SAITO, N., ARAI, S., 'Apparent Specific Resistance and Machining Accuracy'. Bull. of the Japan Soc. of Prec. Engs, Vol. 2, No. 2, p.126. (1967).

44. CRYER, C.W., 'The Approximate Solution of Free Boundary Problems Using Finite Differences', Journal of the Association for Computing Machinery, Vol.17, No. 3, p.397, (July 1970).

45. BODEN, P.J., RABBON, M.F., 'Electrolytes for ECM of Titanium and its Alloys' First International Conference on ECM, Leicester University (March 1973).

46. HOLE, V.H.R., 'Thermistor Temperature Measuring Bridge Circuits Part I'. Electronic Components p.1167 (12 Nov. 1971).

47. HOLE, V.H.R., 'Thermistor Temperature Measuring Bridge Circuits Part II'. Electronic Components, p.26 (14 JAN 1972).

48. PLANT, M. 'The Thermistor as a Thermometer' School Technology, Bul. 18, Vol. 4(3), p.9 (June 1971).